

Methylmercury cycling, bioaccumulation, and export from agricultural and non-agricultural wetlands in the Yolo Bypass

Cooperator Report Prepared by:
U.S. Geological Survey
California Department of Fish and Game
Moss Landing Marine Laboratory
Battelle Marine Sciences
Bachand and Associates
Yolo Basin Foundation

Responsible Organization: San Jose State University Research Foundation

FINAL REPORT September 30, 2010

Title:	Name:	Signature:	Date:
Project Manager	Mark Stephenson	_____	_____
SWRCB Contract Manager	Janis Cooke	_____	_____

Dates: December 2006-December 2008
Watershed: Yolo Bypass, Yolo County, CA
Funds: Central Valley Regional Water Quality Control Board
Cost of Project: \$999,760

This project is supported by Proposition 40 as part of the Agricultural Water Quality Grant Program and local and federal matching funds.

“Funding for this project has been provided in full or in part through an agreement with the State Water Resources Control Board. The contents of this document do not necessarily reflect the views and policies of the State Water Resources Control Board, nor does mention of trade names or commercial products constitute endorsement or recommendation for use.” (Gov. Code 7550, 40 CFR 31.20)

GRANT SUMMARY FORM

2005 - 2006 CONSOLIDATED GRANTS - PROPOSITION 40/50 AGRICULTURE WATER QUALITY
 GRANT PROGRAM
 GRANT AGREEMENT
 BETWEEN THE
 STATE WATER RESOURCES CONTROL BOARD, hereinafter called "State" or "State Water Board"
 AND

SAN JOSE STATE UNIVERSITY FOUNDATION, hereinafter called "Grantee"

Methylmercury cycling and export from agricultural and natural wetlands in the Yolo Bypass,
 hereinafter called "Project"

AGREEMENT NO. 06-232-555-0

State and Grantee hereby agree as follows:

PROVISION(S). The following provision(s) authorize the State Water Board to enter into this type of Grant Agreement:
 PRC §§ 5096.650, 30940(a) (Pr 40 Agricultural Water Quality)
 WC § 79540.1(b), PRC § 30940(a) (Pr 50 Agricultural Water Quality)

PURPOSE. State shall provide a grant to and for the benefit of Grantee for the purpose of developing effective Total Maximum Daily Load (TMDL) by quantifying seasonal and spatial processes through laboratory and statistical analyses.

GRANT AMOUNT. The maximum amount payable under this Agreement shall not exceed \$999,881.00. Global Positioning System (GPS) locations for any monitoring must be identified for this Project prior to any disbursements.

TERM OF AGREEMENT. The term of the Agreement shall begin on DECEMBER 1, 2006 and continue through Project completion plus three (3) years unless otherwise terminated or amended as provided in the Agreement. **HOWEVER, ALL WORK SHALL BE COMPLETED BY MARCH 1, 2009. ABSOLUTELY NO FUNDS MAY BE REQUESTED AFTER APRIL 1, 2009.**

PROJECT REPRESENTATIVES. The Project Representatives during the term of this Agreement will be:

State Water Board		Grantee: San Jose University Foundation	
Name:	Stephanie Fong, Grant Manager	Name:	Mark Stephenson, Project Director
Address:	11020 Sun Center Drive, Suite #200	Address:	544 Sandholt Road
City, Zip:	Rancho Cordova, CA 95670	City, Zip:	Moss Landing, CA 95039
Phone:	(916) 464-4822	Phone:	(831) 771-4177
Fax:	(916) 464-4780	Fax:	(831) 633-0805
e-mail:	swfong@waterboards.ca.gov	e-mail:	mstephenson@mlml.calstate.edu

Direct all inquiries to:

State Water Board		Grantee: San Jose University Foundation	
Section:	Division of Financial Assistance	Section:	
Attention:	Carmen Rios, Program Analyst	Name:	Chris Thompson, Grant Contact
Address:	1001 "I" Street, 16th Floor	Address:	210 N. 4 th Street, 4 th Floor
City, Zip:	Sacramento, CA 95814	City, Zip:	San Jose, CA 95112-5569
Phone:	(916) 341-5659	Phone:	(408) 924-1440
Fax:	(916) 341-5296	Fax:	(408) 924-1496
e-mail:	crios@waterboards.ca.gov	e-mail:	cthompso@foundation.sjsu.edu

Either party may change its Project Representative upon written notice to the other party.

Methylmercury cycling, bioaccumulation, and export from agricultural and non-agricultural wetlands in the Yolo Bypass

Lisamarie Windham-Myers¹, Mark Marvin-DiPasquale¹, Jacob Fleck¹, Charles N. Alpers¹, Josh Ackerman¹, Collin Eagles-Smith¹, Craig Stricker¹, Mark Stephenson^{2,3}, David Feliz², Gary Gill⁴, Philip Bachand⁵, Ann Brice⁶, and Robin Kulakow⁶

¹U.S. Geological Survey

²California Department of Fish and Game

³Moss Landing Marine Laboratory

⁴Battelle Marine Sciences

⁵Bachand and Associates

⁶Yolo Basin Foundation

Executive Summary

This 18-month field study addresses the seasonal and spatial patterns and processes controlling methylmercury (MeHg) production, bioaccumulation, and export from natural and agricultural wetlands of the Yolo Bypass Wildlife Area (YBWA). The data were collected in conjunction with a Proposition 40 grant from the State Water Resources Control Board in support of the development of Best Management Practices (BMP's) for reducing MeHg loading from agricultural lands in the wetland-dominated Yolo Bypass to the Sacramento-San Joaquin River Delta. The four management-based questions addressed in this study were:

- 1. Is there a difference among agricultural and managed wetland types in terms of MeHg dynamics (production, degradation, bioaccumulation, or export)?**
- 2. Does water residence time influence MeHg dynamics?**
- 3. Does the application of sulfate-based fertilizer impact MeHg production rates?**
- 4. Does the presence (or absence) of vegetation influence MeHg production rates?**

Measurements of MeHg concentrations in sediment, water, and biota (plants, invertebrates, and fish) were made to assess management-level patterns in five wetland types, which included three types of shallowly-flooded agricultural wetlands (white rice, wild rice, and fallow) and two types of managed wetlands (permanently and seasonally flooded). To strengthen our understanding of the processes underlying the seasonal and spatial patterns of MeHg cycling, additional explanatory factors were measured including ancillary sediment and water quality parameters, stable isotope fractionation (oxygen, sulfur, carbon, and nitrogen), photodemethylation rates, and daily-integrated hydrologic budgets. Samples and field data were collected from May 2007 to July 2008, and nearly all sample analyses were completed by September 2008 as per the Quality Assurance Program Plan (QAPP) requirements.

Although wetland type was a major factor that drove the study design, within-field hydrology also proved to be an important factor controlling aqueous MeHg and total mercury (THg) concentrations and export. Overall, agricultural wetlands exhibited higher MeHg concentrations in overlying water, sediment, and biota than did managed seasonal and permanent wetlands. This appears to be partly due to higher rates of sediment microbial production of MeHg in agricultural wetlands during the fall through spring period. Both sulfate- and iron-reducing bacteria have been implicated in the MeHg production process, and both were demonstrably active in all wetlands studied; however, sulfate-reducing bacteria were not stimulated by the addition of sulfate-based fertilizer to agricultural wetlands, suggesting that easily-degraded (labile) organic matter, rather than sulfate, was limiting their activity in these field types. The data suggest that agriculturally-managed soils promoted MeHg production through 1) enhanced microbial activity via higher temperatures and larger pools of labile carbon, and 2) enhanced pools of microbially available inorganic divalent mercury (Hg(II)) resulting from a decrease in reduced-sulfur, solid-phase minerals under oxic or only mildly reducing conditions.

MeHg mass balances were assessed by comparing field-specific MeHg loads for inlets vs. outlet flows. The overall mass balance for MeHg in surface water during the summer irrigation period (June – September 2007) indicated little to no net MeHg export from the six agricultural wetlands taken as a whole. Of the six agricultural wetlands, there was net overall MeHg export from two fields (one fallow and one white rice) during August, and from four of the six fields (one fallow, one white rice, and two wild rice) during September. Over the entire summer irrigation period, two of the fields (one fallow and one wild rice) showed net MeHg export, and the other four fields showed either net import or no significant change. Rates of measured photodemethylation and exchange between sediment and water pools suggest that both processes may be responsible for the lack of MeHg export. Despite significant differences during winter months between fields in surface water concentrations of MeHg, MeHg loads were not calculated in mid-winter because flood waters had overtopped field boundaries and field fidelity could not be established.

During the summer 2007 irrigation season, surface water out-flows from agricultural wetlands were 9%-36% of inlet flows, and evaporation rates explained most of this water loss, with infiltration likely accounting for the remainder. Unfiltered aqueous MeHg concentrations increased from $<1 \text{ ng L}^{-1}$ in source waters to up to 10 ng L^{-1} in agricultural wetland drains during the summer irrigation period. Increases in solute concentration caused by evapoconcentration were estimated by determining concentration factors (outflow / inflow) for chloride (a conservative dissolved constituent) and by measuring oxygen isotope ratios ($^{18}\text{O}/^{16}\text{O}$, expressed as $\delta^{18}\text{O}$) in water. Increases in MeHg concentration from inflows-to-outflows exceeded those caused by evapoconcentration on several fields during the summer irrigation season. This was especially true when initial surface water MeHg concentrations were low, as seen in the southern block of fields receiving irrigation water directly from the Toe Drain. The northern block of fields received irrigation water from Greens Lake, which included Toe Drain water plus recirculated drain water from other agricultural fields within the Yolo Bypass and west of the Yolo Bypass; as such, the northern fields showed a smaller percentage increase in MeHg concentration because initial MeHg concentrations in surface water inflows were greater than in inputs to the southern fields.

Mercury concentrations in fish were greater in agricultural wetlands (white rice and wild rice) than in the two permanently flooded wetlands. Additionally, Hg concentrations in biota

showed a general increase from inlets to outlets within agricultural wetlands, but not within permanent wetlands. This was particularly evident in white rice fields where caged western mosquitofish at the outlets had Hg concentrations that were more than 4 times higher than in caged fish held at the inlets. Similar spatial patterns in Hg bioaccumulation in agricultural and permanent wetlands were seen for wild populations of western mosquitofish and Mississippi silversides. In contrast to fish, invertebrates, such as water-boatmen (Corixidae) and back swimmers (Notonectidae), had greater Hg concentrations in permanent wetlands than in temporarily flooded agricultural wetlands. Fish THg concentrations were weakly correlated with water MeHg, and not correlated with sediment MeHg. In contrast, invertebrate MeHg concentrations were more strongly correlated with sediment MeHg than with water MeHg concentrations. These results illustrate the complexity of MeHg bioaccumulation through food webs and indicate the importance of simultaneously using multiple biosentinels when monitoring MeHg production and bioaccumulation.

Despite high sediment MeHg production rates and water concentrations in agricultural wetlands, MeHg export was physically limited by hydrologic export for all wetlands studied. We suggest that load reduction is maximized by limiting water throughput, but that on-site biota exposure is maximized by this longer water residence time. While field-specific hydrologic loads could not be fully quantified during flood conditions in February 2008, we suggest that the primary period of MeHg export from Yolo Bypass Wildlife Area is during those winter flooding periods when overall microbial activity and MeHg production in agricultural soils is fueled by the decomposition of rice straw, and when hydrologic flowthrough is maximal.

Local stakeholders participated in two workshops related to this study, demonstrating an interest in understanding factors controlling MeHg production, export, and bioaccumulation. The results of this field study show that permanently flooded, naturally vegetated wetlands are unlikely to be a large source of MeHg production within the YBWA, in contrast with agriculturally-managed wetlands. MeHg loading to Toe Drain waters of the Yolo Bypass may be reduced by lowering rates of hydrologic export from agricultural wetlands during the growing season and especially during rice harvest. However, under these water-holding conditions, biota living within agricultural wetlands may thus be exposed to higher MeHg concentrations in surface water. As observed in this study, rapid bioaccumulation over a 2-month period led to MeHg concentrations in invertebrates and fish more than 6 and 11 times higher, respectively, than proposed TMDL target values to protect wildlife (0.03 ppm ww).

The results of this field study, together with the information from YBWA stakeholders, provide a more definitive understanding of how MeHg cycling and bioaccumulation respond to habitat differences and specific management practices. These results directly address 4 core components of CBDA's Mercury Strategy for the Bay-Delta Ecosystem (**Wiener et al., 2003a**):

- a) Quantification and evaluation of THg and MeHg sources,
- b) Quantification of effects of ecosystem restoration on MeHg exposure,
- c) Assessment of ecological risk, and
- d) Identification and testing of potential management approaches for reducing MeHg contamination.

In addition, the quantitative results reported here assess the effect of current land use practices in the Yolo Bypass on MeHg production, bioaccumulation and export, and provide process-based advice towards achieving current goals of the RWQCB-CVR's *Sacramento – San Joaquin Delta Estuary TMDL for Methyl & Total Mercury* (**Wood et al., 2010b**). Further work is necessary to evaluate biotic exposure in the Yolo Bypass Wildlife Area at higher trophic levels (e.g. birds), to quantify winter hydrologic flux of MeHg to the larger Delta ecosystem, and to evaluate rice straw management options to limit labile carbon supplies to surface sediment during winter months.

In summary, agricultural management of rice fields — specifically the periodic flooding and production of easily degraded organic matter — promotes the production of MeHg beyond rates seen in naturally vegetated wetlands, whether seasonally or permanently flooded. The exported load of MeHg from these agricultural wetlands may be controlled by limiting hydrologic export from fields to enhance on-site MeHg removal processes, but the tradeoff is that this impoundment increases MeHg exposure to resident organisms.

Table of Contents

Executive Summary iii

List of Tables xi

List of Figures xiii

1 Project Structure 1

2 Introduction 2

 2.1 Mercury contamination in the Sacramento-San Joaquin Delta and the Yolo Bypass 2

 2.2 Mercury cycling in wetlands 2

 2.3 Landuse and socioeconomic context for the Delta Methylmercury TMDL..... 3

 2.4 Land use and previous mercury studies in the Yolo Bypass 3

 2.5 Project Purpose and Scope..... 4

 2.5.1 Management questions as project drivers..... 5

 2.5.2 Project Goals..... 5

 2.5.3 Project Objectives 5

 2.5.4 Project Approach - Overview..... 6

3 Summary of Study Design, Results, and Management Implications..... 7

 3.1 Study Design..... 7

 3.1.1 Research Questions..... 7

 3.1.2 Location..... 7

 3.1.3 Schedule 8

 3.2 Results Summary: Methylmercury Export 8

 3.2.1 Habitat Effect..... 8

 3.2.2 Block Effect 8

 3.2.3 Season Effect..... 9

 3.2.4 Hydrology Effect..... 9

 3.3 Results Summary: Methylmercury Production in Surface Sediment 9

 3.3.1 Habitat Effect..... 9

 3.3.2 Block Effect 10

 3.3.3 Season Effect..... 10

 3.3.4 Hydrology Effect..... 11

 3.3.5 Fertilizer Effect 11

 3.3.6 Rice Straw Effect..... 11

 3.3.7 Plant Effect..... 12

 3.4 Results Summary: Methylmercury Bioaccumulation 12

 3.4.1 Habitat Effect..... 12

 3.4.2 Block Effect 13

 3.4.3 Season Effect..... 13

 3.4.4 Hydrology Effect..... 13

 3.4.5 Biota Hg Correlations with Hg in Water and Sediment..... 13

 3.4.6 Fish and Invertebrate Hg Concentrations Exceed Harmful Levels to Wildlife in Yolo Bypass Wetlands 14

 3.5 Summary / Discussion of Results..... 14

 3.6 Management Implications and Next Steps 15

4 Detailed Results for Hydrology 17

 4.1 Introduction 17

 4.2 Approach..... 17

4.2.1 Site Description 17

4.2.2 Hydrologic measurements..... 18

4.2.3 Meteorological data..... 20

4.2.4 Water sample collection and analyses 20

4.2.5 Mass balance calculations 20

4.3 Results 21

4.3.1 General trends..... 21

4.3.2 Seasonal analyses 22

4.3.3 Annual water budget 24

4.4 Discussion..... 24

5 Detailed Results for Methylmercury loads and Water Quality 26

5.1 Introduction 26

5.2 Approach..... 26

5.2.1 Field sampling 26

5.2.2 Laboratory analyses 28

5.2.3 Meteorological data..... 29

5.2.4 Statistical analyses..... 29

5.2.5 Load calculations..... 29

5.3 Results and Discussion 30

5.3.1 Mercury and Methylmercury Concentrations 30

5.3.2 Biogeochemical relationships 33

5.3.3 Loads 38

5.4 Summary and Conclusions 41

5.4.1 Summary..... 41

5.4.2 Conclusions..... 42

6 Detailed Results for Sediment Methylmercury Production 44

6.1 Introduction 44

6.2 Approach..... 45

6.2.1 Field and Laboratory Analyses 45

6.2.2 Data analysis..... 46

6.3 Results 47

6.3.1 Mercury Parameters..... 47

6.3.2 Non-mercury parameters 48

6.4 Summary/Discussion..... 52

6.4.1 YBWA sediment MeHg concentrations in the larger ecosystem context..... 52

6.4.2 Controls on Methylmercury production..... 53

6.4.3 Agricultural vs Non-agricultural Fields 55

6.4.4 Fertilizer Additions to Agricultural Fields 56

6.4.5 Post-Harvest Impacts on MeHg Production in Rice Growing Fields..... 58

7 Detailed Results for Plant-Mercury Interactions 60

7.1 Introduction 60

7.2 Approach..... 60

7.2.1 Seasonal Comparison 60

7.2.2 Devegetation Experiment..... 61

7.2.3 Decomposition Assay 62

7.2.4 Statistics..... 63

7.3 Results 64

 7.3.1 Vegetation Productivity/Growth 64

 7.3.2 Vegetated vs. Devegetated Responses 65

 7.3.3 Relationship between microbial devegetation effects: implications for sulfur and iron cycling 67

 7.3.4 Decomposition Assay 68

7.4 Summary/Discussion 68

8 Detailed Results for Methylmercury Bioaccumulation 70

8.1 Introduction 70

8.2 Study Design and Methods 70

 8.2.1 Study Site 70

 8.2.2 Invertebrate Study 70

 8.2.3 Caged Fish Study 71

 8.2.4 Wild Fish Study 72

 8.2.5 Mercury Determination 72

 8.2.6 Statistical Analysis: Invertebrates 73

 8.2.7 Statistical Analysis: Fish 73

8.3 Results 75

 8.3.1 Invertebrates 75

 8.3.2 Caged Fish 77

 8.3.3 Wild Fish Mercury Bioaccumulation 81

 8.3.4 Caged vs. Wild Fish 82

 8.3.5 Biota Hg vs. Water MeHg and Sediment MeHg 82

8.4 Discussion 83

8.5 Summary 85

 8.5.1 Objective 85

 8.5.2 Mercury in Invertebrates 85

 8.5.3 Mercury in Caged Fish 85

 8.5.4 Mercury in Wild Fish 86

8.6 Conclusions 86

9 Detailed Results for Methylmercury Photodemethylation 88

9.1 Introduction 88

9.2 Approach 88

 9.2.1 Bottle Incubations 88

 9.2.2 Sampling Locations and Dates 89

 9.2.3 Light Intensity Measurements 89

 9.2.4 Methylmercury Determinations 89

 9.2.5 Quality Assurance Quality Control 90

9.3 Results and Discussion 90

 9.3.1 Light Intensity (PAR) Measurements 90

 9.3.2 Continuous Measurements 90

 9.3.3 Discrete Water Column Profile Measurements 91

 9.3.4 Photodecomposition Experiments 91

 9.3.5 Monomethyl Hg Concentration Dependence on Photodecomposition Rate ... 92

 9.3.6 Modeling MeHg Photodecomposition in the YBWA 93

9.4 Summary 94

10 Detailed Results for Public Outreach and Stakeholder Involvement..... 95
10.1 Pre-Study Workshop 95
10.1.1 Stakeholder Outreach for the Pre-study Workshop 95
10.1.2 Pre-study Questionnaire 97
10.1.3 Conclusion 98
10.2 Post-Study Workshop..... 98
10.2.1 Stakeholder Outreach for the Post-study Workshop 98
10.2.2 Post-Study Questionnaire 100
10.2.3 Conclusion 101
10.3 PAEP Evaluation and Discussion..... 101
11 REFERENCES CITED 103
12 ACKNOWLEDGEMENTS 116

Appendix 1....Quality assurance results for sediment and plant data

Appendix 2....Quality assurance results for water column data

Appendix 3.... Chemical and isotope data for surface water and fertilizer

**Appendix 4.... Summary of Field Data and Quality Assurance Results for
Photodecomposition Studies**

NOTE: *The Quality Assurance Performance Plan (QAPP) and Project Assessment and Evaluation Plan (PAEP) referenced herein are publically available from the Regional Water Quality Control Board – Central Valley Region*

List of Tables

- Table 1.1. Individuals (alphabetically) and organizations involved in the project
- Table 3.1. Study sampling locations and descriptions
- Table 4.1. Field size and associated areas for hydrologic units
- Table 4.2. Seasonal breakdown of operations at the Yolo Wildlife Management Area, by Field, March 2007 through May 2008
- Table 4.3. Water budget for agricultural and non-agricultural fields during the summer irrigated period
- Table 4.4. Water budget for agricultural and non-agricultural fields during the winter irrigated period
- Table 4.5. Water budget estimates for agricultural fields during the 17-day winter flooded period, based on pressure transducer data
- Table 4.6. Water budget for agricultural and non-agricultural fields during the winter drainage period
- Table 4.7. Water budget for agricultural and non-agricultural fields during the combined winter irrigated and winter drainage periods, excluding the 17-day winter flood period
- Table 4.8. Annual total water budget for agricultural and non-agricultural fields
- Table 5.1. Description of water-quality parameters, Yolo Bypass Wildlife Area mercury study
- Table 5.2. Statistical comparison of selected water-quality parameters for agricultural versus non-agricultural fields
- Table 5.3. Statistical comparison of selected water-quality parameters for northern versus southern agricultural fields
- Table 5.4. Statistical comparison of selected water-quality parameters from agricultural fields during growing season versus post-harvest season
- Table 5.5. Statistical comparison of selected water-quality parameters for inlet, center and outlet sampling sites on agricultural fields
- Table 5.6. Non-evaporative changes in concentrations of selected mercury species along flow paths in agricultural and non-agricultural fields during summer and winter sampling periods
- Table 5.7. Methylmercury loads during the summer irrigation period for agricultural and non-agricultural fields
- Table 5.8. Methylmercury loads for agricultural and non-agricultural fields during the winter, excluding the 17-day winter flood period
- Table 5.9. Comparison of annual average MeHg loads from Yolo Bypass Wildlife Area loads with other systems
- Table 5.10. Synthesis table example boxplot for water column portion of model
- Table 6.1. Description of sediment and pore-water parameters, Yolo Bypass Wildlife Area mercury study
- Table 6.2. Summary statistics for sediment and pore water parameters for individual agricultural fields and non-agricultural wetlands
- Table 6.3. ANOVA results comparing sediment and pore water data grouped as agricultural versus non-agricultural fields
- Table 6.4. ANOVA results comparing northern versus southern agricultural fields
- Table 6.5. ANOVA results comparing growing season versus post-harvest season sediment and pore water data from agricultural fields
- Table 6.6. Linear regression results for longitude versus individual mercury metrics

- Table 7.1. Field descriptions of dominant plant species, yield, and leaf area during the 2007–2008 study period
- Table 7.2. Concentrations of carbon, nitrogen, mercury, and methylmercury and biomass of plant tissue in individual fields
- Table 7.3. Devegetation effect on sediment and pore-water parameters during the period of peak plant biomass, by habitat type
- Table 7.4. Plant litter decomposition rates and areal pool sizes
- Table 8.1. Western mosquitofish whole body total mercury concentration and body burden immediately prior to and after 60 days of caged exposure in agricultural and non-agricultural wetlands within the Yolo Bypass Wildlife Area, California
- Table 8.2. Western mosquitofish size and body condition immediately prior to and after 60 days of caged exposure in agricultural and non-agricultural wetlands within the Yolo Bypass Wildlife Area, California
- Table 9.1 Sampling dates and locations for photodemethylation experiments
- Table 9.2. Summary of the linear regression slopes associated with the change in methylmercury concentration as a function of cumulative solar photosynthetically available radiation and ultraviolet radiation measured during the winter and summer photodemethylation experiments
- Table 9.3. Average daily percent loss of methylmercury as a function of daily integrated photosynthetically available radiation or ultraviolet radiation intensity and light attenuation with water-column depth
- Table 9.4. Average daily percent loss of methylmercury as a function of daily integrated photosynthetically available radiation or ultraviolet radiation intensity and initial methylmercury concentration

List of Figures

- Figure 3.1. Northern-looking oblique graphic illustration of the hydrologic contribution of the Yolo Basin Wildlife Area (YBWA) to the Yolo ByPass hydrologic unit
- Figure 3.2. Map illustrating the location of the study area within the Yolo Bypass Wildlife Area, Yolo County, CA
- Figure 3.3. Satellite image (GoogleEarth™) of the study area depicting the five wetland types studied
- Figure 3.4. Satellite image (GoogleEarth™) depicting sampling locations for specific matrices
- Figure 3.5. Satellite image (GoogleEarth™) depicting photodemethylation study sampling locations
- Figure 3.6. Timeline depicting field hydrology, management activities and approximate study collection dates for sediment, plants and biota samples
- Figure 4.1. Schematics for water flow and concentration trends across the fields based on A) the Continuous Flow Stirred Tank Reactor model and B) the Plug Flow Reactor model
- Figure 4.2. Water budget model
- Figure 4.3. Comparison of water flux calculations using pressure transducer and manual measurements for the fields where both data were collected
- Figure 5.1. Time series plot of total mercury concentration in unfiltered surface water
- Figure 5.2. Time series plot of total mercury concentration in filtered surface water
- Figure 5.3. Log-log plot of total mercury concentration in unfiltered versus filtered surface water
- Figure 5.4. Time series plot of methylmercury concentration in unfiltered surface water
- Figure 5.5. Time series plot of methylmercury concentration in filtered surface water
- Figure 5.6. Log-log plot of methylmercury concentration in unfiltered versus filtered surface water
- Figure 5.7. Log-log plot of total mercury concentration versus methylmercury concentration in unfiltered surface water
- Figure 5.8. Log-log plot of total mercury concentration versus methylmercury concentration in filtered surface water
- Figure 5.9. Time series plot of the methylmercury-to-total-mercury ratio (MeHg/THg) in unfiltered surface water
- Figure 5.10. Time series plot of the methylmercury to total mercury ratio (MeHg/THg) in filtered surface water
- Figure 5.11. Scatter plot of oxygen isotope ratio in water versus hydrogen isotope ratio in water
- Figure 5.12. Log-linear plot showing relation between chloride concentration and $\delta^{18}\text{O}$ in water for summer irrigation season (June – September, 2007)
- Figure 5.13. Diel time series plot of surface water unfiltered methylmercury concentration (u-MeHg) in four agricultural fields
- Figure 5.14. Diel time series plot of methylmercury to total mercury ratio (MeHg/THg) in unfiltered surface water from four fields of the Yolo Bypass Wildlife Area
- Figure 5.15. Time series plot of the sulfate-to-chloride molar ratio in filtered surface water
- Figure 5.16. Log-log plot of sulfate-to-chloride molar ratio versus sulfur stable isotope ratio in aqueous sulfate in filtered surface water
- Figure 5.17. Log-linear plots of sulfate-to-chloride molar ratio versus sulfur stable isotope ratio in filtered surface water for (A) wild rice field W32, and (B) fallow field F66

- Figure 5.18. Log-log plot of sulfate-to-chloride molar ratio in filtered surface water versus methylmercury concentration in unfiltered surface water
- Figure 5.19. Linear-log plot of sulfur stable isotope ratio in aqueous sulfate versus unfiltered methylmercury concentration in surface water
- Figure 5.20. Time series plots of (A) iron concentration and (B) manganese concentration in filtered surface water
- Figure 5.21. Log-log plots of (A) iron concentration and (B) manganese concentration versus methylmercury concentration in filtered surface water
- Figure 5.22. Log-log plots of manganese concentration versus methylmercury concentration in filtered surface water from (A) wild rice fields and (B) fallow fields
- Figure 5.23. Scatter plot of surface water dissolved organic carbon (DOC) versus filtered total mercury (f-THg)
- Figure 5.24. Scatter plot of surface water dissolved organic carbon (DOC) versus unfiltered total mercury (u-THg) within 30 days of the initial irrigation of the agricultural fields during early summer
- Figure 5.25. Scatter plot of surface water dissolved organic carbon (DOC) versus filtered methylmercury (f-MeHg)
- Figure 5.26. Scatter plot of surface water dissolved organic carbon (DOC) versus filtered methylmercury (f-MeHg) in the non-agricultural wetlands
- Figure 5.27. Scatter plot of surface water dissolved organic carbon (DOC) versus filtered methylmercury (f-MeHg) for the permanent wetland (PW) site in the Yolo Bypass Wildlife Area and for Browns Island, a tidal wetland in the San Francisco Bay-Delta
- Figure 5.28. Scatter plot of surface water particulate algal concentration (as chlorophyll-a plus pheophytin; Chl-a+Pheo) versus particulate methylmercury (pMeHg) concentration
- Figure 5.29. Scatter plot of surface water particulate detritus (plant residue) concentration versus the [Out/In] ratio of unfiltered methylmercury concentration along a flow path across agricultural and non-agricultural wetlands during winter (December 2007 and February 2008)
- Figure 5.30. Scatter plot of surface water chlorophyll-a (ChlA) fluorescence versus unfiltered methylmercury (u-MeHg) concentration across white rice (R) and wild rice (W) fields during the diel measurements of summer 2007 (fields W65 and R64) and summer 2008 (fields R20 and W31)
- Figure 5.31. Scatter plot of fluorescence index (FI) versus unfiltered methylmercury (u-MeHg) concentration in surface water across white rice (R) and wild rice (W) fields during the diel measurements of summer 2007 (fields W65 and R64) and summer 2008 (fields R20 and W31)
- Figure 5.32. Scatter plot of cumulative potential solar radiation versus fluorescent dissolved organic matter (FDOM) in surface water during the *in situ* deployments of summer 2007 (fields W65 and R64) and summer 2008 (fields R20 and W31)
- Figure 5.33. Scatter plot of the ratio of fluorescent dissolved organic matter (FDOM) to dissolved organic carbon (DOC) (FDOM/DOC) versus the ratio of unfiltered methylmercury to total mercury u-MeHg/THg in surface water during the 2007 and 2008 diel studies
- Figure 5.34. Bar graph showing methylmercury (MeHg) loads from individual fields during the summer irrigation period, the winter period (excluding the 17-day flood), and the annual average
- Figure 5.35. Time series plot of area-normalized, cumulative methylmercury (MeHg) mass net loading for individual fields in the Yolo Bypass Wildlife Area
- Figure 5.36. Schematic diagram showing methylmercury inputs and outputs from a generic managed wetland

- Figure 6.1. Sediment total mercury (THg) concentration data depicted as (A) a box-and-whisker plot by habitat type and (B) in time series for each field
- Figure 6.2. Sediment $^{203}\text{Hg(II)}$ -methylation rate constant (k_{meth}) data depicted as (A) a box-and-whisker plot by habitat type and (B) in time series for each field
- Figure 6.3. Sediment inorganic reactive mercury (Hg(II)_{R}) concentration data depicted as (A) a box-and-whisker plot by habitat type and (B) in time series for each field
- Figure 6.4. Sediment methylmercury production potential (MPP) rate data depicted as (A) a box-and-whisker plot by habitat type and (B) in time series for each field
- Figure 6.5. Sediment methylmercury (MeHg) concentration data depicted as (A) a box-and-whisker plot by habitat type and (B) in time series for each field
- Figure 6.6. Scatter plot of sediment total mercury (THg) concentration versus longitude showing least-squares linear regression
- Figure 6.7. Time series plots of sediment oxidation-reduction potential (E_{h}) as measured in the (A) field and (B) laboratory at the time of sediment sub-sampling, by field
- Figure 6.8. Time series plots of sediment A) microbial sulfate reduction (SR) rate and B) total reduced sulfur (TRS), by field
- Figure 6.9. Time series plots of pore water A) sulfate (SO_4^{2-}) concentration and B) the sulfate to chloride ($\text{SO}_4^{2-} / \text{Cl}^-$) molar ratio, by field
- Figure 6.10. Scatter plots of pore water sulfate-sulfur stable isotope data ($\delta^{34}\text{SO}_4^{2-}$) as a function of (A) sediment microbial sulfate reduction (SR) rate, (B) pore water sulfate-to-chloride concentration ratio, and (C) sediment redox (E_{h})
- Figure 6.11. Time series plots of ferrous iron (Fe(II)) concentration in (A) pore water and (B) sediment, by field
- Figure 6.12. Time series plots of sediment (A) amorphous / poorly-crystalline ferric iron (aFe(III)) and (B) crystalline ferric iron (cFe(III)), by field
- Figure 6.13. Time series plot of sediment organic content, as percent loss on ignition (%LOI), by field
- Figure 6.14. Time series plots of pore water (A) dissolved organic carbon (DOC) and (B) acetate, by field
- Figure 6.15. Bar graph of pore water acetate concentration by season (growing vs post-harvest) for rice (white and wild) fields and fallow fields
- Figure 6.16. Linear-Log plot of sediment ferrous iron to total iron ratio ($\text{Fe(II)}/\text{Fe}_{\text{T}}$) versus $^{203}\text{Hg(II)}$ -methylation rate constant (k_{meth})
- Figure 6.17. Log-Log plot of sediment total reduced sulfur (TRS) versus reactive inorganic mercury (Hg(II)_{R})
- Figure 7.1 Bar graph of above and below-ground plant biomass in each field during the summer growing season, June–August 2007
- Figure 7.2. Box-and-whisker plot of live root density, expressed as the percentage of soil volume occupied by live roots in the top two centimeters of soil
- Figure 7.3. Scatterplot of live root density versus mercury methylation rate constant in actively growing rice fields during July and August 2007
- Figure 7.4. Bar graph depicting the ‘devegetation effect’ on the microbial mercury methylation rate constant in agricultural fields (August 2007) and non-agricultural fields (December 2007)
- Figure 7.5. Bar graph of the percent devegetation effect on sediment and pore-water parameters in agricultural fields during the period of peak biomass (August 2007)

- Figure 7.6. Bar graph of time-integrated daily rates of change in iron species in the surface (0-2 cm) sediment interval of individual agricultural fields for A) vegetated plots and B) devegetated plots, and C) the difference of vegetated minus devegetated plots
- Figure 7.7. Scatterplot of leaf tissue carbon-to-nitrogen ratios versus litter decomposition rate constants for the dominant plant species in each field type
- Figure 7.8. Log-linear plot of sediment pore water acetate concentration versus the mercury methylation rate constant, by sampling period
- Figure 8.1. Scatter plot of Corixidae (water boatmen) methylmercury concentration versus total mercury concentration, by habitat type, in the Yolo Bypass Wildlife Area
- Figure 8.2. Bar graph of total mercury concentration in (A) Corixidae (water boatmen) and (B) Notonectidae (back swimmers) in agricultural fields of the Yolo Bypass Wildlife Area
- Figure 8.3. Bar graphs of total mercury concentration in Corixidae (water boatmen) and Notonectidae (back swimmers) at the inlets, centers, and outlets of shallowly-flooded fallow fields, by field type, in the Yolo Bypass Wildlife Area, during the first (25 June to 6 July 2007) and last (28 August to 19 September 2007) sampling event
- Figure 8.4. Bar graphs of total mercury concentration in (A) Corixidae (water boatmen) and (B) Notonectidae (back swimmers), by habitat type, during the field management periods of flood-up and rice pre-harvest in the Yolo Bypass Wildlife Area
- Figure 8.5. Bar graph of methylmercury concentration in Corixidae (water boatmen), by habitat type, in Yolo Bypass Wildlife Area
- Figure 8.6. Log-Log plot of total mercury concentration versus methylmercury concentration in western mosquitofish introduced into cages within flooded agricultural fields in the Yolo Bypass Wildlife Area, California
- Figure 8.7. Partial leverage plots depicting the relationship between total mercury concentration and standard length or relative condition factor of (A) caged western mosquitofish, (B) wild western mosquitofish, and (C) wild Mississippi silversides in wetlands of the Yolo Bypass Wildlife Area
- Figure 8.8. Bar graphs of (A) total mercury concentration and (B) total mercury body burden in western mosquitofish removed from cages after a 60-day of exposure period at the inlets, centers, and outlets, by field type, during the 2007 rice growing season at the Yolo Bypass Wildlife Area, California
- Figure 8.9. Bar graphs of (A) Standard length, (B) fresh wet mass, and (C) relative condition factor for western mosquitofish removed from cages after a 60-day exposure period at inlets, centers, and outlets, by field type, during the 2007 rice-growing season, in the Yolo Bypass Wildlife Area, California
- Figure 8.10. Time series plots of (A) total mercury concentration and (B) total mercury body burden of caged western mosquitofish over 60 days of exposure at the outlets of white rice, wild rice, and permanent wetland fields, during the 2007 rice growing season at the Yolo Bypass Wildlife Area, California
- Figure 8.11. Bar graphs of total mercury concentrations and total mercury body burden in (A) wild western mosquitofish and (B) wild Mississippi silversides caught at the inlets and outlets, by field type, during the 2007 rice growing season at the Yolo Bypass Wildlife Area
- Figure 8.12. Bar graphs of (A) caged mosquitofish and (B) wild caught mosquitofish total mercury concentrations and total mercury body burden at the inlets, centers (caged only), and outlets, by field type, during the 2007 rice growing season at the Yolo Bypass Wildlife Area
- Figure 8.13. Log-Log plots of caged mosquitofish total mercury concentration versus (A) surface water unfiltered methylmercury concentration and (B) sediment methylmercury concentration, and Corixidae (water boatman) methylmercury concentration versus (C) surface water unfiltered

methylmercury concentration and (D) sediment methylmercury concentration in agricultural and non-agricultural wetlands of the Yolo Bypass Wildlife Area during 2007

- Figure 9.1. Photograph of photodemethylation experiment in the Yolo Bypass Wildlife Area, Calif.
- Figure 9.2. Graph showing light wavelength versus the percentage of light transmission through the incubation bottles used in the photodemethylation experiments
- Figure 9.3. Time series plots of instantaneous flux of photosynthetically available radiation for A) December 3–7, 2007 and B) July 30 – August 1, 2008
- Figure 9.4. Graph showing instantaneous flux of photosynthetically available radiation versus water column depth, as a measure of light attenuation
- Figure 9.5. Scatter plots showing least-squares linear regressions of integrated (cumulative) solar radiation versus aqueous methylmercury concentration for December 3–7, 2007 based on A) PAR wavelengths (400–700 nm) and B) total UV wavelengths (UVa + UVb)
- Figure 9.6. Scatter plots showing least-squares linear regressions of integrated photosynthetically available radiation versus aqueous methylmercury concentration for July–August 2008 incubations
- Figure 9.7. Scatter plots showing least-squares linear regressions of initial aqueous methylmercury concentration versus PAR-dependent photodecomposition rate A) data from all 13 experiments and B) data from 11 experiments (2007 data from 2 northern fields, F20 and R31, not included)
- Figure 9.8. Scatter plots showing linear least-squares regressions of initial aqueous methylmercury concentration versus UV-dependent photodecomposition rate A) data from all 13 experiments and B) data from 11 experiments (2007 data from 2 northern fields, F20 and R31, not included)

Methylmercury cycling, bioaccumulation, and export from agricultural and non-agricultural wetlands in the Yolo Bypass

1 Project Structure

This project involved scientists and land managers from the following institutions:

- U.S. Geological Survey (USGS)
 - California Water Science Center (CWSC)
 - Western Ecological Research Center (WERC)
 - National Research Program (NRP)
- California Department of Fish and Game (CDFG)
- Moss Landing Marine Laboratory (MLML)
- Yolo Basin Foundation (YBF)
- Battelle Marine Sciences Laboratories (BMSL)
- Bachand and Associates

San Jose State University Foundation was the submitting organization and the project manager. There were 11 Principal Investigators for the project, and **Table 1.1** describes the expertise and organizational affiliation of each. Principal Investigators were responsible for the quality assurance of work done by their own institution. The project QA officer was Ms. Autumn Bonnema, Moss Landing Marine Laboratories. She was not involved with any data collection or analyses for this project. Janis Cooke, with the Regional Water Quality Control Board – Central Valley Region (RWQCB-CVR), maintains the official Quality Assurance Program Plan (QAPP) and the Project Assessment and Evaluation Plan (PAEP) for this project, which were approved by the State Water Resources Control Board (SWRCB) on August 29, 2007 and January 29, 2008, respectively.

The project involved 8 Tasks, which included project management, research, monitoring, assessment, and outreach / education. These were as follows:

- i. **Task 1** - Project Management
- ii. Research/Monitoring/Assessment
 - **Task 2** - Manage fields and water levels in Yolo Bypass
 - **Task 3** - Collect and measure MeHg concentrations and loads
 - **Task 4** - Collect and measure water-quality parameters
 - **Task 5** - Measure MeHg production rates and associated factors
 - **Task 6** - Measure MeHg concentrations in bio-indicators
 - **Task 7** - Measure MeHg photodegradation rates in water column
- iii. Education/Outreach/Capacity-building
 - **Task 8** - Administer workshops and produce outreach publications

2 Introduction

2.1 Mercury contamination in the Sacramento-San Joaquin Delta and the Yolo Bypass

The Sacramento–San Joaquin River Delta (hereinafter referred to as “the Delta”) within California’s Central Valley is highly contaminated with mercury (Hg) from historic Hg mining and gold extraction (Davis et al., 2003; Wiener et al., 2003b; Alpers et al., 2005). Elevated Hg concentrations in fish in the Delta have led to fish-consumption advisories to protect human health (Gassel et al., 2007, 2008) as well as concerns regarding exposure of wildlife to methylmercury (MeHg), the toxic organic form of mercury that is readily bioaccumulated (Wiener et al., 2003a,b). Available information indicates that about 60% of MeHg loads to the Delta come from tributary inputs and about 40% is estimated to be produced *in situ* within Delta wetlands and open-water habitats (Foe et al., 2008).

Of the 8 sub-watersheds in the Delta, the wetland-dominated Yolo Bypass has the highest average annual surface water MeHg concentration (Wood et al., 2010a). These high MeHg concentrations in the Yolo Bypass may be due in large part to the predominance of wetlands within this sub-watershed (Wood et al. 2010a). Wetlands within the Delta and Yolo Bypass are estimated to account for 19% of all MeHg loadings into the Sacramento-San Joaquin River Delta (Wood et al. 2010a). However, the relative contribution of MeHg production from different wetland habitats is unknown.

2.2 Mercury cycling in wetlands

Wetlands are known to be significant MeHg production sites in the San Francisco Bay-Delta (SFB-D) (Davis et al., 2003; Marvin-DiPasquale et al., 2003a) and elsewhere (Zillioux et al. 1993; Rudd 1995; St. Louis et al., 1994, 1996; Hurley et al. 1995; Rumbold and Fink 2006). The production of MeHg is facilitated by sulfate-reducing and iron-reducing bacteria (SRB and FeRB, respectively) in sediments (Compeau and Bartha, 1984; Fleming et al., 2006), and is largely controlled by the activity of those bacteria (limited by sulfate, ferric iron and/or organic matter), and by the availability of divalent inorganic Hg(II) to these bacteria (Marvin-DiPasquale and Agee, 2003). The degradation of MeHg is controlled both by a wide range of microbes and by abiotic processes, particularly photodegradation (Hammerschmidt and Fitzgerald, 2006; Byington, 2007; Gill, 2008a).

The role of wetland plants (both type and density) is a critical factor mediating MeHg production by bacteria in sediments, as plant root zones have recently been shown to be locations of enhanced microbial activity and Hg cycling (Windham-Myers et al. 2009). Because Hg forms strong bonds with dissolved organic matter (DOM), the production and flux of DOM from wetlands is a key process controlling both THg and MeHg transport (Ravichandran, 2004). The uptake of MeHg into the base of the food web, and its bioaccumulation up food webs is of particular concern for both wildlife and human health.

The wet-dry cycle experienced by seasonal wetlands, both non-agricultural wetland maintained for wildlife habitat and agricultural wetlands used for rice production, may promote Hg(II)-methylation more than that observed in permanent wetlands (Alpers et al., 2008 and references therein; Marvin-DiPasquale et al., 2009a). This effect is likely caused by the continued cycling of redox-sensitive elements such as sulfur and iron, which are critical to the metabolism of SRB and FeRB. Despite the importance of agricultural wetlands in California and

globally, there are no well-documented studies that examine the detailed cycling of Hg, Fe, and S in adjacent agricultural and non-agricultural wetlands.

2.3 Landuse and socioeconomic context for the Delta Methylmercury TMDL

The Central Valley historically contained 1.6-2.0 million hectares (ha) of natural wetland habitat (U. S. Fish and Wildlife Service, 1978), much of which was comprised of ephemeral wetlands that were primarily inundated in winter and spring. Over 90% of these wetlands have been lost to agriculture and development over the past century, with only 121,000 ha remaining (U. S. Fish and Wildlife Service, 1978; Gilmer et al., 1982; Frayer et al., 1989; Dahl, 1990). In contrast, 216,100 ha of white rice (U. S. Department of Agriculture, National Agricultural Statistics Service, 2007) and 8,575 ha of wild rice (International Wild Rice Association, 2007) were planted in the Central Valley in 2007. In contrast to the historic, ephemeral wetlands, rice fields are shallowly flooded (<50 cm) during spring and summer for rice production. Moreover, rice fields are often allowed to dry immediately post-harvest, then shallowly flooded again during the winter to speed rice straw decomposition (Elphick and Oring, 1998; Bird et al., 2000). These wetting and drying cycles may strongly impact rice field MeHg production and subsequent bioaccumulation.

Currently, the California RWQCB-CVR is developing a MeHg Total Maximum Daily Load (TMDL) for the Sacramento-San Joaquin River Delta, with a goal of meeting water-quality criteria as soon as possible, but no later than 2035 (Wood et al., 2010b). The current version of the Delta TMDL plan recommends an unfiltered aqueous MeHg level goal of 0.06 ng L⁻¹ or below for the entire legal Delta and Yolo Bypass. To meet water-quality goals in the TMDL, substantial reductions of current loads were calculated for each Delta tributary region, with a stated recommendation of a more than 70% reduction in current MeHg loads from the Yolo Bypass specifically (Wood et al., 2010a, 2010b).

The long-term goal of reducing MeHg levels in sport fish has benefits to fish consumers in the area, including several environmental justice communities in Yolo and Sacramento Counties. Native Americans, African Americans, Russian, Ukrainian, Hmong/Mien, and several other southeast Asian and Pacific Islander groups have been identified by the California Dept. of Health Services as groups with below-average socioeconomic profile that consume above-average amounts of sport fish with elevated Hg levels. This situation puts members of these groups, especially children, at risk for Hg-related medical consequences that may affect neurological development and their ability to learn.

2.4 Land use and previous mercury studies in the Yolo Bypass

Within the Yolo Bypass is the 16,000-acre Yolo Bypass Wildlife Area (YBWA), managed by the California Department of Fish and Game (CDFG), which is tasked with restoring wetland habitat (Elphick, 2000) and encouraging agriculture, all while maintaining the primary function of the Yolo Bypass for flood control. Accordingly, there are four predominant wetland management strategies during the rice-growing season: white rice, wild rice, permanent wetlands, and shallowly-flooded fallow fields. Both white rice (*Oryza sativa*) and, to a lesser extent, wild rice (*Zizania palustris*) are grown extensively throughout the YBWA and represent

the largest wetland area during the late spring and summer. Additionally, former rice fields that are rotated out of production and left fallow are shallowly flooded during the late summer (typically during July through September) to provide foraging habitat for migrating shorebirds. Finally, there are several wetlands that are permanently flooded throughout the year. These different wetland types and the various approaches for managing them were expected to result in different rates of MeHg production, bioaccumulation and export. A more definitive understanding of these habitat differences, and the impact of specific management practices, is critical to achieving the stated TMDL MeHg reduction goals.

A pilot study during 2005–06 investigated concentrations of Hg and MeHg in shallow sediment and surface water at two sites within the YBWA (a non-agricultural, seasonal wetland and a permanent wetland) as well as two similar sites in the adjacent Cache Creek Settling Basin (CCSB) (**Marvin-DiPasquale et al., 2009a**). Results of that study indicated:

- (a) a large degree of spatial and temporal variability with regard to Hg concentration and speciation;
- (b) a rapid increase in benthic MeHg production and (or) release of previously formed MeHg to the water column within days of flooding seasonal wetlands;
- (c) the speciation and methylation of Hg in seasonal and permanent wetlands in response to the chemistry of sulfur (S) and iron (Fe), and associated microbial reduction pathways;
- (d) the period of inundation (hydroperiod) as an important factor mediating MeHg production among various wetland types; and
- (e) the YBWA as more active with regard to MeHg production than the CCSB

Despite the predominance of agricultural wetlands in California's Central Valley, MeHg production, export, and bioaccumulation in rice fields has not previously been quantified relative to adjacent seasonal and permanent wetlands. This study represents an initial effort to fill that important information gap.

2.5 Project Purpose and Scope

This 18-month field study addresses the seasonal and spatial patterns and processes controlling methylmercury (MeHg) production, bioaccumulation, and export from natural and agricultural wetlands of the Yolo Bypass Wildlife Area (YBWA). The data were collected in conjunction with a Proposition 40 grant from the State Water Resources Control Board (SWRCB) in support of the development of Best Management Practices (BMP's) for reducing MeHg loading from agricultural lands in the wetland-dominated Yolo Bypass to the Sacramento–San Joaquin River Delta, and in support of the RWQCB-CVR's current *Sacramento – San Joaquin Delta Estuary TMDL for Methyl & Total Mercury*, which is currently in draft form (**Wood et al., 2010a, 2010b**) and can be accessed in its entirety on-line:

http://www.waterboards.ca.gov/centralvalley/water_issues/tmdl/central_valley_projects/delta_hg

Through an assessment of current land use practices in the Yolo Bypass and their effect on MeHg production and export, this study was specifically designed to provide the necessary scientific background in support of achieving the goal of >70% reduction of MeHg export from the Yolo ByPass, as set out in the current Delta TMDL. In addition, the study addresses several core components of the *CALFED Mercury Strategy for the Bay-Delta Ecosystem* (**Wiener et al., 2003a**): 1) Quantification and evaluation of mercury and methylmercury sources, 3)

Quantification of effects of ecosystem restoration on methylmercury exposure, 4) Monitoring of mercury in fish..., and 6) Identification and testing of potential management approaches for reducing methylmercury contamination. This plan was completed in December 2003 and can be accessed in its entirety on-line at:

<http://www.calwater.ca.gov/science/pdf/MercuryStrategyFinalReport.pdf>

2.5.1 Management questions as project drivers

As the TMDL process moves forward, agencies and managers responsible for lands that may be source zones for MeHg to the Delta, have many questions regarding how their current practices may affect MeHg export to the Delta. In anticipation of some of these uncertainties, this study focuses on four questions that are both fundamental (yet currently unresolved) and useful to managers in terms of land use practices in the watershed. These questions were:

1. *Is there a difference among agricultural and managed wetland types in terms of MeHg dynamics (production, degradation, bioaccumulation, or export)?*
2. *Does water residence time influence MeHg dynamics?*
3. *Does the application of sulfate-based fertilizer impact MeHg production rates?*
4. *Does the presence (or absence) of vegetation influence MeHg production rates?*

2.5.2 Project Goals

Given the above management questions, the primary project **goals** were to determine:

1. *the extent to which seasonal and annual MeHg production and export loads differed for dominant wetlands in the Yolo Bypass: managed permanent and seasonal wetlands, white rice fields, wild rice fields, and rotational fields under fallow management;*
2. *the effect of specific management practices on observed differences in Hg cycling and export;*
3. *if MeHg bioaccumulation was measurable and different between wetland habitat types;*
4. *the underlying processes that led to any observed differences in Hg cycling among wetland types or management practices.*

2.5.3 Project Objectives

We considered two overarching project **objectives** to address these goals.

Objective 1: to examine the linkage between Hg/MeHg cycling, bioaccumulation and export with respect to the following environmental variables:

- a) dissolved organic matter quality and quantity
- b) vegetation type and density
- c) flooding duration, timing, and water residence time
- d) post-harvest flooding of rice straw

- e) sulfur-based fertilizer application
- f) sediment microbial processes and geochemistry

Objective 2: to use the information gained to help the SWRCB develop best management practices (BMP's) for rice farming and wetland management that minimize MeHg production and export.

2.5.4 Project Approach - Overview

Measurements of MeHg concentrations in sediment, water, and biota (plants, invertebrates, and fish) were made to assess land management activities in five wetland types, which included: three types of shallowly-flooded agricultural wetlands (white rice, wild rice, and fallow fields) and two types of managed non-agricultural wetlands (permanently and seasonally flooded). To strengthen our understanding of the processes underlying the seasonal and spatial patterns of MeHg cycling, additional explanatory factors were measured including ancillary sediment and water quality parameters, stable isotope fractionation (oxygen, sulfur, carbon, and nitrogen), photodemethylation rates, and daily-integrated hydrologic budgets. Samples and field data were collected from May 2007 to July 2008, and analyses were completed according to methods and procedures described in the project's Quality Assurance Program Plan (QAPP) (**U.S. Geological Survey et al., 2008**). Pre- and post-study workshops associated with this project were held to promote bi-directional information sharing among local stakeholder groups about Hg issues, including the risks from fish consumption from the Yolo Bypass and areas of the Delta and Sacramento River affected by MeHg export from the Yolo Bypass.

The structure of this report is described below. The next section (**Section 3**) includes a summary of the study design, results, and management implications. Following sections provide detailed results for specific aspects of the study: Hydrology (**Section 4**); MeHg loads and water quality (**Section 5**); Sediment MeHg production (**Section 6**); Plant-Hg interactions (**Section 7**); MeHg bioaccumulation (**Section 8**); MeHg photodemethylation (**Section 9**); Public outreach and stakeholder involvement (**Section 10**). Appendices include results of quality assurance / quality control (QA/QC) for sediment and plant samples (**Appendix 1**), QA/QC results for water-quality samples (**Appendix 2**), Tables of water-quality data (**Appendix 3**), and a summary of MeHg photodecomposition data (**Appendix 4**).

3 Summary of Study Design, Results, and Management Implications

3.1 Study Design

3.1.1 Research Questions

The 4 management questions posed above (**Section 2.5.1**) were expanded and structured to address the 6 research questions below, which systematically focus on comparing processes among wetland types undergoing different management regimes.

Question 1: Did MeHg dynamics vary by type of managed wetland (**habitat effect**)?

Question 2: Did MeHg dynamics vary by field locations or source water such as Toe Drain vs. Toe Drain/Davis Drain/ Greens Lake (**block effect**)?

Question 3: Did MeHg dynamics vary seasonally within the different field types (**season effect**)?

Question 4: Did MeHg dynamics vary with hydrologic factors such as water depth and flowrate (**hydrology effect**)?

Question 5: Did application of sulfate-bearing fertilizers influence MeHg production (**fertilizer effect**)?

Question 6: Did the presence of non-disc'd rice straw influence MeHg production (**rice straw effect**)?

3.1.2 Location

The 40-mile-long Yolo Bypass located within the Sacramento River watershed and Yolo County, Calif., is part of the Sacramento River Flood Control Project, and serves to divert excess water from the Sacramento River during flood periods, relieving pressure on the main levee system along the river channel. Water primarily enters the basin through the Fremont Weir in the north, which allows inflows from the Sutter Bypass, the Feather River and the Sacramento rivers (**Figure 3.1**). Excess water safely returns to the Sacramento River at the southern end of the Bypass.

Within the Yolo Bypass is the 16,700 acre YBWA, (**Figures 3.1 and 3.2**) of which the CDFG manages 3,700 acres, the Yolo Wildlife Management Area (YWMA), for mixed-use as both wildlife habitat and agricultural wetlands. The study area for this project was within the YWMA (**Figure 3.2**). The satellite image in **Figure 3.3** depicts the various wetland types (hereafter identified as **fields** (i.e. agricultural fields = white rice, wild rice, and fallow; non-agricultural fields = seasonally and permanently flooded wetlands)) sampled during the study, as well as the flow paths for irrigation waters. Sampling locations for water, sediment, plants and biota are illustrated in **Figure 3.4**. The GPS coordinates for all sampling locations are given in **Table 3.1**. Photodemethylation and solar radiation measurement study site locations are illustrated in **Figure 3.5**. The seasonally flooded wetland sampling site (SW) was also sampled during a recent previous study of Hg cycling within the YBWA and Cache Creek (**Marvin-DiPasquale et al., 2009a**).

3.1.3 Schedule

The sampling schedule reflected the needs and activities of the rice farmer (Jack DeWit) and CDFG wetland managers, with the first sampling occurring in late May 2007, immediately following the first flood-up event for that year, and the last sampling occurring during April 2008 when all fields were again drained in preparation for the 2008 rice planting season. A timeline of the field management activities and project field sampling events is diagrammed in **Figure 3.6**.

3.2 Results Summary: Methylmercury Export

3.2.1 Habitat Effect

Habitat effects were observed regarding several aspects of MeHg loading during the study period.

Wild Rice Harvest: The most prominent habitat effect was the large export of aqueous unfiltered MeHg (hereafter, u-MeHg) that occurred in the wild rice fields. This effect was largely attributed to wet harvest activity activity and elevated particulate MeHg in the surface waters of wild rice fields during September 2007 while outlets were still flowing. Despite relatively low water flow at the outlets during harvest, extremely high concentrations of u-MeHg resulted in increased export from the wild rice agricultural fields during the harvest period.

White Rice Detritus in Late Winter: Another habitat-specific effect occurred during the late winter (February 2008) following the Cache Creek flood event (Jan.24 – Feb.10, 2008). White rice fields had elevated u-MeHg concentrations relative to the other fields and thus exported a larger amount of MeHg compared to the other fields. This effect appears to be related to the amount and quality of decomposing rice straw (detritus) on the field when the flooding occurred. White rice fields had the greatest amount of detritus left on the fields at the time of the flood whereas the other fields had little detritus left by February. The amount of detritus on the field correlated with u-MeHg concentrations. In addition, the two white rice fields were higher than the other agricultural fields in MeHg export during the December period.

Permanent Wetland Water Retention: A significant habitat difference related to differences in water management is that the permanent wetland (PW5) did not have significant MeHg export because there was not much water exported. This, combined with relatively low MeHg concentrations, resulted in the permanent wetland having the lowest export rates of all the fields. Exports of MeHg from the seasonal wetland were not consistently higher or lower than those from the rice fields.

3.2.2 Block Effect

Block (north vs. south) was not a dominant driver of MeHg export over the course of the study. The only observed block effect occurred during the summer irrigation season, when the northern fields were receiving supply waters with elevated MeHg concentrations relative to the southern fields. As a result there was net export of MeHg from two southern fields (fallow and white rice) during August and September whereas the corresponding northern fields showed net import of MeHg during August and had imports approximately equal to exports during September. In terms of concentration factors relative to chloride (a conservative constituent indicative of evapoconcentration), the southern fields showed increases in MeHg from inflow to

outflow that were much greater than the corresponding increases in chloride, whereas the northern fields showed increases in MeHg comparable to those for chloride. In addition to the effect of higher MeHg in the input water, it is possible that longer residence time for water in the northern fields relative to the southern fields contributed to increased photodemethylation.

3.2.3 Season Effect

Season was the major driver of MeHg net export in the study. Winter exports were greater than summer exports for all agricultural fields. Most fields were a sink, or at most a very small source, of MeHg during the summer growing season. This was likely the effect of photo-demethylation and sedimentation processes. In contrast, all fields were a source of MeHg net export during winter/early spring.

3.2.4 Hydrology Effect

Hydrology was a dominant driver of MeHg exports throughout the summer but was less important between seasons. The greatest sink of MeHg in the summer occurred in the fields with restricted outflows and thus longer hydraulic residence times, greater evapo-transpiration (ET), potentially higher rates of photodemethylation, and lower outflow. Despite increases in MeHg concentration across the fields, the water management on the two fallow fields where inflow was ten times that of outflow led to lower MeHg loads leaving the field relative to the inputs. The greatest MeHg exports occurred when the fields were drained in winter/early spring (**Section 5.3.3.3**), and also when the harvest operations dominated export in the wild rice fields (**Section 5.3.3.2**). The importance of hydrology was also seen between blocks, as the block effect observed in August (**Section 5.3.3.2**) was associated with increased flows in southern fields as more water became available.

3.3 Results Summary: Methylmercury Production in Surface Sediment

3.3.1 Habitat Effect

There were a number of statistically significant differences, based upon habitat (agricultural vs non-agricultural fields), associated with both Hg biogeochemistry and factors that directly impact MeHg production. For data grouped by either agricultural or non-agricultural (experimental devegetated sites excluded) and averaged across all sampling events: sediment THg and reactive or bioavailable inorganic mercury (Hg(II)_{R}) concentrations were higher in agricultural fields, while values of k_{meth} (a measure of Hg(II)-methylating bacterial activity) were higher in non-agricultural fields. Calculated rates of MeHg production are a product of both Hg(II)_{R} and k_{meth} , and were not significantly different between the two habitat groupings. However, average sediment MeHg concentrations were significantly higher (1.5-fold) in agricultural fields.

These trends in mercury metrics were driven by strong habitat differences in a number of key biogeochemical and microbial processes. Across all sites Hg(II)_{R} concentrations decreased as sediment solid phase reduced sulfur concentrations increased, as a result of the strong bonds formed between inorganic Hg(II) and reduced sulfur species. Since average total reduced sulfur (TRS) was significantly lower (8-fold) in agricultural sites, compared to non-agricultural sites, concentrations of Hg(II)_{R} were comparatively elevated in agricultural fields. Conversely, the activity of the resident microbial community, as assessed by radiotracer $^{203}\text{Hg(II)}$ amendment

experiments (k_{meth}), increased as sediment conditions transition from those more conducive to microbial iron-reduction to those more conducive to microbial sulfate-reduction. While both processes occur in all fields, iron speciation data indicate that sediments associated with the agricultural fields were generally more poised for iron reduction and non-agricultural fields were more poised for sulfate reduction. As a result, values of k_{meth} were significantly higher in non-agricultural fields. Thus, due to higher Hg(II)_{R} concentrations and lower k_{meth} values in agricultural fields, and lower Hg(II)_{R} concentrations and higher k_{meth} values in non-agricultural fields, average calculated MeHg production rates were similar for both groupings.

Across all sites for both agricultural and non-agricultural habitats, sediment MeHg concentrations were poorly correlated with calculated MeHg production (MP) rates, suggesting that temporal and spatial processes of MeHg degradation and/or loss within sediments are variable, significant and poorly understood. The exception to this was in white rice fields, where calculated MP rates explained 48% of the variability in MeHg concentration. MP, again, was calculated as the product of microbial rate measurements (k_{meth}) and the poolsize of reactive mercury in sediment (Hg(II)_{R}). Sediment MeHg concentrations were also significantly correlated with sediment organic content across all non-agricultural sites, but not across agricultural sites. In fact, no single factor adequately explained MeHg concentration across all agricultural fields.

A strong linear relationship between THg concentration and longitude was found, with THg concentrations increasing 4-fold moving from east to west. Much weaker, yet significant relationships were also found between longitude and other mercury metrics (k_{meth} , Hg(II)_{R} and MeHg concentration), but not for calculated MP rates. Since all of the agricultural sites were located to the west of all of the non-agricultural study sites, we can not exclude the possibility that some of the significant differences found between agricultural and non-agricultural sites were at least partially caused by this spatial gradient in THg concentration.

3.3.2 Block Effect

The effect of northern block fields (F20, W23 and R31) versus southern block fields (F66, W65 and R64) was statistically tested across all agricultural fields. There were no significant differences in any of the measured sediment parameters, with the exception of pH, where northern block fields had slightly (yet significantly) higher average (\pm standard error) pH (7.01 ± 0.05) than southern block fields (6.88 ± 0.03). No mercury metrics were significantly different among the northern and southern blocks.

3.3.3 Season Effect

Seasonal effects were statistically tested by comparing growing season data (June, July and August 2007) to post-harvest data (December 2007 and February 2008) for agricultural sites (only). While there were no significant seasonal differences in most mercury metrics, average sediment MeHg concentrations were almost 2-fold higher during the post-harvest period ($3.70 \pm 0.38 \text{ ng g}^{-1} \text{ dw}$) compared to the growing season ($1.91 \pm 0.17 \text{ ng g}^{-1} \text{ dw}$). In addition, post-harvest agricultural fields had significantly lower pore water chloride and DOC, presumably due to winter flooding.

3.3.4 Hydrology Effect

Hydrology had a pronounced effect on sediment geochemical conditions on agricultural fields, as a function of field flooding and draining/drying cycles. Across all agricultural fields, sediment redox explained 51% of Hg(II)_R concentration. Once flooded, agricultural fields became more chemically reduced as a result of the stimulation of sediment bacteria and the build-up of reduced sulfur and iron end-products. As sediment condition became more reduced (e.g. throughout the June thru September growing season), concentrations of Hg(II)_R decreased. In contrast, once fields were drained (e.g. during the September thru October harvest), fields became more oxidized and Hg(II)_R increased. Post-harvest, fields were reflooded and sediments again became more reduced (during fall/winter) and sediment Hg(II)_R concentrations tended to decrease as a result. Thus, since Hg(II)_R concentrations partially control MeHg production rates, these changes in hydrology and sediment redox had a significant effect on where and when MeHg production rates were elevated or reduced.

3.3.5 Fertilizer Effect

A primary hypothesis of this study was that the addition of sulfate containing fertilizers to rice fields would stimulate microbial sulfate reduction (SR) and subsequently MeHg production. Although sulfate application rates were significant, at approximately $50\text{-}70\text{ kg acre}^{-1}$ on rice fields during the growing season, neither SR nor MeHg production were measurably or systematically stimulated. Prior to fertilizer amendment, sediment pore water sulfate concentrations were elevated ($> 1\text{ mmol L}^{-1}$) at levels where SR is generally not limited by sulfate concentrations, but instead by organic substrates. Thus, the additional sulfate input as fertilizer did nothing to increase microbial SR, nor MeHg produced by resident sulfate reducing bacteria.

3.3.6 Rice Straw Effect

The seasonal increase in MeHg production observed for the white and wild rice fields during the post-harvest season appears to be at least partially driven by decaying rice straw (**Section 6.4.5**). The first line of evidence supporting this is that benthic microbial SR was not limited by sulfate (electron acceptor) concentration (**Section 6.4.4**), and thus was limited by available organic matter (electron donor) and/or temperature. Secondly, MeHg production rates and concentrations were not highest during the summer growing season when temperature was highest ($23 \pm 4^\circ\text{C}$), as might be predicted if temperature was the primary driver of microbially produced MeHg. Instead, MeHg production rates and concentrations were highest during the post-harvest period when sediment temperatures were significantly colder ($12 \pm 4^\circ\text{C}$). Thirdly, pore water acetate concentrations increased from $148 \pm 73\text{ }\mu\text{mol L}^{-1}$ during the growing season to $385 \pm 265\text{ }\mu\text{mol L}^{-1}$ post-harvest in white and wild rice fields (combined), which had decaying rice straw. In contrast, pore water acetate in the fallow fields decreased from $156 \pm 87\text{ }\mu\text{mol L}^{-1}$ during the growing season to $16 \pm 15\text{ }\mu\text{mol L}^{-1}$ post-harvest. Finally, white and wild rice fields (combined) had higher sediment MeHg concentrations by February than did the fields that were fallow during the previous growing season. Taken together, this evidence strongly suggests that the decaying rice straw supplied labile organic matter (in the form of low molecular weight compounds, such as acetate) that readily fueled the microbial community involved in Hg(II) -methylation.

Because none of the agricultural fields were disced in the post-harvest season, we were not able to compare the observed field reflooding effects of decomposing rice straw with discing (physical incorporation of straw into the surface soil horizon), which is another common practice to remove post-harvest rice straw.

3.3.7 Plant Effect

Experimental evidence suggests that the presence of actively growing vegetation increases rates of MeHg production. MeHg production and concentration were significantly greater during the growing season in vegetated (control) plots compared to devegetated (manipulated) plots. This vegetation effect appeared to be due primarily to rhizosphere stimulation of 1) the supply of labile carbon pools such as acetate (fermentation product) that serve as fuel for Hg(II)-methylating bacteria, and to a lesser extent 2) enhanced iron cycling, including the reoxidation of reduced iron pools – Fe(II) to amorphous Fe(III) – an effective electron acceptor for iron-reducing bacteria. Along with comparative data between fields and seasons, these experimental data suggest the potential importance of iron-reducing bacteria in Hg(II)-methylation in these agricultural wetlands.

3.4 Results Summary: Methylmercury Bioaccumulation

3.4.1 Habitat Effect

Mercury in Invertebrates: Wetland habitat type had an important influence on THg concentrations in invertebrates, but this effect depended on the sampling time period and taxa. In particular, Notonectidae, but not Corixidae, THg concentrations were higher in permanent wetlands (average concentrations exceeding $2.0 \mu\text{g g}^{-1} \text{ dw}$) than in white rice, wild rice, or shallowly-flooded fallow fields, which all had similar average concentrations ranging between 1.1 and $1.3 \mu\text{g g}^{-1} \text{ dw}$. The effect of wetland habitat type was especially prevalent at the end of the rice growing season, when Notonectidae THg concentrations increased by approximately 1.5-2 times over their flood-up levels, and were at their highest in permanent wetlands. Additionally, invertebrate THg concentrations were higher at field outlets ($1.14 \pm 0.06 \mu\text{g g}^{-1} \text{ dw}$) than inlets ($0.93 \pm 0.06 \mu\text{g g}^{-1} \text{ dw}$).

Mercury in Caged Fish: THg concentrations and total Hg burdens in caged fish differed among wetland types at all cage sites, with white rice and wild rice fields having higher Hg concentrations than permanent wetlands. THg concentrations were higher at outlets than inlets in white rice, higher at inlets than outlets in wild rice, and did not differ in permanent wetlands. Total Hg burdens were higher at outlets than inlets in white rice, higher at inlets than outlets in permanent wetlands, and did not differ in wild rice. Our results indicate that THg concentrations in caged mosquitofish increased by 12, 6, and 3 times over reference levels in white rice, wild rice, and permanent wetlands outlets in just 60 days, respectively.

Across all wetland habitat types and sites, THg concentrations in mosquitofish removed from cages after 60 days of exposure were $1.07 \pm 0.03 \mu\text{g g}^{-1} \text{ dw}$, $1.13 \pm 0.02 \mu\text{g g}^{-1} \text{ dw}$, and $0.40 \pm 0.01 \mu\text{g g}^{-1} \text{ dw}$ in white rice, wild rice, and permanent wetlands, respectively, and $0.71 \pm 0.02 \mu\text{g g}^{-1} \text{ dw}$, $0.81 \pm 0.02 \mu\text{g g}^{-1} \text{ dw}$, and $0.84 \pm 0.02 \mu\text{g g}^{-1} \text{ dw}$ at the inlets, centers, and outlets, respectively.

Mercury in Wild Fish: Similar to caged fish, THg concentrations in wild fish differed among habitats, with white rice and wild rice having THg concentrations higher than in permanent wetlands. THg concentrations in wild mosquitofish were higher at outlets than inlets in white rice and wild rice, and inlets were higher than outlets in permanent wetlands. THg concentrations in wild silversides also were higher at white rice outlets than inlets, but not in wild rice or permanent wetlands.

Across all wetland habitat types and sites, THg concentrations in wild mosquitofish ($N=140$) were $0.63\pm 0.04 \mu\text{g g}^{-1} \text{ dw}$, $0.69\pm 0.05 \mu\text{g g}^{-1} \text{ dw}$, and $0.45\pm 0.02 \mu\text{g g}^{-1} \text{ dw}$ in white rice, wild rice, and permanent wetlands, respectively, and $0.43\pm 0.03 \mu\text{g g}^{-1} \text{ dw}$ and $0.77\pm 0.03 \mu\text{g g}^{-1} \text{ dw}$ at the inlets and outlets, respectively. THg concentrations in wild silversides ($N=136$) were $0.82\pm 0.05 \mu\text{g g}^{-1} \text{ dw}$, $0.66\pm 0.05 \mu\text{g g}^{-1} \text{ dw}$, and $0.30\pm 0.02 \mu\text{g g}^{-1} \text{ dw}$ in white rice, wild rice, and permanent wetlands, respectively, and $0.48\pm 0.03 \mu\text{g g}^{-1} \text{ dw}$ and $0.62\pm 0.04 \mu\text{g g}^{-1} \text{ dw}$ at the inlets and outlets, respectively.

Wild Versus Caged Fish for Wetland Hg Monitoring: Our results from wild fish are similar to caged fish, except that THg concentrations in caged fish were higher than in wild fish that were presumably exposed to Yolo Bypass Hg concentrations their entire lives. This illustrates the importance of using caged fish as site specific bioindicators of Hg contamination since wild fish are free to move in and out of the wetlands studied and into canals where MeHg concentrations are known to be lower.

3.4.2 Block Effect

We did not test for a block effect on biota Hg concentrations due to inherent intercorrelations between block and habitat type.

3.4.3 Season Effect

We tested for a seasonal effect on biota Hg concentrations using invertebrates that were sampled upon rice flood-up and again just before rice harvest. THg concentrations in Corixidae did not differ between flood-up and pre-harvest time periods (difference: $0.11\pm 0.09 \mu\text{g g}^{-1} \text{ dw}$), whereas THg concentrations in Notonectidae were higher during the pre-harvest than the flood-up time period (difference: $0.40\pm 0.10 \mu\text{g g}^{-1} \text{ dw}$).

3.4.4 Hydrology Effect

As stated above, invertebrate Hg concentrations tended to be higher at the end of the rice growing season than upon flood-up. Additionally, mosquitofish that were experimentally caged at wetland centers had nearly as high Hg concentrations than mosquitofish caged at wetland outlets. These results indicate that Hg bioaccumulation occurred rapidly within wetlands' hydrological gradient from inlets to outlets.

3.4.5 Biota Hg Correlations with Hg in Water and Sediment

Our results indicate that temporarily flooded shallow wetlands, such as white rice and wild rice fields, have elevated THg concentrations in both caged and wild fish compared to permanent wetlands at the Yolo Bypass. In contrast, THg and MeHg concentrations in invertebrates were higher in permanent wetlands than in white rice or wild rice fields.

These conflicting results are partially explained by the fact that fish THg concentrations were correlated with water MeHg, but not with sediment MeHg, whereas invertebrate MeHg concentrations were more correlated with sediment MeHg than with water MeHg. These results illustrate the complexity of MeHg bioaccumulation in food webs and indicate the importance of using several bioindicators simultaneously when monitoring MeHg production and bioaccumulation.

3.4.6 Fish and Invertebrate Hg Concentrations Exceed Harmful Levels to Wildlife in Yolo Bypass Wetlands

Hg concentrations in Yolo Bypass wetlands exceeded levels potentially harmful to wildlife. Hg concentrations in invertebrates and fish were more than 6 and 11 times higher, respectively, in Yolo Bypass wetlands than stated TMDL target values to protect wildlife (0.03 ppm ww). In fact, 99% of wild fish sampled in Yolo Bypass wetlands exceeded stated TMDL target values to protect wildlife (0.03 ppm ww) and 75% of invertebrates sampled in Yolo Bypass wetlands exceeded reported MeHg dietary effect levels of $0.50 \mu\text{g g}^{-1} \text{ dw}$ on avian reproduction. Therefore, Yolo Bypass wetlands should be considered a hot-spot for MeHg bioaccumulation and higher trophic level predators, such as waterbirds, should be monitored to make sure Hg is not having detrimental effects on avian reproduction.

3.5 Summary / Discussion of Results

Despite high benthic MeHg production rates (**Section 6**) and water concentrations in agricultural fields (**Section 5**), MeHg exports were physically limited by hydrologic export (**Section 4**) for all wetlands studied. While photodemethylation may have been partially responsible for limiting MeHg export (see **Section 9**), high aqueous MeHg concentrations led to rapid bioaccumulation of MeHg within caged and wild fish (**Section 8**). We suggest that load reduction is maximized by limiting water throughput, but that on-site biota exposure is maximized by this longer water residence time. Seasonally, we observed that the primary period of MeHg export from the Yolo Bypass Wildlife Area is during winter flooding periods when overall microbial activity and MeHg production in agricultural soils is fueled by the decomposition of rice straw (**Section 7**), and when hydrologic flowthrough is maximal. Because both photodemethylation and particle settling processes of MeHg removal are relatively inactive in winter months, we suggest that efforts to reduce MeHg production during this period would limit export from the fields.

The most dramatic difference in MeHg loads exported from the fields was found in the comparison of permanent ponds with the other fields. There was limited water export from the permanent ponds, and therefore, the MeHg export loads were minimal in comparison to the other fields. The concentrations of MeHg in the permanent ponds were also the lowest of all the fields, which also contributed to the relatively low MeHg exports.

The within-field comparisons are limited because of the variability in MeHg exports both seasonally and spatially and the limited sample size. It is unlikely the loads of MeHg coming from the fields in the Yolo Bypass are raising the concentrations of MeHg in the Delta during the active crop growing season, due to three factors:

1. Water discharge from YBWA agricultural fields are minimized by current management practices.

2. When water is exported, it is generally “recycled” and used again within the YBWA for irrigation.
3. Water use and evapotranspiration losses in rice fields is substantial during the summer irrigation season, such that the net flow of water is from the Delta to the YBWA.

3.6 Management Implications and Next Steps

1. The practice of wet harvesting of wild rice (active harvesting while outflows were open and flowing) led to the highest exports of u-MeHg the study. Restricting outflow during the wet harvest would minimize summer exports and potentially allow MeHg in the field’s water column to be reduced by particle settling and photodemethylation. The efficacy of this control mechanism could be tested during peak MeHg load periods of wild rice post harvest or ag fields in winter months.
2. Lower outflow generally results in lower u-MeHg exports. Minimizing surface water exports, wherever practicable, may limit the export of MeHg loads, as the more water is exported, the higher the loads. For rice management, however, a long residence time with minimal water export might be detrimental. Minimum water depths are needed during critical periods of the rice life cycle (so that flower buds are protected from low evening air temperatures which can cause sterilization). Further, input water is relatively saline, and additional evaporation can cause salt (osmotic) stress on the rice plants. Only the minimal amount of water that is needed should be flowed through the rice fields to minimize MeHg export. More attention to water management to optimize water use might require more resources.
3. MeHg removal from the water column via photodemethylation or particle settling may explain the reduction aqueous MeHg concentrations from inlet to outlet in the permanent wetland. If waters are held continuously in a permanently flooded deep wetland, particle settling and photodemethylation may provide an important MeHg removal function that could be utilized for tail-water cleaning. In future studies, it may be valuable to evaluate the whether the restoration or creation of permanent wetlands at the landscape scale will significantly influence hydrologic export and biotic exposure, especially outside of the wetland boundaries.
4. The surficial layer of rice straw that is generated late in the season is likely responsible for the high MeHg concentrations in surface water and sediments (biota were not monitored in winter). Alternative management that limits the availability of this labile carbon source prior to continuous winter flooding (e.g. discing or rice straw removal) may limit the carbon supply to mercury methylating microbes, and thus limit MeHg production and subsequent export.
5. Source water concentrations of u-MeHg are difficult to mitigate at the field scale, and may be a dominant control on net exports. Next steps may include a tracer experiment and/or measurements of processes related to advection and diffusion, as well as percolation.

6. Yolo Bypass wetlands should be considered a hot-spot for MeHg bioaccumulation and higher trophic level predators, such as waterbirds, should be monitored to make sure Hg within the YBWA is not having detrimental effects on avian reproduction.

4 Detailed Results for Hydrology

4.1 Introduction

Understanding hydrology in aquatic systems is important because many of the factors that control water quality in these systems are dependent on hydrologic conditions. Constituent concentrations provide only a snapshot of water quality at a particular window of time without any insight into the processes that led to the snapshot. Water supply, controls, pathways, and losses are all required to understand the processes leading to the water quality of an aquatic system at any particular moment in time.

The role of hydrology is of particular importance in the YBWA because the various wetland systems managed within the YBWA are largely defined by their hydrologic conditions, such as time and duration of flooding. Other systems within the YBWA have similar hydrologic conditions but differ in other ways such as crop type, fertilization, pesticide use, and a host of other operational variables that may impact water quality. To be able to understand the impact of these variables on water quality in the YBWA, hydrology must first be excluded as a driving factor. The only way to address the role of hydrology, and its impact on these systems, is to measure the hydrology for each field and identify its role prior to assessing the impact of other variables on water quality. Furthermore, hydrology in the YBWA is widely manipulated for water supply and therefore provides a variable that can be relatively easily manipulated by managers in the interest of controlling water quality in the YBWA.

In this study, hydrology was characterized for five wetland types managed within the YBWA to provide a basis for understanding the fate and transport of nutrient, organic carbon and pollutants for different wetland habitats: rice, wild rice and fallow fields as well as seasonal and permanent wetlands. Hydrologic analyses and seasonal water budgets were developed for fields currently being managed by farmers and wildlife managers in Yolo County, CA through routine hydraulic and meteorological data. The objective of the research was to quantify the differences in the water budget and hydrologic management of the different cropping systems in order to better understand the potential drivers for water quality, in particular MeHg.

4.2 Approach

4.2.1 Site Description

Eight fields were studied in this investigation ranging in size from 16 to 78 hectares (**Table 4.1, also see Figures 3.3 and 3.4**). Two fields were fallow under shallow flooding (F20, F66), two fields were in white rice (R31, R64), two fields were in wild rice (W32, W65), and two fields were managed wetlands (SW – seasonal wetland, PW –permanent wetland). The YBWA fields have silty-clay soils and shallow groundwater maintained at 1 to 2 meters below land surface during the irrigation season. Ditch water levels are maintained for routing water from three reservoirs: the Toe Drain, Green's Lake and return water from the Davis Drain. Losses in the recycled water in Greens Lake and Davis Drain are replenished by pumping water up the Toe Drain from the Sacramento - San Joaquin Delta and into the South Supply Ditch. The fields were managed in the spring, summer and fall according to their use: rice, wild rice, fallow or wetlands. The cropped fields were managed by the farmer to maximize crop yields. Wetlands were

managed by the California Department of Fish and Game for wildlife use. Field activities such as planting and harvesting were tracked through discussions with land managers and field observations.

Land managers controlled the hydrology of the study area's fields through the use of various hydraulic control structures. Water enters these fields through either valved pipes or flashboard risers depending upon the hydraulic design of each field. The fields are divided into checks, with a check defined as a subfield with a set bed elevation (plus or minus a few centimeters) with a minimal slope to carry the water from the upstream check to the downstream check. Check berms are set up along field contours, thus enabling the farmer to manage the water depths throughout each check. The number of checks within a field is determined by the total elevation drop across the field from inlet to outlet. Water enters and exits each check through risers with water level and flow controlled through the placement of boards in these weir structures. Each check typically has two weirs at the inlet and two at the outlet although field management may only utilize one weir box for an inlet or outlet from each check based on water demand and field mixing.

4.2.2 Hydrologic measurements

To characterize the hydrology of these systems, a hydrologic unit (HU) was defined for each field (**Table 4.1**). The HU approach was used so that all flow measurements could be made using weirs and thus would be subject to the same constraints and errors. Each HU was defined so that both the inflows and outflows would have weirs. Since all fields do not have weirs at the inflows, the first check berms with weirs for inflows were defined as the upstream end of HUs. The downstream end of the fields, all fitted with weirs, were defined as outflow of the HUs. Thus, all flows were estimated using standard equation describing flow over weirs (**Heald, 2002**):

$$Q = C(L - 0.2H)H^{1.5} \quad \text{Equation 4.1}$$

Where

Q = flow in cubic feet per second,

L = length of weir opening in feet,

H = head on weir in feet

Data from a previous study with similar weirs were used to determine the C-value for this equation ($C = 3.207$, $R^2 = 0.9394$). (**Bachand and Associates et al., 2006**). This equation is valid under critical flow conditions, where water drops over the end of the weir with no backing up of flow or other restrictions to gravity flow. Flow estimates could not be made in the managed wetlands (permanent and seasonal) because beaver dams interfered with the operation of the weirs.

A staff gauge was installed at each inflow and outflow location. Each height over weir measurement was accompanied by a staff gauge reading. These readings were used to provide a quick assessment of changes in water levels and were calibrated against the manual measurements of water height over the weir as a QAQC check. Staff gauge measurements at HU outflow locations were used to estimate changes in water levels across the fields. Along with

quantitative measurements, metadata was collected and photographs were taken to document the hydrologic conditions (e.g. critical flow, signs of disturbance, malfunctioning equipment, staff gauge levels).

For a subset of inflow and outflow locations, pressure transducers were installed and data recorded at 15 minute intervals. In wetland fields, pressure transducers were installed at outflow and center locations. Each pressure transducer was attached to a staff gauge and housed in an open-ended, vented PVC pipe. Pressure transducers measured water levels and were calibrated against staff gauge readings and measurements of heights over the weir. The calibrated data were converted to flow estimates using **Equation 4.1**, providing high frequency calculations of flow rates. Thus, the pressure transducers were used to track rapid changes in water level and flow not captured by discrete measurements.

Measurements began in June 2007 and continued through early April 2008 for the rice, wild rice and fallow fields. Transducer measurements began in July 2007, delayed by contractual issues. Monitoring of the wetland fields began in October 2007. Measurements were most intensive during the irrigation season; sites were visited several times a week during that time. Fewer measurements were made during the fall or spring because little or no water was flowing. Hydrologic measurements were made when possible in the late fall and winter, flooding limited access. After early December, few estimates of flow could be made because critical flow conditions were rarely met.

We were not able to calculate flow rates during the initial flooding of the fields because irrigators removed all boards in the weirs and water flowed freely. This phase occurred during the first week of irrigation; once standing water was present, irrigators began to add boards and measurements could be made. The flood-up period for fallow fields was approximately 50 days and we measured the flow rates during much of that time. We estimated that flow rates during the unmeasured flood-up period as equal to the average of the flows measured in July, the first month of flood-up for the fallow fields.

For rice and wild rice fields, we estimated inflow volume during initial flooding as the amount of water needed to saturate the unsaturated soil above the plow sole plus the height of water in the field at the end of the initial flooding phase. Several studies have shown through empirical data or modeling results that water does not quickly infiltrate the plow sole in rice fields (**Liu et al., 2001; Wopereis et al., 1994, Bouman et al., 1994**). The soils at the YBWA, Sacramento Series (ref) are classified as having very poor drainage and a plow layer approximately 18 cm deep. We estimated that the soil initially had a water content of 25% based upon its field capacity of 30 – 35% and its hygroscopic coefficient (wilting point) of 10 – 18% (**Brady and Weil, 2002**). Based on a porosity of about 50% for cultivated soils (**Brady and Weil, 2002**), we estimated that 6 cm of water was needed to saturate the soil in the plow layer. We then doubled that amount based upon an expectation that some water would flow past the plow layer during the flooding period. Thus, to calculate the total volume of inflow during the initial flooding phase, 12 cm of water was added to the amount necessary to raise surface water levels. Flow rates were calculated for the initial flooding, depending on the elapsed time during this period.

All hydrologic data was entered into an MS-ACCESS database and processed to develop flow rates. Extensive QAQC of the hydrologic data was conducted to ensure that predicted flows were only made for conditions of critical or zero flow, and that instrumentation was working effectively. Data that failed to meet these objectives were excluded from the analyses. Hydrologic trends and statistical significance using ANOVA was conducted using Statistica (Statsoft Inc).

4.2.3 Meteorological data

Precipitation measurements and reference evapotranspiration data was obtained from California Irrigation Management Information System (CIMIS) UCD station, located approximately 15 km to the northwest of YBWA. Actual evapotranspiration (ET) was calculated from ET_0 using crop coefficients (Kc) according to:

$$ET = Kc ET_0 \quad \text{Equation 4.2}$$

where ET is in mm day^{-1} , the Kc value is dimensionless, and ET_0 is the reference crop evapotranspiration measured by CIMIS in mm day^{-1} . During the growing season, Kc was based on crop development stage, as defined by the Food and Agriculture Organization Irrigation and Drainage Paper 56 (FAO 56) (Allen et al., 1998). Kc values for fields and periods where no crop was present and no Kc value published were estimated according to their state of inundation, vegetative condition and soil water content.

4.2.4 Water sample collection and analyses

Water samples were collected for calibration of the hydrologic model using conservative tracers (SC, Cl⁻, Br⁻) measured at inflow, middle and outflow of HUs in late August 2007 to help assess the degree of mixing in the HUs. Specific conductance was measured in the field at the hydrologic monitoring locations using a YSI multiprobe (YSI 6-series). Chloride and bromide samples were collected as part of the water quality sampling effort (see Section 5) at field inlets, outlets and center locations. Laboratory analyses are described in Section 5.

4.2.5 Mass balance calculations

Two models were used to develop mass budgets: the Plug Flow Reactor (PFR) model and Continuous Flow Stirred Tank Reactor (CFSTR). The CFSTR model assumes that the field is well mixed throughout whereas the PFR model assumes that each check is well mixed but independent from each other (Figure 4.1). The equations derived above were used in the PFR and CFSTR model development to estimate the contributions of surface and groundwater to meeting evapotranspiration needs, and to estimate subsurface flow rates into or out of the field system. These equations were applied for selected conditions during the summer irrigation season including 1) Inflow was greater than zero; 2) Outflow was greater than zero; 3) Inflow was greater than outflow; and 4) All flow, electroconductivity and water level data was available for each date. These conditions allow for the best resolution of flow paths that could then be used to guide calculations for the entire hydrologic period.

Water and mass budgets were derived to describe the aquatic crop fields, including the underlying soil near the rootzone as illustrated in Figure 4.2. The total water budget can be described with the following expression:

$$Q_i + Q_{ssf} + Q_{pr} = Q_o + Q_{ET} + Q_{\Delta WL} \quad \text{Equation 4.3}$$

where

Q_i = surface flow into the system,

Q_o = surface flow out from the system

Q_{pr} = flow into the system from precipitation

$Q_{\Delta WL}$ = Change in water storage due to changes in surface water levels

Q_{ET} = flow from the system as evapotranspiration

Q_{ssf} = subsurface flow into the system.

Using the soil water interface as a boundary between the above and below ground water balance, a surface water budget can be described by

$$Q_i + Q_{pr} = Q_o + Q_P + Q_E + Q_{\Delta WL} \quad \text{Equation 4.4}$$

For flooded fields, subsurface soil can be assumed to remain saturated and so no change in water storage occurs. The subsurface water can be described by

$$Q_P = Q_T - Q_{ssf} \quad \text{Equation 4.5}$$

Where

Q_P = flow to root zone through percolation

Q_E = flow out as evaporation (surface) and

Q_T = flow out as transpiration (subsurface).

Q_{ssf} = flow to rootzone from groundwater

Importantly, this water budget separates transpiration and evaporation when describing evapotranspiration.

4.3 Results

4.3.1 General trends

Field based manual measurements tracked *in situ* measurements well and produced similar water fluxes (**Figure 4.3**). Because of the good relationship between manual and automated measurements and because not all fields were equipped with transducers, manual measurements were used to calculate all field water budgets to maintain maximum consistency across all fields in the study.

Using the steady state analysis of a conservative tracer (Cl^-) with the models during the summer irrigation period, white rice fields were found to follow the PFR model where each check is individually well-mixed and concentrations increase along the flow paths, whereas wild rice fields behaved more like the CFSTR model with concentrations being similar across the entire field independent of checks.

4.3.2 Seasonal analyses

Measurements were separated into “seasons” based on agricultural practices, water level, and flow (**Table 4.2**): Two of the “seasons” were periods of inundation for most fields including the summer agricultural production season, in which seven of the fields were flooded for at least 60 days, and the winter flooded period in which all eight of the fields were flooded. The winter flooded period was further broken down into three separate periods: the winter irrigation, winter flood, and winter drainage periods. The spring and autumn seasons are periods of no irrigation when fields are extensively dry so that land preparation and harvest activities can be performed, because no surface water transport occurred during these seasons, no analysis of those seasons is included in this report.

4.3.2.1 *Summer irrigated period*

For all fields, irrigation water dominated the inputs during the summer. **Table 4.3** presents a summer water budget with values reported as cm of water, standardized to the area of the field. Irrigation water applied to the fallow fields was less than that applied to the domestic white and wild rice fields largely because the fallow fields were flooded for a shorter period of time and were not managed as flow-through systems, instead allowing the water to stand in the field and slowly move from check to check. Surface drainage was much less than surface irrigation (12% to 31%) due to significant loss mechanisms during the time water passed over the fields. During stable flow conditions, the CFSTR model predicted that 38% of ET losses were from E and 63% from transpiration whereas the PFR model predicted 27% ET losses were from E and 73% from transpiration. Irrigation management in the summer growing season differed between white and wild rice. Flow across the fields was greater in wild rice than white rice early in the period whereas wild rice flows across the field decreased late in the season and flow across the white rice fields increased. Because the wild rice fields were not drained post-harvest, there is a relatively large amount of water stored on the field whereas the other fields were drained entirely during the irrigation period. Budget imbalance for the season ranged from -7 to +15 cm of water. When including the water deficit of the soils from the spring dry-down the budget imbalances range from -38 to +1 cm. The models suggest groundwater utilization by plants through upward flow in the soil strata during transpiration as the balance for the water deficits; however, these figures are within the error of measurement and are as likely to be the result of the initial flood-up estimates and ET demands during the dry period.

4.3.2.2 *Winter irrigated period*

This period is defined as the period when the fields are reflooded for waterfowl habitat and decomposition of summer vegetation. Precipitation and river flows commonly preclude the need for irrigation except in the fallow fields and seasonal wetlands which require irrigation because they typically get flooded earlier in the year before the rainy season begins. The end of the period was defined by overbanking of the fields by high Cache Creek flows, as this impacted the ability to accurately measure water and constituent fluxes. The value of 25 cm water depth was chosen as the point at which water quality measurements were reasonable for the measured water volumes. Losses due to transpiration were negligible because the plants were either harvested or senesced. Losses to evaporation were small because of cooler temperatures and less solar radiation. As seen in **Table 4.4**, the large calculated imbalance in the fallow fields and W65 likely reflects difficulties encountered in measuring the surface inflows to the fields during the

winter irrigation period. Many of the measurements collected early in this period failed to meet the critical flow requirement for measurement because of the manner in which the managers maintained the weirs. This resulted in a likely underestimation of surface irrigation for the early part of the record.

4.3.2.3 *Winter flood period*

Flow measurements onto and off of the fields could not be made during this period because high storm flows from Cache Creek over-topped the berms used to isolate the fields, resulting in a large, undefined expanse of water encompassing the fields. Unconfined flow dominated this period. Also, access was restricted during the flooded period for safety concerns. Because no measurements were possible during this period, there are no measurements that can be used to estimate this period, we can only estimate water fluxes during this period using theoretical approach. As a means to estimate water on and off the fields during this period, the pressure transducer measurements were used to estimate field depths. Elevation changes more from east to west so fields without pressure transducers that lie on the same longitude as field with transducers were estimated as having similar changes in water depth over the flooded period. Using the most conservative scenario, that there was no flow component to the flood inflow and outflow volumes and water merely rose and dropped on each field, the 17-day flood period accounted for roughly 50% of the annual water budgets for each field (**Table 4.5**). Using the average change in water depth from the beginning of the flood and the end (from 1/25/08 – 2/10/08) and the lower end of published floodplain velocity estimates (0.1 m s^{-1} ; **Sommer et al., 2001**), we estimated a less conservative range of 200 to 500 cm of water flowed onto and off of each field during the 17-day period of inundation. There is little doubt that the flow regime across the greater Yolo Bypass was complex and likely included greater velocities than the 0.1 m s^{-1} used for this estimate, equating to much greater water volumes passing through the fields. We did not further evaluate the less conservative estimates of flow or areal differences between fields during this period because this very rough estimate of water flux was an order of magnitude greater than the irrigation values for the rest of the year, accounting for the vast majority of the annual water budget for each field despite the short duration of the regional flooding.

4.3.2.4 *Winter drainage period*

The winter drainage period is defined as the point at which the fields re-established their boundaries as floodwaters receded below the berms and back to the baseline 25cm depth established as the end to the winter irrigation period. Because the flood breached some berms and open irrigation supply pipes acted as drains following the flood, no direct measurements of flow could be made during this period. Therefore, the drainage period water budget was estimated as the export of water that was present on the field, based on the 25cm baseline assumption pre-flood. Because the start of this period was the re-establishment of individually flooded fields and the end was defined as fully drained conditions, a net export of 25 to 30 cm of water was calculated for all fields (**Table 4.6**). When added to the total winter budget (**Table 4.7**), this outflow of flood water was the greatest term for hydrologic export within all fields.

4.3.2.5 *Spring and autumn dry-down periods*

Precipitation and ET dominated in these periods as they have, by definition, no irrigation inputs or surface drainage from the fields. When drying fields, managers rely on ET to outpace precipitation to dry-out the soils for machinery access for harvest and field preparation activities. These periods make up a minor portion of the annual hydrologic budget except that they set the water deficit for the fields and drive the irrigation requirements at the initial flooding.

4.3.3 Annual water budget

It is apparent that a bulk of the surface irrigation of the agricultural fields occurs in summer (approx. 80%), as would be expected, however, the bulk of the surface water exports occur during winter (approx. 80%) because of lower ET and higher precipitation. As shown in **Table 4.8**, irrigation demand of the managed wetlands was similar to that of the agricultural fields in spite of having lower ET during the flooded period, largely due to longer periods of flooding which resulted in higher ET demand. Also, although we excluded the contribution of the regional flooding from the calculated annual budget because of the large uncertainties in the estimates, estimates of the contribution of the flood to the annual water budget is large even under the highly conservative methods used indicating the relative importance of this event to actual annual loads and the importance for capturing these events in future efforts. The high irrigation demand for field R64 was a result of the herbicide management requirement for that field. To apply the type of herbicide used, the field had to be completely drained and reflooded during the growing season. Irrigation demand for the fallow fields was lowest likely due to the short period of flooding; however, the budget imbalance was greatest for these fields, suggesting a large water deficit which may be a result of difficulties in measuring the initial flooding of these fields.

4.4 Discussion

Much of the irrigation water applied to the agricultural fields was never exported through surface outlets during the summer irrigation period (**Tables 4.3**). Surface outflows constituted only 15 to 30% of the irrigation water in summer. Transpiration was the largest vector of water loss from the surface water column during this period, carrying constituents into the soil stratum, leaving the question of what the ultimate fate of the constituents might be: concentrated in soil root zone, leached out with some seepage into surrounding drains or taken up by plants through the roots, exported during flood periods in the winter due to diffusion from substratum into surface waters. Further impacts include the fact that advective flow of water downward into the soil from the overlying water to meet transpiration demand (during actively transpiring periods) would greatly reduce the diffusion of constituents produced in sediments upward into the surface water column.

In contrast, winter precipitation accounted for at least as much water inputs to the fields as surface irrigation, even without including the 17-day Cache Creek flood period. Also, evaporation was minor and transpiration is negligible during winter. This results in a bulk of the surface export of water to occur in the winter period. The differences in hydrology between seasons are likely to have a profound impact on water quality and constituent exports. Also, it is important to note that in the YBWA, even under the most conservative estimate of the winter flood to the annual budget, the flood waters accounted for at least 50% and more likely in excess

of 99% of the annual water budget despite being only 17 days long. It is imperative that a greater effort be attributed to the examining this winter period in future studies.

Also of note is the difficulty of measuring the water budget in these wetland systems, particularly in the fallow fields. The effort required for assessing hydrology should never be underestimated when designing a study or in prescribing management practices to growers. It was good that manual measurements mirrored *in situ* measurements in this study, but this relationship and dataset should not be expected in all cases or locations, as it required a great amount of time and effort to make the measurements. It is imperative that efforts be made for coordination between irrigation managers in the field and *in situ* data collection to reduce assumptions and error in measurements. Future efforts should be made to instrument flow structures in such a way as to capture flood-up and drainage of large events as they can dominate water flux on and off field as well as uncertainties that are carried on in the calculation of constituent fluxes.

In conclusion, hydrology may be the most important variable in understanding water quality in the YBWA. The flow of supply water, evaporative and plant transpiration demand and impacts of flow path all influenced water quality. Of particular interest in this study was the recognition of the different roles of evaporation (E) and transpiration (T) in the water budget as opposed to evapotranspiration (ET) considered as a single component of the water budget as there is a significant difference in their effect on surface water quality. Distinguishing evaporative losses from transpiration losses was necessary to reconcile the hydrologic and tracer mass budgets. Evaporation acts on the surface water of the system, removing water but not constituents, thus increasing concentrations in surface water (evaporative concentration). In contrast, transpiration occurs in the root zone of the plants which acts similarly to a surface outlet except that the constituents can be trapped in the soil or taken up into the plants. The implications of not capturing these realities in hydrology are profound in that the improper allocation of hydrologic flowpaths can result in the fundamental misunderstanding of ecosystem function and resulting water quality.

5 Detailed Results for Methylmercury loads and Water Quality

5.1 Introduction

There are several reasons to study MeHg cycling and export from wetland habitats hydraulically connected to the Delta: 1) there are fish consumption advisories issued for limiting the amount of fish consumed by anglers in the Delta; 2) there is concern that any changes to restore the Delta, including creating more wetlands, will exacerbate the Hg problem; 3) there are goals by the California Bay Delta Authority to create and restore thousands of acres of wetlands and to drastically alter the structure and functioning of the Delta; and 4) the Central Valley RWQCB has proposed a Basin Plan Amendment (**Wood et al., 2010b**) that would require wetland managers to conduct research to develop BMPs for reducing MeHg releases from wetlands.

There have been few publications reporting loads of MeHg from different wetland habitats, particularly in California's Delta where wetlands are a prominent land type. Internationally, wetlands have been identified as important sources of MeHg. For example, in the experimental lakes area of Ontario, Canada it was shown that watersheds with wetlands contributed far more MeHg than watersheds with lakes (stratified and non-stratified) and riparian habitats (**St. Louis et al., 1994**). In other areas in the U.S.A. and Canada these results were confirmed (**Krabbenhoft et al., 1995; Branfireun et al., 1996; Driscoll et al. 1998**). Of particular interest is that periodically flooded wetlands were found to be habitats with particularly high MeHg production (**Hecky et al., 1991; Rudd, 1995**)

Wetlands and rice fields from the YBWA were selected for study because of their wide wetland variety in close proximity, from typical seasonal wetlands and permanent wetlands to white rice, wild rice, and fallow fields. The YBWA wetlands represent important habitat for birds along the Pacific Flyway, a migratory corridor of many thousands of acres of wetlands throughout California.

The primary objectives of this task element of the study are to quantify and compare mercury and MeHg concentrations and exports from different wetland types within the YBWA and to determine the dominant processes that lead to methylation, export and Hg bioaccumulation under different land management schemes commonly used in the YBWA. Both *in situ* (within the YBWA) concentrations and exports are important because *in situ* concentrations will govern the exposure of local biota to Hg and MeHg, whereas exports may impact sensitive downstream environments.

5.2 Approach

5.2.1 Field sampling

The field sampling plan consisted of four levels of intensity: Schedules A, B, C and D. Schedules A and B were multidisciplinary and designed to coordinate with sediment, plant, and biota sampling teams involved in the greater study objective of providing a wholistic view of Hg cycling in different wetland habitats. These schedules consisted of the most extensive list of analytes collected at five time points considered indicative of the dominant management

activities in the wetlands under study, including initial flooding, mid-irrigation-season (top dressing fertilizer application), pre-harvest, winter flood-up (prior to Bypass flood) and winter pre-drainage (post Bypass flood) (see *Table 11.1* and *11.2* in *QAPP (U.S. Geological Survey et al., 2008)* for sampling schedules and analytes). Schedule C sampling included a subset of analytes from Schedules A and B with the focus of enhancing the time series of particular analytes of interest (i.e., MeHg, DOC, and SO₄) to provide greater certainty in the export loads calculation. Schedule D sampling included a subset of analyses performed for the purpose of calibrating *in situ* measurements used to discern the high frequency temporal variation in water chemistry in the fields that may be important to the methylation or demethylation processes. Procedures for the collection of samples in Schedules A, B, C, and D are described in the project's Quality Assurance Project Plan (*QAPP Table 4.2*) and Management Plan; a summary of procedures is provided below. Abbreviations for water-quality analytes are given in *Table 5.1*.

5.2.1.1 Interdisciplinary study (Schedules A and B)

Schedules A and B were collected as part of the multidisciplinary sampling plan. Sampling was conducted by the USGS Sacramento sampling team. Samples were collected from the inlets, outlets and a central location of each field using 2- or 3-liter acid-cleaned Teflon[®] bottles attached to an acid-rinsed PVC pole (US Geological Survey, 2006). Additional samples were collected from the supply ditches upstream of the inlets to determine if differences existed between concentrations of constituents going onto the fields and the source water in the supply ditches.

Water collected in the Teflon[®] bottles was poured into two acid cleaned 13-L Teflon[®]-lined containers until approximately nine liters had been collected in each container. The 13-L containers were placed on ice in a dark cooler with wet ice for immediate transport to the USGS laboratory in Sacramento for processing. In the cases where fields had multiple inlets or outlets, the water samples were composited in the field in proportion to the flow at each location.

Upon arrival at the USGS laboratory, samples were poured into a 20-L acid cleaned, Teflon[®]-lined, stainless-steel churn splitter to perform sub-sampling for the full suite of analyses for the appropriate sample schedule using clean-hands, dirty-hands techniques (Olson and Dewild, 1999). Aliquots were collected for various analyses, in various containers as per *QAPP Figure 12.1* and *QAPP Table 12.1*. Aliquots for all unfiltered analyses were collected from the churn prior to the collection of any filtered aliquots to ensure there was no biasing of the sample during processing with regard to suspended sediment concentration.

5.2.1.2 Loads assessment extras (Schedule C)

Schedule C samples were collected temporally between the Schedule A and B sample collections and during drainage events. The samples were collected primarily by the California Department of Fish and Game sampling team, although the USGS team from Sacramento assisted with several sampling events. Samples were collected at each sampling location using individual sample bottles. The bottles for MeHg and TSS analyses were preserved and shipped directly to the Moss Landing Marine Laboratory (MLML) in Moss Landing, CA. A single 2-L or 3-L sample was collected for the remaining analytes and was delivered to the USGS Sacramento

laboratory for processing similar to that performed in the Schedule A and B samplings. Aliquots for Schedule C analyses were collected as per *QAPP Figure 12.1* and *QAPP Table 12.1*.

5.2.1.3 Diel study (Schedule D)

Schedule D samples were collected over three deployment periods. Diel measurements were conducted in Field W65 in July 2007; Field R64 in August 2007 and in Fields R20, W31 and PW5 in July 2008. The instrumentation was deployed for at least 48 hours to capture a sense of the diel variability in each field. Hourly to bihourly samples were collected for instrument calibration and to determine relationships between mercury species and the optical measurements. Isolated bottle and bag measurements were collected for comparison to *in situ* measurements of DOM and optical properties to help isolate possible mechanisms for diel trends.

The *in situ* instrumentation package consisted of a similar organic matter characterization system as described by **Downing et al. (2008)**. In summary, the system included a multi-channel spectrophotometer (AC-9, Wetlabs Inc.), a CDOM fluorometer (Wetlabs Inc.), a ChlA fluorometer (Wetlabs Inc.), a YSI multiprobe (YSI 6-series), and an UV-vis spectrophotometer (ISUS, Satlantic Inc.) The system included both filtered and unfiltered flow paths to capture measurements of the dissolved and particulate components of the water at short-term intervals, generally averaged over 15 minutes. The filtered flow path was pumped through a 0.2µm pore diameter filter with a 40-mesh screen and 10 µm pore diameter pre-filter. The unfiltered path was pumped in parallel to the filtered channel. Difficulties organic buildup within the filtered channel led to censoring of large portion of these data; data presented in this report focus primarily on the unfiltered channel.

Discrete grab samples were collected using modified clean-hands methods, as described in the *QAPP*. Samples were collected in acid-cleaned glass bottles. *In situ* flowpaths were cleaned and well rinsed to reduce contamination. For Field W65, filtered samples were collected directly from the instrument flowpath whereas unfiltered samples were collected from the weir next to the instrument set-up. For the other fields, both samples were collected from their respective instrument flowpaths with care to pull from the center of the water column. Additional measurements of DOM character and optical properties were collected from Tedlar bags (http://www.keikaventures.com/s_tedlar.php#FAQ) during the 24-hr grab sampling effort on field R64 to isolate photolytic reactions from biological impacts. Six tedlar bags (3 filtered and 3 unfiltered) were filled with surface water from field R64 following sunset (9PM) and six bags were similarly filled at dawn (5AM). Each bag was left in the field near the *in situ* sampling apparatus to mimic photo-environment at the *in situ* measurement location. The tedlar bags were not tested for mercury cleanliness and thus were used only for DOM evaluations. Results from the tedlar bags were compared to *in situ* measurements and laboratory DOM measurements collected in coordination with the photodemethylation bottle experiments (**Section 9**).

5.2.2 Laboratory analyses

Laboratory analyses were completed for surface water samples using methods described in the *QAPP* (**U.S. Geological Survey et al., 2008**). Results of quality assurance and quality control analyses are given in **Appendix 2**.

5.2.3 Meteorological data

Meteorological data were obtained from the California Irrigation Management System (<http://wwwcimis.water.ca.gov>) site #6, Davis (N38°32'09", W121°46'32") which is located approximately seven miles west of the YBWA.

5.2.4 Statistical analyses

Normality of data was checked using SigmaPlot, version 11 (Systat Software, Inc., San Jose, Calif.). Correlation coefficients for relationships among variables were determined using two different methods, a parametric method for normally distributed data and a non-parametric method for data that are not normally or log-normally distributed. The parametric method used was the Pearson Product Moment Correlation, for which the correlation coefficient is denoted as r_p . The non-parametric method used was the Spearman Rank Order, for which the correlation coefficient is denoted as r_s . Linear least-squares regression, for which the correlation coefficient is denoted as r and the coefficient of determination is R^2 , was done using SigmaPlot, version 11.

A Mann-Whitney test (a non-parametric test for assessing whether two sets of observations come from the same distribution) was applied to various subgroups of the water quality data to assess whether or not statistically significant differences were found. The Mann-Whitney testing was done using MINITAB, version 14 (Minitab, Inc., State College, PA).

5.2.5 Load calculations

Loads were calculated for each field by interpolating measured concentrations for each flow sampling location to create a daily record and then multiplying by the daily flow at that location. The hydrology and flow determination are described in detail in **Section 4**. Water quality interpolations using data collected at the field inflow and outflow locations were combined with flow interpolation data collected at the inflow and outflow locations. These calculations were totaled over the season to estimate total surface load onto and off of the system. Because a concentration gradient exists within each field, and on most fields, the hydrologic measurements were collected at a different location than water-quality inflow measurements, we corrected the load estimates onto the fields using a linear interpolation of water-quality spatial gradients using the average seasonal concentrations. This correction did not need to be applied to outflow locations as the hydrology and water quality measurements were collected concurrently. Surface storage for each constituent was estimated using the total change in water level for the season multiplied by the average concentration on each field during a season.

Mass fluxes through the soil water interface were estimated using chloride as a tracer. Chloride is neither produced nor consumed by chemical reactions involving water and soil, and can be used as a conservative, natural tracer in aquatic systems (e.g. **Schemel et al., 2006**).

Chloride flux to the root zone (percolation) was taken as the difference between chloride inflow and outflow from each field. The percent of the inflow load passing through the soil-water interface was estimated by the differences between the surface-water load of chloride onto the field minus the sum of surface-water export of chloride and surface-water storage. A ratio was calculated for each field relating calculated chloride flux passing through the soil-water interface and surface-water chloride inflow. That ratio was applied to the other constituents to estimate the amount of each constituent fluxing through the soil-water interface because of hydrologic effects.

5.3 Results and Discussion

5.3.1 Mercury and Methylmercury Concentrations

5.3.1.1 *Seasonal trends*

5.3.1.1.1 Total Mercury

Concentrations of THg were highly variable over time. A large increase in THg concentration occurred shortly after early summer flood-up, followed by a quick decline. A second concentration pulse occurred in winter in the rice fields (**Figures 5.1 and 5.2**). A large proportion (about 50%) of the THg released in the initial pulse was in the dissolved ($<0.45\mu\text{m}$) fraction (f-THg), whereas the winter pulses tended to be the result of higher particulate concentrations (**Figures 5.1 and 5.2**). The proportion of THg that passed through $0.45\mu\text{m}$ filters varied from about 5% to about 95% (**Figure 5.3**). This proportion was relatively low in the permanent wetland (5 to 50%), relatively high in the seasonal wetland (30 to 95%), and highly variable (5 to 95%) in the agricultural fields. Over the period of study, u-THg concentrations exceeded the EPA water-quality criterion of 50 ng L^{-1} (California Toxics Rule; U.S. Environmental Protection Agency, 2000b) on 14 occasions, mostly following the initial flooding of the agricultural fields. Although the water-quality criterion in the California Toxics Rule is not typically enforced in agricultural systems, it is often used as an indicator of potential important sources of THg to downstream environments. Concentrations of u-THg and f-THg were consistently higher on agricultural fields (means of 26 and 7.1 ng L^{-1} , respectively) vs. non-agricultural fields (means of 7.8 and 1.9 ng L^{-1} , respectively) (**Table 5.2**). The differences in aqueous THg between agricultural and non-agricultural fields coincide with a general east-west gradient (lower in east, higher in west) noted in THg concentrations in sediment (**Section 6**). The east-west gradient in THg is believed to reflect the source of deposited sediments with high THg sediments from Cache Creek being deposited in the western part of the Bypass and lower THg sediments of the Sacramento River dominating deposition in the eastern portion of the Bypass, according to the east-west gradient of water flows identified by **Sommer et al. (2008)**. No statistically significant differences were noted when comparing aqueous THg data from the northern block of fields to the southern block (**Table 5.3**) or between seasons (**Table 5.4**). The similarity between blocks is consistent with the lack of a north-south spatial gradient for THg in sediment at the scale of the study area (**Section 6**). High variability in THg concentrations explains the lack of statistically significant difference between seasons.

5.3.1.1.2 Methylmercury

Whole-water (u-MeHg) and filter-passing (f-MeHg) concentrations generally increased from inlet to center and inlet to outlet, however there was no significant difference between center and outlet for all fields considered together (**Figures 5.4 and 5.5; Table 5.5**). All measured u-MeHg concentrations far exceeded 0.06 ng L^{-1} , the TMDL goal (**Wood et al. 2010a,b**). Supply water

for the wetlands exceeded the TMDL goal by at least 4-fold throughout the year; the most elevated concentrations entered the northern water supply from the Davis Drain. Center and outlet locations on white rice and fallow fields had the highest u-MeHg concentrations shortly after flooding and maintained similar concentrations through the water year, whereas concentrations on wild rice fields started relatively low following irrigation flooding and increased throughout the growing season, peaking during wet harvest activities and decreasing during the winter to levels similar to those in mid-summer (**Figure 5.4**). The permanent wetland maintained low u-MeHg and f-MeHg concentrations throughout the year, except when inundated by floodwaters that covered much of the bypass in early February 2008. The dissolved fraction ($<0.45 \mu\text{m}$) of MeHg (f-MeHg) exhibited a temporal trend opposite to that of f-THg, starting low in early summer and increasing with time flooded. The temporal trend in f-MeHg mirrored the trend in sediment MeHg (**Figures 5.5 and 6.5**). For MeHg, the percent filter-passing varied from about 10 to 90%; most values were in the range of 30 to 60 % (**Figure 5.6**). Concentrations of f-MeHg on white rice fields increased throughout the year and were markedly higher than the other wetlands in winter. During August, surface-water concentrations of f-MeHg were similar among all of the agricultural fields.

The ratio of MeHg to THg (MeHg/THg) is often used as a measure of the methylation efficiency of a wetland (e.g. **Krabbenhoft et al., 1999**). The MeHg/THg ratio in unfiltered water generally ranged from about 1 to 100% (**Figure 5.7**) whereas the ratio in filtered water was mostly between about 10 and 100% (**Figure 5.8**). In both unfiltered water (**Figure 5.9**) and filtered water (**Figure 5.10**), the MeHg/THg ratio increased markedly throughout the summer growing season in all agricultural fields. In contrast, MeHg/THg ratio in the permanent wetland increased with time only in the filtered fraction (**Figure 5.9**). Although the relatively high MeHg/THg ratio in the northern supply water might confound the use of this metric, the consistency of temporal trends in both the northern and southern field blocks suggest that this effect is minor.

5.3.1.1.3 Evapoconcentration effects

Evapoconcentration was quantified using two independent approaches: (1) concentrations of chloride and (2) stable isotopes of oxygen and hydrogen. Because chloride is a conservative ion, it tends to be residually concentrated in surface water in direct proportion to the amount of evaporation. Stable isotopes of hydrogen and oxygen in water show a systematic trend with evaporation that commonly shown on plots of $\delta^{18}\text{O}$ vs. δH as a characteristic slope between 3 and 5, in contrast to unevaporated waters which tend to follow the Global Meteoric Water Line with a slope of 8 (**Clark and Fritz, 1997**). A plot of $\delta^{18}\text{O}$ vs. δH for water samples collected in this study (**Figure 5.11**) shows a slope of 4.42, which is consistent with evaporation being the dominant mechanism affecting the oxygen and hydrogen isotope ratios. The empirical fraction factor, α , is equal to 1.009 for $\delta^{18}\text{O}$ during evaporation (**Clark and Fritz, 1997**). On a log-linear plot of chloride concentration versus $\delta^{18}\text{O}$, the expected slope for water affected by evapoconcentration, based on Raleigh fractionation (**Clark and Fritz, 1997**) is 20.7 (9 times 2.303). The data from this study plot in a distribution very close to the expected slope (**Figure 5.12**), and a linear least-squares regression indicates a slope of 20.1, which corresponds to an empirical α value of 1.0087 (20.1 divided by 2.303).

The degree of evapoconcentration for given “snapshots” in time can be quantified by taking the ratio of chloride concentration of outflow to that of the inflow (Out/In) for each field. A similar ratio can be computed for other constituents to assess whether observed changes in concentration from inflow to outflow might be due entirely or in part to evaporative

concentration. By normalizing the Out/In ratio of MeHg to the Out/In ratio for chloride, the resulting values, if greater than 1.0, indicate the enhancement of MeHg caused by processes other than evaporative concentration. In **Table 5.6**, the Out/In ratio of u-MeHg and u-THg relative to chloride is shown for each season for each field. In general, the non-evaporative enhancement for u-MeHg was much higher for agricultural fields in the southern block than those in the northern block in the summer period. This effect is caused primarily by lower concentrations of u-MeHg in the inflow water for this zone compared with the inflow water to the northern block, which tended to include a higher degree of recirculated agricultural drainage water that was higher in MeHg. In contrast, the greatest non-evaporative enhancement in the winter period occurred in the white rice fields, one of the wild rice field (W32) and the seasonal wetland (SW). The enhancement for THg was largely caused by evaporative concentration, as indicated by values near 1.0. Only field F20 showed non-evaporative enhancement of THg.

5.3.1.2 Diel Trends

Diel trends were found to be widely variable between fields and years. During a series of intensive, high-frequency 24-hour sampling events in 2007, a strong diel trend in u-MeHg concentration was observed in a wild rice field (W65) varying from less than 1.0 ng L^{-1} to 2.1 ng L^{-1} . In contrast, no trend was observed in a white rice field (R64) with concentrations remaining around $0.73 (\pm 0.08) \text{ ng L}^{-1}$ (**Figure 5.13**) throughout a 24-hr period. In 2008, there was a trend in the white rice field R20 varying from 0.53 to 0.95 ng L^{-1} , although the trend was not clearly diel like the trend observed in W65 in 2007. No trend was observed in a wild rice field (W31) monitored in 2008, with concentrations holding constant at $0.51 (\pm 0.02)$. The higher MeHg concentrations observed in field W65 during 2007 were likely caused by the higher THg concentrations in the wild rice field relative to the other fields (11.6 vs 3.2 , 3.9 and 4.3 ng L^{-1}) because the percentage of THg as MeHg (MeHg/THg) was similar between fields. No significant diel trends were observed in THg concentrations at either site. The MeHg/THg ratios in unfiltered surface water (**Figure 5.14**) followed similar diel trends as u-MeHg concentrations in all fields, except with a greater skew towards dawn for W65. The primary difference between observed diel trends in MeHg concentration and those in MeHg/THg are the relative magnitudes between the sites.

The diel trends differed markedly between fields. The trend for u-MeHg in field W65 during the 2007 experiment was nearly sinusoidal; rising at night, peaking in the early morning hours (3 AM) and slowly decreasing throughout the daylight hours. In contrast, in field R20 during the 2008 diel experiment, MeHg concentrations remained relatively constant through much of the diel cycle but spiked in the early evening through midnight. During the 2007 experiment, the white rice field (R64) had a consistently high MeHg/THg (20%), whereas the wild rice field (W65) had a similar MeHg/THg at dawn (18%) and lower ratios during daylight hours (8%), suggests that the diel trend was more likely a result of a removal mechanism affecting MeHg during daylight than an increase in MeHg production during nighttime hours. In contrast, during the 2008 experiment, the fields had relatively constant MeHg/THg ratios around 15% with R20 decreasing slightly to 13% near sunset and increasing to 22% near midnight, before returning to 15% in the early AM which suggests a source of MeHg increasing concentrations in field R20.

The differences in the diel trends suggest different mechanisms affecting MeHg in R20 and W65; however, the influence of hydrology cannot be ruled out. The location of each deployment

differed because of differences in field management and condition of the crop. The field with the most pronounced diel trend, W65, was the field with the lowest flow rates during the deployments; in comparison the fields monitored in 2008 were observed to have greater flow rates and denser stands than the fields monitored in 2007. These differences in hydrology and crop density may explain some differences in trends between years do not explain differences observed within years.

5.3.2 Biogeochemical relationships

The complexities of Hg cycling can be explained in part by relationships of various forms of mercury with various forms of sulfur, iron, manganese, and DOM, all of which are redox-active constituents. With regard to DOM, both quantity (concentration) and quality (composition) may be important to THg and MeHg cycling (e.g. **Barkay et al., 1997; Haitzer et al., 2003; Ravichandran, 2004**).

5.3.2.1 Sulfur

Sulfate-reducing bacteria (SRB) are thought to play a major role in methylation of mercury in many environments (**Compeau and Bartha, 1984; Benoit et al., 2003**). Because sulfate (SO_4) was added to the white rice and wild rice fields as part of fertilizer applications, possible effects on Hg cycling were investigated. Because evapoconcentration affected all solutes, chloride (Cl) concentrations were used as a natural tracer to understand the degree of this effect. The ratio SO_4/Cl was higher on the white rice and wild rice fields relative to the fallow fields which did not receive fertilizer (**Figure 5.15**). The temporal trend on all irrigated fields during the summer months was toward lower values of SO_4/Cl . One explanation for the observed decrease in SO_4/Cl during the period June through September 2007 is the reduction of SO_4 by SRB. During late February, 2008, a series of water samples taken from white rice fields showed marked decrease in SO_4/Cl (**Figure 5.15**).

In some situations, stable isotopes of sulfur can provide a tracer both for sulfate-reduction processes as well as for sources of sulfur in hydrogeochemical systems (e.g. **Seal et al., 2000**). During periods of active sulfate reduction, the ratio $^{34}\text{S}/^{32}\text{S}$ (expressed as $\delta^{34}\text{S}$ relative to the reference standard Vienna Cañon Diablo Troilite or VCDT) becomes enriched in residual sulfate because SRB preferentially reduce ^{32}S relative to ^{34}S . The end-member fertilizer products used on the white rice and wild rice fields had $\delta^{34}\text{S}$ values ranging from 1.2 to 8.3 permil VCDT (**Appendix 3, Table A3-8**). The fertilizers were applied in mixtures such that the material applied to each field had $\delta^{34}\text{S}$ values ranging from 2.5 to 4.0 permil VCDT (**Figure 5.16**). Values of $\delta^{34}\text{S}$ in sulfate of input water ranged from about -2 to +2 permil. Aqueous sulfate from numerous water samples from field centers and outlets had $\delta^{34}\text{S}$ values greater than 4.0 permil (**Figure 5.16**), indicating that sulfate reduction was active. A significant correlation ($p < 0.001$) was found between $\log(\text{SO}_4/\text{Cl})$ and $\delta^{34}\text{S}$ for all water samples (**Figure 5.16**), with a Spearman rank order correlation coefficient (r_s) of -0.74. This correlation was considerably stronger on two individual fields, W32 and F66, where r_s values were -0.87 and -0.96, respectively (**Figure 5.17**). These data provide additional evidence that SRB were actively removing sulfate from the water column. Furthermore, it is unlikely that interactions between sulfate and plants are responsible for the variations in aqueous $\delta^{34}\text{S}$, because isotope fractionation during plant uptake of sulfate is minimal (**Trust and Fry, 1992**).

Because SRB have been frequently mentioned in the literature as the main cause of Hg methylation, the relations between SO_4/Cl , $\delta^{34}\text{S}$ and u-MeHg concentration are of interest. Plots of $\log(\text{SO}_4/\text{Cl})$ vs. $\log(\text{u-MeHg})$ (**Figure 5.18**) and $\delta^{34}\text{S}$ vs. $\log(\text{u-MeHg})$ (**Figure 5.19**) show poor correlations ($R^2 = 0.13$ and 0.20 , respectively). Working with data for individual fields for plots similar to those in **Figure 5.18** and **5.19**, R^2 values were universally less than 0.5 . These analyses suggest that SRB activity explains less than half of the variability in u-MeHg. It is important to consider that the fields are not closed systems, in that mass transfer between geochemical reservoirs (i.e. sediments, pore water, surface water, biofilms, etc.) is likely occurring to some extent. This is true both for sulfur species and MeHg, for which production and consumption are co-occurring and are not distinctly tied to one particular reservoir. Therefore one would not expect a perfect correlation in plots such as **Figures 5.18** and **5.19** even if SRB were the dominant process in u-MeHg production. These results are consistent with the conclusions from the sediment and pore water analyses (**Section 6**), which suggest that microbial reduction of iron (and perhaps also manganese) may be important in the study area.

5.3.2.2 Iron (Fe) and Manganese (Mn)

Because iron-reducing bacteria (and possibly manganese-reducing bacteria) also have been identified as contributors to mercury methylation (**Fleming et al., 2006; Kerin et al., 2006**), the relations between filtered iron (f-Fe), filtered manganese (f-Mn), and f-MeHg are also of interest. In the circum-neutral pH range for the surface waters in this study, f-Fe is likely to occur primarily as Fe(II) and f-Mn as Mn(II) because the more oxidized forms of Fe and Mn are relatively insoluble. Fe(II) and Mn(II) represent the end products of iron-reduction and manganese-reduction reactions, respectively. Measuring their concentration in surface water represents an indication of the extent to which Fe reduction and Mn reduction are taking place. Time series plots of f-Fe and f-Mn concentration (**Figure 5.20**) indicate that both of these metals were higher in concentration during the *early winter* and *late winter* sampling periods compared with the *summer irrigation season*. This suggests a flux of reduced species from the soils during winter flooding. The plots of f-Fe vs. u-MeHg (**Figure 5.21A**) shows a relatively weak positive correlation ($R^2 = 0.20$, Spearman rank order correlation = 0.492), whereas the plot of f-Mn vs. u-MeHg (**Figure 5.21B**) shows a relatively stronger correlation ($R^2 = 0.52$, Spearman rank order correlation = 0.718). Analysis of correlation between f-Mn vs. u-MeHg for specific field types indicates a stronger correlation for wild rice (**Figure 5.22A**, $R^2 = 0.58$) and fallow fields (**Figure 5.22B**, $R^2 = 0.68$). Because $\log(\text{f-Mn})$ and $\log(\text{f-MeHg})$ are normally distributed for these individual field types, but $\log(\text{f-Mn})$ is not normally distributed for the full data set, the non-parametric Spearman rank order correlation is more appropriate. These results indicates that f-Mn potentially explains more than half of the variation in f-MeHg in selected wetland types, and suggests the hypothesis that Mn-reducing bacteria may play a role in Hg methylation, perhaps to a greater extent than Fe-reducing bacteria. **Gill (2008b)** showed significant correlations between MeHg and dissolved Fe and Mn in pore water from two tidal marshes in the Delta, Little Break and Mandeville Cut. Additional work on distribution of Mn species in pore water and sediment, as well as microbial assays to demonstrate the presence of Mn-reducing bacteria, would be needed to demonstrate this hypothesis.

5.3.2.3 Organic Matter (OM)

Relationships between organic matter and mercury were highly variable in both space and time. For the ease of comparison, the analysis of the relationship is separated into two temporal scales: seasonal and diel.

5.3.2.3.1 Seasonal scale

Aqueous THg concentrations were closely related to DOC concentrations but the relationships varied across three distinct periods of field conditions (**Figure 5.23**). The relationship between f-THg and DOC during the first 30 days following the initial irrigation of the rice fields was poor. This poor relationship was likely a result of THg partitioning to suspended particles or algal uptake as u-THg was strongly related with DOC during this period (**Figure 5.24**). The linear least-squares regression between f-THg vs. DOC was strong throughout the growing season and into the winter during normal flow-through conditions prior to the regional flooding of the YBWA by Cache Creek (**Figure 5.23**; $R^2 = 0.66$). Finally, a strong relationship between f-THg and DOC was also observed following the flood of the Bypass, but THg was elevated relative to DOC during this period resulting in a different regression slope (**Figure 5.23**).

The relationship between DOC and f-MeHg was poor because both MeHg and DOC concentrations were highly variable within and between fields in the YBWA (**Figure 5.25**). However, a strong relationship was observed between DOC and f-MeHg in the seasonal and permanent wetlands although the relationship was markedly different after the regional flooding of Cache Creek (**Figure 5.26**). The relationship between DOC and f-MeHg in the permanent wetland was strikingly similar to that observed in a Delta tidal wetland, with both wetlands having nearly identical linear least-squares regression slopes (**Figure 5.27**). This may indicate a similar fundamental driving process in the permanent wetland as the tidal wetland with the difference in intercept being the result of differences in background conditions in each system.

DOM character appeared to be less important than concentration in relation to Hg cycling over the seasonal time-scale of this study. No strong relationships were observed between measurements of DOM character and either THg or MeHg across sites or seasons. One explanation for this result is that DOM and Hg are both subjected to extreme cycling in these low-flow, shallow water systems that disconnects them from the dominant processes that control them in other habitats where the biogeochemical controls on the production of MeHg and DOM are more tightly linked. The character of the DOM in this study appeared to be a result of extensive production and processing within the water column (via algal processing and photochemical reactions) more than the result of different sources (sediment vs. algal). It is likely to be similar for Hg and MeHg speciation.

In contrast to DOM character, particulate organic matter (POM) character appeared to have an impact on Hg cycling. MeHg in suspended particulates was very high with all concentrations exceeding 7 ng g^{-1} , which is an order of magnitude greater than typical environmental levels (e.g. **Rudd 1995**). Relationships between aqueous concentrations of MeHg in the particulate fraction (measured by difference between unfiltered and filtered subsamples) and particle concentration and character were mixed. TSS and POM concentration did not appear to be related to particulate MeHg (data not shown); however, MeHg was related to algae-derived particles (**Figure 5.28**).

The relationship was dependent on field type with white rice and fallow fields having the highest MeHg-to-algae ratio followed by wild rice and the permanent wetland with the lowest (**Figure 5.28**). This trend in MeHg-to-algae ratio corresponds well with biota Hg concentration trends across fields reported in **Section 8** of this report, potentially linking water column processes with Hg contamination in consumer organisms.

The importance of solid-phase OM to Hg cycling was further expressed in the winter period. Within the winter period, the amount of plant residue, or detritus, remaining on the fields in December and February was closely related to the ratio of MeHg (outlet/inlet) across field types and blocks (**Figure 5.20**; also see **Section 7**: plant interactions). The greater degree of scatter in February is likely due to uncertainty in the inlet water concentrations following the regional flooding of Cache Creek and any impacts the flooding had on resetting the relationship between the soils, detritus and water columns. This suggests that MeHg production in the winter season is largely driven by the amount of readily available organic matter for stimulating the microbial activity that produces MeHg (see **Sections 6 and 7**).

5.3.2.3.2 Diel scale

The relationships between DOM and MeHg differed markedly between seasonal and diel time-scales. Diel trends in MeHg were observed to differ greatly between fields but were much more tightly coupled to DOM character than over the seasonal timescale. MeHg concentrations were most closely related to ChlA fluorescence (**Figure 5.30**) and the fluorescence index of the DOM (FI) across all sites (**Figure 5.31**). The relationship between MeHg and ChlA is dominated by W65 which had the greatest magnitude and range in ChlA fluorescence (**Figure 5.30**). In contrast, the FI varied over the diel cycle in three of the four sites. In 2007, MeHg concentrations were positively correlated with FI, indicating higher MeHg concentrations corresponded with more algal or microbial DOM, whereas in R20 in 2008, MeHg concentrations were negatively correlated with FI, which suggests MeHg increases were more related to terrestrial DOM (**McKnight et al., 2001**). These results indicate the potential for different MeHg sources for diel trends with algal cycling likely driving MeHg diel trends in W65 and soil exchange with the water column likely driving the trend in R20.

Alternatively, photodemethylation may play a pivotal role in the MeHg diel trends in the fields (see **Section 9**: photodemethylation). Coincident decreases in MeHg and FDOM were observed in both the bottle experiments and *in situ* measurements. FDOM, an indicator of DOM photobleaching (**Frimmel 1998 a,b; Del Vecchio and Blough, 2002**), decreased with increasing radiation for all fields in the bottle experiments, and all fields except field W31 and part of the deployment in field R64 (when grab samples were collected) for the *in situ* measurements (**Figure 5.32**). Although there was not a direct relationship between MeHg concentration and FDOM, the MeHg/THg ratio was related to the carbon normalized fluorescence (FDOM/DOC) across the three fields where FDOM changed with photoexposure (**Figure 5.33**).

The absence of measurable MeHg diel trends in fields R64 and W31 is difficult to explain given the available data. All fields had similarly extreme weather conditions and relatively constant inorganic water chemistry. Optical measurements collected *in situ* revealed that field R64 optical measurements changed over the diel cycle, just not during the period of MeHg sampling (**Figure 5.32**). Furthermore, the Tedlar bags deployed at R64 showed changes in DOM

over the period of photo-exposure (especially S_r , HI). Perhaps shading was not equal across all sites as spot measurements of leaf area indices (LAI) suggested (see **Section 7**). Qualitative field observations suggest that W65 probably had the highest photoexposure due to poor canopy development in large areas of the field not included in the LAI assessment. Qualitative observations would support W31 having the greatest shading; however, measurements of PAR penetration through the canopies and water columns conducted in 2008 showed little difference between fields R20 and W31 ($22\% \pm 9\%$ vs $29\% \pm 21\%$, respectively). Perhaps differences in hydrology impacted the potential diel trends as higher flow rates in a field could limit the impact of photobleaching by reducing residence time and the cumulative photoexposure of DOM. The field with the strongest diel cycle, W65, had the lowest flow rate during the deployments. Also, some optical measurements of DOM character suggested W65 had more overall photoexposure ($S_{r_{UV-vis}}$, HI); however, these optical measurements are not merely measures of photoexposure but also of DOM source which complicates interpretation without supporting ancillary measurements.

Results from the bottle experiment suggest that DOM from fields R20 and W65 monitored in 2008 (which had similar properties as W64, monitored in 2007) were more susceptible to photoexposure than field W31 (2008), suggesting that DOM character may play a role in overall diel cycling as well. Further research is necessary to address these potential mechanisms driving diel trends. Another explanation for the differences in the trends observed in 2007 and 2008 was that the measurements in 2007 were made in the southern fields which received relatively clean irrigation water from the Toe Drain whereas the fields measured in 2008 were in the north unit which received a higher proportion of recycled agricultural drain water that had higher MeHg concentrations in the irrigation water and may have suppressed the diffusional exchange between soil and water column, thus minimizing MeHg exchange mechanisms responsible for diel trends.

The strength of observed relationships suggests that algal activity was the greatest driving force for diel trends in MeHg in field W65; however, there are some perplexing aspects to this hypothesis. First, the maximum chlorophyll measurements would not normally be expected during the night. Potential explanations include: 1) the algae migrated from the benthos to the water column during the night and back to the sediments during the day to escape extreme environmental conditions such as low dissolved oxygen in the sediments at night or high temperatures and extreme solar radiation in the water column or 2) bioturbation caused by migrating invertebrates and feeding by zooplankton may have elevated chlorophyll in the water column at night. Perhaps the most important difference between fields that may have impacted algal activity was the application of herbicides. W65 was the most pristine of the fields studied, having not received herbicide in several years whereas the white rice fields receive several applications during the growing season and W31 had received herbicide applications the previous year when the field was used for white rice production. The application of herbicides would negatively impact the benthic algal community which may impact both the DOM and the algal activity. Reduced benthic ChlA was observed in the white rice fields when compared to W65 in 2007 (see **Section 7**).

The importance of understanding diel variations in these systems cannot be overstated. The disconnect between diel-scale and seasonal-scale relationships may indicate a decoupling of the mechanisms over time because of different rates of production and degradation, which merely

exposes the limitation that seasonal-scale sampling is insufficient for understanding Hg cycling. Furthermore, diel variations in MeHg concentration provide a potential large source of error in loads assessments depending on the time of sampling for each field. In fields where diel variations occur, early morning sampling would bias MeHg loads high whereas late afternoon sampling would bias loads low - assuming diel variations are caused by processes occurring within the fields such as photodemethylation and biological (algal) forcings which may not be equal for all fields. A need to better understand the processes that control diel cycling of MeHg in different systems and managements is essential to identifying optimal representative sampling strategies and may also provide insights to mitigations strategies for MeHg by identifying source and loss mechanisms that may be manipulated for MeHg control. The evidence for possible biological impacts on the diel trends of MeHg also provides potentially vital information for the entry of MeHg into the food web. If there is active movement of algae into the sediment, which is the primary source of MeHg, that would likely increase MeHg movement into the pelagic food web as rates of MeHg movement would likely increase compared to diffusive movement from the soil to water column. Also the diel pattern of possible algal movement and MeHg concentrations could affect biota differently through different temporal or event-based feeding patterns (e.g. **Krumme et al., 2008**).

5.3.3 Loads

5.3.3.1 *General trends*

Loading rates of MeHg in the YBWA fields differed greatly over both space and time. There was a wide range in area-normalized average daily export rates ranging from $-195 \mu\text{g m}^{-2} \text{d}^{-1}$ in field F20 during the summer irrigation period to $+310 \mu\text{g m}^{-2} \text{d}^{-1}$ in field R64 in winter (**Figure 5.34**). The most prominent difference was between the summer and winter seasons. Differences were observed between field blocks, type and management within seasons. For this reason, data analyses were performed within each season to explore the dominant controlling processes leading to the differences in MeHg loadings in the differently managed fields of the YBWA.

5.3.3.2 *Summer irrigation*

Within the summer irrigation season, there was a significant difference ($p < 0.01$) in MeHg loadings between field units (north versus south) as the northern fields acted as MeHg sinks whereas the southern fields acted as sources of MeHg (**Figure 5.34**). The driver for this pattern is likely the irrigation source water because the northern fields' irrigation source water was higher in MeHg concentration than the southern irrigation source water leading to a greater enhancement of MeHg in the southern fields (**Table 5.6**). The two fields with net MeHg surface water losses, F20 and R31, received a large portion of their irrigation water from the Davis Drain, which had high MeHg concentrations during the mid- to late-summer irrigation period. The other fields received irrigation water dominated by Toe Drain water which had consistently lower MeHg concentrations throughout the summer period compared to the Davis Drain (see **Section 4**: hydrology). The load losses from transpiration were calculated according to the fields' mean concentrations and the percolation rates of water into the soil from plant water demand according to the water balance of the conservative tracers (see **Section 4**: hydrology). The ultimate fate of the MeHg percolated into the soil via transpiration demand is unknown but may build up in the soil strata, be taken up into plant components or possibly converted to Hg(0) and released to the atmosphere. Evidence exists for soil build-up (see **Section 6**: sediment) and plant uptake (see **Section 7**: plant interactions) supporting the total imbalance for the period which

points towards net MeHg production of about 1 to 1.5 $\mu\text{g m}^{-2} \text{d}^{-1}$ produced in the fields, except F20 and PW which remained net sinks for the period (**Table 5.7**). Actual benthic flux from sediment to the water column, however, was not measured, so this estimate represents a potential flux.

We propose three mechanisms responsible for the trends observed during summer. First, the source of MeHg to the water column is assumed to be at least partially dependent on diffusion from the soils and into the water column. In the northern fields, the relatively high concentration of MeHg present in the irrigation supply water reduced the diffusional gradient of MeHg from the soils into the water column compared to the low MeHg concentration irrigation supply in the southern fields. Therefore, the MeHg flux from soil to water column would be greater in the southern fields than in the northern fields. In fact, the concentrations in the Davis Canal water were high enough in mid-summer to potentially promote diffusion from the water column into the soil. This mechanism also explains the relatively low MeHg concentrations in the permanent wetland (PW). Because the PW remains flooded throughout the year, diffusion gradients are minimized by the absence of the wet-dry cycle of flooding and draining and by the presence of a larger ratio of water volume to sediment area than the agricultural fields. The second mechanism we propose is a MeHg loss term: photodemethylation. In the fields with higher irrigation MeHg concentrations, more photodemethylation would be acting on the irrigation waters as the same MeHg coming into the field would be exposed to solar radiation throughout its residence time in the field whereas the fields where MeHg is diffused from soil to water column, there would be a lower solar radiation exposure rate.

The loss of MeHg by photodemethylation is further supported by the differences in loss rates within the blocks. The greatest loss rates in the northern block occur on the fields with the greatest residence times and thus greatest exposure to solar radiation (F20>R31>W32). The third mechanism that would contribute to summer losses of MeHg across the fields is particle settling. The higher concentrations of inlet waters would lead to greater particle loss across the fields.

Differences between fields were multifaceted. The management on F20 turned out to be optimal for MeHg removal with high inlet concentrations and minimal outlet flow following a long residence time on the field. The wild rice field monitored in 2008 (W32) had the lowest loss rate because the majority of the MeHg export from W32 occurred during the harvest operations. Wild rice requires a wet harvest to optimize harvest yield but this disturbs the soils such that MeHg concentrations increased markedly. During the 2007 harvest, outlets were allowed to flow during the operations thus greatly increasing outlet loads during and following this activity. Within the southern unit, the agricultural fields were all net sources of MeHg (F66>R64>W65). The MeHg loss observed in F20 was not reflected in F66, which showed the highest MeHg export rate in the southern unit. However, F66 acted as a MeHg sink for most of the summer period except for a large export due to the final drainage at the end of the summer period (**Figure 5.35**). The high export from F66 may be attributed to high bird use in the field, particularly a large pelican colony. If the management of W65 and R64 are taken into account, F66 loads were even higher relative to the other agricultural fields. W65 was wet harvested in 2007, thus increasing the outlet loads markedly during those operations compared to pre-harvest when there was a net MeHg loss in the field. The white rice field, R64, was drained in mid July 2007 for herbicide application, thus also increasing the outlet loads relative to F66.

5.3.3.3 *Winter*

The trends in the winter season were very different from those in the summer irrigation period (**Figure 5.34**), due in part to different hydrologic patterns, as summarized in **Section 4.3.2**. The absence of percolation due to transpiration demands and photodemethylation lead to a strong connection between MeHg concentration ratios and loads. The white rice fields were clearly the greatest exporters of MeHg in the winter, mirroring the MeHg production fueled by plant residues during this period (**Figure 5.34**; also **Section 7**). With the assumption of no MeHg loss from the water column due to transpiration-driven percolation, the total imbalance suggests higher MeHg production in the white rice fields and relatively low MeHg production in the wild rice fields (**Table 5.8**). The seasonal wetland (SW) shows a similar net MeHg production ($1 \mu\text{g m}^{-2}$) as in the white rice fields and all the agricultural fields in the summer period. The relatively low export from field W32 was due to the backing up of Green's Lake, which limited exports from this field and increased imports onto the field and was not a result of typical management conditions.

Unfortunately, the study design was focused on the irrigation period and water sampling was sparse during the winter period making interpretation difficult and limiting our ability to evaluate the dominant processes occurring during that period. Nonetheless, it appeared that the white rice fields produced the greatest amount of MeHg due to drying of fields for harvest operations, ample plant residue at flood-up and low photodemethylation and transpiration post-flooding for winter irrigation – all of which promote enhanced methylation (see **Sections 6, 7, and 9**). The seasonal wetland (SW) also showed high MeHg production in winter with ample plant residue, extended drying period, and relatively low transpiration, but water management was limited to maintaining the water level of the wetland and, similar to F20, the flooding began early in the season while the rice fields were still in the summer irrigation period such that the removal mechanisms dominating the summer loads in the rice fields discussed earlier might have an impact on the export from the seasonal wetland that would not have been observed in the white rice fields in the winter period. We note that our initial study design was to have “replicate” field types, but given water source differences and hydrologic management variation between fields, the pairs of agricultural fields with similar land use did not serve as replicates.

5.3.3.4 *Comparison between seasons*

The stark differences in MeHg loadings between seasons in the agricultural fields were likely the result of the different mechanisms responsible for both production and loss within each season. Summer exports from the water column were split between surface outlets, percolation into the soil from transpiration demands, and photodemethylation. In contrast, both photodemethylation and transpiration losses from the water column were small in the winter. Transpiration was nearly zero in winter because most vegetation was either senesced or had been cut during the rice harvest, with little growth of new vegetation following harvest. Photodemethylation was much lower in winter because the solar intensity and duration was reduced to a fraction of that occurring in the summer. The lack of these two loss mechanisms in winter would permit greater diffusion of MeHg from the soils into the water column, thus increasing surface water MeHg concentration available for surface transport off the fields. The MeHg production rates also increased in winter despite lower temperatures because of the large reservoir of organic matter left on the fields in the form of plant residue (see **Sections 6 and 7**: sediment and plant interactions).

The annual average exports measured in this study fall into a similar range as other wetland and agricultural systems (**Table 5.9**). MeHg losses in rice systems have been observed elsewhere in recent Delta studies (**Fleck, unpublished data; Heim, unpublished data**).

Comparing the loads measured in this study to the *Delta Methylmercury Mass Balance* (Foe et al. 2008), the contribution from the entire 6,500 hectares of the YBWA would range from -1.3 g d^{-1} to $+0.2 \text{ g d}^{-1}$ in the summer depending on the distribution of management types and operations. In winter, the range would be from -0.06 g d^{-1} for permanent wetlands to $+2 \text{ g d}^{-1}$ for the white rice fields. The contribution from the entire 24,000 hectares of the greater Yolo Bypass would be -5 g d^{-1} to $+0.8 \text{ g d}^{-1}$ in summer and -0.2 g d^{-1} to 7 g d^{-1} in winter. It is not feasible to manage the entire YBWA or the entire Yolo Bypass as permanent wetlands so the loss of MeHg in winter is an unrealistic scenario. Furthermore, the winter numbers do not include any regionally flooded conditions when the greatest loadings are likely to occur in the Bypass. The higher end of the estimated loadings calculated in this study concur with previous speculation that the Yolo Bypass contributes a large proportion of the tributary MeHg loads to the Delta in winter (16.6 g d^{-1} total tributary load estimated by Foe et al. 2008). The range of winter loads is comparable to other sources in the Delta including total benthic flux and wastewater exports (0.6 g d^{-1} , each) whereas summer loads are more comparable to the smaller sources to the Delta such as urban runoff and precipitation inputs ($< 0.1 \text{ g d}^{-1}$). The annual average loads for the entire YBWA (-0.1 to 0.5 g d^{-1}) are similar in magnitude to the estimated agricultural return loads in the Delta Mass Balance (0.3 g d^{-1}).

Opportunities for improved management of MeHg loads from the Yolo Bypass are difficult to pinpoint because of the large variability in loads over both space and time observed in this study. Perhaps most important to note is that the annual loads from the Yolo Bypass are dominated by winter loads when agricultural operations are largely suspended. However, the impact of agriculture on the winter loads cannot be entirely ruled out. The highest winter loads were measured in the fields that had been used to grow white rice and where plant residues were left on the field and may have stimulated MeHg production. In contrast, wild rice fields had relatively low loading rates in winter, possibly due to the decomposition of plant residues during the period of no outflow. The holding of water on the field post-harvest reduced the export of MeHg from the fields but did not reduce *in situ* MeHg concentrations which may still lead to an ecological impact on birds and other animals that feed off the biota within the wild rice fields. Management of the fallow fields suggest a possible mitigation strategy for MeHg exports but the feasibility of this management option for widespread use in the Bypass is questionable. Another option for export management is the use of holding ponds or permanent ponds at the outlets of agricultural and seasonal wetlands. The ponds would remove suspended sediments through settling and promote photodemethylation in the drainage water prior to its release to downstream environments.

5.4 Summary and Conclusions

5.4.1 Summary

THg concentrations were high, exceeding 50 ng L^{-1} on 14 separate occasions, mostly following initial irrigation of rice fields and following the Cache Creek flood in February. On average 30% (stdev=20%) of the THg was in the filter-passing phase. This is of interest

because THg in the dissolved and colloidal phases have a greater potential for further cycling and transport than Hg bound to suspended sediments (e.g. Benoit et al. 2003). Concentrations of THg were positively correlated to DOC, iron, and manganese concentrations.

The multiple abiotic and biotic interactions affecting water MeHg concentrations and export are diagrammed in **Figure 5.36**. As shown in the synthesis table (**Table 5.10**), despite a marked increase in MeHg concentrations from inlets to outlets within individual fields in the YBWA wetlands, net exports of aqueous MeHg were minimal because outlet flows were small relative to inlets (approx 10%) because of evaporative losses and percolation into the soil to meet plant transpiration demands (see **Section 4**). MeHg was produced in the fields but concentrations in water were likely reduced *in situ* through a combination of loss mechanisms including photo-demethylation (see **Section 9**), percolation of surface waters into the soil (see **Section 4**), algal uptake, sedimentation, and uptake into plants (see **Section 7**) and bioaccumulation in the foodweb (see **Section 8**). The concentration of MeHg in irrigation source water appeared to control summer loads via two possible mechanisms:

- 1) source water MeHg concentrations affected the diffusion gradients from the soils to the water column, with high concentration source water depressing the diffusion of constituents upward, and

- 2) MeHg losses to photodemethylation, where the rate of photodemethylation is concentration-dependent with high concentrations having higher loss rates, especially in the case of source water where the exposure to solar radiation is maximized as the water crosses the field (see **Section 9**). Observed seasonal and diel trends illustrate the complex and highly variable nature of both Hg cycling and Hg-organic matter (Hg-OM) interactions in natural systems. Dissolved organic matter (DOM) and particulate organic matter (POM) appear to play significant roles in Hg cycling in ways that may impact both estimates of exports and uptake of MeHg into the foodweb.

5.4.2 Conclusions

MeHg cycling in the water column of the YBWA wetlands is variable and complex. Comparison with MeHg flux data from other wetland systems (**Table 5.9**), a wide range of imports and exports is shown within the YBWA complex. In this study the most important variable controlling net MeHg export from all the wetland types during the agricultural production period (summer) was the MeHg concentration of the irrigation source water. It appears that irrigation water already high in MeHg reduces the primary source of MeHg to the water column: diffusion of MeHg from the soil and promotes the losses: settling, advection into the soil via transpiration demand and photodemethylation. Summer net exports of MeHg could be minimized by utilizing irrigation water already high in MeHg if the option is available. However, the ultimate fate of MeHg in these fields is still in question. The impact of this approach only addresses net export concerns and does not consider impacts of MeHg in the rice grain (see **Section 7**) or resident biota on birds using the wetlands for foraging (see **Section 8**). Also, winter MeHg loads exceeded those of summer even though the period of regional flooding, when greatest loads would be expected, was left out of the calculations because it could not be reasonably estimated. The fields in winter were more consistent exporters across all field types and blocks. The magnitude of MeHg export appeared to be most dependent on the amount of plant residue present upon flooding, though a more extensive study of this mechanism is necessary to confirm this finding. Natural

seasonal flooding is difficult to manage but efforts to reduce outlet flow, increase particulate deposition and maximize exposure of the aqueous MeHg to sunlight, and finally to remove plant materials that may enhance MeHg formation prior to winter flooding could be utilized to minimize MeHg loads during winter.

6 Detailed Results for Sediment Methylmercury Production

The data reported in this section relates to summary **Section 3.3: Methylmercury Production in Surface Sediment**.

6.1 Introduction

Microbial processes are at the root of the Hg ‘problem’. If certain microbes did not readily convert inorganic mercury (Hg(II)) to toxic and readily bioaccumulated MeHg, the Hg problem in the San Francisco Bay – Delta region and elsewhere would be largely a non-issue. The fact is that select bacteria that are common in freshwater and saline environments do indeed readily carry out the Hg(II)-methylation process. Thus, understanding the key environmental factors that stimulate their activity, as well as make Hg(II) readily available to them, is at the heart of managing the Hg problem in aquatic systems everywhere.

Some general things are well established in terms of what controls the activity of Hg(II)-methylating bacteria and what controls the availability of Hg(II) to those bacteria, with reviews on the subject of microbial Hg(II)-methylation previously published (**Ullrich et al., 2001; Barkay and Wagner-Döbler, 2005; Merritt and Amirbahman, 2009**). First, only a comparatively small subset of all microbes can convert Hg(II) to MeHg, and most of these are sub-sets from two general classes bacteria, sulfate reducers and iron reducers, both of which are anaerobic (i.e. do not persist in the presence of oxygen) and heterotrophic (i.e. require small organic substrates for energy and growth). The role of sulfate reducing bacteria in the Hg(II)-methylation process has been recognized since the mid-1980’s (**Compeau and Bartha, 1985**), while the role of iron reducing bacteria in this process has only recently been established (**Fleming et al., 2006; Kerin et al., 2006**). A defining feature of all sulfate reducing bacteria is that they transfer electrons from the breakdown of organic substrates (the electron donor) to sulfate (the electron acceptor) and generate sulfide as an end-product (**Skyring, 1987**). Likewise, a defining feature of all iron reducing bacteria is that they transfer electrons from the breakdown of organic substrates to ferric iron (Fe(III), the oxidized form of Fe) and generate ferrous iron (Fe(II), the reduced form of Fe) (**Thamdrup, 2000**). Thus, in addition to universal effect of temperature on microbial rates, the availability of organic substrates and the above noted electron acceptors are key factors that mediate the activity of these bacteria, and thus MeHg formation in the environment.

A second important factor in understanding and managing the Hg problem is that only a comparatively small percentage of total Hg(II) in the environment is readily available for bacteria to methylate. However, measuring this fraction of bioavailable Hg(II), or even defining its exact chemical composition, remains both a challenge and an area of active research on the part of many mercury scientists. Since Hg(II) and reduced forms of sulfur (S) form very strong bonds, it is not surprising that Hg(II) availability for methylation has been shown to be affected by the relative availability of reduced sulfur compounds (**Benoit et al., 1999**) (REFS). In addition factors such as DOC concentration (**Benoit et al., 2001; Drexel et al., 2002; Waples et al., 2005**) (ref) and particle grain size (**Marvin-DiPasquale et al., 2009b**) have all been shown to play a role in mediating the relative ‘availability’ of Hg(II).

In recent years a number of mercury studies have been conducted that focus on reconciling the relative contributions of the activity of the resident Hg(II)-methylating microbial community

and the availability of Hg(II) to those microbes, both within the San Francisco Bay ecosystem (Grenier et al., 2010; Marvin-DiPasquale and Agee, 2003; Marvin-DiPasquale et al., 2003a, 2007, 2009a; Yee et al., 2008) and elsewhere (Marvin-DiPasquale et al., 2009b). Habitat type clearly plays a major role in determining if a particular location is a ‘hot spot’ for MeHg production or not, and wetland environments appear to be particularly efficient areas for Hg(II)-methylation (Lacerda and Fitzgerald, 2001; Marvin-DiPasquale, et al., 2003a; Zillioux et al., 1993). A national study of 20 U.S. watersheds concluded that wetland density was the leading determinant of MeHg productions within a study basin (Krabbenhoft et al., 1999), and that MeHg concentrations in water were correlated with Hg accumulation in fish (Brumbaugh et al., 2001). There are many reasons why wetlands may be effective zones for MeHg production, including that a) they are typically organic rich, thus supplying plenty of organic ‘fuel’ for microbial processes, b) they generally have anoxic sediment, which is important for both iron and sulfate reducing bacteria, c) there are generally emergent plants, the root zones of which have been shown to be important zones of MeHg production (Windham et al., 2009), and d) they often go through wetting and drying cycles that is thought to ‘reset’ the pool of available Hg(II) (Gilmour et al. 2004; Marvin-DiPasquale et al., 2009a).

A primary focus of the current project is to better understand what controls MeHg production in the various agricultural and non-agricultural wetland habitats that dominate the Yolo Bypass, and specifically in terms of what environmental factors regulate both the activity of the resident Hg(II)-methylating microbial community and the availability of Hg(II) to that community. This work is a follow-up to a recent study conducted within the YBWA and Cache Creek (including the settling basin), which focused exclusively on non-agricultural wetlands (Marvin-DiPasquale et al., 2009a).

6.2 Approach

6.2.1 Field and Laboratory Analyses

Three agricultural settings (white rice, wild rice and fallow fields) and two hydrologically distinct non-agricultural settings (seasonally flooded and permanently flooded wetlands) were studied as part of the sediment biogeochemistry portion of the larger YBWA Mercury Project. Prior to the initial sampling, fixed sites were selected for sediment collection and mapped with GPS. All were located near the field centers, as opposed to near hydrologic inputs and outputs, (Figures 3.3 and 3.4). During the first sampling event (June '07) two separate sites, approximately 100 meters apart, were sampled to examine within-field variability. Afterwards only one site was sampled per field, with the exception of permanent wetland PW5, which contained three sub-habitats (non-vegetated open-water (PW5-ow), cattail dominated (PW5-cat) and tule dominated (PW5-tule)), all of which were within 20 meters of each other. To increase the number of non-agricultural sites, and for comparison to PW5-ow, an extra open water permanent wetland site (PW2) was added later in the study (December '07).

There were six sediment sampling events (Figure 3.6), which included: June '07 (soon after initial fertilization and rice seed planting; white and wild rice fields and PW5), July '07 (all agricultural fields and PW5), August '07 (all agricultural fields and PW5), October '07 (seasonal wetland SW only; two weeks following initial flooding), December '07 (all sites including PW2), February '08 (all sites). This sampling schedule reflected the fact that only flooded fields were sampled for sediment Hg cycling studies (Figure 3.6).

In all cases, the surface 0-2 cm depth interval was sampled, with sediment transferred to glass mason jars, which were filled to the brim such that no trapped air remained. To slow all microbial processes and abiotic reactions, the jars of sediment were stored on ice until further sub-sampling at the USGS laboratory in Menlo Park. Sample holding times prior to sub-sampling under laboratory conditions ranged from 1 to 2 days.

To understand what factors control temporal and spatial mercury dynamics across the range of YBWA habitats studied, a large suite of both mercury-related and non-mercury parameters were measured (**Table 6.1**). Field parameters measured include sediment temperature, pH, and redox (oxidation-reduction) potential. Samples that were incubated to measure microbial rates of MPP and SR were incubated at the average field temperature (± 1 °C) for that sampling event. Further details describing field sampling techniques, subsequent sediment and pore water sub-sampling under anaerobic laboratory conditions, and individual analyses associated with all of the parameters listed in **Table 6.1** are published elsewhere (**Marvin-DiPasquale et al., 2008** and references within) and are described in the Quality Assurance Performance Plan (QAPP) developed for the current study (**U.S. Geological Survey et al., 2008**).

The one method not detailed in the QAPP is the one used for assaying ^{34}S isotope fractionation in pore water sulfate ($\delta^{34}\text{SO}_4^{2-}$), which is described briefly here. Pore water was initially sub-sampled into crimp sealed vials under anaerobic conditions by the USGS Menlo Park group (**Marvin-DiPasquale et al., 2008; U.S. Geological Survey et al., 2008**), preserved frozen, and subsequently shipped frozen to the Denver, CO, USGS facility. Sample preparation was conducted according to previously published methods (**Carmody et al., 1998**). Upon thawing, samples were acidified with HCl to a pH of 3-4, then stripped of dissolved sulfide with nitrogen gas. Samples were then diluted with deionized water and dissolved SO_4^{2-} was precipitated as BaSO_4 . The precipitate was filtered onto 0.45 μm cellulose acetate membrane filters, dried at 50° C, and transferred into borosilicate glass vials until further processing. Precipitate subsamples (ca. 1.5 mg) were transferred into 5 x 9 mm tin capsules, amended with V_2O_5 , and crimp sealed. Samples were then combusted and analyzed for $\delta^{34}\text{S}$ according to methods of **Giesemann et al. (1994)** using a Costech Analytical Inc. elemental analyzer (model ECS4010) coupled to a Thermo-Finnigan Delta Plus XP mass spectrometer operated in continuous flow mode. Stable isotope compositions are expressed in delta (δ) notation:

$$\delta = (R_{\text{sample}} / R_{\text{standard}}) - 1 \quad \text{Equation 6.1}$$

where R refers to $^{34}\text{S}/^{32}\text{S}$. Values of $\delta^{34}\text{S}$ are expressed relative to Vienna-Cañon Diablo Troilite (V-CDT) with a precision of $\pm 0.2\text{‰}$. Samples are normalized to the V-CDT scale using internationally accepted standards (IAEA-SO-6 = -34.1‰ , NBS127 = 21.1‰).

6.2.2 Data analysis

The MeHg production potential (MPP) rate was calculated as a pseudo-first order reaction:

$$\text{MPP} = \text{Hg(II)}_{\text{R}} - \text{Hg(II)}_{\text{R}} * \text{EXP}(-k_{\text{meth}} * t) \quad \text{Equation 6.2}$$

Where: Hg(II)_{R} is 'inorganic reactive mercury' and a measure of the pool of inorganic Hg(II) that is available to microbes for Hg(II) -methylation; k_{meth} is the radiotracer derived $^{203}\text{Hg(II)}$ -methylation rate constant' and a measure of the activity of the sediment Hg(II) -methylating

community; t equals time (set to 1 day); and EXP indicates exponent (base e). At moderate to low values of k_{meth} , **Equation 6.2** approximates:

$$\text{MPP} = \text{Hg(II)}_{\text{R}} \times k_{\text{meth}} \quad \text{Equation 6.3}$$

Data was analyzed for both temporal and spatial trends using S-Plus® 7.0 (Insightful Corp.) statistical software. Type II error probability was set at $p < 0.05$ for all statistical tests. Analysis of variance (ANOVA) was used to compare three primary paired relationships: a) agricultural vs non-agricultural fields, b) northern vs southern block fields (agricultural fields only), and c) growing season [June, July and August data] vs the post-harvest period [December and February data] (agricultural fields only).

6.3 Results

6.3.1 Mercury Parameters

Key mercury parameters (THg, Hg(II)_{R} , k_{meth} , MPP, and MeHg) are plotted by ‘habitat type’ and in ‘time series’ to best illustrate both spatial and temporal data trends (**Figures 6.1** thru **6.5**). Summary statistics (mean, standard error and median) for individual fields are given in **Table 6.2** for all mercury and non-mercury parameters. ANOVA results for tests of spatial and temporal differences between paired groupings (agricultural vs non-agricultural fields; northern vs southern agricultural blocks; growing vs post-harvest season) are given in **Tables 6.3** thru **6.5**. While sediment THg concentration varied little over time at any given site, there were differences among habitat types (**Figure 6.1**), with agricultural fields having significantly more THg in surface sediments than did non-agricultural fields (**Table 6.3**). This difference in THg concentration among habitat types was unexpected, and was at least partially due to an east-west gradient in THg, with concentrations increasing approximately 4-fold overall from east to west (**Figure 6.6**). However, there was no significant east-west gradient in the data when grouped solely by agricultural or by non-agricultural habitat type (not shown). Instead there appeared to be a marked increase in overall THg concentration west of -121.603 degrees longitude, with a more than 2-fold higher average THg concentration in the agricultural field (west) grouping than for the non-agricultural field (east) grouping (**Table 6.3**). Further, the overall range of THg concentrations in the agricultural (western) fields was significantly larger than the range of concentrations observed for the non-agricultural fields (**Figure 6.6**). There were no significant differences in THg concentration among agricultural fields grouped by block (northern vs southern; **Table 6.4**) or by season (growing vs post-harvest, **Table 6.5**). For individual fields, median THg concentrations ranged 3-fold, from 124 ng g⁻¹ (PW2) to 382 ng g⁻¹ (white rice field R31), across all sampling dates (**Table 6.2**).

Average values of k_{meth} were significantly higher in non-agricultural wetlands compared to agricultural fields, across all sampling dates (**Table 6.3**, **Figure 6.2A**). After initially rising through the June through August growing season, k_{meth} values in most fields decreased during the period surrounding the rice harvest (**Figure 6.2B**), when agricultural fields were drained between early September thru mid-November (duration varied for individual fields; see **Figure 3.6**). Values of k_{meth} then increased again between early December and February, particularly for the white rice fields. There were no significant differences in k_{meth} values among agricultural fields grouped by block (northern vs southern; **Table 6.4**) or by season (growing vs post-harvest, **Table 6.5**). For individual fields, median k_{meth} values ranged 200-fold, from 0.003 d⁻¹ (white rice field R31) to 0.52 d⁻¹ (PW5-cat), across all sampling dates (**Table 6.2**).

Both spatial and temporal trends in sediment Hg(II)_R concentration were largely the mirror opposite of what was seen for k_{meth} . Agricultural fields had significantly higher Hg(II)_R concentrations than did non-agricultural wetlands (**Table 6.3, Figure 6.3A**). During the June through August growing season, Hg(II)_R concentrations decreased in agricultural fields, followed by an increase during the September thru November periods the fields were drained, and finally a decrease again (post-reflooding) between early December and February (**Figure 6.3B**). There were no significant differences in Hg(II)_R concentrations among agricultural fields grouped by block (northern vs southern; **Table 6.4**) or by season (growing vs post-harvest, **Table 6.5**). For individual fields, median Hg(II)_R concentrations ranged 46-fold, from 0.14 ng g^{-1} (SW) to 6.4 ng g^{-1} (fallow field F66) across all sampling dates (**Table 6.2**).

Since MPP is a function of both k_{meth} and Hg(II)_R , the opposing spatial and temporal trends of these two parameters (**Figures 6.2 and 6.3**) resulted in overall similar trends in calculated MPP rates (**Figure 6.4**), with no significant difference between agricultural and non-agricultural sites (**Table 6.3**), by block (**Table 6.4**) or by season (**Table 6.5**). For individual fields, median MPP rates ranged 22-fold, from $5.4 \text{ pg g}^{-1} \text{ d}^{-1}$ (PW2) to $120 \text{ pg g}^{-1} \text{ d}^{-1}$ (PW5-CAT), across all sampling dates (**Table 6.2**).

In contrast to MPP, MeHg concentrations (and %MeHg) did show significant differences by both habitat type (agricultural fields > non-agricultural wetlands; **Table 6.3 and Figure 6.5A**) and by season (post-harvest > growing season; **Table 6.5 and Figure 6.5B**), but not by block (**Table 6.4**). Rice growing fields had the widest range of MeHg concentrations over the study period, although pooled by habitat type, fallow fields had the highest median MeHg concentration (**Figure 6.5A**). For individual fields, median MeHg concentrations ranged over 4-fold, from 0.65 ng g^{-1} (PW2) to 3.0 ng g^{-1} (wild rice field W65) across all sampling dates (**Table 6.2**).

6.3.2 Non-mercury parameters

Of the many sediment and pore water parameters measured during this study (**Table 6.1 and 6.2**), the ones that are discussed in detail below are the most relevant with respect to the ensuing discussion regarding what controls Hg(II) -methylation among the multiple habitat types studied.

6.3.2.1 Sediment Redox

Sediment ‘redox’ or oxidation-reduction potential (ORP) is a semi-quantitative and qualitative measure of the net impact of all competing chemical oxidation and reduction reactions occurring in the sediment aqueous (pore water) phase. When ORP probe measurements (in millivolts; mV) are corrected for the ‘reference’ half-reaction associated with hydrogen, redox is expressed in terms of E_h (in mV). Conditions of $E_h > 0$ are said to be ‘oxidized’, while those < 0 are said to be ‘reduced’. Sediment redox was measured both in the field at the time of sample collection, and once again in the laboratory at the time the mason jars of sediment were again sub-sampled under anaerobic conditions. This repeated measure gives some indication as to if sediment chemistry changed significantly during the intervening holding period. There was an average decrease in E_h of $-75 \pm 9 \text{ mV}$ ($n = 55$) between the time of field collection and laboratory sub-sampling (**Figure 6.7**), which is modest given the $> 430 \text{ mV}$ range in values (-80

to +353 mV) for the complete dataset of field measurements. Apart from this modest decrease in E_h during the 1-4 day holding period, the qualitative integrity of the sediment samples was verified to be preserved, as the plots for both field and laboratory E_h track each other very closely over the study period and by individual field (**Figure 6.7**).

Similarly, temporal changes in sediment redox at a given location indicate whether sediment chemistry is changing significantly throughout the year. Sediment redox changed dramatically throughout the study period in the agricultural fields, where in a pattern strikingly similar to that for $Hg(II)_R$ (**Figure 6.3B**), E_h decreased during the June through August growing season, then increased during the September thru November when the fields were drained, and finally decreased again (post-reflooding) between early December and February (**Figure 6.7**). There were significant habitat differences in E_h with agricultural fields more chemically oxidized and non-agricultural fields more chemically reduced (**Table 6.3**). While there was no significant north-south block effect for agricultural fields, there was a significant seasonal difference with the growing season being more reduced than the post-harvest period (reflooded) (**Table 6.5**), although this effect was only seen in the laboratory measurements, and not with the field collected E_h data.

6.3.2.2 Sediment Sulfur Chemistry

Microbial sulfate reduction (SR) rate varied by both site and season, with no consistent spatial or temporal trend (**Figure 6.8A**) among fields. However, a number of the agricultural fields showed a general rise in SR rates during the growing season, followed by a decrease during the draining period, and varied responses during the post-harvest winter. Site-specific median values ranging by a factor of 10-fold (6.9 to 69.4 $\text{nmol g}^{-1} \text{d}^{-1}$; **Table 6.2**). Most sites exhibited comparatively low rates throughout the year ($< 100 \text{ nmol g}^{-1} \text{d}^{-1}$), with the exception of PW5-ow, which exceeded 300 $\text{nmol g}^{-1} \text{d}^{-1}$ in July, and wild rice field W32, which exceeded 1200 $\text{nmol g}^{-1} \text{d}^{-1}$ during February (**Figure 6.8A**). There were no significant differences in SR rates among agricultural fields grouped by habitat (agricultural vs non-agricultural), by block (northern vs southern) or by season (growing vs post-harvest).

In contrast to SR rates, solid-phase TRS exhibited a similar seasonal pattern among all agricultural fields, which included an increase during the growing season, a decrease during the draining period, and an increase again during the post-harvest winter period (**Figure 6.8B**), a pattern which was mirror opposite of that for sediment redox (**Figure 6.7**). Both TRS and AVS (poorly crystalline FeS) were significantly higher (approximately 10-fold) in non-agricultural sites as compared to agricultural fields (**Table 6.3** and **Figure 6.8B**), with median TRS concentrations by site ranging 77-fold (1.2 to 93.4 $\mu\text{mol g}^{-1}$) and median AVS concentrations by site ranging 128-fold (0.4 to 53.9 $\mu\text{mol g}^{-1}$) (**Table 6.2**). No significant differences in TRS or AVS concentrations were found when data was grouped by block or by season.

Pore water sulfate concentration ($\text{pw}[SO_4^{2-}]$) was significantly higher (> 5 -fold) in agricultural fields than in non-agricultural wetlands (**Table 6.3; Figure 6.9A**). Similar to TRS, $\text{pw}[SO_4^{2-}]$ exhibited a similar seasonal pattern among most agricultural fields (**Figure 6.9A**). This pattern was the mirror opposite of TRS (and similar to sediment redox), including a decrease during the growing season, an increase during the draining period, and a decrease again during the post-harvest winter period. An exception to this general pattern in agricultural fields

was noted for wild rice field W65 and fallow field F66, in which $\text{pw}[\text{SO}_4^{2-}]$ appeared to rise during the growing season (**Figure 6.9A**). However, in the case of wild rice field W65, this was largely due to an overall increase in salinity in this field during that period, as evidenced by pore water chloride concentration data (not shown). Since chloride is a conservative element in the environment, affected almost exclusively by physical processes of dilution and evaporative concentration, normalizing sulfate to chloride concentration (i.e. calculating the sulfate-to-chloride ($\text{pw}[\text{SO}_4^{2-}/\text{Cl}^-]$) molar ratio) allows us to separate changes in sulfate concentration due to microbiological and abiotic chemical reactions, from those based solely on physical dilution or evaporative concentration (**Marvin-DiPasquale et al., 2003b**). Time series plots of $\text{pw}[\text{SO}_4^{2-}/\text{Cl}^-]$ ratio data (**Figure 6.9B**) more clearly show the relative changes in $\text{pw}[\text{SO}_4^{2-}]$ concentration due to microbiological and/or abiotic reaction, with field W65 also exhibiting a general decrease during the growing season. However, F66 was still shown to increase during this period, which is suggestive of the continued reoxidation of reduced-S compounds during the growing and draining periods. The significant decrease in the $\text{pw}[\text{SO}_4^{2-}/\text{Cl}^-]$ ratio between December '08 and February '09 for all agricultural fields suggests stimulated sulfate reduction during this period. Pore water sulfide concentration ($\text{pw}[\text{H}_2\text{S}]$) was uniformly low for all sites, rarely exceeding $2 \mu\text{mol L}^{-1}$ (**Table 6.2**), which suggests either reoxidation or precipitation into solid-phase Fe-S minerals. There were also no significant differences in $\text{pw}[\text{H}_2\text{S}]$ among fields grouped by habitat, by block or by season. The above results indicate comparable rates of microbial SR in the two habitat types, but a much higher degree of reduced sulfur preservation (and less reoxidation) in the non-agricultural wetland sites, most likely from the precipitation of H_2S with dissolved iron to form Fe-S minerals.

Pore water sulfate isotope data ($\text{pw}[\delta^{34}\text{SO}_4^{2-}]$; June thru December 2007 data only) sheds even more light on sulfur cycling across the habitats studied, as agricultural fields were significantly lighter isotopically (lower values) compared to non-agricultural wetlands (**Table 6.3**). This is consistent with generally more microbial SR in non-agricultural fields, as the process of SR tends to fractionate sulfate and sulfide such that the remaining (unused) pore water sulfate is enriched in the heavier ^{34}S isotope and the end-product reduced-sulfur (e.g. sulfide) is isotopically depleted in ^{34}S (Sharp, 2007). This trend is apparent in the positive correlation between SR rates and $\text{pw}[\delta^{34}\text{SO}_4^{2-}]$ (**Figure 6.10A**). Similarly, the negative correlation between the $\text{pw}[\text{SO}_4/\text{Cl}]$ ratio and $\text{pw}[\delta^{34}\text{SO}_4^{2-}]$ (**Figure 6.10B**) indicates that sites comparatively depleted in sulfate (also suggestive of enhanced SR) are enriched in $\delta^{34}\text{SO}_4^{2-}$. So while statistically significant differences in SR rates were not found between the two field types, the data suggests that overall there was a more $\text{pw}[\delta^{34}\text{SO}_4^{2-}]$ enrichment due to SR in non-agricultural fields, while agricultural fields spanned a much wider range of both SR rates and $\text{pw}[\delta^{34}\text{SO}_4^{2-}]$ enrichment factors (**Figure 6.10A**).

The $\text{pw}[\delta^{34}\text{SO}_4^{2-}]$ data also gives us some evidence as to the extent of reduced-sulfur reoxidation among the various habitat types. When reduced-sulfur compounds are reoxidized back to SO_4^{2-} , the isotopic signature of the resulting SO_4^{2-} is similar to the parent reduced-sulfur compound (i.e. isotopically depleted) (**Balci et al., 2007**). We note that the only instances of isotopically depleted $\text{pw}[\delta^{34}\text{SO}_4^{2-}]$ (values < 0) occurred exclusively in agricultural fields, and only at sites with high redox values ($\text{Eh} > +150 \text{ mv}$; **Figure 6.10C**). This suggests that there is a significant amount of reduced-sulfur reoxidation that occurs on agricultural fields, compared to non-agricultural fields. Further, during the post-harvest season (December data only),

agricultural fields exhibited significantly lighter $_{pw}[\delta^{34}\text{SO}_4^{2-}]$ values than during the June-August growing season (**Table 6.5**), indicating that this reoxidation takes place largely during the post-harvest season.

6.3.2.3 *Sediment Iron Chemistry*

While microbial Fe(III)-reduction was not directly measured, multiple iron pools were tracked throughout the study, and provide a dynamic picture of seasonal and spatial iron cycling. As the name implies, microbial heterotrophic Fe(III)-reduction describes the process by which certain bacteria can use organic carbon as an electron donor and various forms of ferric iron (Fe(III)) as an electron acceptor, thereby reducing Fe(III) to the ferrous (Fe(II)) form. Since a) some Fe(III)-reducing bacteria have been shown to form MeHg (**Fleming et al., 2006; Kerin et al., 2006**), b) multiple forms of Fe react with both S and Hg (**Hylander et al., 2000; Slowey and Brown, 2007**), and c) there is abundant total iron ($\text{Fe}_T = \text{Fe(II)} + \text{aFe(III)} + \text{cFe(III)} = 15.6 \pm 0.8 \text{ mg g}^{-1}$, average for all sites) in the YBWA study area, understanding Fe-biogeochemistry is key to understanding Hg cycling in this system.

One measure of the general activity of Fe(III)-reducing bacteria is the build-up of the Fe(II) concentrations over time. Agricultural fields exhibited large seasonal changes in both pore water and sediment Fe(II) concentrations (**Figures 6.11A and 6.11B**), with periods of Fe(II) increase observed during the June-August growing season and the December-February post-harvest season. In contrast, while non-agricultural areas often had higher Fe(II) concentrations, temporal changes in these were much less pronounced. The large drop in Fe(II) concentrations in pore water and sediment in the agricultural fields during the September-November field draining period coincided with the increase in sediment redox conditions (**Figure 6.7**), and thus likely reflects the abiotic reoxidation of Fe(II) back to Fe(III). Median Fe(II) concentrations across all sites ranged more than 160-fold (0.03 to 4.5 mg L^{-1}) in pore water, and only 3-fold (2.4 to 7.6 mg g^{-1}) in sediment (**Table 6.2, Figure 6.11**). Agricultural sites had significantly higher sediment Fe(II), than did non-agricultural sites (**Table 6.3**). Significant differences were not found for pore water Fe(II) based on habitat, nor for sediment or pore water Fe(II) for data grouped by block or by season.

Previous studies (**Lovley and Phillips, 1987a; Roden and Zachara, 1996**) have shown that amorphous (poorly crystalline) forms of Fe(III) (herein referred to as aFe(III)) are more readily available to Fe(III)-reducing bacteria than are more crystalline forms (herein referred to as cFe(III); e.g. crystalline goethite (αFeOOH), hematite (Fe_2O_3), Ferrihydrite ($\text{Fe}(\text{OH})_3$), lepidocrocite (γFeOOH), and magnetite (Fe_3O_4)). Average sediment aFe(III) and cFe(III) concentrations were significantly higher (> 7 -fold and 2 -fold, respectively) in agricultural fields, compared to non-agricultural fields, with cFe(III) concentrations being significantly larger (20X to $> 180\text{X}$, all sites) than aFe(III) concentrations (**Table 6.3, Figure 6.12**). There were no other significant differences for either Fe(III) species, grouped by either block or season. To the extent that aFe(III) is the preferred form of Fe(III) for microbial Fe(III)-reduction, due to increased surface area (**Roden and Zachara, 1996**), and that the aFe(III) concentration has been shown to be proportional to rates of microbial Fe(III)-reduction (**Roden and Wetzel, 2002**), the current data suggests that agricultural fields exhibit an overall higher rate of Fe(III)-reduction, than do non-agricultural fields (**Windham et al., 2009**).

6.3.2.4 Organic Carbon

Sediment total organic matter, as measured by %LOI, was generally constant with time and similar in magnitude among all sites, with the exception of vegetated non-agricultural sites (i.e. SW, PW5-CAT, PW5-TULE), which were somewhat more organic rich (**Figure 6.13, Table 6.2**). As a group, sediment in agricultural fields was slightly, yet significantly, less organic rich compared to non-agricultural fields (**Table 6.3**). There were no significant differences in sediment organic content for data group by block or season.

In contrast to whole sediment organic content, dissolved organic metrics (pore water DOC (pw[DOC] and pore water acetate (pw[Ac])) exhibited much more dynamic seasonal and spatial differences. While pw[Ac] is only a minor subset of the total pw[DOC] pool, it is a key indicator of substrates for heterotrophic bacteria (including sulfate and iron reducers), a low molecular weight end product of bacteria fermentation, and thus a good surrogate for the specific class of low molecular weight organic molecules that fuel microbial processes in sediment. There were there was a general rise on both pw[DOC] and pw[Ac] concentrations through the growing season, followed by a decrease during the field harvest and draining period (**Figures 6.14A and 6.14B**). There was no significant difference in the concentration of either pore water constituent when data was grouped by habitat (agricultural vs non-agricultural sites) or by block. However, pw[DOC] was statistically greater during the growing season across all agricultural fields (**Table 6.5**). Further statistical analysis indicated that among agricultural fields only, those planted with rice (white and wild) and which had decaying rice straw (post harvest), increased significantly in pw[Ac] concentration between the growing and post harvest season, while those that were held fallow during the study period, decreased in pw[Ac] between the growing and post-harvest periods (**Figure 6.15**).

6.4 Summary/Discussion

6.4.1 YBWA sediment MeHg concentrations in the larger ecosystem context

While wetlands in general are known to be important zones for MeHg production (**Zillioux et al., 1993; Rudd, 1995; St. Louis et al., 1996; Marvin-DiPasquale et al., 2003a**), there is very little known about the influence of land management and agricultural practices on the cycling of mercury in freshwater wetlands. The upper range of MeHg concentrations measured in surface sediments of the YBWA (this study; 75th-100th percentile range = 2.7 – 6.2 ng g⁻¹ dry wt.) are high compared to other reports of surface sediment MeHg concentrations made in a number of open-water locations throughout the San Francisco Bay system, including an extensive estuarine transect from the Guadalupe R. to the SFB-Delta (0.1-1.0 ng g⁻¹ dry wt., n = 52; **Conaway et al., 2003**), San Pablo Bay (< 1 ng g⁻¹; **Marvin-DiPasquale et al., 2003a**), the Frank's Tract region (SFB central delta; 75th-100th percentile range = 0.5-0.9 ng g⁻¹; **Marvin-DiPasquale et al., 2007**), the larger central SFB-Delta region (< 1 – 3 ng g⁻¹ dry; all data; **Heim et al., 2007**) and Englebright Lake (a Sierra Nevada foothill reservoir; range = 0.7-1.5 ng g⁻¹ dry; n = 12; **Alpers et al., 2006**). However, the YBWA MeHg concentrations are in the range of values measured in the Cosumnes R. region (freshwater) and its associated floodplain (75th-100th percentile range = 4-22 ng g⁻¹; **Marvin-DiPasquale et al., 2007**) and in the range of salt marsh settings in the central SFB-Delta (2-8 ng g⁻¹ dry; **Heim et al., 2007**), adjacent to San Pablo Bay (average = 5.4 ng g⁻¹ dry wt.; **Marvin-DiPasquale et al., 2003a**), and associated with the Petaluma R. (75th-100th percentile range = 4.0 – 14.5 ng g⁻¹ dry wt.; **Yee et al., 2008**). Thus, the

concentrations of sediment MeHg measured in this study are similar to other wetland settings (both freshwater and saline) measured throughout the larger San Francisco Bay system.

6.4.2 Controls on Methylmercury production

While the overall range of sediment MeHg concentrations in the YBWA are similar to other wetlands within the SFB watershed, large seasonal variations and differences among habitat types were observed for both MeHg concentrations (**Figure 6.5**) and MPP rates (**Figure 6.4**) in this study. To better understand what natural and land management actions controls these temporal and spatial variations, our focus is ultimately on what controls the activity of the Hg(II)-methylating community (i.e. k_{meth}) and the availability of inorganic Hg(II) to be methylated (i.e. Hg(II)_{R}), as these two terms control gross MeHg production (see **Equation 6.3**). Based on the literature and our previous research experience, we hypothesized that interactions with the biogeochemical cycles governing S, Fe and C chemistry would play a significant role in governing Hg cycling in the YBWA. The relevant interrelationships between these elemental cycles are brie discussed below.

Sulfate reducing bacteria (SRB) mediate the conversion of dissolved sulfate (SO_4^{2-}) to sulfide (H_2S), while iron reducing bacteria mediate the conversion of Fe(III) to Fe(II). Both sulfate reducing (**Gilmour et al., 1992; Jeremiason et al., 2006**) and Fe(II) reducing (**Mehrotra et al., 2003; Fleming et al., 2006; Kerin et al., 2006**) bacteria are known to carry out Hg(II)-methylation in freshwater sediments, although not all species within these two group have this capability (**King et al., 2001; Kerin et al., 2006**). Both microbial sulfate and iron reduction take place largely in sediments, typically under oxygen depleted conditions, and both are facilitated by bacteria that require suitable forms of organic C as the electron donor, as well as for cellular growth. Due to the thermodynamics of both processes, Fe(III)-reduction typically outcompetes SR for commonly used organic substrates such as acetate (**Thullner and Van Cappellen, 2007**). So it is common that when suitable forms of Fe(III) are available, microbial Fe(III)-reduction is active, and at the expense of microbial SR, at least in terms of commonly used organic substrates (**Lovley and Phillips, 1987b**). However, not all forms of Fe(III) are equally available to Fe(III)-reducing bacteria. Amorphous (poorly crystalline) forms of Fe(III) (i.e. aFe(III)) have more surface area and are more readily susceptible to microbial reduction, than are crystalline forms (i.e. cFe(III)) (**Roden and Zachara, 1996**). Thus, while Fe(III)-reducing bacteria can use both Fe(III) forms, they utilize cFe(III) much more slowly. Since electron acceptor availability is a key determinate as to which microbial groups are active at a given time or place, as aFe(III) becomes limiting, conditions for microbial SR become more favorable.

Reduced forms of both S and Fe can readily react to form a suite of solid phase reduced Fe-S minerals (e.g. FeS, FeS_2 , etc...), thus diminishing the concentration of either sulfide or Fe(II) (or both) in the dissolved phase, depending on which is in limited supply. Further, both dissolved and solid phase reduced sulfur compounds can form strong bonds with inorganic Hg(II) (**Benoit et al., 1999, 2001**) and MeHg (**Qian et al., 2002**). To the extent that Hg(II) is bound to various solid phase reduced-S compounds, it may be less available for Hg(II)-methylation (**Marvin-DiPasquale and Cox, 2007; Marvin-DiPasquale et al., 2009a, 2009b**). Thus, the presence, form and concentration of both S and Fe species exert a very strong influence on each other and on the Hg cycle.

In the current study, as with our previous research (**Marvin-DiPasquale et al., 2003a, 2007; Marvin-DiPasquale and Agee, 2003; Yee et al., 2008**), the activity of the resident Hg(II)-methylating community in sediment was assessed using the radioactive $^{203}\text{Hg}(\text{II})$ isotope derived k_{meth} parameter. If the community of sulfate reducing bacteria were the only microbial group involved in the Hg(II)-methylation process, we would expect to see a good correlation between k_{meth} and our independent parallel measure of microbial SR rates across all sites. While a significant positive linear relationship was found between these two parameters, microbial SR rates explained only 33% of the variability in k_{meth} values across all sites and dates of the YBWA dataset (i.e. linear regression $R^2 = 0.33$, data not shown). A much stronger relationship ($R^2 = 0.69$) was found when k_{meth} was regressed against the term $[\% \text{Fe}(\text{II})/\text{Fe}_T]$ (**Figure 6.16**), where Fe_T (total Fe) is the sum of all solid phase Fe species ($\text{Fe}(\text{II}) + a\text{Fe}(\text{III}) + c\text{Fe}(\text{III})$). While not a direct measure of Fe(III)-reduction rate, $[\% \text{Fe}(\text{II})/\text{Fe}_T]$ represents a measure of the percentage of all (measured) solid phase iron species that have already been reduced to Fe(II), presumably via microbial Fe(III)-reduction. We interpret that sites with low $[\% \text{Fe}(\text{II})/\text{Fe}_T]$ values as having a high potential for Fe(III)-reduction, as much of the Fe is still in the oxidized Fe(III) form. Conversely, high $[\% \text{Fe}(\text{II})/\text{Fe}_T]$ values would suggest sites with a lower potential for further Fe(III)-reduction, as much of the Fe(III) pool (includes $a\text{Fe}(\text{III}) + c\text{Fe}(\text{III})$) has already been converted to Fe(II). Since $a\text{Fe}(\text{III})$ is more readily available and always much lower in concentration than $c\text{Fe}(\text{III})$ (**Table 6.2, Figure 6.12**), we would also expect that as $[\% \text{Fe}(\text{II})/\text{Fe}_T]$ values increase, the actual rate of Fe(III)-reduction slows, as the remaining Fe(III) is in the less available crystalline form. Further, since Fe(III)-reduction is thermodynamically more favorable than microbial SR, sites with a high potential for Fe(III)-reduction (low $[\% \text{Fe}(\text{II})/\text{Fe}_T]$ values) would be expected to have a low potential for SR, and vice versa. Therefore, the $[\% \text{Fe}(\text{II})/\text{Fe}_T]$ metric also provides some measure of the geochemical conditions along a continuum of sites and dates that transition from those more favorable to Fe(III)-reduction (low $[\% \text{Fe}(\text{II})/\text{Fe}_T]$) to those more favorable for SR (high $[\% \text{Fe}(\text{II})/\text{Fe}_T]$) (**Figure 6.16**).

The distribution of data along the regression line indicates that for agricultural sites (white rice, wild rice and fallow fields), $[\% \text{Fe}(\text{II})/\text{Fe}_T]$ ranges anywhere from 5-60%, depending on the site and time (**Figure 6.16**). For non-agricultural fields $[\% \text{Fe}(\text{II})/\text{Fe}_T]$ ranges from 30-75% for most sites. For data grouped by these two habitat types, $[\% \text{Fe}(\text{II})/\text{Fe}_T]$ was statistically larger for non-agricultural sites compared to agricultural sites (**Table 6.3**). These results suggests that the agricultural fields are generally more poised for microbial Fe(III)-reduction, while the non-agricultural fields are generally more poised for SR. This is supported by the fact that there was significantly higher $a\text{Fe}(\text{III})$ and $c\text{Fe}(\text{III})$ concentrations in the agricultural sites (**Table 6.3**), since the concentration of $a\text{Fe}(\text{III})$ has been shown to be proportional to the actual rate of Fe(III)-reduction in wetland settings (**Roden and Wetzel, 2002; Bonneville, et al., 2004**). However, there is certainly overlap in both processes in both settings, as evidenced by the fact that there was no statistical difference in SR rates between the two habitat types, even though the non-agricultural sites had significantly more solid phase AVS and TRS and lower concentrations of $\text{pw}[\text{SO}_4^{2-}]$ (**Table 6.3**). Overall, this data indicates that the community of Hg(II)-methylating bacteria is active under conditions favoring both Fe(III)-reduction and SR, but as conditions transition from those favoring the former to those favoring the latter, the activity of the Hg(II)-methylating community increases.

Apart from the activity of the Hg(II)-methylation bacterial community, the other factor that ultimately mediates MeHg production is the availability of inorganic Hg(II) for methylation. The concentration of Hg(II)_R exhibited a strong negative linear relationship with the solid phase TRS concentration ($R^2 = 0.62$; **Figure 6.17**). Agricultural sites, which had significantly lower TRS concentrations (**Table 6.3**) had much higher Hg(II)_R concentrations, while the reverse was true for the non-agricultural sites. Similar relationship between Hg(II)_R and TRS (or AVS) have been shown in a number of recent studies, including San Francisco Bay saltmarshes and the central Delta region (**Marvin-DiPasquale et al., 2007; Yee et al., 2008**), southern Louisiana wetlands (**Marvin-DiPasquale, unpublished data**), and across a diversity of stream systems (**Marvin-DiPasquale et al., 2009b**). This is interpreted to reflect the strong binding of Hg(II) to the surfaces of solid phase reduced-S compounds, making less of the total Hg(II)_R available with increasing TRS concentration.

6.4.3 Agricultural vs Non-agricultural Fields

Agricultural fields differed from non-agricultural fields in the YBWA in many ways that were reflected in the sediment chemistry associated with Hg, S, Fe and C. Most notably with respect to mercury, the resident microbial population responsible for Hg(II)-methylation was generally less active in the agricultural sites, while the pool size of Hg(II)_R available for methylation was generally higher in agricultural sites (**Tables 6.2 and 6.3; Figures 6.2 and 6.3**). These opposing trends in k_{meth} and Hg(II)_R resulted in no significant difference in calculated MPP rates between agricultural and non-agricultural sites (**Table 6.3; Figure 6.4**), although MeHg concentrations were significantly higher in agricultural fields, particularly during the post-harvest season (**Table 6.3, Figure 6.5**). The comparison of agricultural vs non-agricultural fields is potentially confounded by the general east-to-west increase in THg concentration in the study area (**Figure 6.6**), and the fact that all of the agricultural sites lay to the west and the non-agricultural sites to the east. However, we conclude that the differences observed between the two habitat groupings is much more related to actual land use, than to longitude. First, THg is generally a very poor predictor of MeHg concentrations, as many of the other factors (discussed herein) have a much stronger influence on where and when MeHg is produced by bacteria. Statistical analysis demonstrated that THg was poorly correlated with all other mercury metrics across all sites, indicating that THg alone had little impact on rates of MeHg production, or Hg(II)_R and MeHg concentrations. Second, while a number of the other key mercury metrics also exhibited significant linear relationships as a function of latitude (**Table 6.6**), they also varied greatly with season for any given field. This indicates dynamic microbial and abiotic reactions are playing a dominant role. Third, within each of the two habitat groupings, there was no significant relationship between latitude and THg or any other mercury metric.

Redox sensitive species associated with both Fe and S were markedly different between the two habitat groupings. In general, the agricultural fields had higher concentrations of more oxidized species, including aFe(III), cFe(III), and pw[SO₄²⁻], while non-agricultural fields had higher concentrations of more reduced species including solid phase AVS, TRS, Fe(II), and pw[Fe(II)] (**Table 6.3, Figures 6.7, 6.8B, 6.11, and 6.12**). Multiple land management factors likely drive these overarching differences in redox chemistry, including a) seasonal draining of agricultural fields, b) tilling of agricultural fields, and c) shallower water depths in agricultural fields, particularly compared to the open water permanent wetland sites (PW2 and PW5). As a result of these physical and hydrological manipulations, surface sediment associated with

agricultural fields tends to be more oxidized, and reduced species have a higher likelihood of getting reoxidized. Extensive reoxidation in the agricultural fields is strongly suggested by the $\text{pw}[\delta^{34}\text{SO}_4^{2-}]$ data (**Table 6.5, Figure 6.10**). By extension, the reoxidation of Fe(II) to aFe(III) is presumably also better facilitated in this habitat grouping. This is evidenced by the strong seasonal changes in Fe-speciation associated with agricultural fields (but not for the non-agricultural fields) which are temporally synchronous with seasonal field draining and reflooding events (e.g. **Figures 6.7 and 6.11**). All of this supports the conclusion that agricultural fields are more poised for microbial Fe(III)-reduction (and less so for SR) than are non-agricultural fields. More importantly, these findings point to the primary influence of hydrology management on sediment chemistry, microbial processes and ultimately on Hg cycling. Previous research has also suggested that newly flooded areas (**Kelly et al., 1997**) or aquatic systems which undergo periods of both wetting and drying (**Gilmour et al., 2004**) are zones of enhanced MeHg production.

The significantly higher pore water alkalinities ($\text{pw}[\text{ALK}]$, **Table 6.3**) in the agricultural fields also suggest a larger degree of organic carbon mineralization, compared to non-agricultural wetlands. The higher potential for the reoxidation of reduces S and Fe species in agricultural fields (as discussed above) would support of this conclusion. Further, laboratory degradation studies conducted with dominant plant material collected from each of the YBWA field types indicates that white and wild rice detritus degrades much faster than does cattail or tule detritus (see **Section 7.3.4**). Thus, while rates of overall sediment organic matter degradation were not measured directly, the above observations indicate that there may be more overall organic mineralization associated with the agricultural fields. If so, this may also be a factor that leads to significantly higher MeHg concentrations in agricultural fields, compared to the non-agricultural wetlands (**Table 6.3**).

6.4.4 Fertilizer Additions to Agricultural Fields

One of the key questions initially posed by this study was whether or not the addition of SO_4^{2-} containing fertilizers to agricultural fields stimulates microbial SR, and ultimately MeHg production. Based on fertilizer application rates used during the study and the on chemical composition of the various fertilizers (Jack DeWit, cooperating rice farmer, *personal communication*), we estimate that approximately 4-11 kg of SO_4^{2-} was applied per acre (as starter fertilizer) to white and wild rice fields during the June 2007 application, immediately prior to rice seed amendment (**Figure 3.6**). Subsequently, another 41-66 kg of SO_4^{2-} per acre was applied, as ammonium sulfate ($(\text{NH}_4)_2\text{SO}_4$), to rice growing fields during July 2007. White rice field R64 received an additional 66 kg SO_4^{2-} per acre (as $(\text{NH}_4)_2\text{SO}_4$) during August 2007. If instantaneously dissolved, these application rates would represent to an increase in overlying water SO_4^{2-} concentrations (above background) of approximately $5\text{-}26 \text{ mg L}^{-1}$ ($0.06\text{-}0.28 \text{ mmol L}^{-1}$) for the July starter fertilizer application, and approximately $70\text{-}100 \text{ mg L}^{-1}$ ($0.7\text{-}1.1 \text{ mmol L}^{-1}$) for the June / August applications of $(\text{NH}_4)_2\text{SO}_4$, assuming optimal water depths of 4 inches for white rice and 7 inches for wild rice. However, actual SO_4^{2-} concentration increases due to fertilizer are likely lower, as the form of application is as a solid and dissolution is not instantaneous. Given that surface water SO_4^{2-} concentrations measured at the inlets of white and wild rice fields were $67 \pm 22 \text{ mg L}^{-1}$ ($0.7 \pm 0.2 \text{ mmol L}^{-1}$; avg. \pm std. dev.; $n = 19$; **Appendix 3, Table A3.8**), and assuming that these represent background concentrations, the above additional

amendments from fertilizer potentially represent significant pulsed inputs of SO_4^{2-} to overlying water.

Even though the potential increase in overlying water SO_4^{2-} concentrations are significant, the direct effect of fertilizer amendments on benthic microbial SR rates and MeHg production is less clear. While all four rice fields exhibited overall higher June through December $\text{pw}[\text{SO}_4^{2-}]$ concentrations compared to non-agricultural fields, so did the fallow fields, particularly F66 (**Figure 6.9A**). So while higher $\text{pw}[\text{SO}_4^{2-}]$ concentrations associated with rice fields may well have been a direct result of fertilizer amendments from the current growing, the higher concentration also associated with fallow fields suggest the possibility that some of the $\text{pw}[\text{SO}_4^{2-}]$ may be from legacy SO_4^{2-} applied in previous years and/or the reoxidation of reduced-S, which the agricultural fields appear more prone to (**Section 6.3.2.2**). Since non-agricultural fields also have higher SR rates, the relative difference in $\text{pw}[\text{SO}_4^{2-}]$ concentrations between the two habitat groupings is in some part a function of the more rapid depletion of $\text{pw}[\text{SO}_4^{2-}]$ in the non-agricultural settings. In 3 of 4 cases $\text{pw}[\text{SO}_4^{2-}]$ increased in rice fields for at least part or all of the June thru August growing season (i.e. W32, W65 and R34), while declining throughout this period in white rice field R31 (**Figure 6.9A**). However, these observed increases in $\text{pw}[\text{SO}_4^{2-}]$ largely reflected simple evaporative concentration, as all rice fields, with the exception of R64, showed steady decrease in $\text{pw}[\text{SO}_4^{2-}/\text{Cl}^-]$ ratio through the same June thru August period (**Figure 6.9B**). Further, fallow field F66 also exhibited a rise in both $\text{pw}[\text{SO}_4^{2-}]$ and the $\text{pw}[\text{SO}_4^{2-}/\text{Cl}^-]$ ratio between June and August, and no fertilizer was applied to this field in 2007, again suggesting reoxidation reactions. Thus, simply considering $\text{pw}[\text{SO}_4^{2-}]$ concentrations by site and time does not clearly illustrate the effect of fertilizer addition on the $\text{pw}[\text{SO}_4^{2-}]$ pool.

The concentration at which SO_4^{2-} begins to limit the rate of microbial sulfate reduction is approximately 1 mmol L^{-1} in marine sediments (**Martens and Berner, 1974**) and may be even lower in freshwater systems (**Roden and Tuttle, 1993**). Through most of the study (except for February 2008) $\text{pw}[\text{SO}_4^{2-}]$ concentrations in agricultural fields were very near or above this 1 mmol L^{-1} threshold (**Figure 6.9A**), suggesting that microbial SR was not limited by $\text{pw}[\text{SO}_4^{2-}]$ concentrations. Whether the higher concentrations in agricultural fields was a direct result of current and/or past fertilizer applications is unclear, but to the extent that fertilizer additions pushed $\text{pw}[\text{SO}_4^{2-}]$ concentrations much above 1 mmol L^{-1} , we would expect this to have no effect on SR rates.

While there was a general increase in microbial SR and solid phase TRS concentrations in all four rice fields during the growing season, there was also a rise in both parameters for fallow fields F20 and F66, neither of which received fertilizer during the study period (**Figures 6.8A and 6.8B**). There was also a rise in SR rates in the non-agricultural PW5 open water site from June to July, followed by a decrease in August. Thus, any conclusions regarding the impact of fertilizer amendments based upon temporal changes in SR rates alone are also equivocal.

In addition to the assessment of the $\text{pw}[\text{SO}_4^{2-}]$ concentration and the SR rate data discussed above, a number of other observations lead us to conclude that the addition of fertilizer did little to stimulate microbial SR rates in agricultural fields. First, rates of microbial SR were generally higher in non-fertilized non-agricultural fields during the June-August growing season (**Figures 6.8A**). Second, the high activity of Fe(III)-reducing bacteria in the agricultural fields during the

growing season, as evidenced by the overall increase in solid phase and dissolved Fe(II) (**Figure 6.11**) and the decreases in both forms of Fe(III) (**Figure 6.12**), coupled with the fact that Fe(III)-reduction generally outcompetes SR (**Lovley and Phillips, 1987b**). Since the agricultural fields were largely poised for Fe(III)-reduction, and because $\text{pw}[\text{SO}_4^{2-}]$ concentration were already near or above levels no longer limiting to sulfate reducing bacteria, the additional SO_4^{2-} from fertilizer did little to additionally stimulate SR rates. On the contrary, SR rates were likely limited by organic substrate due to the competition with Fe(III)-reduction.

Finally, while calculated MPP rates did increase substantially in the rice fields during the growing season (**Figure 6.4B**), and it was largely due to the increase in the activity of the Hg(II)-methylating community (as measured by k_{meth} ; **Figure 6.2B**), similar increases in k_{meth} were also seen on the non-fertilized fallow fields, and between June and July in the non-fertilized PW5 open water site. Temporal trends in sediment MeHg concentrations were not so consistent for either fertilized or non-fertilized fields during the growing season (**Figure 6.5B**), suggesting that variable degrees of MeHg degradation (not measured) affected the site specific MeHg concentrations. Since k_{meth} was found to be more strongly correlated with the $[\% \text{Fe(II)}/\text{Fe}_T]$ metric (**Figure 6.16**) than with SR rates (**Section 6.4.2**), we conclude that the increase in k_{meth} and associated MPP rates in fertilized rice fields reflects the overall increase in heterotrophic microbial activity (both Fe(III)-reduction and SR) brought on by the stimulatory effect of actively growing rice plants supplying organic exudates to the Hg(II)-methylating community (**Windham et al., 2009**).

6.4.5 Post-Harvest Impacts on MeHg Production in Rice Growing Fields

Another key question this study was designed to address is: How and to what extent and do post-harvest management practices impact MPP rates and MeHg concentrations? The original study design sought to compare the effects of field discing (plowing the remaining rice straw into the surface soil layer) versus allowing the standing rice straw to decay aboveground by simply draining and reflooding the field after harvest. Due to 2007 field conditions and other constraints, the cooperating rice farmer decided not to conduct discing on any of the rice fields studied during the growing season. Instead, post-harvest rice fields were reflooded and the standing rice straw was allowed to decay in all four cases. While we were not able to compare the two post-harvest approaches as planned, one benefit to the ultimate outcome was our ability to better replicate the study of the reflooding approach exclusively.

The biggest obvious effect of reflooding post-harvest rice fields and allowing the rice straw to decay aboveground, was the conversion of large amounts of particulate organic matter (rice straw) into dissolved organic matter that can fuel microbial processes. The degradation of organic matter does not happen in a single step, but instead through multiple steps each facilitated by a consortium of microbes (**Capone and Kiene, 1988**), including the exoenzymatic breakdown of particulate material into large macromolecules (polymers) by fungi, the breakdown of polymers into simpler low molecular weight monomers (e.g. simple sugars, amino acids, and fatty acids), the fermentation of monomers into even simpler organic molecules (e.g. acetate, volatile fatty acids, alcohols). It is this class of simple organic molecules that fuel terminal electron accepting processes such as Fe(III)-reduction and sulfate reduction. Statistical analysis of agricultural fields only (both previously in-rice and fallow) indicates that both MeHg concentration and the %MeHg were higher in surface sediments in the post-harvest

season, as compared to the growing season (**Table 6.5; Figure 6.5B**). None of the other key mercury metrics showed a significant difference for agricultural field data grouped into these two temporal classes. One factor that may have limited our ability to detect statistical differences among parameters grouped in this manner is that there were big differences in geochemical and microbial conditions between December 2007 and February 2008, both of which fell under the ‘post-harvest’ data grouping. Sediment metrics measured in December 2007 may be more reflective of the geochemical changes associated of recently reflooding previously drained sediments. In contrast, the geochemical data from February indicates comparatively reducing conditions have been re-established, and potentially exacerbated by the decaying rice straw. For example, compared to the last time point in the growing season (August), sediment was substantially more oxidized (**Figure 6.7**), TRS and Fe(II) concentrations were lower (**Figures 6.8B and 6.11**), and $\text{pw}[\text{SO}_4^{-2}]$, aFe(III) and cFe(III) concentrations were higher (**Figures 6.9A and 6.12**) in December. However, all of these trends were reversed by February 2008. This suggests that both Fe(III)-reduction and SR were substantially enhanced between the December and February ‘post-harvest’ sampling dates.

In terms of the two dissolved organic parameters, $\text{pw}[\text{DOC}]$ and $\text{pw}[\text{Acetate}]$, the wild rice fields exhibited a much more pronounced increase in both, compared to the white rice fields (**Figure 6.14**). This may well be due to the fact that the wild rice fields were drained and harvested a full 1.5 months prior to the white rice fields (**Figure 3.6**). Thus, the remaining straw associated with the wild rice fields had that much longer to decay, and the concentrations of these parameters to build up in surface sediments. This longer time frame for organic matter decay may be reflecting in the significantly higher February $\text{pw}[\text{Fe(II)}]$ concentrations in the wild rice fields compared to the white rice fields (**Figure 6.11A**), suggesting a stronger response of the Fe(III)-reducing bacterial community. Acetate concentration is a much better surrogate measure of the class of organic matter used by Fe(III)-reducers and sulfate reducers, than is DOC. It is thus noteworthy that only the agricultural fields with decaying rice straw exhibited a significant increase in $\text{pw}[\text{Ac}]$ in the post-harvest season (compared to the growing season), while fallow fields exhibited a significant decrease in $\text{pw}[\text{Ac}]$ (**Figure 6.15**). This finding, coupled with the fact that by February, Fe(II) and TRS build-up was significantly higher, and SR rates were generally higher, in fields with decaying rice straw than in fallow agricultural fields (**Figures 6.8 and 6.11**), supports our conclusion that the management practice of decaying rice straw via reflooding alone stimulates heterotrophic microbial activity, and subsequently Hg(II)-methylation, in surface sediment.

7 Detailed Results for Plant-Mercury Interactions

The data reported in this section relates to summary **Section 3.3: Methylmercury Production in Surface Sediment**.

7.1 Introduction

Vegetation can influence sediment biogeochemistry in both terrestrial and wetland ecosystems through plant:soil feedbacks (**Ehrenfeld et al., 2005**). A primary influence on sediment biogeochemistry is rhizosphere activity and physiology (**Marschner, 1986**). Root:soil interactions affect a number of processes and geochemical characteristics in the rhizosphere zone, including a) microbial community structure and activity (**Bagwell et al., 1998; Hines et al., 1989; Borga et al., 1994; Westover et al., 1997**), b) dissolved organic carbon quality (**Hines et al., 1994; Garland et al., 1996; Cheng et al., 2003**), c) the concentration and availability of electron acceptors to microbes (**Roden and Wetzel, 1996; Blaabjerg and Finster, 1998; Lee et al., 1999**), and d) nutrient/contaminant speciation (**Marins et al., 1997; Windham and Ehrenfeld, 2003; Jacob and Otte, 2003**). Further, the structure and quality of aboveground biomass influences physical dynamics (e.g. sediment irradiation) as well as the pulsed supply of decaying litter post-senescence. The abiotic processes and microbial activities that influence MeHg production are likely influenced spatially and temporally by this suite of physical, chemical and biological feedbacks from plants. Surface soils, with high root densities or supplies of aboveground labile carbon, are perhaps the most important ecosystem horizons for MeHg production, as MeHg production is typically the greatest in these zones (**Gilmour et al., 1998**) and because MeHg pools from this horizon are most likely to become suspended or diffuse into surface waters (**Langer et al., 2001**). Temporal inputs of organic matter have also been shown to drive MeHg in field and lab conditions (e.g. **Hall et al., 2004**).

7.2 Approach

7.2.1 Seasonal Comparison

In the Yolo Bypass Wildlife Area (YBWA), three types of flooded agricultural wetlands (white rice, wild rice and fallow fields) and three non-agricultural managed wetland areas (one seasonally flooded and two permanently flooded) were studied. Plant samples and structure were assessed in order to determine their physical and biogeochemical influences on mercury cycling, as well as carbon, nitrogen, sulfur, and iron. Of the two agricultural fallow fields, one was devoid of vegetation (barren fallow) and the other had a densely rooted mixed plant community (vegetated fallow). Field and dominant vegetation descriptions are given in **Table 7.1**. Vegetation sampling overlapped with sediment sampling schedules (**Figure 3.6**). Seeds were collected at the time of maturity - August for wild rice, August and December for white rice, and December for cattail and tule plants in the permanent wetland.

The above and belowground plant community was characterized for each field at all 5 major sampling events (June, July, August, December 2007 and February 2008) for total live biomass (g m^{-2}), rooting depth, and leaf area index (a ratio of leaf area to planar area). Samples were collected in triplicate for each sampling event, and a mean and standard deviation were calculated for seasonal and spatial comparisons.

Fresh leaf, root and seed tissues (50-100 g wet weight) were subsampled in the field, with ~50g refrigerated until further processing, and ~20-50 g flash frozen for Hg and MeHg analyses.

Within 72 hours of collection, refrigerated leaf surfaces and live root tissues (separated from sediments as described below) were rinsed with deionized water and a 1% EDTA solution to remove loosely sorbed THg particles and other particulates, and then freeze-dried. Tissue concentrations and isotopic ratios of carbon (C) and nitrogen (N) were measured using a Carlo-Erba elemental analyzer in tandem with a Micromass Optima system. Tissue THg concentrations were analyzed using a microwave-assisted nitric acid (HNO_3) digestion followed by Hg analysis on a Tekran 2600 automated CVAFS unit, according to **DeWild et al. (2004)**, a modified version of EPA 1630. MeHg concentrations were measured with a KOH:methanol extraction followed by ethylation and CVAFS, as per **Bloom (1993)**. Along with biomass data, these concentrations were used to calculate standing stocks of C, N, THg and MeHg, as well as ratios of carbon:nitrogen (an index of carbon lability) and MeHg:Hg (an index of MeHg production and uptake).

Root density and depth profiles were collected from plots using 30 cm deep cores, which were temporarily preserved on wet ice to slow microbial processes. The cores were cut into 2 cm depth intervals in the laboratory. Surface sediment (0-2 cm depth) was sampled concomitantly in neighboring devegetated and vegetated plots, using 2 cm deep (6 cm i.d.) pre-cut polycarbonate core rings. Between 5 and 10 surface sediment cores (0-2cm, “patties”) were collected per plot using 6cm (i.d.) polycarbonate rings and composited into two glass mason jars (1 pt). These surface sediment composites were analyzed for sediment chemistry and physical characteristics as listed in **Table 6.1**. Three additional surface sediment cores (patties) were collected at each site for analysis of root biomass and root density in the 0-2 cm depth interval. Live roots were manually harvested with forceps and rinsed of soil particles, then visually identified by turgidity and color. A subsample of live roots were subjected to a vital stain (1% tetrazolium red) followed by dissection under 40x magnification, to assess errors of commission (< 5% for all samples collected). Live roots for each replicate surface sediment core were rinsed thoroughly and then assessed for volume by displacement of deionized water in a 50 or 100ml graduated cylinder. These samples were then freeze dried and weighed to assess root dry biomass. These root density data, collected from discrete 0-2 cm cores, were compared with the 0-2 cm data from the 0-30cm deep root profiles, and in all cases, the root profile biomass from this 0-2cm surface interval was found to be within ± 1 standard deviation of the biomass calculated using the surface sediment cores.

7.2.2 Devegetation Experiment

For each vegetated plot, a neighboring devegetated plot with similar initial edaphic conditions was established. Prior to seeding and floodup, and at least 2.5 months prior to sample collection, 1 m² devegetation plots were established in triplicate in each of the agricultural fields to prevent the growth of plant material. In the already vegetated permanent wetlands, a single 2 m² plot was established by clipping aboveground biomass (live and dead) to the ground surface and removing this material from the plot. A spade was used to cut roots with a 30 cm deep slit along the edge of the plots to inhibit root growth and root-mediated inputs to the devegetated plots. All plots were covered with professional-grade water-permeable landscape cloth, to shade the sediment and inhibit vegetation regrowth during the study period. Plots were revisited 2-3 times during the growing season to retrench devegetated plots and to measure primary productivity in adjacent vegetated (control) plots.

At the growing season peak (June-December depending on the wetland type), plots were revisited and the landscape cloth lifted to access the underlying sediment surface, and sampled the same way as described in **Section 6.2**. In addition, surface sediment (0-1 cm depth) were collected to assess concentrations of benthic microalgal abundance using a modified version of **Parsons et al. (1984)**, with centrifugation, extraction and spectral analysis of chlorophyll a and phaeophytin pigments.

Net concentration changes in the three measured sediment iron species (Fe(II), aFe(III) and cFe(III)) (normalized per day) were calculated in the agricultural fields – using the *in situ* concentration difference between July and August for the fallow fields, and June and August for the rice fields, the dates most closely related to flood-up and peak biomass for a given field type. Although Fe(III)-reduction rates were not directly measured in short term incubations, as were rates of microbial sulfate reduction, total measured iron concentration in bulk sediment ($Fe_T = Fe(II) + aFe(III) + cFe(III)$) was generally consistent through time (17-19 mg g⁻¹), which allowed us to calculate an average net daily rate of change in each of the three iron pools as a surrogate for iron-cycling rates over the growing season. The aFe(III) concentration data was also used as an indicator of conditions favorable for iron reduction (**Roden, 2008**), as discussed in **Section 6.4.2**.

7.2.3 Decomposition Assay

Carbon mineralization and the release of THg during tissue decomposition were assessed experimentally with laboratory incubations of August 2008 samples from the six agricultural fields and the 2 permanent wetland communities. Leaves were first rinsed in a 1% EDTA solution, followed by deionized water and blotted dry. For each treatment, 4.8-5.2 g of freeze-dried ground leaf tissue were added to each of 40 Pyrex glass centrifuge tubes (50ml), with 5 additional centrifuge tubes acting as a control solution with no leaf material added. A 40.0 ml aliquot of deionized water (Ultrapur MQ) was added to each of the 45 vials at the start of the incubation. Samples were incubated under oxic conditions (tested weekly for sulfide presence) at 30°C while gently shaken (50 rpm) on a gyration table within a temperature-regulated incubator. Subsamples (5ml) were collected from each vial days 0, 1, 7, 14 and 28 for time-point processing. The incubation water was monitored for volume each week and used to correct for total mass of solution. Hg concentrations in this initial incubation water were less than 0.2 ng L⁻¹, and in control vial concentrations remained within 25% RSD of the initial concentration throughout the experiment

Upon retrieval, splits were made for dissolved THg analysis (filtration through acid-clean 0.45 nylon filters) and DOC analysis (GFF filtration at 0.6 μm and preservation at 0.1%v/v phosphoric acid). Particulate mass (detritus) removal was calculated from mass on these preweighed GFF filters. A subsample of filtrate was acid-preserved for dissolved organic carbon concentrations, analyzed on a Shimadzu TOC analyzer. The remaining filtrate was returned to the centrifuge tube and 200 ul of BrCl (0.5% v/v) was added to preserve and extract any Hg that may have adsorbed to the vial walls. This incubation filtrate was then heated overnight at 70°C and analyzed for total Hg concentration by CVAFS according to EPA 1630. Tissue decomposition rates were assessed with laboratory incubations on freeze-dried, ground leaf tissues from all fields except F20 (fallow, barren). A single dominant species - *Cyperus difformis* (sedge)- was chosen to represent decomposition within the mixed fallow field (F66).

Tissue samples of known weight ($5\text{g} \pm 0.2\text{g}$) were added to pyrex centrifuge tubes, followed by 40ml of deionized water. Replicate ($n=5$) vials were filled for all 8 treatments (7 field treatments + 1 control). Vials were incubated at 30°C for 28 days and were kept aerobic and non-stratified by continuous shaking at 40rpm. On days 1, 7, 14, and 28, subsamples of 5ml of water were removed from the vials and prepared for analysis of particulate material, aqueous THg and DOC by filtration and preservation. Subsamples were also checked for dissolved oxygen concentrations and were $> 10\%$ saturation in all cases. Volume loss to evaporation was recorded to the nearest ml, and represented approximately 2-3ml per week. Final calculations of mass loss included the initial vs. final particulate material in each vial. These differences were used to calculate a logarithmic decay rate (k) based on laboratory conditions. To estimate decay rates under field conditions, laboratory measurements were scaled according to a Q_{10} of 2.44 (Gu et al., 2004), on monthly timesteps of average monthly temperatures as recorded by CDFG at El Macero Station (Yolo Bypass). These rates were then combined with initial biomass pools (aboveground biomass in August), and the date of litter deposition (harvest date or for fallow fields, drawdown date) to estimate the poolsize of surface detritus through time within each field type.

7.2.4 Statistics

Statistical analyses were performed using SPlus 7.0 (Insightful Corp. 2001). Data from the 10 sites were categorized by site and/or treatment (vegetated control plot versus devegetated plot). Data were assessed for significance between discrete field types and for Pearson correlation and/or linear or logarithmic regression analysis of parameters within given field types. Only significant correlations are reported ($p < 0.05$), as assessed by comparison with t_{crit} for a two-tailed distribution and $df=1$. Regressions are reported for predictive relationships with $p < 0.05$. We do not report absolute difference between vegetated and devegetated plots, unless explicitly noted. Instead, we focus on the relative effects of devegetation, as a way to interpret the major vegetation effects across multiple habitat types. For each site specific vegetated-devegetated plot pair, a relative metric for the magnitude and direction of the devegetation effect (%DevegEffect) had on a given parameter (e.g. $X = k_{\text{meth}}$, Hg(II)R , MeHg , etc...) was calculated as the % difference between devegetated and vegetated control plots, such that:

Equation 7.1

$$\% \text{DevegEffect} = (X_{\text{vegetated plot}} - X_{\text{devegetated plot}}) / X_{\text{vegetated plot}} \times 100$$

Normality of each parameter was assessed with Kolomogorav-Smirnov tests, and non-parametric data were log-transformed. Although the devegetation effect was profound enough for some measured parameters to warrant direct ANOVA comparisons of vegetation status (vegetated vs. devegetated), the calculation of the %DevegEffect metric for paired plots provides a clearer sense of the devegetation effect across a continuum of wetland conditions. Pairwise t-tests were used to test paired (vegetated / devegetated) plots for the significant influence of devegetation within a given habitat category.

7.3 Results

7.3.1 Vegetation Productivity/Growth

Vegetative growth was rapid in the cropped fields (**Figure 7.1**). Over 76 days, between the June and August sampling events, the white rice fields generated $2.1 \pm 0.2 \text{ kg m}^{-2}$ above ground plus below ground biomass (average of R31 and R64), and the wild rice fields generated $1.5 \pm 0.3 \text{ kg m}^{-2}$ above ground plus below ground biomass (average of W32 and W65).

Leaf area index, a function of above ground growth, also rose quickly over the growing season for agricultural fields, reaching maximum cover in August at greater than 2.5 in three of the four rice fields (**Table 7.1**). In comparison, live aboveground biomass was consistently high in the vegetated permanent wetland sites, with leaf area indices greater than 2 for most of the year. Fallow fields were barren until flooded, and then gained $0.4 \pm 0.1 \text{ kg m}^{-2}$ at field F66. Belowground biomass (roots/rhizomes) represented less than 20 % of total biomass in white rice fields, less than 10% of total biomass in wild rice fields, but up to 35% of total biomass in the permanent wetland tule stand.

Density of live roots in surface sediments reached a seasonal maximum in August within agricultural fields, but remained constant in the permanent wetland sites. Live root densities were greatest for surface soils in white rice fields, reaching up to 10% of soil volume, whereas wild rice fields were fairly consistent with root densities of 5% (**Figure 7.2**). White and wild rice fields in the southern block (R64 and W65) had 3-9 fold greater variation between samples within a given sampling date than did fields in the northern block (R31 and W32), which is likely due to uneven early recruitment within these fields. Live root biomass and density increased over the growing season (**Figures 7.1, 7.3**), with the exception of white rice in field R31, where the average density of live roots decreased from 10% to 6% from July to August (**Figure 7.3**). High root mortality was observed on R31, where the highest surface water temperatures of the study were also observed ($>38^{\circ}\text{C}$, see QA for water quality parameters in **Appendix 1**).

The most significant differences in tissue quality parameters were found between plant type, and not between blocks ($p>0.05$) or across season ($p>0.05$). Not only was leaf tissue biomass more abundant than seed or root biomass, they also showed the highest concentrations of nitrogen (**Table 7.2**). Tissue nitrogen concentrations varied strongly between species, with the highest leaf N concentrations observed in fallow field weeds (2.9%), followed by white rice ($1.4 \pm 0.4\%$), and then by wildrice ($0.5 \pm 0.1\%$). This led to over a 3-fold variation in carbon:nitrogen (C:N) ratios between the two crops, white rice (28 ± 11) and wildrice (92 ± 21), and to over a 4-fold variation in biomass N pools between white rice ($18 \pm 4 \text{ g m}^{-2}$) and wild rice ($4 \text{ g} \pm 1 \text{ g m}^{-2}$). The fallow field weed (sedge, *Cyperus difformis*) was similar to white rice in C:N ratios (20 ± 3), but its low biomass led to a low pool of N in biomass ($5.6 \text{ g} \pm 0.6 \text{ g m}^{-2}$). Surprisingly, the leaf tissue C:N ratios of cattail (59 ± 23) and tule (50 ± 14) were similar, and tended to be lower than wild rice C:N ratios. Another notable difference by species was the high ash content (loss on ignition, LOI) in white rice (up to 2% leaf tissue composition). Elemental analysis by ICP-AES suggested that the silica comprised the majority of this mineral component in all species. Although ash, silica or %C contents were not significantly different between species, LOI and %C were positively correlated ($r = 0.86$), suggesting that the mineral or ash component directly reduced carbon concentrations, and thus, plays a direct role in diluting carbon pools in standing stock biomass and later during litter decay on the sediment surface.

Tissue concentrations of THg also varied by species, but not between blocks ($p < 0.05$) or across season ($p < 0.05$). THg concentrations were greatest in roots, ranging from 104 ng g^{-1} in cattail fine roots to 282 ng g^{-1} in white rice fine roots. Analysis of aluminum concentrations in root tissues (and all tissues) illustrated that soil contamination represented less than 0.1% of the root sample, and thus cannot account for these high concentrations. No differences were observed between plant types for root concentrations of THg, but leaf concentrations varied by almost 1 order of magnitude between species, with leaf [THg] of $104 \pm 8 \text{ ng g}^{-1}$ in wild rice leaves and $14 \pm 3 \text{ ng g}^{-1}$ in white rice leaves. Non-crop species (sedges and cattails) all showed similar leaf tissue concentrations of $30\text{-}55 \text{ ng g}^{-1}$. The low THg concentration in white rice leaf tissue was notable, considering the comparably high THg concentrations in plant roots. Further, there was greater than a 6-fold difference in THg pools associated with leaf tissue biomass between white rice and wild rice fields ($15 \mu\text{g m}^{-2}$ and $100 \mu\text{g m}^{-2}$, respectively). The importance of these THg leaf tissue biomass pools, however, are small compared to the sediment THg pools in all agricultural fields ($5240\text{-}6270 \mu\text{g m}^{-2}$ for the surface 0-2 cm interval), and comparable to sediment Hg(II)_{R} pools ($44\text{-}120 \mu\text{g m}^{-2}$ for the surface 0-2 cm depth interval), as calculated from the summary data given in **Table 6.2**.

Tissue concentrations of MeHg were similar among agricultural crops, but the permanent wetland species (tule and cattail) had 3-fold lower concentrations in their leaves (0.5 ng g^{-1}), 10-fold lower concentrations in their roots (1.1 ng g^{-1}), and 5-fold lower concentrations in their seeds (0.5 ng g^{-1}). MeHg concentrations were not correlated with THg concentrations and in many cases showed opposite patterns. While MeHg represented 8-9% of the THg pool in white rice seeds, MeHg constituted 37-60% of the THg pool in wild rice seeds (**Table 7.2**). No seasonal or block patterns were observed, but MeHg concentrations were significantly greater in agricultural crop tissues than permanent wetland species roots ($p = 0.0032$), leaves ($p = 0.0004$) and seeds ($p < 0.0001$), following the same pattern observed in sediment MeHg concentrations (**Tables 6.2 and 6.3**). The highest tissue MeHg concentrations observed were in seeds ($4.2 \pm 1.1 \text{ ng g}^{-1}$ in white rice, $6.2 \pm 1.5 \text{ ng g}^{-1}$ in wild rice), and seed [MeHg] was better correlated with root [MeHg] ($r = 0.90$) than leaf [MeHg] ($r = 0.61$). A separate analysis of [MeHg] on seed husks for wild rice showed the highest concentrations of all tissues (up to 9 ng g^{-1}), but this portion is usually removed in the crop storage and preparation process.

7.3.2 Vegetated vs. Devegetated Responses

Despite differences in hydrology and vegetation among the freshwater wetland types studied, the activity of Hg(II) -methylation bacteria (as k_{meth}) consistently decreased (17 to 87%) as a result of devegetation, in all sub-habitats except in the cattail dominated wetland (**Figures 7.4 and 7.5, Table 7.3**). Similarly, sediment MeHg concentration significantly decreased (13 to 55%) in all sub-habitats except for wild rice fields. The effect of devegetation on sediment Hg(II)_{R} concentration was more varied, with a decrease in the vegetated fallow field, and an increase in the barren fallow field and in both the tule- and cattail-dominated wetlands, and non-significant changes in both rice field settings and in the Yolo seasonal wetland. The combined effect of k_{meth} and Hg(II)_{R} concentrations on calculated MP rates thus resulted in the situation where MP significantly decreased due to devegetation in both rice field sub-habitats and the vegetated fallow field in Yolo. The concentration of pw[Ac] consistently decreased (63 to 99%) with devegetation across all freshwater sub-habitats (**Table 7.3**). While we found a significant

devegetation effect on benthic ChlA (an indicator of algal biomass in surface sediment), estimated algal biomass was quite low in all fields ($<1.0 \text{ g m}^{-2}$), and was especially low in the white rice fields ($<0.2 \text{ g m}^{-2}$) where the largest devegetation effects were observed. The devegetation effects on pw[Ac] and microbial activity are thus more likely to come from decreases in root density, as pw[Ac] concentrations were highly correlated with root density in agricultural fields through the growing season ($r = 0.92$).

Agricultural fields showed the strongest devegetation responses with respect to solid phase iron species (**Table 7.3**), including an increase in sediment Fe(II) and a decrease in sediment aFe(III) concentrations, whereas concentrations for the more abundant cFe(III) fraction were varied and not significantly different between treatments. Despite sulfate loading to both white and wild rice fields through fertilizer application ($>50\text{-}75 \text{ kg SO}_4^{2-} \text{ acre}^{-1}$), no significant effect from devegetation was observed in the white or wild rice fields for microbial SR rates or for reduced sulfur species concentrations. Devegetation-driven decreases in microbial SR rates were observed, however, in both fallow field settings and in the densely rooted tule permanent wetland (**Table 7.3**).

An examination of the change in Fe-species concentrations in agricultural fields showed significant decreases in cFe(III) and increases in Fe(II) over the growing season (from flood-up [June/July] until August), both trends indicative of net Fe(III)-reduction (**Figure 7.6A**). Devegetated plots showed the same general pattern of Fe(III)-reducing activity (a net decrease in cFe(III) and a net increase in Fe(II)) across all agricultural fields (**Figure 7.6B**). A direct comparison of vegetated versus devegetated plots, by difference [vegetated minus devegetated], indicates that the rates of Fe(II) increase were greater for devegetated plots (negative differences) for 5 of the 6 fields studied (**Figure 7.6C**), suggesting modestly higher net rates of Fe(III)-reduction in the devegetated sites associated with both white rice and wild rice fields, and a significantly higher net rate of Fe(III)-reduction in the devegetated site associated with fallow field F66. The exception to this trend was seen for the “devegetated” barren fallow field F20, where the [vegetated minus devegetated] difference in the Fe(II) net rate of change was clearly positive and the difference in the cFe(III) net rate of change was clearly negative (**Figure 7.6C**), suggesting that for field F20 the devegetated site had a significantly lower rate of net Fe(III)-reduction than its vegetated pair for the July thru August time period. For most of the other fields, the [vegetated minus devegetated] difference in the net rate of change for the cFe(III) pool was non-significant, based upon the error bars, the exception being wild rice field W65, which was strongly positive and again reinforces the conclusion that the devegetated site had a higher net rate of Fe(III)-reduction than did its vegetated pair.

In terms of elucidating the spatial trends in microbial Fe(III)-reduction among fields and for the vegetated versus devegetated plots (to explore the ‘plant effect’), the above examination of the net changes in the Fe(II) and cFe(III) pools seems obvious, simply from their abundance on the three plots of **Figure 7.6**, relative to aFe(III). However, aFe(III) is a critical component of the Fe-cycle in that it is much more readily available to Fe(III)-reducing bacteria than is cFe(III) due to the very high surface area associated with its poorly crystalline (amorphous) structure (**Roden and Zachara, 1996**). Further, aFe(III) is an active intermediary component of the iron cycle, and thus not likely to build up over longer periods of time. Thus, the small aFe(III) pool size in sediment relative to cFe(III) (e.g. 20 to 36-fold smaller across all agricultural fields, 33 to 850-

fold smaller across all non-agricultural wetland sites; based on mean values in **Table 6.2**) may be particularly important due to its relevance as an electron acceptor in these wetland habitats; as Fe(III)-reducing bacteria are effective at utilizing it when it is available. Further, aFe(III) concentrations were shown to be proportional to Fe(III)-reduction rates (**Roden and Wetzel, 2002**), as noted in **Section 6.4.2**. Thus, while the absolute concentrations (**Table 6.2**) and subsequently the calculated net rates of change of aFe(III) pools appear small (**Figure 7.6**), that pool is likely turning over very quickly at shorter time scales than were addressed in this study.

During the growing season, there was a significant net decrease in aFe(III) concentration over time in three of the four rice fields (R64, R31 and W32) for both the vegetated (**Figure 7.6A**) and devegetated (**Figure 7.6B**) plots, as well as the devegetated plot in fallow field F66 (**Figure 7.6B**). All of these net changes in aFe(III) corroborate the conclusions reached from the above examination of the Fe(II) and cFe(III) data, and again suggest active Fe(III)-reduction in these locations. In further support for active Fe cycling, sites/treatments that exhibited a significant net increase in aFe(III) over time, indicative of the (re)oxidation of Fe(II) to aFe(III), included vegetated sites W65, F66 and F20 (**Figure 7.6A**), as well as devegetated site F20 (**Figure 7.6A**). In examining the [vegetated minus devegetated] differences in the aFe(III) rate of change (**Figure 7.6C**), a few things are evident: a) there is no statistical difference between vegetated and de-vegetated plots in two of the rice fields (R64 and W32); b) there is a modestly higher rate of aFe(III) production (Fe(II) reoxidation) in the vegetated sites associated with the other two rice fields (R31 and W65), and there is strong evidence for this in fallow field F66. In contrast, there is evident for a moderately lower rate of Fe(II) reoxidation in the vegetated site, compared to the devegetated site, for field F20.

The importance in considering the rate changes associated with this seemingly small aFe(III) pool is that it represents the portion of the Fe-cycle that cycling quickly between processes of Fe(III)-reduction and Fe(II)-reoxidation. While the absolute changes are small, compared to Fe(II) and cFe(III) when assessed over these relatively long time periods (1-2 months), the direction and magnitude of shift may shed some light onto what sites are most dynamic with respect to Fe-cycling in general. Thus, those sites exhibiting small but significant increases in aFe(III) in the [vegetated minus devegetated] comparison over time – and especially sites exhibiting increased aFe(III) concentrations at the same time that Fe(II) concentrations are increasing (especially F66, and W65) – may be reflective of the sites that are actually most active with respect to microbial Fe(II)-reduction, and Hg(II)-methylation, under typical vegetated conditions.

7.3.3 Relationship between microbial devegetation effects: implications for sulfur and iron cycling

Pearson correlation analysis was used to assess the correspondence of devegetation effects among the parameters, and to identify significant biogeochemical interactions. When compared across all wetland settings, %DevegEff for aFe(III) positively correlated with both the %DevegEffect for Hg(II)_R ($r = 0.66$) and the %DevegEffect for MP ($r = 0.73$). Thus, in wetlands where sediment aFe(III) concentration were significantly decreased due to devegetation, MP showed the most substantial decreases (**Windham et al., 2009**). Because lower rates of aFe(III) production is indicative of a lack of Fe(II)-reoxidation back to aFe(III), this relationship suggests that Fe(II)-reoxidation may be important in driving higher rates of MP in the vegetated (control)

sites, by resupplying aFe(III) as an electron acceptor for a subset of the Fe(III)-reducing microbial community that may be involved in Hg(II)-methylation (e.g. geobacter; **Roden, 2008**). Because the most significant revegetation effects associated with mercury cycling (ie. k_{meth} , MP, %MeHg, Hg(II)_{R} and MeHg concentration) were predominantly associated with significant changes in iron speciation, our data point to an important linkages between iron Fe biogeochemistry and MeHg production dynamics in these agricultural and managed wetlands.

7.3.4 Decomposition Assay

Laboratory assays of decomposition rates were rapid for rice, wild rice and fallow species (>4% day) and significantly slower for permanent wetland species tule and cattail (2%, **Table 7.4**). Log-based calculations of k (d^{-1}) were similar through the entire incubation except for initial leaching. With 5-14% of initial mass lost in the first day of incubation for rice, wild rice and the fallow species, these plant tissues were highly labile as compared with the more waxy and lignin-rich tissues of tule and cattail (<2% mass lost on the first day of incubation). Loss on ignition showed high ash contents in wild rice ($1.3 \pm 0.9\%$) and white rice ($1.9 \pm 1.0\%$). Elemental analyses suggest high silicate concentrations in both rice tissues, approaching 2% in white rice. Rates of mass loss were clearly a function of tissue quality, specifically C:N ratios ($R^2=0.71$, **Figure 7.7**) as per **Melillo et al. (1982)**, and less so a function of lignin concentrations were ($R^2=0.24$). Multiple regression analyses support the importance of %N as the primary driver of decay dynamics.

When scaled to field conditions, surface litter areal mass was highest in white rice fields and lowest in fallow fields (**Table 7.4**). These patterns were found to be correlated with two key sediment characteristics expected to relate to labile carbon supply: pw[Ac] ($r = 0.71$) and microbial Hg(II)-methylation rate constants (k_{meth} , $r = 0.68$). The role of labile carbon as a driver of Hg(II)-methylating bacteria activity was particularly apparent during February 2008, the period during which the decay of rice straw was being actively facilitated with managed reflooding of the previously harvested rice fields and when the strongest relationship between pw[Ac] and k_{meth} was seen (**Figure 7.8**). Further, the terrestrial signal associated with the characterization of surface water DOC quality was correlated with estimates surface litter areal mass (Jacob Fleck, pers. obs).

7.4 Summary/Discussion

The role of vegetation was significant at different timepoints of the year based on the importance of key processes. During the growing season, remarkably high production of biomass in the white and wild rice fields led to large amounts of root material ($180\text{-}300 \text{ g m}^{-2}$) concentrated within the upper 5cm of sediment. In cropped fields, root density was highly correlated with mercury methylation rates in the top 0-2cm of soil. Further, the experimental removal of active rhizosphere processes led to significant biogeochemical changes – specifically a reduction in MeHg production and sediment MeHg pools. These were accompanied by sharp drops in the concentration of pw[Ac] , suggesting that the primary influence of vegetation in active ricefields is the production of labile carbon for microbial activity. Further, it suggests these relationships suggest that microbial methylation was carbon limited within these fields. In

addition, significant limitations of aFeIII supply were observed in devegetated plots, accompanied by decreases in Cl concentrations. These data, in conjunction with hydrologic estimates of evaporation (**Section 5**) and isotopic evidence of pore water sulfide reoxidation (**Section 6**), suggest that transpiration-driven oxidation of the surface soil may have played a key role in regenerating pools of amorphous iron for use by iron-reducing bacteria. These are among the first data to support the significance of iron reducing bacteria in MeHg production at the ecosystem scale (**Windham et al., 2008**).

During vegetative senescence in winter months, live roots were observed but were not correlated with MeHg production or concentration. Instead, abundant surficial detritus in white ricefields was observed and estimated poolsizes at the field scale were significantly correlated with rates of MeHg production. Estimates of surface detritus were correlated with both pw[Ac] concentrations (labile carbon) and the relative terrestrial signature of DOC in surface water (index of fresh carbon supply), suggesting that MeHg production is also carbon-limited in winter months, and that decaying ricestraw is a key driver in C supply (**Figure 7.8**).

Pools of THg and MeHg in plant biomass were <10-100 fold lower than surface sediment pools (0-1cm depth), suggesting that although uptake may be active, vegetation represents a relatively small sink for MeHg and Hg compared to sediment processes. In aboveground biomass, MeHg concentrations were lowest in stem tissue (<1 ng g⁻¹) and elevated in seed (up to 6 ng g⁻¹ in wild rice).

8 Detailed Results for Methylmercury Bioaccumulation

The data reported in this section relates to summary **Section 3.4: Methylmercury Bioaccumulation**.

8.1 Introduction

It is widely recognized that MeHg biomagnifies through aquatic food chains and is a potent neurotoxin (**Wiener et al., 2003a**). In addition, wetlands often have higher rates of MeHg production than other aquatic habitats, in part because ambient conditions common within wetlands are generally conducive to MeHg production (**Zillioux et al., 1993; Marvin-DiPasquale et al., 2003; Hall et al., 2008**). Fluctuating water levels that are typical of intermittently and shallowly-flooded wetlands also can enhance the release of MeHg from sediments (**Morel et al., 1998**). As such, wetlands are known to contribute substantially to MeHg bioavailability within downstream environments (**Hurley et al., 1995; Krabbenhoft et al., 1995; Rudd, 1995; Krabbenhoft et al., 1999**) as well as to *in situ* bioaccumulation (**Snodgrass et al., 2000**). Unfortunately, specific wetland habitat types and management practices that might alter MeHg production and bioavailability remain unclear (but see **Snodgrass et al., 2000; Harmon et al., 2005; Rumbold and Fink, 2006**).

Our goal in the current study was to evaluate how different wetland management practices influenced MeHg bioavailability. We used invertebrates and fish as our indicators of Hg bioaccumulation. Specifically, our main objectives were to determine if invertebrate and fish Hg concentrations (1) differed among wetland habitat types, and (2) varied within fields from water inlets to outlets. Although not funded as part of this original study, data collected in addition to that supporting the above project objectives included Hg contamination in caged fish, and in a second species of invertebrate (Notonectidae). Subsequently, we have included that recently published data (**Ackerman and Eagles-Smith, 2010; Ackerman et al., 2010**) as part of this report for a more comprehensive assessment of Hg bioaccumulation within the Yolo Bypass.

8.2 Study Design and Methods

8.2.1 Study Site

We assessed MeHg bioaccumulation within wetlands at the Yolo Bypass Wildlife Area (38.33° N, 121.4° W). The Yolo Bypass Wildlife Area is approximately 6,475 ha and is located within the Yolo Bypass - a 23,877 ha floodway that provides flood protection as part of the Sacramento River Flood Control Project. It is common for the Yolo Bypass to flood each spring when Sacramento River waters are high due to spring runoff. During these flood events, MeHg is transported downstream into the Sacramento-San Joaquin River Delta. Both seasonal wetlands and agricultural fields are flooded during the fall and winter to provide habitat for wintering waterfowl and shorebirds.

8.2.2 Invertebrate Study

We studied MeHg bioaccumulation within two fields each of white rice, wild rice, permanent wetlands, and shallowly-flooded fallow fields. We sampled two taxa of aquatic macroinvertebrates at the inlets, centers, and outlets of each of the 8 wetlands during two time periods bounding the rice growing season and corresponding to flood-up and pre-harvest (96 total samples). White rice fields were initially flooded, then the water was discharged within two

weeks for weed control, and thereafter re-flooded; we conducted our first sampling time period immediately after the fields were re-flooded for rice production. Because fallow fields were managed for migrating shorebirds, they were not initially flooded until late July. Our pre-harvest invertebrate sampling time period occurred immediately before the wild rice harvest in mid September. Thus, our flood-up invertebrate sampling occurred from 25 June to 6 July and our pre-harvest sampling occurred from 28 August to 19 September for all habitats, with the exception that fallow fields were sampled at flood-up on 30 July 2007.

We sampled aquatic invertebrates in the water column and submerged vegetation using D-ring sweep nets with 0.5 mm mesh (diurnal) and floating light traps (nocturnal). Light traps were constructed as described by **Marchetti and Moyle (2000)**, and were set at night and retrieved at dawn the following morning. We also used sweep nets at each site during trap deployment and retrieval to increase the biomass of invertebrates captured. We transported invertebrates from the field in fresh source water on wet ice and stored them in the refrigerator for 24 hrs to allow the passage of inorganic Hg present in their digestive tracts. We then identified and sorted invertebrates with a dissecting microscope (10×) following **Merritt and Cummins (1996)**; genera were independently confirmed by the R. M. Bohart Museum of Entomology, University of California, Davis. We sampled invertebrates from each site until we reached a biomass of >3 g wet weight each of Corixidae (Order Hemiptera, Family Corixidae, Genus *Corisella*, water boatmen) and Notonectidae (Order Hemiptera, Family Notonectidae, Genus *Notonecta*, back swimmers). We stored invertebrates in Whirl-paks[®] (Nasco, Modesto, California, U.S.A.) at -20°C until Hg analysis.

8.2.3 Caged Fish Study

We built rectangular enclosures that were 454 L and measured 122 cm × 61 cm × 61 cm (L × W × H) using 6 mm polypropylene aquaculture mesh (Industrial Netting, Minneapolis, Minnesota, USA) affixed with cable ties to a polyvinyl chloride (PVC) pipe frame. We drilled holes in the PVC pipe frame to reduce buoyancy. A similar cage design was used successfully to examine diet and growth rates of caged juvenile chinook salmon (*Oncorhynchus tshawytscha*), and they showed that the 6 mm mesh netting allowed adequate movement of prey items such as zooplankton and macroinvertebrates to enter the enclosure (**Jeffres et al., 2008**). For cages in permanent wetlands, we affixed two 130 cm long × 7 cm diameter closed-cell foam floats to each side of the cage so that the top of the cages floated about 15 cm out of the water. In white rice and wild rice fields, we attached each cage with cable ties to 3/16 inch rebar stakes that were driven into the substrate on each side of the fish cages. To avoid fatalities from accidental drainage or low water events, we positioned the cages in slightly deeper locations of the field so that the top also was about 15 cm out of the water. We placed fish cages approximately 15 m from the water inlet and outlet within each wetland.

Western mosquitofish for our study originated from the same stock at the Sacramento-Yolo Mosquito and Vector Control District's aquaculture facility (D. Dokos, Elk Grove, California, USA). We transported mosquitofish from the aquaculture facility to the Yolo Bypass Wildlife Area (about 25 miles) during the early morning in water-filled, closed ice chests that were kept oxygenated with battery powered aerators. We measured standard length (mm) with a ruled fish board, fresh wet mass (g) using an electronic balance (Ohaus Adventurer™ Pro, Pine Brook, New Jersey, USA), and visually determined sex (**Moyle, 2002**) before their introduction into

cages. To determine baseline THg concentrations in fish at the time of introduction, we randomly selected 37 female mosquitofish from our stock population and recorded their fresh wet weight (g) and standard length (mm), and stored them frozen in Whirl-paks[®] (Nasco, Modesto, California, USA) at -20°C until Hg analysis.

We randomly selected 30 female mosquitofish for each cage and introduced them into cages placed at the inlet, center, and outlet of each of three wetland habitat types (white rice, wild rice, and permanent wetlands) on 28 June 2007, shortly after the white rice fields were re-flooded after being seeded. All fish were removed 60 days after introduction on 27 August 2007. Additionally, during deployment at each outlet, we placed 30 female mosquitofish into a second cage that was 15-20 m from the first outlet cage and these fish were removed at the mid-point of the 60 day exposure period on 27 July 2007 (29 days of exposure) to assess temporal bioaccumulation patterns. Each wetland habitat type was replicated twice; thus, we introduced a total of 24 fish cages (720 total fish) into six different wetlands. The density of mosquitofish introduced into cages was 0.07 fish L⁻¹ of cage space, and the average biomass was 0.11 g of fish L⁻¹, which is a much lower density than most caging experiments assessing contaminant bioaccumulation (review by **Oikari, 2006**). Upon removal from cages, we re-measured each fish's fresh wet weight (g) and standard length (mm), and stored them frozen in Whirl-paks[®] (Nasco, Modesto, California, USA) at -20°C until Hg analysis.

8.2.4 Wild Fish Study

Using beach seines (3 mm mesh, 3 m or 6 m × 1.5 m) and dip nets, we also collected wild western mosquitofish and wild Mississippi silversides at each of the same wetland's inlets and outlets at the time when caged fish were removed (from 27 August to 19 September 2007). As with caged fish, we weighed (g) and measured the standard length (mm) of each fish, and stored them frozen in Whirl-paks[®] (Nasco, Modesto, California, USA) at -20°C until Hg analysis.

8.2.5 Mercury Determination

Prior to Hg analysis, invertebrates and fish were dried at 60°C for 24-48 h, ground, and then homogenized to a fine powder using a porcelain mortar and pestle. Initially, an aliquot of each Corixidae sample and a subset of caged fish were analyzed for MeHg at Battelle Marine Sciences Laboratory (Sequim, Washington, U.S.A.) using cold vapor atomic fluorescence following EPA method 1630 (**U. S. EPA 2001**). We then analyzed the remaining aliquots of the same Corixidae samples and all the Notonectidae and fish samples for THg at the USGS Davis Field Station Mercury Lab, on a Milestone DMA-80 Direct Mercury Analyzer (Milestone Inc., Monroe, Connecticut, U.S.A.) following EPA method 7473 (**U. S. EPA 2000**). For 11 of the 92 invertebrate samples, we could not analyze THg because we were unable to collect enough biomass for both analyses. Because MeHg and THg were highly correlated (see Results), and the percent MeHg did not vary as a function of THg levels (see Results), we used MeHg concentrations and the average percent MeHg in Corixidae to estimate THg concentrations for 11 Corixidae samples. Quality assurance measures included analysis of two certified reference materials (either dogfish muscle tissue [DORM-2; National Research Council of Canada, Ottawa, Canada], dogfish liver [DOLT-3; National Research Council of Canada, Ottawa, Canada], or lobster hepatopancreas [TORT-2; National Research Council of Canada, Ottawa, Canada]), two system and method blanks, two duplicates, one matrix spike, and one matrix spike duplicate per batch. For invertebrate THg, recoveries (\pm SE) averaged 106.3 \pm 1.7% ($N=9$) and

101.1±1.7% ($N=14$) for certified reference materials and calibration checks, respectively. Matrix spike recoveries for THg averaged 98.3±1.3% ($N=10$), and absolute relative percent difference for all duplicates and matrix spike duplicates averaged 7.5±2.9%. For invertebrate MeHg, recoveries averaged 91.20±3.8% ($N=3$) for certified reference materials. Matrix spike recoveries for MeHg averaged 97.3±1.8% ($N=12$), and absolute relative percent difference for all duplicates and matrix spike duplicates averaged 7.8±1.6%. For fish THg, recoveries (\pm SE) averaged 99.4±1.8% ($N=60$) and 97.9±0.8% ($N=90$) for certified reference materials and calibration checks, respectively. Matrix spike recoveries for THg averaged 103.0±0.5% ($N=30$), and absolute relative percent difference for all duplicates and matrix spike duplicates averaged 3.4±0.5%. We report mean±SE THg and MeHg concentrations on a dry weight (dw) basis because Hg is associated with the solid protein lattice in fish tissue, and differences in moisture content among samples can substantially bias Hg results. However, for ease of comparison to other studies and regulation targets, moisture content (mean±SE) was 75.9±0.1% in caged mosquitofish, 73.1±0.2% in wild mosquitofish, and 72.8±0.1% in wild silversides.

8.2.6 Statistical Analysis: Invertebrates

We tested whether THg and MeHg concentrations in invertebrates differed among factors using backward elimination mixed effect analysis of variance (ANOVA), with $\alpha > 0.10$ to remove interactions using JMP® version 5.0 (SAS Institute, Cary, North Carolina, U.S.A.). The global mixed model included wetland habitat type (white rice, wild rice, permanent wetland, and fallow fields), site (inlet, center, and outlet), time period (flood-up and pre-harvest), taxa (Corixidae and Notonectidae; for THg model only) as fixed effects, wetland replicate as a random effect, and all 2-way and 3-way interactions of fixed effects. We found significant 2-way interactions for taxa \times time period, taxa \times wetland type, and time period \times wetland type for the THg model, therefore we used conditional F-tests (slices) to test the effects of wetland type, time period, and taxa separately while accounting for all the other variables in the model. We then used pair-wise t -tests to make multiple comparisons. We calculated the proportion of THg in Corixidae that was in the form of MeHg by dividing the MeHg concentration by the THg concentration. We used linear regression to test whether MeHg concentrations were related to THg concentrations in Corixidae, and to test whether THg concentrations in Corixidae were related to THg concentrations in Notonectidae.

8.2.7 Statistical Analysis: Fish

We tested whether whole-body THg concentrations (\log_e -transformed) in caged mosquitofish exposed for 60 days differed among factors using a mixed effect analysis of covariance (ANCOVA) while accounting for any effects of fish size or body condition with JMP® version 8.0 (SAS Institute, Cary, North Carolina, USA). The global ANCOVA model for THg concentrations included wetland habitat type (white rice, wild rice, and permanent wetland), site (inlet, center, and outlet), fish standard length (\log_e -transformed), and relative body condition as fixed effects, wetland replicate as a random effect, and the wetland type \times site interaction. We estimated the relative body condition of fish using the Relative Condition Factor to account for potential changes in shape as fish grow (Anderson and Neumann, 1996), such as often occurs in gravid female mosquitofish. The Relative Condition Factor was calculated as $K_n = W/W'$, where W was mass in g and W' was the predicted length-specific mean mass from a predictive model calculated for that population. To determine W' for the caged mosquitofish population,

we used \log_{10} -transformed standard length (mm) and \log_{10} -transformed fresh wet mass (g) data for the mosquitofish that were introduced into cages as well as the reference mosquitofish analyzed for Hg (caged mosquitofish linear regression: $N=756$, $R^2=0.76$, intercept=-4.3379, slope=2.8584). We also calculated W' for each species of wild fish using all the wild fish captured and analyzed for Hg (wild mosquitofish linear regression: $N=140$, $R^2=0.95$, intercept=-5.5443, slope=3.5573; wild silverside linear regression: $N=135$, $R^2=0.95$, intercept=-5.0217, slope=2.9583).

Total body burden of THg was calculated for each sample as the product of fish body mass (dw) and whole-body THg concentration. The global ANOVA model for total Hg burden (\log_e -transformed) in caged mosquitofish exposed for 60 days was similar to that for THg concentrations, except that this model did not include fish standard length or relative body condition as covariates since fish size was incorporated when calculating total body burden. Similarly, we tested whole-body THg concentrations (\log_e -transformed) and total Hg burden in wild mosquitofish and wild silversides using the same model structure as for caged fish, except that we only sampled wild fish from inlets and outlets, and not centers. There were significant interactions between wetland type and site in all models; we therefore used conditional F-tests (slices) to test the effects of habitat separately by site, and site separately by habitat, while also accounting for the other variables in the models. We then used pair-wise t -tests to examine which habitats and sites differed. We also used two-sample t -tests to compare THg concentrations and total Hg burdens of reference mosquitofish at introduction to values of mosquitofish removed from cages 60 days later, and we applied a sequential Bonferroni corrected alpha level to account for the number of tests performed (**Rice, 1989**). Unless otherwise noted, we reported model-based mean \pm SE THg concentrations and total Hg burdens based on back-transformed least-square means \pm SEs. The model-based SEs of the means were calculated by the delta method (**Williams et al., 2002**).

We also tested whether the size of mosquitofish removed from cages after 60 days of exposure differed among habitats and sites using a mixed effects analysis of variance (ANOVA). We performed separate ANOVAs for each of three size parameters (\log_e -transformed standard length [mm], \log_e -transformed fresh wet mass [g], and relative body condition). For each ANOVA, we included wetland habitat type (white rice, wild rice, and permanent wetland) and site (inlet, center, and outlet) as fixed effects, wetland replicate as a random effect, and the wetland type \times site interaction. There were significant interactions between wetland type and site in all models (see Results); we therefore used conditional F-tests to test the effects of habitat separately by site, and site separately by habitat, while also accounting for the other variables in the models. We then used pair-wise t -tests to examine which pairs of habitats and sites differed. We also used two-sample t -tests to compare the size of fish at introduction to values 60 days later when fish were removed from cages, and we applied a sequential Bonferroni corrected alpha level to account for the number of tests performed for each variable.

Lastly, we assessed temporal THg bioaccumulation using only reference fish at introduction and mosquitofish caged at wetland outlets. For this analysis, we compared THg concentrations and body burdens among three time periods: 1) reference mosquitofish at introduction, 2) mosquitofish within the second outlet cage that was removed after 29 days of exposure, and 3) mosquitofish within the primary outlet cage that was removed after the full 60 days of exposure.

We used a similar mixed effects ANCOVA to our primary models, where THg concentration (\log_e -transformed) was the dependent variable and wetland habitat type (white rice, wild rice, and permanent wetland), time period (reference, 29-day exposure, and 60-day exposure), fish standard length (\log_e -transformed), and relative body condition were fixed effects, wetland replicate was a random effect, and wetland type \times time period was included as an interaction. The global ANOVA model for THg body burden (\log_e -transformed) was similar to that for THg concentrations, except that this model did not include fish standard length or relative body condition. For these temporal analyses, we randomly selected 12 of the 37 reference mosquitofish at introduction to be assigned to each of the three wetland habitat types at time zero to avoid pseudoreplication of reference fish among habitats.

8.3 Results

8.3.1 Invertebrates

Across all wetland habitat types and sampling time periods, THg concentrations were $0.89 \pm 0.06 \mu\text{g g}^{-1} \text{ dw}$ in Corixidae ($N=36$) and $1.18 \pm 0.08 \mu\text{g g}^{-1} \text{ dw}$ in Notonectidae ($N=45$). Notonectidae THg concentrations were not correlated with Corixidae THg concentrations (linear regression: $N=31$, $R^2=0.01$, $P=0.96$) or Corixidae MeHg concentrations (linear regression: $N=43$, $R^2=0.02$, $P=0.42$) collected at the same locations and time periods. MeHg concentrations in Corixidae were $0.74 \pm 0.05 \mu\text{g g}^{-1} \text{ dw}$ ($N=46$). Corixidae MeHg concentrations were highly correlated with Corixidae THg concentrations (linear regression: $N=34$, $R^2=0.80$, $p<0.0001$; **Figure 8.1**). In addition, most of the THg in Corixidae was comprised of MeHg ($88.0 \pm 3.1\%$) and the proportion of Hg in the form of MeHg was not correlated with THg concentrations (linear regression: $N=34$, $R^2=0.01$, $P=0.99$), indicating that the proportion of THg in the MeHg form did not vary with THg concentrations.

The final model from our backward elimination mixed effect ANOVA model for THg concentrations in invertebrates included wetland type, site, time period, and taxa as fixed effects, wetland replicate as a random effect, and taxa \times time period, taxa \times wetland type, and time period \times wetland type as 2-way interactions (ANOVA: wetland type: $F_{3,3.94}=3.16$, $P=0.15$; site: $F_{2,71.88}=3.84$, $P=0.03$; time period: $F_{1,71.88}=5.12$, $P=0.03$; taxa: $F_{1,71.88}=29.36$, $p<0.0001$; time period \times wetland type: $F_{3,71.88}=4.03$, $P=0.01$; taxa \times wetland type: $F_{3,71.88}=10.37$, $p<0.0001$; taxa \times time period: $F_{1,71.88}=15.83$, $P=0.001$). We therefore used conditional F-tests to further interpret the significant interactions to assess whether invertebrate THg concentrations differed among wetlands, taxa, and time periods.

8.3.1.1 Site

THg concentrations in invertebrates tended to increase from water inlets (least squares mean \pm SE: $0.92 \pm 0.08 \mu\text{g g}^{-1} \text{ dw}$) and wetland centers ($1.01 \pm 0.08 \mu\text{g g}^{-1} \text{ dw}$) to water outlets ($1.14 \pm 0.08 \mu\text{g g}^{-1} \text{ dw}$; **Figures 8.2 & 8.3**). In pairwise comparisons, THg concentrations in invertebrates at the outlet were significantly higher than THg concentrations at the inlets (difference: $0.21 \pm 0.08 \mu\text{g g}^{-1} \text{ dw}$; $t_{2,71.89}=2.76$, $P=0.01$) and THg concentrations at wetland centers did not differ from concentrations at inlets (difference: $0.09 \pm 0.08 \mu\text{g g}^{-1} \text{ dw}$; $t_{2,71.89}=1.15$, $P=0.25$) nor outlets (difference: $0.12 \pm 0.08 \mu\text{g g}^{-1} \text{ dw}$; $t_{2,71.86}=1.61$, $P=0.11$).

8.3.1.2 *Taxa × time*

THg concentrations in Notonectidae increased from the time of flood-up to pre-harvest (difference: $0.40 \pm 0.09 \mu\text{g g}^{-1} \text{ dw}$; $F_{1,71.86}=18.14$, $p < 0.0001$), whereas THg concentrations in Corixidae did not differ between time periods (difference: $0.11 \pm 0.09 \mu\text{g g}^{-1} \text{ dw}$; $F_{1,71.90}=1.60$, $P=0.21$; **Figure 8.4**). Accordingly, THg concentrations in Corixidae did not differ from Notonectidae during the flood-up time period (difference: $0.09 \pm 0.10 \mu\text{g g}^{-1} \text{ dw}$; $F_{1,71.90}=0.94$, $P=0.33$), but Notonectidae were higher than Corixidae during the pre-harvest time period (difference: $0.61 \pm 0.09 \mu\text{g g}^{-1} \text{ dw}$; $F_{1,71.86}=48.99$, $p < 0.0001$).

8.3.1.3 *Wetland type × time*

THg concentrations in invertebrates, overall, increased from the time of flood-up to pre-harvest in permanent wetlands (difference: $0.40 \pm 0.14 \mu\text{g g}^{-1} \text{ dw}$; $F_{1,71.86}=7.57$, $P=0.01$) and wild rice (difference: $0.29 \pm 0.13 \mu\text{g g}^{-1} \text{ dw}$; $F_{1,71.95}=5.19$, $P=0.03$), but not white rice (difference: $0.10 \pm 0.12 \mu\text{g g}^{-1} \text{ dw}$; $F_{1,71.86}=0.62$, $P=0.43$) or shallowly-flooded fallow fields (difference: $0.20 \pm 0.12 \mu\text{g g}^{-1} \text{ dw}$; $F_{1,71.86}=2.54$, $P=0.12$; **Figure 8.4**). THg concentrations in invertebrates did not significantly differ between wetland habitats within the flood-up time period ($F_{3,6.64}=3.14$, $P=0.10$; differences: permanent wetland vs white rice: $0.21 \pm 0.21 \mu\text{g g}^{-1} \text{ dw}$; permanent wetland vs wild rice: $0.48 \pm 0.21 \mu\text{g g}^{-1} \text{ dw}$; fallow vs permanent wetland: $0.09 \pm 0.21 \mu\text{g g}^{-1} \text{ dw}$; fallow vs white rice: $0.29 \pm 0.20 \mu\text{g g}^{-1} \text{ dw}$; fallow vs wild rice: $0.57 \pm 0.20 \mu\text{g g}^{-1} \text{ dw}$; white rice vs wild rice: $0.27 \pm 0.20 \mu\text{g g}^{-1} \text{ dw}$) or pre-harvest time period ($F_{3,5.78}=3.78$, $P=0.08$; differences: permanent wetland vs white rice: $0.51 \pm 0.20 \mu\text{g g}^{-1} \text{ dw}$; permanent wetland vs wild rice: $0.59 \pm 0.20 \mu\text{g g}^{-1} \text{ dw}$; permanent wetland vs fallow: $0.50 \pm 0.20 \mu\text{g g}^{-1} \text{ dw}$; fallow vs white rice: $0.01 \pm 0.20 \mu\text{g g}^{-1} \text{ dw}$; fallow vs wild rice: $0.09 \pm 0.20 \mu\text{g g}^{-1} \text{ dw}$; white rice vs wild rice: $0.08 \pm 0.20 \mu\text{g g}^{-1} \text{ dw}$).

8.3.1.4 *Wetland type × taxa*

THg concentrations differed among wetland habitats for Notonectidae ($F_{3,6.51}=7.97$, $P=0.01$). Notonectidae THg concentrations were higher in permanent wetlands than in wild rice (difference: $1.01 \pm 0.21 \mu\text{g g}^{-1} \text{ dw}$; $t_{3,6.51}=4.81$, $P=0.002$), white rice (difference: $0.72 \pm 0.21 \mu\text{g g}^{-1} \text{ dw}$; $t_{3,6.51}=3.44$, $P=0.01$), and fallow fields (difference: $0.67 \pm 0.21 \mu\text{g g}^{-1} \text{ dw}$; $t_{3,6.51}=3.19$, $P=0.01$), but there were no differences between white rice and wild rice (difference: $0.29 \pm 0.20 \mu\text{g g}^{-1} \text{ dw}$; $t_{3,6.51}=1.47$, $P=0.19$), white rice and fallow fields (difference: $0.05 \pm 0.20 \mu\text{g g}^{-1} \text{ dw}$; $t_{3,6.51}=0.26$, $P=0.80$), or wild rice and fallow fields (difference: $0.34 \pm 0.20 \mu\text{g g}^{-1} \text{ dw}$; $t_{3,6.51}=1.73$, $P=0.14$; **Figures 8.2 & 8.3**). Corixidae THg concentrations did not differ between wetland habitats ($F_{3,5.89}=0.99$, $P=0.46$; differences: white rice vs permanent wetland: $0.01 \pm 0.20 \mu\text{g g}^{-1} \text{ dw}$; permanent wetland vs wild rice: $0.06 \pm 0.20 \mu\text{g g}^{-1} \text{ dw}$; fallow vs permanent wetland: $0.25 \pm 0.20 \mu\text{g g}^{-1} \text{ dw}$; fallow vs white rice: $0.24 \pm 0.20 \mu\text{g g}^{-1} \text{ dw}$; fallow vs wild rice: $0.31 \pm 0.20 \mu\text{g g}^{-1} \text{ dw}$; white rice vs wild rice: $0.07 \pm 0.20 \mu\text{g g}^{-1} \text{ dw}$). THg concentrations in Notonectidae were higher than Corixidae in permanent wetlands (difference: $1.00 \pm 0.14 \mu\text{g g}^{-1} \text{ dw}$; $F_{1,71.86}=48.39$, $p < 0.0001$) and white rice (difference: $0.27 \pm 0.12 \mu\text{g g}^{-1} \text{ dw}$; $F_{1,71.86}=4.84$, $P=0.03$), but THg concentrations in Notonectidae and Corixidae were similar in wild rice (difference: $0.05 \pm 0.13 \mu\text{g g}^{-1} \text{ dw}$; $F_{1,71.95}=0.16$, $P=0.69$) and fallow fields (difference: $0.08 \pm 0.12 \mu\text{g g}^{-1} \text{ dw}$; $F_{1,71.86}=0.39$, $P=0.53$).

8.3.1.5 MeHg in Corixidae

Because we used THg concentrations in our main model, we repeated the backward elimination ANOVA model using only the MeHg data in Corixidae and there were no significant interactions. Wetland habitat type, site, and time period were not significant factors influencing MeHg concentrations in Corixidae (ANOVA: wetland type: $F_{3,4}=0.61$, $P=0.64$; site: $F_{2,37}=1.48$, $P=0.24$; time period: $F_{1,37}=1.17$, $P=0.29$; **Figure 8.5**), although Corixidae MeHg concentrations in permanent wetlands and shallowly-flooded fallow fields tended to be elevated (differences: fallow vs white rice: $0.35\pm 0.32 \mu\text{g g}^{-1} \text{ dw}$; fallow vs wild rice: $0.35\pm 0.32 \mu\text{g g}^{-1} \text{ dw}$; permanent wetland vs white rice: $0.24\pm 0.32 \mu\text{g g}^{-1} \text{ dw}$; permanent wetland vs wild rice: $0.24\pm 0.32 \mu\text{g g}^{-1} \text{ dw}$; fallow vs permanent wetland: $0.12\pm 0.32 \mu\text{g g}^{-1} \text{ dw}$; wild rice vs white rice: $0.01\pm 0.32 \mu\text{g g}^{-1} \text{ dw}$).

8.3.2 Caged Fish

8.3.2.1 Caged fish mercury bioaccumulation after 60-days of exposure

Baseline THg concentrations and body burdens in reference mosquitofish at the time fish were introduced into cages within wetlands were $0.14\pm 0.01 \mu\text{g g}^{-1} \text{ dw}$ ($N=37$; range: $0.08\text{-}0.27 \mu\text{g g}^{-1} \text{ dw}$) and $0.05\pm 0.01 \mu\text{g fish}^{-1} \text{ dw}$ ($N=37$; range: $0.01\text{-}0.29 \mu\text{g fish}^{-1} \text{ dw}$), respectively. To confirm that most Hg in mosquitofish was in the MeHg form, we determined MeHg concentrations in a subset of individuals from both the experimental and reference samples. MeHg concentrations were highly correlated with THg concentrations (linear regression: $N=9$, $R^2=0.98$, $p<0.0001$; **Figure 8.6**), and MeHg accounted for $94.3\pm 4.8\%$ of the THg concentrations.

Across all wetland habitat types and sites, THg concentrations in mosquitofish removed from cages after 60 days of exposure were significantly higher than reference levels at introduction (**Table 8.1**). Total body burden of THg also was higher than reference levels at all sites, but some sites within permanent wetlands and at white rice inlets were not statistically significant after applying the sequential Bonferroni correction. THg concentrations and body burdens in mosquitofish caged at each site increased by a range of 135% to 1197% and 29% to 1566%, respectively (**Table 8.1**). Overall, model-based average THg concentrations in caged mosquitofish ($N=304$) at removal were $1.07\pm 0.09 \mu\text{g g}^{-1} \text{ dw}$, $1.09\pm 0.09 \mu\text{g g}^{-1} \text{ dw}$, and $0.41\pm 0.04 \mu\text{g g}^{-1} \text{ dw}$ in white rice, wild rice, and permanent wetlands, respectively, and $0.69\pm 0.04 \mu\text{g g}^{-1} \text{ dw}$, $0.83\pm 0.04 \mu\text{g g}^{-1} \text{ dw}$, and $0.83\pm 0.04 \mu\text{g g}^{-1} \text{ dw}$ at the inlets, centers, and outlets, respectively.

In our global models, we found that THg concentrations in mosquitofish caged for 60 days were positively related to fish length and negatively related to body condition, while accounting for wetland habitat type and cage site (**Figure 8.7A**). We found significant habitat type \times site interactions for both THg concentrations (habitat: $F_{2,3,0}=43.28$, $P=0.01$, site: $F_{2,291.9}=13.02$, $p<0.0001$, habitat \times site: $F_{4,290.9}=165.66$, $p<0.0001$, length: $F_{1,292.8}=38.85$, $p<0.0001$, condition: $F_{1,292.5}=35.20$, $p<0.0001$) and total Hg burdens (habitat: $F_{2,3,1}=70.04$, $P=0.01$, site: $F_{2,294.0}=58.83$, $p<0.0001$, habitat \times site: $F_{4,293.9}=61.89$, $p<0.0001$). We therefore used conditional F-tests to further interpret whether THg concentrations and total Hg burdens in caged mosquitofish differed among habitats and sites.

8.3.2.1.1 THg concentrations in caged mosquitofish.

THg concentrations in caged mosquitofish differed among wetland habitats at the inlets ($F_{2,4,8}=73.09$, $P=0.001$), centers ($F_{2,3,5}=56.51$, $P=0.01$), and outlets ($F_{2,3,6}=63.50$, $P=0.01$; **Figure**

9.8A). At the inlets, THg concentrations were higher in wild rice than in either white rice ($t_{4,8}=9.82$, $P=0.001$) or permanent wetlands ($t_{4,8}=11.00$, $P=0.001$), but white rice and permanent wetlands did not differ ($t_{4,8}=0.85$, $P=0.43$). At the centers and outlets, THg concentrations were higher in white rice than in either wild rice (center: $t_{3,5}=4.40$, $P=0.02$; outlet: $t_{3,6}=5.98$, $P=0.01$) or permanent wetlands (center: $t_{3,5}=10.61$, $P=0.001$; outlet: $t_{3,6}=11.26$, $P=0.001$), and wild rice was higher than permanent wetlands (center: $t_{3,5}=6.32$, $P=0.01$; outlet: $t_{3,6}=5.45$, $P=0.01$).

THg concentrations also differed among cage sites within white rice ($F_{2,290,7}=194.89$, $p<0.0001$) and wild rice ($F_{2,292,0}=70.87$, $p<0.0001$), but not permanent wetlands ($F_{2,290,5}=0.01$, $P=0.99$; **Figure 8.8A**). Within white rice fields, THg concentrations were higher at field outlets than at the inlets ($t_{290,7}=19.16$, $p<0.0001$) or centers ($t_{290,7}=2.25$, $P=0.03$), and centers were higher than inlets ($t_{290,7}=18.35$, $p<0.0001$). Within wild rice fields, THg concentrations were higher at field inlets than at centers ($t_{292,0}=10.27$, $p<0.0001$) or outlets ($t_{292,0}=11.86$, $p<0.0001$), and centers were higher than outlets ($t_{292,0}=2.73$, $P=0.01$).

8.3.2.1.2 THg body burden in caged mosquitofish.

THg body burdens in caged mosquitofish differed among wetland habitats at inlets ($F_{2,8,0}=28.34$, $P=0.001$), centers ($F_{2,4,2}=91.46$, $P=0.001$), and outlets ($F_{2,4,2}=117.33$, $P=0.001$; **Figure 8.8B**). At the inlets, THg body burdens were higher in wild rice than in white rice ($t_{8,0}=6.26$, $P=0.0001$) or permanent wetlands ($t_{8,0}=6.71$, $P=0.001$), but body burdens in white rice and permanent wetlands did not differ ($t_{8,0}=0.01$, $P=0.99$). At the centers and outlets, THg body burdens were higher in white rice than in either wild rice (center: $t_{4,2}=2.79$, $P=0.05$; outlet: $t_{4,2}=4.46$, $P=0.01$) or permanent wetlands (center: $t_{4,2}=12.96$, $P=0.0001$; outlet: $t_{4,2}=14.91$, $P=0.0001$), and wild rice was higher than permanent wetlands (center: $t_{4,2}=10.29$, $P=0.001$; outlet: $t_{4,2}=10.66$, $P=0.001$).

THg body burdens also differed among cage sites within white rice ($F_{2,292,6}=151.91$, $p<0.0001$) and permanent wetlands ($F_{2,293,8}=4.19$, $P=0.02$), but not wild rice ($F_{2,293,3}=2.31$, $P=0.10$; **Figure 8.8B**). Within white rice fields, THg body burdens were higher at field outlets than at the inlets ($t_{292,6}=17.04$, $p<0.0001$) or centers ($t_{292,6}=2.80$, $P=0.01$), and body burdens at centers were higher than inlets ($t_{292,6}=15.66$, $p<0.0001$). In contrast, within permanent wetlands, THg body burdens were higher at field inlets than at centers ($t_{293,8}=1.99$, $P=0.05$) or outlets ($t_{293,8}=2.88$, $P=0.01$), but body burdens at centers and outlets did not differ ($t_{293,8}=0.91$, $P=0.36$).

8.3.2.2 *Caged fish growth after 60-days of exposure*

Upon introduction into cages, mosquitofish did not differ in standard length or mass among cage sites or habitat types (fish length: habitat: $F_{2,3}=0.42$, $P=0.69$; site: $F_{2,532}=2.81$, $P=0.06$; fish mass: habitat: $F_{2,3}=0.53$, $P=0.64$; site: $F_{2,531}=0.60$, $P=0.55$; **Table 8.2**). After 60 days of exposure, there were significant habitat type \times site interactions for the length (habitat: $F_{2,3,0}=4.68$, $P=0.12$; site: $F_{2,294,4}=34.57$, $p<0.0001$; habitat \times site: $F_{4,294,5}=22.43$, $p<0.0001$), mass (habitat: $F_{2,3,0}=0.53$, $P=0.64$; site: $F_{2,527}=0.61$, $P=0.54$; habitat \times site: $F_{4,527}=2.89$, $P=0.02$), and relative condition factor (habitat: $F_{2,3,0}=0.34$, $P=0.74$; site: $F_{2,294,8}=16.08$, $p<0.0001$; habitat \times site: $F_{4,294,8}=4.65$, $P=0.001$) of mosquitofish removed from cages. We therefore used conditional F-tests to further test whether body measurements differed among habitats or sites.

8.3.2.2.1 Fish length

The standard length of mosquitofish removed from cages differed among habitats at the centers ($F_{2,3.7}=11.55$, $P=0.03$) and outlets ($F_{2,3.7}=14.51$, $P=0.02$), but not at the inlets ($F_{2,6.1}=1.18$, $P=0.37$; **Figure 8.9A**). At the centers and outlets, fish length was greater in white rice (center: $t_{3.7}=3.74$, $P=0.02$; outlet: $t_{3.7}=4.28$, $P=0.01$) and wild rice (center: $t_{3.7}=4.55$, $P=0.01$; outlet: $t_{3.7}=4.99$, $P=0.01$) than in permanent wetlands, but fish length in white rice and wild rice did not differ (center: $t_{3.7}=0.84$, $P=0.46$; outlet: $t_{3.7}=0.69$, $P=0.53$).

Fish length also differed among cage sites within white rice ($F_{2,293.4}=19.44$, $p<0.0001$), wild rice ($F_{2,295.0}=52.38$, $p<0.0001$), and permanent wetlands ($F_{2,294.3}=3.21$, $P=0.04$; **Figure 8.9A**). Within white rice and wild rice fields, fish length was lower at field inlets than at either the centers (white rice: $t_{293.4}=5.37$, $p<0.0001$; wild rice: $t_{295.0}=8.98$, $p<0.0001$) or outlets (white rice: $t_{293.4}=6.18$, $p<0.0001$; wild rice: $t_{295.0}=9.93$, $p<0.0001$), whereas there was no difference in fish length between centers and outlets (white rice: $t_{293.4}=1.49$, $P=0.14$; wild rice: $t_{295.0}=1.22$, $P=0.22$). Within permanent wetlands, fish length was greater at field inlets than at either the centers ($t_{294.3}=2.31$, $P=0.02$) or outlets ($t_{294.3}=2.23$, $P=0.03$), whereas there was no difference in fish lengths between centers and outlets ($t_{294.3}=0.19$, $P=0.85$).

8.3.2.2.2 Fish mass

The fresh wet mass of mosquitofish removed from cages differed among habitats at the outlets ($F_{2,3.3}=8.98$, $P=0.05$), but not the inlets ($F_{2,4.4}=1.69$, $P=0.28$) or centers ($F_{2,3.3}=5.78$, $P=0.08$; **Figure 9.9B**). At the outlets, fish mass was greater in white rice ($t_{3.3}=3.48$, $P=0.03$) and wild rice ($t_{3.3}=3.84$, $P=0.03$) than in permanent wetlands, but white rice and wild rice did not differ ($t_{3.3}=0.35$, $P=0.75$).

Fish mass also differed among cage sites within white rice ($F_{2,293.2}=27.07$, $p<0.0001$), wild rice ($F_{2,294.5}=75.40$, $p<0.0001$), and permanent wetlands ($F_{2,293.7}=4.23$, $P=0.02$; **Figure 8.9B**). Within white rice and wild rice fields, fish mass was lower at field inlets than at either the center (white rice: $t_{293.2}=6.88$, $p<0.0001$; wild rice: $t_{294.5}=11.14$, $p<0.0001$) or outlet (white rice: $t_{293.2}=7.02$, $p<0.0001$; wild rice: $t_{294.5}=11.68$, $p<0.0001$), whereas there was no difference between centers and outlets (white rice: $t_{293.2}=0.50$, $P=0.62$; wild rice: $t_{294.5}=0.66$, $P=0.51$). Within permanent wetlands, fish mass was higher at the inlets than at the outlets ($t_{293.7}=2.89$, $P=0.01$), but did not differ between centers and inlets ($t_{293.7}=1.48$, $P=0.14$) or centers and outlets ($t_{293.7}=1.49$, $P=0.14$).

8.3.2.2.3 Fish relative body condition

The relative body condition of mosquitofish removed from cages did not differ among habitats at the inlets ($F_{2,7.4}=1.98$, $P=0.20$), centers ($F_{2,4.0}=0.41$, $P=0.69$), or outlets ($F_{2,4.0}=1.80$, $P=0.28$; **Figure 8.9C**). However, fish body condition varied among cage sites within white rice ($F_{2,293.5}=6.32$, $P=0.01$), wild rice ($F_{2,294.6}=12.95$, $p<0.0001$), and permanent wetlands ($F_{2,294.6}=4.55$, $P=0.01$; **Figure 8.9C**). Within white rice and wild rice fields, fish body condition was lower at field inlets than at either the centers (white rice: $t_{293.5}=3.50$, $P=0.001$; wild rice: $t_{294.6}=5.01$, $p<0.0001$) or outlets (white rice: $t_{293.5}=2.35$, $P=0.02$; wild rice: $t_{294.6}=4.30$, $p<0.0001$), whereas there was no difference between centers and outlets (white rice: $t_{293.5}=1.63$, $P=0.10$; wild rice: $t_{294.6}=1.00$, $P=0.32$). Within permanent wetlands, fish body condition did not differ

between inlets and centers ($t_{294.6}=1.06$, $P=0.29$) or inlets and outlets ($t_{294.6}=1.61$, $P=0.11$), but body condition at wetland centers was higher than at outlets ($t_{294.6}=2.99$, $P=0.01$).

8.3.2.3 Temporal mercury bioaccumulation in caged fish

In addition to our assessment of THg bioaccumulation in caged fish after 60 days of exposure, we also examined how quickly Hg was bioaccumulated. We did so only at wetland outlets, where we removed separate cages of fish after 29 and 60 days of exposure. We found a significant habitat type \times time period interaction for both THg concentrations (habitat: $F_{2,3.4}=18.59$, $P=0.01$, time period: $F_{2,7.1}=75.32$, $p<0.0001$, habitat \times time period: $F_{4,11.89}=10.17$, $P=0.001$, length: $F_{1,204.5}=56.93$, $p<0.0001$, condition: $F_{1,203.8}=5.64$, $P=0.02$) and THg body burdens (habitat: $F_{2,4.1}=35.49$, $P=0.01$, time period: $F_{2,6.9}=35.31$, $P=0.001$, habitat \times time period: $F_{4,21.0}=13.35$, $p<0.0001$). We therefore used conditional F-tests to further examine whether THg concentrations and THg body burdens in caged mosquitofish differed among habitats and within habitats among time periods.

8.3.2.3.1 Temporal THg concentrations in caged mosquitofish.

THg concentrations in caged mosquitofish differed among time periods within white rice ($F_{2,8.0}=65.09$, $p<0.0001$), wild rice ($F_{2,7.9}=29.26$, $P=0.001$), and permanent wetlands ($F_{2,8.0}=21.98$, $P=0.001$; **Figure 8.10A**). Within white rice and wild rice fields, THg concentrations were higher after 60 days of exposure than after 29 days (white rice: $t_{8.0}=8.01$, $p<0.0001$; wild rice: $t_{7.9}=4.50$, $p<0.0001$) and both 29-day and 60-day exposed mosquitofish were higher than reference fish at introduction (29-day white rice: $t_{8.0}=7.44$, $P=0.01$; 29-day wild rice: $t_{7.9}=5.76$, $P=0.01$; 60-day white rice: $t_{8.0}=9.54$, $P=0.001$; 60-day wild rice: $t_{7.9}=6.95$, $P=0.01$). Within permanent wetlands, THg concentrations were higher after 60-days of exposure than after 29-days ($t_{8.0}=5.97$, $p<0.0001$) and only 60-day exposed mosquitofish were higher than reference fish at introduction (29-day: $t_{8.0}=2.46$, $P=0.08$; 60-day: $t_{8.0}=4.00$, $P=0.02$). Overall, 57%, 71%, and 50% of the THg concentrations at day 60 occurred within the first 29 days in white rice, wild rice, and permanent wetlands, respectively.

THg concentrations in caged mosquitofish did not differ among wetland habitats for reference fish at introduction ($F_{2,203.0}=0.64$, $P=0.53$), however THg concentrations differed among wetlands at 29 and 60 days of exposure (29-day: $F_{2,3.6}=17.10$, $P=0.01$; 60-day: $F_{2,3.2}=21.79$, $P=0.01$; **Figure 8.10A**). At 29 days of exposure, THg concentrations were higher in white rice and wild rice than in permanent wetlands (white rice: $t_{3.6}=5.82$, $P=0.01$; wild rice: $t_{3.6}=3.47$, $P=0.03$), but white rice and wild rice did not differ ($t_{3.6}=2.36$, $P=0.09$). At 60 days of exposure, THg concentrations were higher in white rice and wild rice than in permanent wetlands (white rice: $t_{3.2}=6.59$, $P=0.01$; wild rice: $t_{3.2}=3.06$, $P=0.05$), and white rice also was higher than wild rice ($t_{3.2}=3.59$, $P=0.04$).

8.3.2.3.2 Temporal THg body burden in caged mosquitofish

THg body burdens in caged mosquitofish differed among time periods within white rice ($F_{2,9.2}=46.04$, $p<0.0001$) and wild rice ($F_{2,9.2}=23.45$, $P=0.001$), but not permanent wetlands ($F_{2,9.3}=1.93$, $P=0.20$; **Figure 8.10B**). Within white rice and wild rice fields, THg body burdens were higher after 60 days of exposure than after 29 days (white rice: $t_{9.2}=5.23$, $p<0.0001$; wild rice: $t_{9.2}=4.17$, $p<0.0001$) and both 29-day and 60-day exposed mosquitofish were higher than

reference fish at introduction (29-day white rice: $t_{9,2}=6.79$, $P=0.01$; 29-day wild rice: $t_{9,2}=4.41$, $P=0.01$; 60-day white rice: $t_{9,2}=9.10$, $P=0.001$; 60-day wild rice: $t_{9,2}=6.19$, $P=0.01$). Overall, 49%, 53%, and 71% of the THg body burdens at day 60 were bioaccumulated within the first 29 days in white rice, wild rice, and permanent wetlands, respectively.

THg body burdens in caged mosquitofish did not differ among wetland habitats for reference fish at introduction ($F_{2,205.0}=1.56$, $P=0.21$), however THg body burdens differed among wetlands at 29 and 60 days of exposure (29-day: $F_{2,4.7}=23.79$, $P=0.01$; 60-day: $F_{2,3.4}=46.02$, $P=0.01$; **Figure 8.10B**). At both 29 and 60 days of exposure, fish THg body burdens were higher in white rice and wild rice than in permanent wetlands (29-day white rice: $t_{4,7}=6.69$, $P=0.001$; 29-day wild rice: $t_{4,7}=4.79$, $P=0.01$; 60-day white rice: $t_{3,4}=9.31$, $P=0.001$; 60-day wild rice: $t_{3,4}=6.72$, $P=0.01$), but white rice and wild rice did not differ (29-day: $t_{4,7}=1.90$, $P=0.12$; 60-day: $t_{3,4}=2.69$, $P=0.07$).

8.3.3 Wild Fish Mercury Bioaccumulation

THg concentrations in wild mosquitofish ($N=140$) were $0.67\pm 0.13 \mu\text{g g}^{-1}$ dw, $0.75\pm 0.15 \mu\text{g g}^{-1}$ dw, and $0.44\pm 0.08 \mu\text{g g}^{-1}$ dw in white rice, wild rice, and permanent wetlands, respectively, and $0.47\pm 0.06 \mu\text{g g}^{-1}$ dw and $0.79\pm 0.09 \mu\text{g g}^{-1}$ dw at the inlets and outlets, respectively. THg concentrations in wild silversides ($N=135$) were $0.82\pm 0.14 \mu\text{g g}^{-1}$ dw, $0.92\pm 0.16 \mu\text{g g}^{-1}$ dw, and $0.28\pm 0.05 \mu\text{g g}^{-1}$ dw in white rice, wild rice, and permanent wetlands, respectively, and $0.48\pm 0.05 \mu\text{g g}^{-1}$ dw and $0.74\pm 0.08 \mu\text{g g}^{-1}$ dw at the inlets and outlets, respectively.

Similar to our caged fish models, we found significant interactions between habitat type \times site for wild mosquitofish (THg concentrations: habitat: $F_{2,2.7}=2.10$, $P=0.28$, site: $F_{1,131.8}=51.95$, $p<0.0001$, habitat \times site: $F_{2,130.6}=42.71$, $p<0.0001$, length: $F_{1,126.8}=1.57$, $P=0.21$, condition: $F_{1,131.4}=7.01$, $P=0.01$; total Hg burdens: habitat: $F_{2,3.1}=0.47$, $P=0.66$, site: $F_{1,134.0}=26.98$, $p<0.0001$, habitat \times site: $F_{2,133.1}=6.07$, $P=0.01$) and wild silversides (THg concentrations: habitat: $F_{2,2.9}=14.70$, $P=0.03$, site: $F_{1,126.9}=49.94$, $p<0.0001$, habitat \times site: $F_{2,126.1}=24.01$, $p<0.0001$, length: $F_{1,126.6}=53.81$, $p<0.0001$, condition: $F_{1,126.1}=1.77$, $P=0.19$; total Hg burdens: habitat: $F_{2,3.2}=10.98$, $P=0.04$, site: $F_{1,122.7}=7.54$, $P=0.01$, habitat \times site: $F_{2,121.6}=8.96$, $P=0.001$). THg concentrations were positively related to fish length for wild silversides, but not for wild mosquitofish, and negatively related to body condition for wild mosquitofish, but not wild silversides (**Figure 8.7B and 8.7C**). To interpret the effects of habitat type and site further, we used conditional F-tests.

8.3.3.1 THg concentrations in wild fish

THg concentrations in both wild mosquitofish and wild silversides differed among wetland habitat types at outlets (mosquitofish: $F_{2,2.9}=8.90$, $P=0.05$; silversides: $F_{2,3.5}=23.92$, $P=0.01$), but not inlets (mosquitofish: $F_{2,3.6}=1.13$, $P=0.42$; silversides: $F_{2,3.3}=6.68$, $P=0.07$; **Figure 8.11A and 8.11B**). At the outlets, THg concentrations were higher in white rice (mosquitofish: $t_{2,9}=3.95$, $P=0.03$; silversides: $t_{3,5}=6.16$, $P=0.01$) and wild rice (mosquitofish: $t_{2,9}=3.22$, $P=0.05$; silversides: $t_{3,5}=5.59$, $P=0.01$) than in permanent wetlands, but wild rice and white rice did not differ (mosquitofish: $t_{2,9}=0.74$, $P=0.51$; silversides: $t_{3,5}=0.03$, $P=0.98$).

THg concentrations in both wild mosquitofish and wild silversides also differed among sites within white rice (mosquitofish: $F_{1,130.0}=126.60$, $p<0.0001$; silversides: $F_{1,124.5}=76.36$, $p<0.0001$) and wild rice (mosquitofish: $F_{1,126.8}=10.83$, $P=0.001$; silversides: $F_{1,126.4}=16.29$, $p<0.0001$), but not permanent wetlands (mosquitofish: $F_{1,129.0}=2.57$, $P=0.11$; silversides: $F_{1,124.0}=0.28$, $P=0.60$; **Figure 8.11A and 8.11B**). Within white rice and wild rice fields, THg concentrations were higher at field outlets than at the inlets (mosquitofish in white rice: $t_{130.0}=11.25$, $p<0.0001$; silversides in white rice: $t_{124.5}=8.74$, $p<0.0001$; mosquitofish in wild rice: $t_{126.8}=3.29$, $P=0.001$; silversides in wild rice: $t_{126.4}=4.04$, $P=0.0001$).

8.3.3.2 THg body burdens in wild fish

Total body burden of THg in wild mosquitofish did not differ among habitats at inlets ($F_{2,4.1}=0.95$, $P=0.46$) or outlets ($F_{2,3.2}=1.00$, $P=0.46$; **Figure 8.11A**). However, total body burden differed among sites within white rice ($F_{1,131.6}=19.54$, $p<0.0001$) and wild rice ($F_{1,132.1}=13.96$, $P=0.001$), but not permanent wetlands ($F_{1,131.1}=0.32$, $P=0.57$; **Figure 8.11A**). Within white rice and wild rice fields, body burden was higher at field outlets than at the inlets (white rice: $t_{131.6}=4.42$, $p<0.0001$; wild rice: $t_{132.1}=3.74$, $P=0.001$).

Total body burden of THg in wild silversides differed among habitats at outlets ($F_{2,5.4}=20.42$, $P=0.01$), but not inlets ($F_{2,5.7}=2.50$, $P=0.17$; **Figure 8.11B**). At the outlets, body burden was higher in white rice ($t_{5,4}=6.33$, $P=0.01$) and wild rice ($t_{5,4}=3.17$, $P=0.01$) than in permanent wetlands, but body burdens in wild rice and white rice did not differ ($t_{5,4}=1.57$, $P=0.15$). Total body burden of THg in wild silversides also differed among sites within white rice ($F_{1,127.3}=23.64$, $p<0.0001$), but not wild rice ($F_{1,99.4}=1.09$, $P=0.30$) or permanent wetlands ($F_{1,126.3}=0.91$, $P=0.34$; **Figure 8.11B**). Within white rice fields, body burden was higher at field outlets than at the inlets ($t_{127.3}=4.86$, $p<0.0001$).

8.3.4 Caged vs. Wild Fish

In general, although caged mosquitofish were only introduced for 60 days, caged mosquitofish bioaccumulated THg to higher concentrations than wild mosquitofish that were exposed to Yolo Bypass Hg concentrations presumably their entire lives (**Figure 8.12**). This illustrates the value of using caged fish as site specific bioindicators of Hg contamination. Because wild fish are free to move in and out of the wetlands studied and into canals where MeHg concentrations are known to be lower, their concentrations represent exposure within each wetland for an unknown time period. Alternatively, caged fish not only allow for sampling over a known and discrete time period, but the method also allows for the calculation of bioaccumulation rates over time.

8.3.5 Biota Hg vs. Water MeHg and Sediment MeHg

We used linear regression to compare biota Hg concentrations with sediment MeHg concentrations and MeHg in unfiltered surface water using each site (inlet, center, or outlet) as an independent replicate (**Figure 8.13**). We found that caged mosquitofish THg concentrations at removal were slightly more correlated with MeHg in unfiltered surface water collected at deployment ($N=13$, $R^2=0.44$, $P=0.01$), than in water collected upon retrieval ($N=13$, $R^2=0.33$, $P=0.04$), suggesting that bioaccumulation into fish occurs rapidly upon early exposure. Interestingly, we found no correlation between THg concentrations in mosquitofish and MeHg in sediment sampled upon introduction ($N=5$, $R^2=0.01$, $P=0.86$) or retrieval ($N=5$, $R^2=0.01$,

$P=0.85$). In contrast, invertebrate (Corixidae) MeHg concentrations were more correlated with MeHg in sediment ($N=14$, $R^2=0.40$, $p<0.01$) than with MeHg in unfiltered surface water ($N=39$, $R^2=0.24$, $p<0.01$) across all time periods.

8.4 Discussion

The Yolo Bypass Wildlife Area, like many other state and federal refuges in California's Central Valley, is primarily managed as waterfowl and shorebird habitat. Therefore, wetlands are typically managed using shallow and intermittent flooding because seasonal wetlands typically have greater invertebrate abundance than permanent wetlands that have longer hydroperiods (Neckles et al., 1990). In particular, reverse-cycle seasonal wetlands are intermittently flooded during the spring and summer to increase invertebrate production for breeding ducks (Neckles et al., 1990; de Szalay et al., 2003), which switch from a diet primarily of seeds to that of invertebrates in order to attain the required protein for egg formation (reviews by Alisauskas and Ankney, 1992; Krapu and Reinecke, 1992), and ducklings, that require invertebrate protein for rapid growth (review by Sedinger, 1992). Unfortunately, cyclical wetting and drying of wetland habitats often is associated with increased MeHg production and concentrations in biota (Hall et al., 1998; Snodgrass et al., 2000).

We found that wetland habitat type had an important influence on Hg concentrations in invertebrates and fish, but this effect differed among taxa. Specifically, our results indicate that THg concentrations in Notonectidae, but not Corixidae, increased from wetland flood-up to draw-down, whereas invertebrate THg concentrations in temporarily flooded habitats were not higher than permanent wetlands. In fact, THg concentrations in Notonectidae were higher in permanent wetlands than in white rice, wild rice, or shallowly-flooded fallow fields, but did not differ among wetland types for Corixidae. The effect of habitat on invertebrate THg concentration was especially prevalent at the end of the rice growing season, when Notonectidae THg concentrations were higher in permanent wetlands than in any other wetland habitat. Similarly, THg concentrations in amphipods (Crangonyctidae) were highest in permanent wetlands compared to intermittently flooded sites in the Okefenokee Swamp in Georgia (George and Batzer, 2008).

Importantly, our results are in direct contrast to the companion studies we conducted simultaneously using caged and wild fish, highlighting the importance of evaluating multiple biosentinels simultaneously. In fish, we found strong evidence for higher THg concentrations in white rice and wild rice fields compared to permanent wetlands. However, we did find similar within-field spatial patterns between invertebrates and fish, with both taxa groups tending to have higher THg concentrations at field outlets than at field inlets. These incongruent results for THg concentrations in invertebrates and fish among wetland habitats indicate that bioaccumulation pathways in wetlands are complex and underscore the importance of using several taxa at different trophic levels to examine MeHg bioaccumulation in wetlands. The complexity of MeHg bioaccumulation in wetlands is further illustrated by the fact that we did not find a correlation between THg concentrations in Notonectidae and Corixidae, even though the paired samples were collected at the same sites and on the same days. Notonectidae (*Notonecta*) typically forage at a higher trophic level than Corixidae (*Corisella*; Menke, 1979; Merritt and Cummins, 1996). Thus, the lack of correlation between their THg concentrations indicates that

they are foraging on different prey items, and that the two invertebrates are not tightly linked within the foodweb.

Furthermore, we found that caged fish THg concentrations were correlated with water MeHg concentrations, but not with sediment MeHg concentrations, whereas invertebrate MeHg concentrations were more correlated with sediment MeHg concentrations than with water MeHg concentrations. Thus pelagic-feeding fish may be better indicators of MeHg availability within the water column, and demersal invertebrates better indicators for MeHg availability in sediment, however simultaneously using several bioindicators when monitoring MeHg production and bioaccumulation is important. Top predators often forage on both benthic and pelagic prey, and an important exposure source may be overlooked if bioindicators of only one habitat are examined.

Notably, Corixidae THg and MeHg concentrations were higher at the Yolo Bypass Wildlife Area wetlands than in wetlands located downstream within the same watershed in San Francisco Bay (THg: $0.63 \mu\text{g g}^{-1} \text{ dw}$, MeHg: $0.59 \mu\text{g g}^{-1} \text{ dw}$; A. K. Miles, U. S. Geological Survey, unpublished data). Overall, 75% and 48% of all Corixidae samples at the Yolo Bypass Wildlife Area exceeded reported MeHg dietary effect levels of $0.50 \mu\text{g g}^{-1} \text{ dw}$ for mallard reproduction (*Anas platyrhynchos*; **Heinz, 1979**) and $0.70 \mu\text{g g}^{-1} \text{ dw}$ for American kestrel reproduction (*Falco sparverius*; **Albers et al., 2007**), respectively. Considering that Corixidae are common in waterfowl diets (**Euliss et al., 1991**), higher trophic level predators may be negatively affected by current Hg concentrations in invertebrate prey within Yolo Bypass wetlands.

Furthermore, all caged fish and 99% of wild fish sampled exceeded the Central Valley Regional Water Quality Control Board's Total Maximum Daily Load (TMDL) target for Hg concentrations in small fish ($0.03 \mu\text{g g}^{-1} \text{ ww}$ or approximately $0.11 \mu\text{g g}^{-1} \text{ dw}$ assuming 73% moisture in wild) that is meant to be protective of wildlife in the Sacramento-San Joaquin River Delta (**Wood et al., 2010a**). Although this TMDL target is likely below actual effects to many wildlife, like piscivorous waterbirds, 38% of caged mosquitofish, 19% of wild mosquitofish, and 13% of wild silversides exceeded the dietary concentration of $0.30 \mu\text{g g}^{-1} \text{ ww}$ which is commonly associated with impaired bird reproduction (**Barr, 1986; Albers et al., 2007; Burgess and Meyer, 2008**). In addition to wildlife, fish health might also be affected at current concentrations. Fifty-nine percent of caged mosquitofish and 36% of wild mosquitofish and silversides sampled exceeded $0.20 \mu\text{g g}^{-1} \text{ ww}$ (approximately 0.74 and $0.83 \mu\text{g g}^{-1} \text{ dw}$ assuming 73% and 76% moisture in wild and caged fish, respectively), the fish health risk threshold associated with sublethal endpoints (**Beckvar et al., 2005**).

Thus, there may be substantial risk of MeHg toxicity to waterbirds and other wildlife that forage in Yolo Bypass wetlands. Of particular concern within these wetlands are wading birds such as egrets, herons, ibis, shorebirds, and ducks. Recent lab studies (**Heinz et al., 2009**) have confirmed that wading birds are among the most sensitive species to mercury-induced egg hatching failure, thus future research should evaluate potential effects to these abundant birds in the area. MeHg concentrations in these waterbirds, such as black-necked stilts, should be evaluated to determine wildlife exposure and risk. For example, within San Francisco Bay, we found that black-necked stilt chicks (*Himantopus mexicanus*) found dead near nesting sites had higher THg concentrations than those in randomly-sampled live chicks of similar age

(Ackerman et al., 2008a) and that failed-to-hatch Forster's tern (*Sterna forsteri*) eggs had higher THg concentrations than randomly-sampled live eggs (Ackerman et al., 2008b). Similar deleterious effects of Hg on waterbird reproduction may be occurring within Yolo Bypass wetlands where Hg concentrations in prey are considerably higher than in San Francisco Bay wetlands.

8.5 Summary

8.5.1 Objective

Wetlands typically have higher rates of MeHg production than other aquatic habitats, but it is unclear whether there are specific wetland habitat types that enhance MeHg bioaccumulation. We examined MeHg bioavailability in invertebrates and fish within four of the most predominant wetland habitats in California's Central Valley agricultural region during the spring and summer: white rice, wild rice, permanent wetlands, and shallowly-flooded fallow fields.

8.5.2 Mercury in Invertebrates

We sampled THg and MeHg concentrations in two aquatic macroinvertebrate taxa at the inlets, centers, and outlets of four replicated wetland habitats (8 wetlands total) during two time periods bounding the rice growing season and corresponding to flood-up and pre-harvest (96 total samples). In general, THg concentrations (mean±standard error) in Notonectidae (*Notonecta*, back swimmers; $1.18 \pm 0.08 \mu\text{g g}^{-1} \text{ dw}$) were higher than in Corixidae (*Corisella*, water boatmen; $0.89 \pm 0.06 \mu\text{g g}^{-1} \text{ dw}$, MeHg: $0.74 \pm 0.05 \mu\text{g g}^{-1} \text{ dw}$). MeHg concentrations were correlated with THg concentrations in Corixidae ($R^2=0.80$) and 88% of THg was in the MeHg form. Wetland habitat type had an important influence on THg concentrations in aquatic invertebrates, but this effect depended on the sampling time period and taxa. In particular, THg concentrations in Notonectidae, but not Corixidae, were higher in permanent wetlands than in white rice, wild rice, or shallowly-flooded fallow fields. THg concentrations in Notonectidae were higher at the end of the rice growing season than near the time of flood-up, whereas THg concentrations in Corixidae did not differ between time periods. The effect of wetland habitat type was more prevalent near the end of the rice growing season, when Notonectidae THg concentrations were highest in permanent wetlands. Additionally, invertebrate THg concentrations were higher at water outlets than at inlets of wetlands. Our results indicate that although invertebrate THg concentrations increased from the time of flood-up to draw-down of wetlands, temporarily flooded habitats such as white rice, wild rice, and shallowly-flooded fallow fields did not have higher THg or MeHg concentrations in invertebrates than permanent wetlands.

8.5.3 Mercury in Caged Fish

We introduced western mosquitofish (*Gambusia affinis*) into cages placed within white rice, wild rice, and permanent wetlands at hydrologic sites associated with their surface water inlets, centers, and outlets. We introduced 30 individual fish into each of the 24 cages that were used, for a total of 720 fish that were introduced into Yolo Bypass Wildlife Area wetlands. Baseline THg concentrations in reference mosquitofish at the time cages were introduced into wetlands were $0.14 \pm 0.05 \mu\text{g g}^{-1} \text{ dw}$ ($N=37$). THg concentrations and whole body burdens of caged mosquitofish increased rapidly, exceeding reference values at introduction by 135% to

1197% and 29% to 1566% among sites, respectively, after only 60 days. Mercury bioaccumulation in caged mosquitofish was greater in rice fields than in permanent wetlands. For example, THg concentrations in mosquitofish caged at wetland outlets increased by 12.1, 5.8, and 2.9 times over reference values at introduction in white rice, wild rice, and permanent wetlands, respectively. Within wetlands, THg concentrations and body burdens of caged fish increased from water inlets to outlets in white rice fields, and tended to not vary among sites in permanent wetlands. Overall, model-based average THg concentrations in caged mosquitofish ($N=304$) at removal after 60 days of exposure were $1.07\pm 0.09 \mu\text{g g}^{-1} \text{ dw}$, $1.09\pm 0.09 \mu\text{g g}^{-1} \text{ dw}$, and $0.41\pm 0.04 \mu\text{g g}^{-1} \text{ dw}$ in white rice, wild rice, and permanent wetlands, respectively, and $0.69\pm 0.04 \mu\text{g g}^{-1} \text{ dw}$, $0.83\pm 0.04 \mu\text{g g}^{-1} \text{ dw}$, and $0.83\pm 0.04 \mu\text{g g}^{-1} \text{ dw}$ at the inlets, centers, and outlets, respectively.

8.5.4 Mercury in Wild Fish

We also collected wild western mosquitofish and wild Mississippi silversides (*Menidia beryllina*) at each wetland's inlets and outlets when caged fish were removed. Across all wetland habitat types and sites, THg concentrations in wild mosquitofish ($N=140$) were $0.67\pm 0.13 \mu\text{g g}^{-1} \text{ dw}$, $0.75\pm 0.15 \mu\text{g g}^{-1} \text{ dw}$, and $0.44\pm 0.08 \mu\text{g g}^{-1} \text{ dw}$ in white rice, wild rice, and permanent wetlands, respectively, and $0.47\pm 0.06 \mu\text{g g}^{-1} \text{ dw}$ and $0.79\pm 0.09 \mu\text{g g}^{-1} \text{ dw}$ at the inlets and outlets, respectively. THg concentrations in wild silversides ($N=135$) were $0.82\pm 0.14 \mu\text{g g}^{-1} \text{ dw}$, $0.92\pm 0.16 \mu\text{g g}^{-1} \text{ dw}$, and $0.28\pm 0.05 \mu\text{g g}^{-1} \text{ dw}$ in white rice, wild rice, and permanent wetlands, respectively, and $0.48\pm 0.05 \mu\text{g g}^{-1} \text{ dw}$ and $0.74\pm 0.08 \mu\text{g g}^{-1} \text{ dw}$ at the inlets and outlets, respectively. Similar to caged fish, THg concentrations in wild fish differed among habitats, with white rice and wild rice having higher THg concentrations than permanent wetlands. THg concentrations in wild fish were higher at outlets than inlets in white rice and wild rice, but there was no difference between sites in permanent wetlands. Our results from wild fish are similar to caged fish, except that THg concentrations in caged fish were considerably higher than wild fish that were presumably exposed to Yolo Bypass Hg concentrations their entire lives. This illustrates the importance of using caged fish as site specific bioindicators of Hg contamination since wild fish are free to move in and out of the wetlands studied and into canals where MeHg concentrations are known to be lower.

8.6 Conclusions

Our results indicate that temporarily flooded shallow wetlands, such as white rice and wild rice fields, have elevated THg concentrations in both caged and wild fish compared to permanent wetlands at the Yolo Bypass. In contrast, THg and MeHg concentrations in invertebrates were higher in permanent wetlands than in white rice or wild rice fields. These conflicting results are partially explained by the fact that fish THg concentrations were correlated with water MeHg, but not with sediment MeHg, whereas invertebrate MeHg concentrations were more correlated with sediment MeHg than with water MeHg. These results illustrate the complexity of MeHg bioaccumulation through food webs and indicate the importance of simultaneously using multiple biosentinels when monitoring MeHg production and bioaccumulation.

Hg concentrations exceeded levels that are potentially harmful to wildlife - Hg concentrations in invertebrates and fish were more than 6 and 11 times higher, respectively, in Yolo Bypass wetlands than stated TMDL target values to protect humans and wildlife (0.03 ppm ww). In fact, 99% of wild fish sampled in Yolo Bypass wetlands exceeded this TMDL target

value to protect wildlife and 75% of invertebrates sampled in Yolo Bypass wetlands exceeded MeHg dietary levels of $0.50 \mu\text{g g}^{-1}$ dw that have been previously shown to impair avian reproduction.

9 Detailed Results for Methylmercury Photodemethylation

The data reported in this section relates to summary **Section 3.2: Methylmercury Export** and **Section 3.3: Methylmercury Production in Surface Sediment**.

9.1 Introduction

MeHg photodecomposition – the destruction of MeHg to inorganic mercury (Hg(II) or Hg⁰) by exposure to solar radiation – is an important process which can dramatically influence the abundance and cycling of MeHg in aquatic surface waters. In fact, photodecomposition (e.g. photodegradation) has been shown to account for 80% of the loss of MeHg from an Alaskan lake (**Hammerschmidt and Fitzgerald, 2006**). Previous work in the Bay-Delta has shown that photodecomposition is highly significant in the biogeochemical cycling of mercury, particularly during summertime low river flow conditions (**Byington et al., 2005; Byington, 2007; Stephenson et al., 2008**). It was hypothesized that agricultural rice fields are aquatic systems with high production of MeHg. If this hypothesis is supported by field measurements, then MeHg concentrations in water on agricultural rice fields will likely be elevated compared to ambient waters in the Delta region. Given their shallow water depths, photodecomposition may therefore play an important role in the biogeochemical cycling and transport of Hg in the rice fields.

This current report on the photodecomposition of MeHg in agriculturally-managed and non-agricultural wetlands in the YBWA is part of a larger effort to understand the biogeochemical cycling and transport of Hg and MeHg associated with agricultural rice field activities. The rate of MeHg destruction by photochemical processes was investigated to determine how this process varies relative to the various manipulations and Best Management Practices (BMP) of rice farmers. Special attention was focused on investigating the role of dissolved organic matter concentrations and light intensity on MeHg destruction rates.

9.2 Approach

9.2.1 Bottle Incubations

Photodemethylation experiments were conducted following the *in situ* Teflon® bottle incubation experiments described by **Byington et al. (2005)** and **Byington (2007)**. In preparation for the experiment, a large volume (~ 10 liters) of filtered surface water was collected in a polycarbonate carboy by pumping water through a 0.45 µm filter cartridge using a peristaltic pump. The peristaltic pump was equipped with C-flex pump head tubing and FEP Teflon® tubing on both the inlet and outlet. Sampling was conducted using ultra-clean protocols.

For the winter sampling event only, MeHg was added to the samples to raise the ambient MeHg concentration by ~0.4 ng L⁻¹. Spiking was deemed necessary to maintain concentrations above the method detection limits and to assure good analytical reproducibility. After rigorous mixing of the carboy, ~ 400 mL of the filtered water was aliquoted into 5 darkened (control) and 6 clear 500 mL FEP Teflon® bottles. A duplicate of one time point (usually the final time point) was collected with each experiment, which is why 6 clear bottles were used. Sample bottles were placed in a 13 mm polypropylene mesh and floated on the surface of an open water area of

the YBWA (**Figure 9.1**). One dark and one light bottle were harvested immediately before deployment, and these served as the time zero samples. A pair of samples (dark and light) was retrieved periodically over a 2-3 day exposure period providing a total of five time points of increasing total light exposure. Following retrieval, samples were immediately preserved in the field by acidification with high purity hydrochloric acid to 0.5% acid (v/v). After preservation, samples were kept dark and at ambient temperature (not exposed to heat) until analysis.

Sample bottles, carboys, and tubing were cleaned using 7.5 N reagent grade nitric acid (HNO₃) except for C-flex tubing which was cleaned using 1.2 N reagent grade hydrochloric acid (HCl). All bottles and carboys were filled with 0.5% v/v reagent grade HCl and stored until use. Ultra clean handling protocols (**EPA 1669**) were followed throughout equipment cleaning, sample collection, experimental manipulation, and analysis (**Gill and Fitzgerald, 1985**).

9.2.2 Sampling Locations and Dates

Sampling was conducted in five separate agricultural and wetland types in the YBWA: (1) two rotational white rice fields (after fallow, R31 and R64); (2) two wild rice fields (after fallow, R32 and R65); (3) two fallow fields after wild rice planting and harvesting (rotational fallow, F20 and F66); (4) a seasonal wetland (SW1); and (5) a permanent wetland (PW5). Sampling of these rice fields and wetlands were conducted in a winter (December 2007) period, and for a subset, in the summer (July 2008) period. Whereas the summer photodecomposition sampling effort was off-cycle with most other summer measurements, the same layout of field conditions was used for comparability across years. Sampling locations and field types are given in **Table 9.1** and depicted in **Figure 4.5**. No sampling could be conducted on the seasonal wetland (SW1), field W32 and W65 during July 2008 because the seasonal wetland was dry and these two agricultural fields were in fallow and also dry.

9.2.3 Light Intensity Measurements

Measurements of ultraviolet (UV-A plus UV-B) and photosynthetically available radiation (PAR) were made continuously using a quantum sensor with nanologger from Apogee Instruments, Inc. during the experiments (December 2007 and July-August 2008) to relate light intensity to degradation rate. The light sensor was located approximately 4 km from the location used for deployment of bottle incubations. PAR measurements ($\text{mol m}^{-2} \text{s}^{-1}$) refer to the moles of photons in the UV or PAR wavelengths striking a square meter of (water) surface every second. PAR measurements were multiplied by the number of seconds for each PAR integration interval, giving an estimate of total light exposure (mol m^{-2}): the moles of photons per square meter. For the remainder of this report, MeHg concentrations will be presented in ng L^{-1} whereas light will be presented in units of mol m^{-2} . **Byington (2007)** determined that clear FEP Teflon[®] bottles have a high optical transparency for 280-800 nm light wavelengths (**Figure 9.2**). In addition to the light intensity measurements made during the degradation experiments, measurements were made of light penetration into the water column during several different periods of rice growth to assess seasonal effects of shading on light penetration into the water column.

9.2.4 Methylmercury Determinations

The MeHg concentration in the incubated waters was determined using a distillation and aqueous phase ethylation method with cold vapor atomic fluorescence spectrometry (CVAFS) detection (**Bloom, 1989; Horvat et al., 1993**). Prior to analysis, 45 to 80 mL aliquots were

distilled to minimize recovery artifacts associated with the sample matrix. The distilled sample was buffered to pH 5.0 with 2 M acetate buffer, and reacted with 35 μL of a 1% sodium tetraethylborate (NaBEt) solution to create volatile ethyl analogs of the solution mercury species. The sample was then purged with nitrogen and the ethylated complexes (e.g. monomethylmercury becomes methylethylmercury) are collected onto a Carbotrap™. The trap is then heated and the products flow into an isothermal gas chromatography (GC) column where separation occurs. At the exit of the GC the mercury species were pyrolyzed at high temperature ($>500\text{ }^\circ\text{C}$) and converted to elemental mercury (Hg^0) for subsequent determination by Cold Vapor Atomic Fluorescence Spectrometry (CVAFS). The method detection limit for MeHg determinations was 0.012 ng L^{-1} based on 7 replicate measurements of a low MeHg content substrate.

9.2.5 Quality Assurance Quality Control

Because of the nature of this work, Quality Assurance and Quality Control (QA/QC) for the field sampling can be handled slightly differently than normal field sampling where replication and blank checks are used to verify quality. With each experiment, a set of exposure bottles (clear) are contrasted with a set of control (darkened bottles). Any difference between the concentration of MeHg in the clear bottles and the dark bottles can be taken to result from decomposition due to exposure to light. In addition, all 5 time points are considered together by treating them as an exposure-dependent set using linear regression analysis. In addition, one field replicate was collected with each exposure set. The replicate collected was usually the final time point in the clear bottle. The data used in calculations, and the relative percent difference (RPD) of the replicate pairs, are summarized in **Appendix 4**. QAQC associated with the analytical determinations of MeHg followed the data quality objectives outlined in EPA method 1630, *Methyl Mercury in Water by Distillation, Aqueous Ethylation, Purge and Trap, and CVAFS (EPA, 2001)*.

9.3 Results and Discussion

9.3.1 Light Intensity (PAR) Measurements

Two types of PAR measurements were obtained during this study, continuous measurements associated with the exposure experiments, and discrete measurements in individual fields to evaluate light attenuation with depth in the water column and shading of light reaching the surface due to emergent rice. Ultra-violet (UV) exposures were assessed by established UV:PAR predictive relationships (**Byington 2007**).

9.3.2 Continuous Measurements

Continuous light intensity (PAR) measurements for the two experimental time periods are depicted in **Figures 9.3**. The integrated flux for each individual time point in an experiment is given in the appendices. Note that the maximum intensity of light reaching the surface of the water in the winter ($\sim 800\text{ }\mu\text{mol m}^{-2}\text{ s}^{-1}$) is about half that observed in the summer ($\sim 1700\text{ }\mu\text{mol m}^{-2}\text{ s}^{-1}$). In addition, during the winter period there were periods of cloudy and stormy weather that substantially reduced light intensity reaching the water surface.

9.3.3 Discrete Water Column Profile Measurements

PAR depth profile measurements taken in the water column of the rice fields and wetlands areas are summarized in the Appendix. An example of the water column profile measurements for field R20 taken on June 26, 2008 is given in **Figure 9.4**. The attenuation of the PAR flux with depth can be determined by performing a logarithmic (natural log) regression analysis of the profiles. An attenuation coefficient is determined by taking the reciprocal (m^{-1}) of the logarithmic coefficient associated with equation of the line for a logarithmic (natural log) regression of the PAR data with depth:

$$y = m \ln(x) + b \quad \text{Equation 9.1}$$

The PAR at depth (z) is then given by:

$$PAR_{(z)} = PAR_{(0)} e^{\mu(z)} \quad \text{Equation 9.2}$$

Where, $PAR_{(z)}$ is the intensity of light at depth z , $PAR_{(0)}$ is the intensity of PAR at the water surface ($z=0$), μ is an extinction coefficient or attenuation coefficient and has units of cm^{-1} , and z is depth, in units of centimeters.

The PAR extinction coefficient was observed to be highly variably, ranging from -0.019 to -0.041 cm^{-1} , and averaging $-0.029 \pm 0.011 \text{ cm}^{-1}$. This corresponded to a light intensity at a water depth of 20 cm (the average depth of surface water on rice fields) of 38-82% of surface light intensity. Unfortunately, no UV light penetration data were obtained, so it is not possible to directly assess how UV light was attenuated with depth. Thus, PAR extinction coefficients were applied to UV-calculations to estimate UV radiation attenuation in the water column.

9.3.4 Photodecomposition Experiments

Illustrated in **Figures 9.5A, 9.5B** and **9.6** are individual photodecomposition experiment for the two time periods, December 2007 and July/August 2008. The green circles represent the bottles exposed to light, and the red circles represent samples in darkened bottles. Note that MeHg concentration data (in units of $ng \text{ L}^{-1}$) are plotted relative to total light exposure ($mol \text{ m}^{-2}$). Hence, this is not a typical kinetic experiment where the independent variable would time. The choice to use total light exposure rather than time stems from the fact that the photodegradation rate is linearly proportional to light exposure, and because the light exposure rate varied with time. This means that the photodegradation rate can be treated in kinetic terminology, as first-order with respect to light intensity:

$$\text{MeHg Photodegradation Rate (ng L}^{-1} \text{ mol}^{-1} \text{ m}^2) = k [\text{light flux}] \quad \text{Equation 9.3}$$

Where light flux concentration is represented by the photons of light striking a surface area ($mol \text{ m}^{-2}$) and is independent of time. The rate constant (k) has units of $ng \text{ L}^{-1} \text{ mol}^{-2} \text{ m}^4$. The slope associated with the linear regression analysis for the five exposure periods of each experiment provides the photodecomposition rate constant for the individual experiment. The results for the darkened bottles serve as the control to each experiment. A summary of the linear regression data which provides the photodecomposition rate constant for both experimental periods is given in **Tables 9.2 and 9.3** for PAR and UV as the portion of the light spectrum

driving MeHg photodecomposition. A recent paper by **Li et al. (2010)** has suggested that it is UVb radiation that is responsible for the photodegradation of MeHg. Both treatments (PAR and UV) are provided in this report.

Note that the regression slope for each individual experiment varies significantly. This preliminary information suggests that another parameter is also influencing the rate at which MeHg undergoes photodegradation. In a later section it will be demonstrated that MeHg concentration also influences the photodegradation rate and that the rate is linear with concentration. Hence, the MeHg photodegradation rate is second-order, varying with the amount of light flux and MeHg concentration:

$$\text{MeHg Photodegradation Rate (ng L}^{-1} \text{ mol}^{-1} \text{ m}^2) = k [\text{light flux}][\text{MeHg}] \quad \text{Equation 9.4}$$

Tabulated results of the individual photodecomposition experiments for the two sampling events are given in **Appendix 4**.

9.3.5 Monomethyl Hg Concentration Dependence on Photodecomposition Rate

As noted previously, there is evidence that the photodegradation rate of mercury is dependent on another parameter besides light flux since the slopes of the individual photodegradation experiments varied significantly. Illustrated in **Figures 9.8A and 9.8B** is the dependence of MeHg concentration on the photodecomposition rate using PAR and UV, respectively, as the portion of the light spectrum responsible for MeHg photodecomposition. Rate dependence is determined by plotting the photodecomposition rate (regression slope) obtained for the individual experiments from **Table 9.2** against the initial MeHg concentration. **Figure 9.7A** represents the dependence based on PAR decomposition obtained using all the experimental data and **Figure 9.7B** represents the dependence observed when two experiments are removed (sites 20 and 31 in December). **Figures 9.8A and 9.8B** are similarly structured to represent dependence on UV as driving photodecomposition. Removing the two experimental points from the dependence determination increases the regression coefficient significantly. In both cases, the regression is forced through zero, restricting MeHg decomposition to light driven processes only. Using the selected experimental results the concentration dependence on the photodecomposition rate is given by:

$$\text{PAR Photodecomposition Rate (ng L}^{-1} \text{ mol}^{-1} \text{ m}^2) = -0.0048 [\text{MeHg, ng L}^{-1}]_i [\text{PAR Flux, mol}^{-1} \text{ m}^2] \quad \text{Equation 9.5}$$

$$\text{UV Photodecomposition Rate (ng L}^{-1} \text{ mol}^{-1} \text{ m}^2) = -0.118 [\text{MeHg, ng/L}]_i [\text{UV Flux, mol}^{-1} \text{ m}^2] \quad \text{Equation 9.6}$$

The UV photodecomposition rate of $-0.118 \text{ ng L}^{-1} \text{ mol}^{-1} \text{ m}^2$ represents the rate for all surface waters, and will be used as the starting point for all calculations involved with mass balance calculations (i.e. loss term) of MeHg from the rice fields and wetlands in the YBWA. Additional corrections on a field wide basis need to be made for light attenuation with depth and shading from emergent rice.

9.3.6 Modeling MeHg Photodecomposition in the YBWA

Mass balance modeling of the photodecomposition of MeHg in the Yolo Wildlife Area needs to account for variations due to:

1. Temporal changes in solar irradiation (both daily and seasonal)
2. MeHg concentration dependence on the photodegradation rate
3. Light attenuation with water column depth (TSS dependent)
4. Shading by emergent macrophytes

The resulting output can then be expressed as the mass of MeHg lost in a square meter of the water column per day ($\text{ng MeHg m}^{-2} \text{ d}^{-1}$). This loss rate can also be expressed as a percent loss per day using information on the mass loading of MeHg in the YBWA. Given in **Table 9.4** is the percent loss of MeHg as a function of water column light attenuation and daily integrated PAR (Panel A) and UV (Panel B) light flux. This particular assessment was conducted for a water depth of 30 cm, approximating that of the water depths over a typical rice field in the YWA. The range in light flux spans typical winter and summer integrated light intensity conditions (**Figure 9.3**). Given in **Table 9.4** are the average water column mass losses of MeHg ($\text{ng MeHg m}^{-2} \text{ d}^{-1}$) as function of MeHg concentration. This tabulation was conducting using an attenuation coefficient for PAR and UV of -0.029 and a total water depth of 30 cm. **Table 9.5A** shows the loss driven solely by PAR radiation and **Table 9.5B** shows the loss where UV radiation is responsible for MeHg photodecomposition. Again, the range in light flux spans typical winter and summer integrated light intensity conditions (see **Figure 9.3**).

Several important observations are apparent in these simulations of typical conditions in a rice field.

1. The loss of MeHg, when modeled as driven by UV light is significantly larger (typically greater than 2 times) than the loss that would result from a PAR driven light flux.
2. Assuming that the hydraulic residence time on a rice field is on the order of 12-25 days, then the potential for photodegradation of MeHg, whether driven by PAR or UV becomes very significant in the mass balance of MeHg on the rice fields.
3. The photodecomposition loss of MeHg in the winter is far less than that in summer when photoperiod is longer and days are typically less cloud cover.

Shading of the water surface by emergent grasses was highly variable and difficult to incorporate into a modeling effort. While there were a paucity of measurements (~10 observations), the range in shading observed at the water surface between open water and rice fields varied between 45 and 89%. A typical shading value was around 70% of the incident light, meaning that only around 30% of the ambient light reached the water surface. The attenuation with depth in the emergent grasses appeared to be similar to that observed in the open water. To factor this into the modeling effort one would have to reduce the photodegradation predictions given in **Tables 9.3** and **9.4** by approximately 70% for that portion of the rice field where emergent grass exists, and for the time periods where emergent grass existed.

9.4 Summary

Photodecomposition of MeHg in the YWA was observed to be a direct function of both total light exposure (total photons of light, mol m^{-2}) and MeHg concentration (ng L^{-1}). No significant photodecomposition was observed with dark controls suggesting that the destruction of MeHg was abiotic and mediated by sunlight. The dependence of MeHg concentration on photodecomposition can be modeled based either on degradation by PAR or the UV portions of the light spectrum according to:

$$\text{PAR Photodecomposition Rate (ng L}^{-1} \text{ mol}^{-1} \text{ m}^2) = -0.0048 [\text{MeHg, ng/L}]_t [\text{PAR Flux, mol}^{-1} \text{ m}^2]$$

$$\text{UV Photodecomposition Rate (ng L}^{-1} \text{ mol}^{-1} \text{ m}^2) = -0.118 [\text{MeHg, ng/L}]_t [\text{UV Flux, mol}^{-1} \text{ m}^2]$$

The combination of these two controlling factors results in a much more significant MeHg photodecomposition in summer periods than in winter periods. The significant increase in summer is due primarily to two factors, more total light exposure (both intensity and period) and generally higher MeHg concentrations in the summer period compared to winter periods. A recent paper by **Li et al. (2010)** suggests that the photodegradation of MeHg is driven primarily by UV radiation, although most previous research related photodegradation to the PAR portion of the light spectrum. Both approaches are provided here, but it is clear that if driven solely by UV radiation, then the loss would be much more significant. Knowledge of environmental factors that influence photodegradation will clearly be useful in developing management strategies to mitigate MeHg problems and for controlling high MeHg inputs into the Delta. Environmental parameters that could potentially be manipulated to influence MeHg concentrations in open water areas such as YWA include: water clarity (TSS), shading by emergent aquatic vegetation, water residence time, and water depth.

10 Detailed Results for Public Outreach and Stakeholder Involvement

The data reported in this section addresses outreach support and environmental justice goals of the project.

10.1 Pre-Study Workshop

GOAL: To increase community and stakeholder understanding of MeHg exposure and share information between the research and stakeholder community.

TASK : Organize one (1) pre-study workshop in conjunction with the Yolo Bypass Working Group to discuss design and goals of project.

The Yolo Basin Foundation hosted a two-part Workshop on Mercury in the Yolo Bypass on Thursday, February 8, 2007. The meeting was facilitated by long-time Yolo Bypass Working Group facilitator, Dave Ceppos, with the Center for Collaborative Policy associated with California State University Sacramento. The morning session (10 a.m. to noon) introduced the new project. There were presentations on:

1. Mining history in northern California
2. Methylmercury and the TMDL process
3. Wetland Management in the Yolo Bypass Wildlife Area

After the presentation, project objectives, approach and expected outcome were discussed with questions and answers. There was a short break for lunch.

The second part of the meeting covered general information on mercury in the waterways of Yolo and Sacramento Counties and the status of fish-consumption advisories, TMDLs and other regulatory processes. There was an overview of ongoing education and outreach efforts including the Delta Fish Mercury Project.

10.1.1 Stakeholder Outreach for the Pre-study Workshop

TASK: Invite stakeholders representing a variety of potentially interested constituencies, including farmers, landowners, fish consumers, local and state government agencies, and other interested stakeholders.

A significant outreach effort ensured that 54 stakeholders attended the workshop. A press release announcing the workshop was sent to all of the local papers using Yolo Basin Foundation's press list. The over 200 participants on the Yolo Bypass Working Group listserv were invited by email to attend the workshop. Additionally several email invitations were sent to over 60 stakeholders in the public and private sector who are involved in water quality, environmental health, and advocacy concerns related to environmental justice issues.

The following organizations and agencies were represented at the pre-study workshop:
Government:

City of Davis Public Works
Yolo County Department of Health
Yolo County Planning Department
Irvington High School
Delta Protection Commission
Sacramento Area Flood Control Agency
State Water Resources Control Board
California State Department of Fish and Game Water Branch
California State Department of Fish and Game, Yolo Bypass Wildlife Area
California Wildlife Conservation Board
California State Department of Water Resources Division of Environmental Services
Central Valley Regional Water Quality Control Board
Office of Environmental Health Hazard Assessment, CA Environmental Protection Agency
California State Department of Water Resources
Solano County Environmental Management Department
California Department of Health Services
University of California Davis
University of California Cooperative Extension
US Geological Survey

Private Sector Business and Industry:

Techlaw Inc.
Homestake Mine
Larry Walker Associates
Shaw Environmental
Cal Test Analytical Lab
URS Corporation

Press:

Davis Enterprise

Agriculture Industry:

DeWit Farms, Rice Grower in Yolo Bypass
Schene Enterprises, Rancher in Yolo Bypass
California Rice Commission

Private Wetland Management:

Glide In Ranch (hunting club)

Conservation:

Delta Keeper
Yolo Basin Foundation
California Waterfowl Association
Ducks Unlimited
Solano Land Trust
Tuleyome

Sacramento River Watershed Program
California Indian Environmental Alliance

10.1.2 Pre-study Questionnaire

TASK: Prepare a questionnaire to be distributed at the workshops with goals of determining principal areas of stakeholder interest, level of knowledge of mercury issues with regard to fish consumption and human health, level of knowledge with regard to the THg-MeHg TMDL process.

A two-sided questionnaire was distributed to participants when they arrived for the workshop. One side had pre-workshop questions, and participants were asked to fill that out before the workshop started. The second side had the same questions but the attendees were asked to fill it out before they left.

The questionnaire listed various interests in the Bypass and the attendees were asked to check which applied to them. There were 34 respondents. Most people checked more than one area of interest. The interest tallies were as follows:

Land Use 15

Agriculture: 12

Wildlife: 15

Fishing: 13

Mercury advisories: 17

Mercury TMDL: 25

Other interests included: science behind wetland MeHg process; analytical; land management (Yolo Bypass Wildlife Area).

The first question on both the pre-workshop and post workshop questionnaires asked: “On a scale of 1 to 10 rate your knowledge of fish consumption advisories in the Yolo/Sacramento Area (1= not familiar, 10= very familiar.)” Pre-workshop responses ranged from 1 to 10 with an average of 5.79. Post-workshop responses ranged from 4 to 10 with an average of 7.10, indicating that participants felt that they had gained some more knowledge of the subject.

The second question on both the pre-workshop and post-workshop questionnaire asked: “On a scale of 1 to 10 rate your knowledge of the TMDL process with regard to mercury and methylmercury (1=not familiar, 5=moderately familiar, 10=very familiar).” The pre-workshop responses ranged from 1 to 10 with an average of 5.35. The post-workshop responses ranged from 2 to 10 with an average of 7.10, indicating that participants felt that they had also gained some additional knowledge on this subject.

Comments received included: “Helpful presentations describing recent research and upcoming studies in the Bypass;” “great gathering, looking forward to future updates;” “Good for scientific community, not so great for public health and local government attendees who deal with social issues, I enjoyed it a lot!” “Lots of information, what would be helpful next time is for all presenters to have copies of their PowerPoint presentations (maybe one big packet handed out to attendees before the meeting starts);” “Very good, thanks! Good presentations;” “would be great

to get semi-annual or annual updates on studies regarding MeHg characterization, control and BMPs;” “very good line-up of speakers;” “very informative;” “great turnout;” “good selection of speakers;” “At the beginning an objective was mentioned of including diversity and low income in this meeting – I didn’t see it.” “Helpful for basic overview of mercury processes and present issues.”

10.1.3 Conclusion

The workshop was well attended, and many participants thanked the workshop organizers for making the opportunity available. People asked to be kept up-to-date on the issue of MeHg in the Yolo Bypass and with the research project during the year.

10.2 Post-Study Workshop

GOAL: To update the stakeholder community on research results of the project and increase community and stakeholder understanding of MeHg exposure.

TASK : Organize one (1) post-study workshop in conjunction with the Yolo Bypass Working Group to discuss design and goals of project.

The first part of the post-study workshop focused on results from the project. Dave Ceppos (with the Center for Collaborative Policy) facilitated the workshop. After Dave Feliz, Yolo Bypass Wildlife Area Manager, introduced the project, Mark Stephenson (with the Moss Landing Marine Laboratory) described the project and its hypotheses. Project scientists Mark Stephenson, Lisa Windham-Myers (with the U.S. Geological Survey, USGS), Phil Bachand (with Bachand and Associates), Charlie Alpers (USGS), Jacob Fleck (USGS), Mark Marvin-DiPasquale (USGS), and Josh Ackerman (USGS) presented the results by subject: hydrology, water quality, THg and MeHg loads, MeHg photo degradation, sediment, plants, and bioaccumulation. Part I concluded with a panel discussion by the project team on conclusions and evaluation of the hypotheses. The panel also discussed management practices that may affect MeHg bioaccumulation and export. After a lunch break, Part 2 of the workshop began with general information on mercury in Yolo and Sacramento Counties. Robert Brodberg (with the California Office of Environmental Health Hazard Assessment) discussed fish- consumption advisories related to MeHg as well as public health outreach and education. Patrick Morris (with the Regional Water Quality Control Board – Central Valley Region, RWQCB-CVR) and Dave Ceppos gave an update on the MeHg TMDL process in the Sacramento–San Joaquin Delta. Chris Foe (RWQCB-CVR) presented information based on MeHg studies conducted in the flooded Yolo Bypass in 2006. Mark Stephenson described current research on developing Best Management Practices for MeHg in the Yolo Bypass Wildlife Area. The workshop ended in a group discussion led by Dave Ceppos.

10.2.1 Stakeholder Outreach for the Post-study Workshop

TASK: Invite stakeholders representing a variety of potentially interested constituencies, including farmers, landowners, fish consumers, local and state government agencies, and other interested stakeholders.

A significant outreach effort resulted in 72 stakeholders attending the workshop. A press release announcing the workshop was sent to all of the local papers using Yolo Basin Foundation's press list. An article appeared in the *Davis Enterprise* the day before the workshop. More than 200 participants on the Yolo Bypass Working Group listserve were invited by email to attend the workshop. Additionally several email invitations were sent to over 60 stakeholders in the public and private sector that are involved in water quality, environmental health, and advocacy issues related to environmental justice issues. Members of the Lower Yolo Bypass Planning Forum were also invited.

The following organizations and agencies were represented at the post-study workshop:

Government:

City of Davis Public Works

City of Vacaville

Yolo County Department of Public Health

Delta Protection Commission

California Assembly Water, Parks and Wildlife Committee

State Water Resources Control Board

California State Department of Fish and Game Water Branch

California State Department of Fish and Game, Yolo Bypass Wildlife Area

California State Department of Fish and Game, Bay Delta Region

California State Department of Water Resources Division of Environmental Services

Central Valley Regional Water Quality Control Board

North Coast Regional Water Quality Control Board

Office of Environmental Health Hazard Assessment, CA Environmental Protection Agency

California Bay Delta Authority

North Delta Water Agency

Reclamation District 2068

Sacramento County Regional Sanitation District

Solano County Water Agency

University of California Davis

US Army Corps of Engineers

US Bureau of Land Management

US Fish and Wildlife Service

US Geological Survey

Private Sector Business and Industry:

AMEC

Burkeson Consulting

Clean Water Vision

EDAW

G. Fred Lee and Associates

A. Teichert and Son

Larry Walker Associates

Cal Test Analytical Lab

Wallace Kuhl & Associates

Agriculture Industry:

Conaway Ranch
DeWit Farms, Rice Grower in Yolo Bypass

Conservation:

Clean Water Action
Yolo Basin Foundation
California Waterfowl Association
Ducks Unlimited
Solano Land Trust
Tuleyome
The Nature Conservancy

10.2.2 Post-Study Questionnaire

TASK: Prepare a questionnaire to be distributed at the workshops with goals of determining principal areas of stakeholder interest, level of knowledge of mercury issues with regard to fish consumption and human health, level of knowledge with regard to the THg/MeHg TMDL process.

As with the pre-study workshop, a two-sided questionnaire was distributed to participants when they arrived for the post-study workshop. One side had pre-workshop questions that participants were asked to fill that out before the workshop started. The second side had the same questions but the attendees were asked to fill it out before they left. There was also a space for comments.

The questionnaire listed various interests in the Bypass and the attendees were asked to check which applied to them.

There were 32 respondents. Most people checked more than one area of interest. The interest tallies were as follows:

Land Use 14
Agriculture: 12
Wildlife: 21
Fishing: 8
Mercury advisories: 12
Mercury TMDL: 24

Other interests included: research on fish, plants and microbes, mining and abandoned mine lands, impacts of MeHg on subsistence fishing, mercury hotspots, making a documentary, wetland management, hunting, beneficial uses of the Bay-Delta, and policy issues related to MeHg and habitat restoration.

The first question on both the pre-workshop and post-workshop questionnaires asked: “On a scale of 1 to 10 rate your knowledge of fish consumption advisories in the Yolo/Sacramento Area (1= not familiar, 10= very familiar.)” Pre-workshop responses ranged from 1 to 10 with an

average of 5.75. Post-workshop responses ranged from 4 to 10 with an average of 7.83, indicating that participants felt that they had gained some more knowledge of the subject.

The second question on both the pre-workshop and post-workshop questionnaire asked: “On a scale of 1 to 10 rate your knowledge of the TMDL process with regard to mercury and methylmercury (1=not familiar, 5=moderately familiar, 10=very familiar).” The pre-workshop responses ranged from 1 to 10 with an average of 5.75. The post-workshop responses ranged from 2 to 10 with an average of 8.07, indicating that participants felt that they had gained some additional knowledge on the subject.

Comments received included: “great research project;” “very informative;” “great presentation of the study;” and “good update on status of current studies in the Yolo Bypass.” The majority of comments were positive, but some indicated that the agenda was rushed and too ambitious and that the information was too technical.

10.2.3 Conclusion

The Workshop was well attended. People asked to be kept up-to-date on the issue of MeHg in the Yolo Bypass and with future research projects. Several participants expressed the opinion that MeHg research projects should be continued, as much more information is needed in order to develop effective Best Management Practices to reduce MeHg releases to the Bay Delta estuary.

10.3 PAEP Evaluation and Discussion

A Project Assessment and Evaluation Plan (PAEP) was used to evaluate the results of our field-based studies for use in developing BMP’s for agricultural fields and managed wetlands within the Yolo Bypass of the S-SJ Delta. Project Goals and Desired Outcomes are as follows:

- a. Project Goals for Research/Monitoring/Assessment**
 - i. Aid in the development of an effective TMDL for MeHg in the Delta
 - ii. Aid in development of cost-efficient BMP’s to reduce MeHg production, export and bioaccumulation
- b. Desired Outcomes for Research/Monitoring/Assessment**
 - i. Regional Water Board staff will have a better understanding of patterns and processes of MeHg production and export over an annual cycle through quantification of wetland management practices for the Yolo Bypass.

The results reported here have not yet been used directly in the TMDL for MeHg in the Delta, but are being considered by members of the SWRCB as quantitative information to modify BMP guidelines. Our goal of 50% acceptance and use of the resulting BMP guidelines for the MeHg TMDL by land managers has not yet been tested, as the BMPs have yet to be developed by the SWRCB.

- c. Project Goals for Education/Outreach/Capacity-building**
 - i. Increase community and stakeholder understanding of MeHg exposure
 - ii. Increase bi-directional sharing of information between the research and stakeholder community

d. Desired Outcomes for Education/Outreach/Capacity-Building

- i. Wetland managers understand how to aid in reducing MeHg production and export from wetlands of the Yolo Bypass.
- ii. Disadvantaged communities become more informed as to the risk and causes of Hg contamination of sport fish in the Yolo Bypass.

We exceeded targets for the following project goals in education and outreach:

GOAL 1: Greater literacy among land managers regarding Hg cycling in the Yolo Bypass and the proposed MeHg TMDL for the Delta.

RESULT: 20% greater understanding of Hg cycling in the Yolo Bypass, 20% greater understanding of fish consumption guidelines and relation to land management, and 20% greater understanding of biogeochemical conditions related to fish Hg levels

GOAL 2: Greater awareness among disadvantaged communities of the risks of consuming Hg in specific fish.

RESULT: 20% greater awareness of MeHg consumption risks among stakeholders.

We still seek to evaluate the use of MeHg risk information in an additional 20% of school and community newsletters or other documents.

GOAL 3: Direct sharing of study results with designated stakeholders.

RESULT: Formal presentation and distribution of project fact sheet with CALFED-abstracts to 100% of designated stakeholders at post-study meeting

In summary, quantifiable goals of the PAEP research agenda have been largely met, but BMP development and implementation has a longer timeframe for evaluation. In addition to positive public evaluation of the pre- and post-study meetings, high stakeholder turnout and interaction with PI's both at the meeting and in subsequent telephone and e-mail conversations are evidence of the successful outreach effort to share the patterns and processes of MeHg production, bioaccumulation and export on managed wetlands of the YBWA.

11 REFERENCES CITED

- Ackerman, J.T., and Eagles-Smith C.A., 2008, A dual life-stage approach to monitoring the effects of mercury concentrations on the reproductive success of Forster's Terns in San Francisco Bay: Final Administrative Report, U. S. Geological Survey, Western Ecological Research Center, Davis, Calif., 41 p.
- Ackerman J.T., and Eagles-Smith C.A., 2010, Agricultural wetlands as potential hotspots for bioaccumulation: experimental evidence using caged fish: *Environmental Science and Technology*, v. 44, p. 1451–1457.
- Ackerman, J.T., Miles, A.K., and Eagles-Smith, C.A., 2010, Invertebrate mercury bioaccumulation in permanent, seasonal, and flooded rice wetlands within California's Central Valley: *Science of the Total Environment*, v. 408, p. 666–671.
- Ackerman, J.T., Takekawa, J.Y., Eagles-Smith, C.A., and Iverson, S.A., 2008, Mercury contamination and effects on survival of American avocet and black-necked stilt chicks in San Francisco Bay: *Ecotoxicology*, v. 17, p. 103–116.
- Albers, P.H., Koterba, M.T., Rossman, R., Link, W.A., French, J.B., Bennett, R.S., and Bauer, W.C., 2007, Effects of methylmercury on reproduction in American kestrels: *Environmental Toxicology and Chemistry*, v. 26, p. 1856–1866.
- Alisauskas, R.T., and Ankney, C.D., 1992, The cost of egg laying and its relationship to nutrient reserves in waterfowl, *in* Batt, B.D.J., Afton, A.D., and others, eds., *Ecology and management of breeding waterfowl*: Minneapolis, University of Minnesota Press, p. 30–61.
- Allen, R.G., Pereira, L.S., Raes, D., and Smith, M., 1998, Crop evapotranspiration — guidelines for computing crop requirements: Irrigation and Drainage Paper 56, Food and Agriculture Organization of the United Nations, Rome, Italy.
<http://www.fao.org/docrep/X0490E/X0490E00.htm> (accessed Sept. 30, 2010).
- Alpers, C.N., Eagles-Smith, C., Foe, C., Klasing, S., Marvin-DiPasquale, M.C., Slotton, D.G., and Windham-Myers, L., 2008, Mercury conceptual model. Sacramento, Calif.: Delta Regional Ecosystem Restoration Implementation Plan, 62 p.
http://www.science.calwater.ca.gov/pdf/drerip/DRERIP_mercury_conceptual_model_final_012408.pdf
- Alpers, C.N., Hunerlach, M.P., Marvin-DiPasquale, M.C., Antweiler, R.C., Lasorsa, B.K., De Wild, J.F., and Synder, N.P., 2006, Geochemical data for mercury, methylmercury, and other constituents in sediments from Englebright Lake, California, 2002: U.S. Geological Survey, Data Series 151, 107 p. <http://pubs.er.usgs.gov/usgspubs/ds/ds151>
- Anderson, R.O., and Neumann, R.M., 1996, Length, weight, and associated structural indices, *in* Murphy, B.R., and Willis, D.W., eds., *Fisheries techniques*, second edition: American Fisheries Society, Bethesda, Maryland, p. 447–482.
- Bachand and Associates, Hydrofocus, Inc., University of California, Davis, U.S. Geological Survey, Ducks Unlimited, and Contra Costa Water District, 2006, Reducing non-point DOC and nitrogen exports from rice fields: A pilot study and quantitative survey to determine the effects of different hydrologic management practices: Final Report to State Water Resources Control Board, Agreement 03-165-555-0, Davis, Calif., May 19, 2006, 194 p., appendices.
http://aquacomm.fcla.edu/2072/1/FINAL_REPORT_2006.pdf (accessed Sept. 30, 2010).
- Bagwell, C.E., Piceno, Y.M., Ashburne-Lucas, A.L., and Lovell, C.R., 1998, Physiological diversity of the rhizosphere diazotroph assemblages of selected salt marsh grasses: *Applied Environmental Microbiology*, v. 64, no. 11, p. 4276–4282.

- Balci, N., Shanks III, W.C., Mayer, B., and Mandernack, K.W., 2007, Oxygen and sulfur isotope systematics of sulfate produced by bacterial and abiotic oxidation of pyrite: *Geochimica et Cosmochimica Acta*, v. 71, p. 3796–3811.
- Barkay, T., Gillman, M., and Turner, R.R., 1997, Effects of dissolved organic carbon and salinity on bioavailability of mercury: *Applied and Environmental Microbiology*, v. 63, no. 11, p. 4267–4271.
- Barkay, T., and Wagner-Döbler, I., 2005, Microbial transformations of mercury — potentials, challenges, and achievements in controlling mercury toxicity in the environment: *Advances in Applied Microbiology*, v. 57, p. 1-52.
- Barr, J.F., 1986, Population dynamics of the common loon (*Gavia immer*) associated with mercury-contaminated waters in northwestern Ontario: Canadian Wildlife Service Occasional Paper No. 56, Ottawa, Canada, 25 p.
- Beckvar, N., Dillon, T.M., and Read, L.B., 2005, Approaches for linking whole-body fish tissue residues of mercury or DDT to biological effects thresholds: *Environmental Toxicology and Chemistry*, v. 24, p. 2094–2105.
- Benoit J.M., Gilmour C.C., Heyes A., Mason R., and Miller, C., 2003, Geochemical and biological controls over methylmercury production and degradation in aquatic systems, *in* Chai, Y., and Braids, O.C., eds., *Biochemistry of Environmentally Important Trace Elements: ACS Symposium Series 835*, American Chemical Society, Washington, D.C., p. 262–297.
- Benoit, J.M., Gilmour, C.C., and Mason, R.P., 2001, The influence of sulfide on solid-phase mercury bioavailability for methylation by pure cultures of *Desulfobulbus propionicus* (1pr3): *Environmental Science and Technology*, v. 35, no. 1, p. 127–132.
- Benoit, J.M., Gilmour, C.C., Mason, R.P., and Heyes, A., 1999, Sulfide controls on mercury speciation and bioavailability to methylating bacteria in sediment porewaters: *Environmental Science and Technology*, v. 33, p. 951–957.
- Benoit, J.M., Mason, R.P., Gilmour, C.C., and Aiken, G.R., 2001, Constants for mercury binding by dissolved organic matter isolates from the Florida Everglades: *Geochimica et Cosmochimica Acta*, v. 65, no. 24, p. 4445-4451.
- Bird, J.A., Pettygrove, G.S., and Eadie, J.M., 2000, The impact of waterfowl foraging on the decomposition of rice straw: mutual benefits for rice growers and waterfowl: *Journal of Applied Ecology*, v. 37, p. 728–741.
- Blaabjerg, V. and Finster, K., 1998, Sulphate reduction associated with roots and rhizomes of the marine macrophyte *Zostera marina*: *Aquatic Microbial Ecology*, v. 15, p. 311–314.
- Bloom, N.S., 1993, Determination of picogram levels of methylmercury by aqueous phase ethylation, followed by cryogenic gas chromatography, with cold vapour atomic fluorescence detection: *Canadian Journal of Fisheries and Aquatic Sciences*, v. 46, p. 1131–1140.
- Bonneville, S., Van Cappellen, P., and Behrends, T., 2004, Microbial reduction of iron (III) oxyhydroxides: effects of mineral solubility and availability: *Chemical Geology*, v. 212, p. 255–268.
- Borga, P., Nilsson, M., and Tunlid, A., 1994, Bacterial communities in peat in relation to botanical composition as revealed by phospholipid fatty acid analysis: *Soil Biology and Biochemistry*, v. 26, p. 841–848.
- Bouman, B.A.M., Wopereis, M.C.S., Kropff, M.J., ten Berge, H.F.M., and Tuong, T.P., 1994, Water use efficiency of flooded rice fields. II. Percolation and seepage losses: *Agricultural Water Management*, v. 26, p. 291–304.

- Brady, N.C. and Weil, R.R., 2002, *The Nature and Properties of Soils* (13th ed.): Upper Saddle River, N.J., Prentice Hall, 960 p.
- Branfireun, B., Heyes, A., and Roulet, N., 1996, The hydrology and methylmercury dynamics of a Precambrian Shield headwater peatland: *Water Resources Research*, v. 32, no. 6, p. 1785–1794.
- Brumbaugh, W.G., Krabbenhoft, D.P., Helsel, D.R., Wiener, J.G., and Echols, K.R., 2001, A national pilot study of mercury contamination of aquatic ecosystems along multiple gradients — Bioaccumulation in fish: U.S. Geological Survey, Biological Science Report USGS/BRD/BSR-2001-0009, 26 p.
- Burgess N.M., and Meyer, M.W., 2008, Methylmercury exposure associated with reduced productivity in common loons: *Ecotoxicology*, v. 17, p. 83–91.
- Byington, A., 2007, Photo-degradation of methylmercury in the Sacramento–San Joaquin Delta Estuary: San Jose, Calif., San Jose State University and Moss Landing Marine Laboratory, Master's thesis, 64 p.
- Byington, A., Coale, K., Gill, G., and Choe, K.-Y., 2005, Photo-degradation of methyl mercury (MeHg) in the Sacramento-San Joaquin Delta [abs.]: State of the San Francisco Estuary Conference, 7th Biennial, Oakland, Calif., October 4–6, 2005.
http://www.abag.ca.gov/abag/events/estuary/pdfs/SOE_2005_abstracts_poster.pdf (accessed Sept. 30, 2010)
- Capone, D.G., and Kiene, R.P., 1988, Comparison of microbial dynamics in marine and freshwater sediments: Contrasts in anaerobic carbon catabolism: *Limnology and Oceanography*, v. 33, p. 725–749.
- Carmody, R.W., Plummer, L.N., Busenberg, E., and Coplen, T.P., 1998, Methods for collection of dissolved sulfate and sulfide and analysis of their sulfur isotopic composition: U.S. Geological Survey Open-File Report 97-234, 91 p.
- Cheng, S., Johnson, D.W., and Fu, S., 2003, Rhizosphere effects on decomposition: controls of plant species, phenology, and fertilization: *Soil Science Society of America Journal*, v. 67, p. 1418–1427.
- Clark, I.D., and Fritz, P., 1997, *Environmental Isotopes in Hydrogeology*: New York, Lewis Publishers, 328 p.
- Compeau, G., and Bartha, R., 1984, Methylation and demethylation of mercury under controlled redox, pH, and salinity conditions: *Applied and Environmental Microbiology*, v. 50, p. 498–502.
- Compeau, G.C., and Bartha, R., 1985, Sulfate-reducing bacteria — Principal methylators of mercury in anoxic estuarine sediment: *Applied and Environmental Microbiology*, v. 50, p. 498-502.
- Conaway, C.H., Squire, S., Mason, R.P., and Flegal, A.R., 2003, Mercury speciation in the San Francisco Bay estuary: *Marine Chemistry*, v. 80, p. 199–225.
- Dahl, T.E., 1990, Wetland losses in the United States 1780's to 1980's: U.S. Department of the Interior, Fish and Wildlife Service, Washington, D.C., 13 p.
<http://www.fws.gov/wetlands/documents/gSandT/NationalReports/WetlandsLossesUS1780sto1980s.pdf> (accessed Sept. 30, 2010)
- Davis, J.A., Yee, D., Collins, J.N., Schwarzbach, S.E., and Louma, S.N., 2003, Potential for increased mercury accumulation in the estuary food web, *in* Brown, L.R., ed., *Issues in San Francisco Estuary Tidal Wetlands Restoration*: San Francisco Estuary and Watershed Science:

- v. 1, issue 1, article 4 <http://repositories.cdlib.org/jmie/sfews/vol1/iss1/art4> (accessed Sept. 30., 2010)
- de Szalay, F.A., Carroll, C., Beam, J.A, and Resh, V.H., 2003, Temporal overlap of nesting duck and aquatic invertebrate abundances in the Grasslands Ecological Area, California, USA: *Wetlands*, v. 23, p. 739–749.
- Del Vecchio, R., and Blough, N.V., 2002, Photobleaching of chromophoric dissolved organic matter in natural waters: kinetics and modeling: *Marine Chemistry*, v. 78, p. 231–253.
- DeWild, J., Olund, S.D., Olson, M.L., Tate, M.T., 2004, Methods for the preparation and analysis of solids and suspended solids for methylmercury: U.S. Geological Survey Techniques and Methods for Water Investigations, Book 5, A-7, 21 p. <http://pubs.usgs.gov/tm/2005/tm5A7/>
- Downing, B.D., Bergamaschi, B.A., Evans, D.G., and Boss, E., 2008, Estimating source-specific contributions of DOC into a drinking-water reservoir using optical profiling: *Lake and Reservoir Management*, v. 24, p. 381–391.
- Drexel, R.T., Haitzer, M., Ryan, J.N., Aiken, G.R., and Nagy, K.L., 2002, Mercury (II) sorption to two Florida Everglades peats: Evidence for strong and weak binding and competition by dissolved organic matter released from the peat: *Environmental Science and Technology*, v. 36, p. 4058-4064.
- Driscoll, C.T., Holsapple, J., Schofield, C.L., and Munson, R., 1998, The chemistry and transport of mercury in a small wetland in the Adirondack Region of New York, USA: *Biogeochemistry*, v. 40, no. 2/3, p. 137–146. [Mercury as a Global Pollutant, 4th International Conference.]
- Ehrenfeld, J.G., Ravit, B., and Elgersma, K., 2005, Feedback in the plant-soil system: *Annual Review of Environmental Resources*, v. 30, p. 75–115.
- Elphick, C.S., 2000. Functional equivalency between rice fields and seminatural wetland habitats: *Conservation Biology*, v. 14, p. 1–13.
- Elphick, C.S., and Oring, L.W., 1998, Winter management of California rice fields for waterbirds: *Journal of Applied Ecology*, v. 35, p. 95–108.
- Fleming, E.J., Mack, E.E., Green, P.G., and Nelson, D.C., 2006, Mercury methylation from unexpected sources: molybdate-inhibited freshwater sediments and an iron-reducing bacterium: *Applied and Environmental Microbiology*, v. 72, p. 457–464.
- Foe, C., Louie, S., and Bosworth, D., 2008, Methyl mercury concentrations and loads in the Central Valley and freshwater Delta, *task 2 of Transport, Cycling, and Fate of Mercury and Monomethyl Mercury in the San Francisco Delta and Tributaries: An Integrated Mass Balance Assessment Approach: Final report to Calif. Dept. of Fish and Game and California Bay-Delta Authority*, Sept. 2008, 41 p., 37 figs., 21 tpls. http://mercury.mlml.calstate.edu/wp-content/uploads/2008/10/04_task2mmhg_final.pdf (accessed Sept. 30, 2010)
- Frayer, W.E., Peters, D.D., and Pywell, H.R., 1989, Wetlands of the California Central Valley Status and Trends: 1939 to mid-1980's: U.S. Department of the Interior, Fish and Wildlife Service, Washington, D.C. 28 p.
- Frimmel, F.H., 1998a, Characterization of natural organic matter as major constituents in aquatic systems: *Journal of Contaminant Hydrology*, v. 35, p. 201–216.
- Frimmel, F.H., 1998b, Impact of light on the properties of aquatic natural organic matter: *Environment International*, v. 24, p. 559–571.
- Gassel, M., Brodberg, R.K., Klasing, S., and Roberts, S., 2007, Draft safe eating guidelines for fish and shellfish from the San Joaquin River and South Delta (Contra Cost, San Joaquin,

- Stanislaus, Merced, Madera, and Fresno Counties): Sacramento, Calif., California Office of Environmental Health Hazard Assessment, March 2007, 124 p.
http://www.oehha.ca.gov/fish/so_cal/centralsouthdelta.html (accessed Sept. 30, 2010)
- Gassel, M., Brodberg, R.K., Klasing, S., and Roberts, S., 2008, Draft safe eating guidelines for fish and shellfish from the Sacramento River and Northern Delta: Sacramento, Calif., California Office of Environmental Health Hazard Assessment, April 2008, 31 p., 9 tbls., 6 figs., appendices. http://www.oehha.ca.gov/fish/so_cal/srnd041108.html (accessed Sept. 30, 2010)
- George, B.M., Batzer, D., 2008, Spatial and temporal variations of mercury levels in Okefenokee invertebrates, southeast Georgia: *Environmental Pollution*, v. 152, p. 484–490.
- Giesemann, A., Jager, H.J., Norman, A.L., Krouse, H.R., Brand, W.A., 1994, On-line sulfur-isotope determination using an elemental analyzer coupled to a mass spectrometer: *Analytical Chemistry*, v. 66, p. 2816–2819.
- Gill, G., 2008a, Methylmercury photo-degradation studies, *Task 5.1 in Transport, Cycling, and Fate of Mercury and Methylmercury in the San Francisco Delta and Tributaries: An Integrated Mass Balance Assessment Approach: Final report to the California Department of Fish and Game and the California Bay Delta Authority*, 21 p.
http://mercury.mlml.calstate.edu/wp-content/uploads/2008/10/09_task5_1_final.pdf (accessed Sept. 30, 2010)
- Gill, G., 2008b, Sediment biogeochemistry studies in Delta wetlands, *Task 5.3b in Transport, Cycling, and Fate of Mercury and Methylmercury in the San Francisco Delta and Tributaries: An Integrated Mass Balance Assessment Approach: Final report to the California Department of Fish and Game and the California Bay Delta Authority*, 16 p.
http://mercury.mlml.calstate.edu/wp-content/uploads/2008/10/17_task5_3b_final.pdf (accessed Sept. 30, 2010)
- Gill, G.A., and Fitzgerald, W.F., 1985, Mercury sampling in open ocean waters at the picomolar level: *Deep-Sea Research*, v. 32, p. 287–297.
- Gilmer, D.S., Miller, M.R., Bauer, R.D., LeDonne, J.R., 1982, California's Central Valley wintering waterfowl: concerns and challenges: *Transactions, North American Wildlife and Natural Resources Conference*, v. 47, p. 441–452.
- Gilmour, C.C., Henry, E.A., and Mitchell, R., 1992, Sulfate stimulation of mercury methylation in freshwater sediments: *Environmental Science and Technology*, v. 26, p. 2281–2287.
- Gilmour, C., Krabbenhoft, D., Orem, W., and Aiken, G., 2004, Influence of drying and rewetting on mercury and sulfur cycling in Everglades and STA Soils, *Appendix 2B-1 in 2004 Everglades Consolidated Report: South Florida Water Management District and Florida Department of Environmental Protection*, 19 p.
https://my.sfwmd.gov/pls/portal/docs/PAGE/PG_GRP_SFWMD_SFER/PORTLET_PREVREP_ORF/FINAL/INDEX.HTML (accessed Sept. 30, 2010)
- Grenier, L., Marvin-DiPasquale, M., Drury, D., Hunt, J., Robinson, A., Bezalel, S., Melwani, A., Agee, J., Kakouros, E., Kieu, L., Windham-Myers, L., and Collins, J., 2010, South Baylands Mercury Project. Cooperator Report prepared for the California State Coastal Conservancy by San Francisco Estuary Institute, U.S. Geological Survey, and Santa Clara Valley Water District, February 10, 2010, 97 p.
http://www.sfei.org/sites/default/files/SBMP_Final%20Report%2010FEB2010.pdf

- Gu, L., Post, W.M., and King, A.W., 2004, Fast labile carbon turnover obscures sensitivity of heterotrophic respiration from soil to temperature: a model analysis: *Global Biogeochemical Cycles*, v.18, GB1022, doi:10.1029/2003GB002119
- Haitzer, M., Aiken, G.R., and Ryan, J.N., 2003, Binding of mercury (II) to aquatic humic substances: influence of pH and source of humic substances: *Environmental Science and Technology*, v. 37, p. 2436–2441.
- Hall, B.D., Aiken, G.R., Krabbenhoft, D., Marvin-DiPasquale, M., Swarzenski, C.M., 2008, Wetlands as principal zones of methylmercury production in southern Louisiana and the Gulf of Mexico region: *Environmental Pollution*, v. 154, p.124–134.
- Hall, B.D., Rosenberg, D.M., Wiens, A.P., 1998, Methyl mercury in aquatic insects from an experimental reservoir: *Canadian Journal of Fisheries and Aquatic Sciences*, v. 55, p. 2036–2047.
- Hall, B.D., St. Louis, V.L., and Bodaly, R.A., 2004, The stimulation of methylmercury production by decomposition of flooded birch leaves and jack pine needles: *Biogeochemistry*, v. 68, p.107–129.
- Hammerschmidt, C.R. and Fitzgerald, W.F., 2006, Photodecomposition of methylmercury in an Arctic Alaskan Lake: *Environmental Science and Technology*, v. 40, p. 1212–1216.
- Harmon, S.M., King, J.K., Gladden, J.B., Chandler, G.T, Newman, L.A., 2005, Mercury body burdens in *Gambusia holbrooki* and *Erimyzon sucetta* in a wetland mesocosm amended with sulfate: *Chemosphere*, v. 59, p. 227–233.
- Heald, C.C., ed., 2002, *Cameron Hydraulic Data -- A handy reference on the subject of hydraulics and steam* (19th ed.): Irving, Tex., Flowserve, Inc.
- Hecky, R.E., Ramsey, D.J., Bodaly, R.A., and Strange, N.E., 1991, Increased methylmercury contamination in fish in newly formed freshwater reservoirs, *in* Suzuki, T., Imura, N., and Clarkson, T.W., eds., *Advances in Mercury Toxicity: Proceedings of a Conference held in Tokyo, Japan, Aug. 1–3, 1990*. Springer, p. 33–52.
- Heim, W., Coale, K., Stephenson, M., Choe, K.-Y., Gill, G., and Foe, C., 2007, Spatial and habitat-based variations in total and methyl mercury concentrations in surficial sediments in the San Francisco Bay-Delta: *Environmental Science and Technology*, v. 41, p. 3501–3507.
- Heim, W.A., Deverel, S., Ingrum, T., Piekarski, W., and Stephenson, M., 2009, Assessment of Methylmercury Contributions from Sacramento-San Joaquin Delta Farmed Islands: Final report submitted to the Central Valley Regional Water Quality Control Board, contract 04-235-150-0, August 2009, 54 p.
http://www.waterboards.ca.gov/centralvalley/water_issues/tmdl/central_valley_projects/delta_hg/other_technical_reports/ (accessed Sept. 30, 2010)
- Heinz, G.H., 1979, Methylmercury: reproductive and behavioral effects on three generations of mallard ducks: *Journal of Wildlife Management*, v. 43, p. 394–401.
- Heinz, G.H., Hoffman, D.J., Klimstra, J.D., Stebbins, K.R., Konrad, S.L., and Erwin, C.A., 2009, Species differences in the sensitivity of avian embryos to methylmercury: *Archives of Environmental Contamination and Toxicology*, v. 56, p. 129–138.
- Hines, M.E, Banta, G.T., Giblin, A.E., Hobbie, J.E., and Tugel, J.B., 1994, Acetate concentrations and oxidation in salt-marsh sediments: *Limnology and Oceanography*, v. 39, p.140–148.
- Hines, M.E., Knollmeyer, S.L., and Tugel, J.B., 1989, Sulfate reduction and other sedimentary biogeochemistry in a northern New England salt marsh: *Limnology and Oceanography*, v. 34, p. 578–590.

- Horvat, M., Bloom, N.S., and Liang, L., 1993, A comparison of distillation with other current isolation methods for the determination of methyl mercury compounds in low level environmental samples. Part 2, water: *Analytica Chimica Acta*, v. 282, p. 153–168.
- Hurley, J.P., Benoit, J.M., Babiarz, C.L., Shafer, M.M., Andren, A.W., Sullivan, J.R., Hammond, R., Webb, D.A., 1995, Influences of watershed characteristics on mercury levels in Wisconsin rivers: *Environmental Science and Technology*, v. 29, p. 1867–1875.
- Hylander, L.D., Meili, M., Oliveira, L.J., de Castro e Silva, E., Guimaraes, J.R.D., Araujo, D.M., Neves, R.P., Stachiw, R., Barros, A.J.P., and Silva, G.D., 2000, Relationship of mercury with aluminum, iron and manganese oxy-hydroxides in sediments from the Alto Pantanal, Brazil: *The Science of the Total Environment*, v. 260, no. 1-3, p. 97–107.
- International Wild Rice Association, 2007, *The Manomin News*: v. 17, no. 4, November 2007, Outing, Minn.
- Jacob, D.L. and Otte, M.L., 2003, Conflicting processes in the wetland plant rhizosphere: metal retention or mobilization?: *Water, Air, and Soil Pollution*, v. 3, p. 91–104.
- Jeffres, C.A., Opperman, J.J., Moyle, P.B., 2008, Ephemeral floodplain habitats provide best growth conditions for juvenile Chinook salmon in a California river: *Environmental Biology of Fishes*, v. 83, p. 449–458.
- Jeremiason, J.D., Engstrom, D.R., Swain, E.B., Nater, E.A., Johnson, B.M., Almendinger, J.E., Monson, B.A., and Kolka, R.K., 2006, Sulfate addition increases methylmercury production in an experimental wetland: *Environmental Science and Technology*, v. 40, p. 3800–3806.
- Kelly, C.A., Rudd, J.W.M., Bodaly, R.A., Roulet, N.P., St.Louis, V.L., Heyes, A., Moore, T.R., Schiff, S., Aravena, R., Scott, K.J., Dyck, B., Harris, R., Warner, B., and Edwards, G., 1997, Increases in fluxes of greenhouse gases and methyl mercury following flooding of an experimental reservoir: *Environmental Science and Technology*, v. 31, p. 1334–1344.
- Kerin, E., Gilmour, C.C., Roden, E., Suzuki, M.T., Coates, J.D., and Mason, R.P., 2006, Mercury methylation among the dissimilatory iron-reducing bacteria: *Applied and Environmental Microbiology*, v. 72, p. 7919–7921.
- King, J.K., Kostka, J.E., Frischer, M.E., Saunders, F.M., and Jahnke, R.A., 2001, A quantitative relationship that demonstrates mercury methylation rates in marine sediments are based on the community composition and activity of sulfate-reducing bacteria: *Environmental Science and Technology*, v. 35, no. 12, p. 2491–2496.
- Krabbenhoft, D.P., Benoit J.M., Babiarz C.L., Hurley J.P., and Andren A.W., 1995, Mercury cycling in the Allequash Creek Watershed, northern Wisconsin: *Water, Air, and Soil Pollution*, v. 80, p. 425–433.
- Krabbenhoft, D.P., Wiener, J.G., Brumbaugh, W.G., Olson, M.L., DeWild, J.F., Sabinal, T.J., 1999, A national pilot study of mercury contamination of aquatic ecosystems along multiple gradients, *in* Morganwalp, D.W., and Buxton, H.T., eds., U.S. Geological Survey Toxic Substances Hydrology Program — Proceedings of the Technical Meeting, Charleston, SC, March 8-12, 1999 – Volume 2 of 3 – Contamination of Hydrologic Systems and Related Ecosystems, USGS Water-Resources Investigations Report: 99-4018, p. 147-160. Available at: http://toxics.usgs.gov/pubs/wri99-4018/Volume2/sectionB/2301_Krabbenhoft/pdf/2301_Krabbenhoft.pdf (accessed: August, 2007)
- Krapu, G.L., and Reinecke, K.J., 1992, Foraging ecology and nutrition, *in* Batt, B.D.J., Afton, A.D., Anderson, M.G., Ankney, C.D., Johnson, D.H., Kadlec, J.A., and Krapu, G.L., eds.,

- Ecology and management of breeding waterfowl: Minneapolis, University of Minnesota Press, p. 1–29.
- Krumme, U., Brenner, M., and Saint-Paul, U., 2008, Spring-neap cycle as a major driver of temporal variations in feeding of intertidal fishes: Evidence from the sea catfish *Sciades herzbergii* (Ariidae) of equatorial west Atlantic mangrove creeks: *Journal of Experimental Marine Biology and Ecology*, v. 367, no. 2, p. 91–99.
- Lacerda, L.D., and Fitzgerald, W.F., 2001, Biogeochemistry of mercury in wetlands: *Wetlands Ecology and Management*, v. 9, p. 291–293.
- Langer, C.S., Fitzgerald, W.F., Visscher, P.T., and Vandal, G.M., 2001, Biogeochemical cycling of methylmercury at Barn Island Salt Marsh, Stonington, CT, USA: *Wetlands Ecology and Management*, v. 9, p. 295–310.
- Lee, R., Kraus, D.W., and Doeller, J.E., 1999, Oxidation of sulfide by *Spartina alterniflora* roots: *Limnology and Oceanography*, v. 44, p. 1155–1159.
- Li, Yanbin, Mao, Y., Liu, G., Tachiev, G., Roelant, D., Feng, X., Cai, Y., 2010, Degradation of methylmercury and its effects on mercury distribution and cycling in the Florida Everglades: *Environmental Science and Technology*, v. 44, p. 6661–6666.
- Lovley, D.R., and Phillips, E.J.P., 1987a, Rapid assay for microbially reducible ferric iron in aquatic sediments: *Applied and Environmental Microbiology*, v. 53, p. 1536–1540.
- Lovley, D.R., and Phillips, E.J.P., 1987b, Competitive mechanisms for inhibition of sulfate reduction and methane production in the zone of ferric iron reduction in sediments: *Applied and Environmental Microbiology*, v. 53, p. 2636–2641.
- Liu, C.W., Chen, K., Jou, S.W., and Kuo, S.F., 2001, Estimation of the infiltration rate of a paddy field in Yun-Lin, Taiwan: *Agricultural Systems*, v. 68, p. 41–54.
- Marchetti, M.P., and Moyle, P.B., 2000, Spatial and temporal ecology of native and introduced fish larvae in lower Putah Creek, California: *Environmental Biology of Fishes*, v. 58, p. 75–87.
- Marins, R.V., Lacerda, L.D., Goncalves, G.O., de Paiva, E.C., 1997, Effect of root metabolism on the post-depositional mobilization of mercury in salt marsh soils: *Bulletin of Environmental Contamination and Toxicology*, v. 58, p. 733–738.
- Marschner, H., 1995, *The mineral nutrition of higher plants* (2nd ed.): London, Academic Press, 889 p.
- Martens, C.S., and Berner, R.A., 1974, Methane production in the interstitial waters of sulfate depleted marine sediments: *Science*, v. 185, p. 1167–1169.
- Marvin-DiPasquale, M., and Agee, J.L., 2003, Microbial mercury cycling in sediments of the San Francisco Bay-Delta: *Estuaries*, v. 26, no. 6, p. 1517–1528.
- Marvin-DiPasquale, M., Agee, J., Bouse, R., and Jaffe, B., 2003a, Microbial cycling of mercury in contaminated pelagic and wetland sediments of San Pablo Bay, California: *Environmental Geology*: v. 43, no. 3, p. 260–267.
- Marvin Di-Pasquale, M., Alpers, C.N., and Fleck, J.A., 2009a, Mercury, methylmercury, and other constituents in sediment and water from seasonal and permanent wetlands in the Cache Creek Settling Basin and Yolo Bypass, Yolo County, California, 2005–06: U.S. Geological Survey, Open File Report 2009-1182, 69 p. <http://pubs.usgs.gov/of/2009/1182/> (accessed Sept. 30, 2010)
- Marvin-DiPasquale, M.C., Boynton, W.R., and Capone, D.G., 2003b, Benthic sulfate reduction along the Chesapeake Bay central channel. II. Temporal controls: *Marine Ecology Progress Series*, v. 260, p. 55–70.
- Marvin-DiPasquale, M., and Cox, M.H., 2007, Legacy mercury in Alviso Slough, South San Francisco Bay, California: Concentration, speciation and mobility: U.S. Geological Survey

- Open-File Report 2007-1240, 98 p. <http://pubs.usgs.gov/of/2007/1240/> (accessed Sept. 30, 2010)
- Marvin-DiPasquale, M.C., Lutz, M.A., Brigham, M.E., Krabbenhoft, D.P., Aiken, G.R., Orem, W.H., and Hall, B.D., 2009b, Mercury cycling in stream ecosystems. 2. Benthic methylmercury production and bed sediment-pore water partitioning: *Environmental Science and Technology*, v.43, p. 2726–2732.
- Marvin-DiPasquale, M.C., Lutz, M.A., Krabbenhoft, D.P., Aiken, G.R., Orem, W.H., Hall, B.D., DeWild, J.F., and Brigham, M.E., 2008, Total mercury, methylmercury, methylmercury production potential, and ancillary streambed-sediment and pore-water data for selected streams in Oregon, Wisconsin, and Florida, 2003–04: U.S. Geological Survey Data Series 375, 24 p.
- Marvin-DiPasquale, M., Stewart, A.R., Fisher, N.S., Pickhardt, P., Mason, R.P., Heyes, A., and Windham-Myers, L., 2007, Evaluation of mercury transformations and trophic transfer in the San Francisco Bay/Delta: Identifying critical processes for the Ecosystem Restoration Program: final report to California Bay Delta Authority, project ERP-02-P40, 40 p.
- McKnight, D.M., Boyer, E.W., Westerhoff, P.K., Doran, P.T., Kulbe, T., and Anderson, D.T., 2001, Spectrofluorometric characterization of dissolved organic matter for indication of precursor organic material and aromaticity: *Limnology and Oceanography*, v. 46, no. 1, p. 38–48.
- Mehrotra, A.S., Horne, A.J., and Sedlak, D.L., 2003, Reduction of net mercury methylation by iron in *Desulfobulbus propionicus* (1pr3) cultures: implications for engineered wetlands: *Environmental Science and Technology*, v. 37, p. 3018–3023.
- Melillo, J.M., Aber, J.D., and Muratore, J.M., 1982, Nitrogen and lignin control of hardwood leaf litter decomposition dynamics: *Ecology*, v. 63, p. 621–626.
- Menke, A.S., ed., 1979, The semiaquatic and aquatic Hemiptera of California: *Bulletin of the California Insect Survey*, v. 21, p. 1–166.
- Merritt, K.A., and Amirbahman, A., 2009, Mercury methylation dynamics in estuarine and coastal marine environments — A critical review: *Earth-Science Reviews*, v. 96, p. 54–66.
- Merritt, R.W., Cummins, K.W., eds., 1996, *An introduction to the insects of North America* (3rd ed.): Dubuque, Iowa, Kendall-Hunt Publishing Co., 862 p.
- Morel, F.M.M., Kraepiel, A.M.L., and Amyot, M., 1998, The chemical cycle and bioaccumulation of mercury: *Annual Review of Ecology and Systematics*, v. 29, p. 543–566.
- Moyle, P.B., 2002, *Inland Fishes of California* (2nd ed.): Berkeley, Calif., Univ. of California Press, 517 p.
- Neckles, H.A., Murkin, H.R., and Cooper, J.A., 1990, Influences of seasonal flooding on macroinvertebrate abundance in wetland habitats: *Freshwater Biology*, v. 23, p. 311–322.
- Oikari, A., 2006, Caging techniques for field of fish to chemical contaminants: *Aquatic Toxicology*, v. 78, p. 370–381.
- Olson, M.L., and Dewild, J.F., 1999, Techniques for the collection and species-specific analysis of low levels of mercury in water.: U. S. Geological Survey - Toxic Substance Hydrology Program. Water-Resources Investigation Report 99-4018B, 191-199 p.
- Parsons, T. R., Y. Maita and C. M. Lalli, 1984. *A manual of chemical and biological methods for seawater analysis*. Pergamon Press. Oxford, UK. 173 pp.
- Qian, J., Skyllberg, U., Frech, W., Bloom, P.R., and Petit, P.E., 2002, Bonding of methyl mercury to reduced sulfur groups in soil and stream organic matter as determined by X-ray

- absorption spectroscopy and binding affinity studies: *Geochemica et Cosmochemica Acta*, v. 66, no. 22, p. 3873–3885.
- Ravichandran, M., 2004, Interactions between mercury and dissolved organic matter—a review: *Chemosphere*, v. 55, no.3: p. 319–331.
- Rice, W.R., 1989, Analyzing tables of statistical tests: *Evolution*, v. 43, p. 223–225.
- Roden, E.E., 2008, Microbiological controls on geochemical kinetics 1: Fundamentals and case study on microbial Fe(III) oxide reduction, *in* Brantley, S.L., Kubicki, J.D., and White, A.F., eds., *Kinetics of Water-Rock Interactions*: New York, Springer, p. 335–415.
- Roden, E.E., and Tuttle, J.H., 1993, Inorganic sulfur turnover in oligohaline estuarine sediments: *Biogeochemistry*, v. 22, p. 81–105.
- Roden, E.E., and Wetzel, R.G., 2002, Kinetics of microbial Fe(III) oxide reduction in freshwater wetland sediments: *Limnology and Oceanography*, v. 47, p. 198–211.
- Roden, E.E., and Zachara, J.M., 1996, Microbial reduction of crystalline iron(III) oxides: Influence of oxide surface area and potential for cell growth: *Environmental Science and Technology*, v. 30, p.1618–1628.
- Rudd, J.W.M., 1995, Sources of methyl mercury to freshwater ecosystems: a review: *Water, Air, and Soil Pollution*, v. 80, p. 697–713.
- Rumbold, D.G., and Fink, L.E., 2006, Extreme spatial variability and unprecedented methylmercury concentrations within a constructed wetland: *Environmental Monitoring and Assessment*, v. 112, p. 115–135.
- Sassone, E., Bonnema, A., Stephenson, M., Heim, W.A., Newman, A., Fleck, J., and Coale, K., 2008, Methylmercury loading studies in Delta wetlands – Twitchell Island, *task 5.3a in* Transport, Cycling, and Fate of Mercury and Monomethyl Mercury in the San Francisco Delta and Tributaries: An Integrated Mass Balance Assessment Approach: Final report to the California Department of Fish and Game and the California Bay Delta Authority, 13 p. http://mercury.mlml.calstate.edu/wp-content/uploads/2008/10/12_task5_3a_twitchell_final.pdf (accessed Sept. 30, 2010)
- Schlemel, L.E., Cox, M.H., Runkel, R.L., and Kimball, B.A., 2006, Multiple injected and natural conservative tracers quantify mixing in a stream confluence affected by acid mine drainage near Silverton, Colorado, *Hydrologic Processes*, v. 20, p. 2727–2743.
- Seal II, R.R., Alpers, C.N., and Rye, R.O., 2000, Stable isotope systematics of sulfate minerals, *in* Alpers, C.N., Jambor, J.L, and Nordstrom, D.K., eds., *Sulfate Minerals: Crystallography, Geochemistry, and Environmental Significance*: Washington, D.C., Mineralogical Society of America and Geochemical Society, *Reviews in Mineralogy and Geochemistry*, v. 40, p. 541–602.
- Sedinger, J.S., 1992, Ecology of prefledging waterfowl, *in* Batt, B.D.J., Afton, A.D., Anderson, M.G., Ankney, C.D., Johnson, D.H., Kadlec, J.A., and Krapu, G.L., eds., *Ecology and management of breeding waterfowl*: Minneapolis, University of Minnesota Press, p.109–127.
- Sharp, Z., 2007, *Principles of Stable Isotope Geochemistry*: New Jersey, Pearson-Prentice Hall, 344 p.
- Skyring, G.W., 1987, Sulfate reduction in coastal ecosystems: *Geomicrobiology Journal*, v. 5, p. 295-374.
- Slowey, A.J., and Brown Jr., G.E., 2007, Transformations of mercury, iron, and sulfur during the reductive dissolution of iron oxyhydroxide by sulfide: *Geochimica et Cosmochimica Acta*, v. 71, p. 877–894.

- Snodgrass, J.W., Jagoe, C.H., Bryan, Jr. A.L., Brant, H.A., and Burger, J., 2000, Effects of trophic status and wetland morphology, hydroperiod, and water chemistry on mercury concentrations in fish: *Canadian Journal of Fisheries and Aquatic Sciences*, v. 57, p. 171–180.
- Sommer, T., Harrell, B., Nobriga, M., Brown, R., Moyle, P., Kimmerer, W. and Schemel, L., 2001, California's Yolo Bypass — Evidence that flood control can be compatible with fisheries, wetlands, wildlife, and agriculture: *Fisheries*, v. 26, p. 6-16.
- Sommer, T.R., Harrell, W.C., and Swift, T.J., 2008, Extreme hydrologic banding in a large-river floodplain, California, U.S.A.: *Hydrobiologia*, v. 598, p. 409–415.
- St. Louis, V.L., Rudd, J.W.M., Kelly, C.A., and Barrie, L.A., 1995, Wet deposition of methylmercury in northwestern Ontario compared to other geographic locations: *Water, Air, and Soil Pollution*, v. 80, p. 405–414.
- St. Louis, V.L., Rudd, J.W.M., Kelly, C.A., Beaty, K.G., Bloom, N.S. and Flett, R.J., 1994, Importance of wetlands as sources of methylmercury to boreal forest ecosystems: *Canadian Journal of Fisheries and Aquatic Sciences*, v. 51, p. 1065–1076.
- St. Louis, V.L., Rudd, J.W.M., Kelly, C.A., Beaty, K.G., Robert, J.F., Roulet, N.T., 1996, Production and loss of methylmercury and loss of total mercury from boreal forest catchments containing different types of wetlands: *Environmental Science and Technology*, v. 30, p. 2719–2729.
- Stephenson, C., Foe, C., Gill, G.A., and Coale, C., 2008, Transport, Cycling, and Fate of Mercury and Monomethyl Mercury in the San Francisco Delta and Tributaries: An Integrated Mass Balance Assessment Approach: Final report to the California Department of Fish and Game and the California Bay Delta Authority, September, 2008.
<http://mercury.mlml.calstate.edu/reports/reports/> (accessed Sept. 30, 2010)
- Thamdrup, B., 2000, Bacterial manganese and iron reduction in aquatic sediments: in Schink, Bernhard (Ed.), *Advances in Microbial Ecology*, Vol 16. Springer, p. 41-84
- Thullner, M., and Van Cappellen, P., 2007, Modeling microbially induced carbon degradation in redox-stratified subsurface environments: concepts and open questions: *Geomicrobiology Journal*, v. 24, p. 139–155.
- Trust, B.A., and Fry, B., 1992, Stable sulfur isotopes in plants - a review: *Plant, Cell, and Environment*, v.15, p. 1105–1110.
- U.S. Department of Agriculture, National Agricultural Statistics Service, 2007,
<http://www.nass.usda.gov/> (accessed July 22, 2009)
- U.S. Environmental Protection Agency, 2000a, Mercury in solids and solutions by thermal decomposition, amalgamation, and atomic absorption spectrophotometry: Method 7473, Test methods for evaluating solid waste, physical/chemical methods SW 846, Update IVA, Washington, D.C.
- U.S. Environmental Protection Agency, 2000b, Water Quality Standards - Establishment of Numeric Criteria for Priority Toxic Pollutants for the State of California, 40 CFR Part 131.
<http://www.epa.gov/fedrgstr/EPA-WATER/2000/May/Day-18/w11106.pdf> (accessed Sept. 30, 2010)
- U.S. Environmental Protection Agency, 2001, Methyl mercury in water by distillation, aqueous ethylation, purge and trap, and cold-vapor atomic fluorescence spectrometry: Method 1630, EPA-821-R-01-020. Office of Water and Office of Science and Technology, Washington, D.C.
- U.S. Fish and Wildlife Service, 1978, Concept plan for waterfowl wintering habitat and preservation, Central Valley, California: Portland, Oregon.

- U.S. Geological Survey, 2006, Collection of water samples (ver. 2.0): U.S. Geological Survey Techniques of Water-Resources Investigations, book 9, chap. A4, revised September 2006, accessed May, 23, 2007 at <http://pubs.water.usgs.gov/twri9A4/>
- U.S. Geological Survey, Calif. Department of Fish and Game, Yolo Basin Foundation, Moss Landing Marine Lab, and Battelle Marine Sciences, 2008, Quality Assurance Project Plan (version 3.1), Methylmercury cycling and export from agricultural and natural wetlands in the Yolo Bypass: prepared for the California State Water Resources Control Board, January 7, 2008, 419 p.
- Ullrich, S.M., Tanton, T.W., and Abdrashitova, S.A., 2001, Mercury in the aquatic environment: A review of factors affecting methylation: *Critical Reviews in Environmental Science and Technology*, v. 31, p. 241-293.
- Waples, J.S., Nagy, K.L., Aiken, G.R., and Ryan, J.N., 2005, Dissolution of cinnabar (HgS) in the presence of natural organic matter: *Geochemica et Cosmochemica Acta*, v. 69, p. 1575-1588.
- Westover, K.M., Kennedy, A.C., and Kelley, S.E., 1997, Patterns of rhizosphere microbial community structure associated with co-occurring plant species: *Journal of Ecology*, v. 85, p. 863–873.
- Wiener, J.G., Gilmour, C.C., Krabbenhoft, D.P., 2003b, Mercury strategy for the Bay-Delta ecosystem: a unifying framework for science, adaptive management, and ecological restoration: Final report to the California Bay Delta Authority, Sacramento, California. <http://calwater.ca.gov/science/pdf/MercuryStrategyFinalReport.pdf> (accessed Sept. 30, 2010)
- Wiener, J.G., Krabbenhoft, D.P., Heinz, G.H., Scheuhammer, A.M., 2003a, Ecotoxicology of Mercury, *Chapter 16 in Hoffman, D.J., Rattner, B.A., Burton, G.A., Jr., and Cairns J., Jr., eds., Handbook of Ecotoxicology (2nd ed.)*: Boca Raton, Fla., CRC Press, p. 409–463.
- Williams, B.K., Nichols, J.D., Conroy, M.J., 2002, Analysis and management of animal populations: Modeling, estimation, and decision making: San Diego, Calif., Academic Press, 818 p.
- Windham, L. and Ehrenfeld, J.G., 2003, Net impact of a plant invasion on nitrogen cycling processes within a brackish tidal marsh: *Ecological Applications*, v. 13, p. 883–897.
- Windham-Myers, L., Marvin-DiPasquale, M., Krabbenhoft, D.P., Agee, J.L., Cox, M.H., Heredia-Middleton, P., Coates, C., and Kakouros, E., 2009, Experimental removal of wetland emergent vegetation leads to decreased methylmercury production in surface sediment: *Journal of Geophysical Research, Biogeosciences*, v. 114, G00C05, doi:10.1029/2008JG000815 <http://www.agu.org/journals/pip/jg/2008JG000815-pip.pdf> (accessed Sept. 30, 2010)
- Wood, M.L., Foe, C., Cooke, J., and Louie, S.J., 2010a, Sacramento – San Joaquin Delta Estuary TMDL for Methylmercury: Staff report, Regional Water Quality Control Board – Central Valley Region, Sacramento, Calif., April 2010, 234 p. http://www.swrcb.ca.gov/rwqcb5/water_issues/tmdl/central_valley_projects/delta_hg/april_20_10_hg_tmdl_hearing/index.shtml (accessed Sept. 30, 2010)
- Wood, M.L., Morris, P., Cooke, J., and Louie, S.J., 2010b, Amendments to the Water Quality Control Plan for the Sacramento River and San Joaquin River Basins for the Control of Methylmercury and Total Mercury in the Sacramento-San Joaquin Delta Estuary: Staff Report, Regional Water Quality Control Board – Central Valley Region, April 2010, 332 p. http://www.swrcb.ca.gov/rwqcb5/water_issues/tmdl/central_valley_projects/delta_hg/april_20_10_hg_tmdl_hearing/index.shtml (accessed Sept. 30, 2010)

- Wopereis, M.C.S., Bouman, B.A.M., Kropff, M.J., ten Berge, H.F.M., and Maligaya, A.R., 1994, Water use efficiency of flooded rice fields. I. Validation of the soil-water balance model SAWAH: Agricultural Water Management, v. 26, p. 277–289.
- Yee, D., Collins, J., Grenier, L., Takekawa, J., Tsao-Melcer, D., Woo, I., Schwarzbach, S., Marvin-DiPasquale, M., Windham, L., Krabbenhoft, D., Olund, S., and DeWild, J., 2008, Mercury and Methylmercury Processes in North San Francisco Bay Tidal Wetland Ecosystems – Final Report for Project # ERP02D-P62. Cooperator Report to CALFED Ecosystem Restoration Program, Prepared by the San Francisco Estuary Institute and the U.S. Geological Survey. May 2, 2008, 65 p.
- YSI, Inc., 2009, YSI 6-series Multiparameter Water Quality Sondes — User’s Manual (revision F): Yellow Springs, Ohio, Sept. 2009, 377 p. <http://www.ysi.com/media/pdfs/069300-YSI-6-Series-Manual-RevF.pdf> (accessed Sept. 30, 2010)
- Zillioux, E.J., Porcella, D.B., and Benoit, J.M., 1993, Mercury cycling and effects in freshwater wetland ecosystems: Environmental Toxicology and Chemistry, v. 12, p. 2245–2264.

12 ACKNOWLEDGEMENTS

This report integrates a large and diverse data set that would be difficult to understand without review comments from two agencies: 1) the review panel within the RWQCB-CVR – especially Janis Cooke, and 2) Joann Holloway, USGS – Denver, Colorado, whose comments were invaluable as an independent sounding board, due to her detailed and comprehensive understanding of each part and how it should link together. We are grateful to the SWQCB for supporting this project with Proposition 40 funding. Task-specific acknowledgements follow here:

Acknowledgements for Section 5: Special thanks to California Department of Fish and Game staff (especially Chris Rocco), USGS field and laboratory staff (especially Frank Anderson, Elizabeth Beaulieu, and Will Kerlin), SWRCB/ RWQCB-CVR staff and the Yolo Basin Foundation staff. Thanks to the residents of California for funding from Proposition 40 and the USGS for contributions of matching funds from the Cooperative Hydrology Program as well as in-kind funds from the National Research Program in Water Resources and other USGS programs in support of the work conducted in this study. Particular USGS in-kind contributions include supportive laboratory analyses by Craig Stricker (USGS-Denver), Howard Taylor (USGS-Denver), and George Aiken (USGS-Boulder).

Acknowledgements for Sections 6 & 7: We thank Jack DeWit, of DeWit farms for sharing field-based management decisions and for sharing post-harvest estimates of yield for each field. We thank Mark Rollog (USGS, Menlo Park) for providing high quality analyses of plant tissue carbon and nitrogen concentrations and isotopic signatures. We thank many field and laboratory technicians for both initial experimental set up and for continued sampling and processing during the 1 year study, including Sherrie Wren, Steven Quistad, Justin Kanerva, and Kathy Akstin. This research was made possible by careful wetland management by California Fish and Game staff and Chris Rocco of the Yolo Bypass Wildlife Area.

Acknowledgements for Section 8: This research was funded by the California State Water Resources Control Board with additional support from the USGS Western Ecological Research Center. We thank Carson Jeffres for fish cage design and advice on deployment, Sarah Stoner-Duncan, Robin Keister, Danika Tsao, Mark Ricca, Erica Caceres, Jill Bluso, Sarah Spring, Cody Massing, Meg Harper, Jessica Mellinger, and Whitney Thornton for field and lab work, and Julie Yee for statistical advice. We also thank Dave Feliz and the California Department of Fish and Game staff of the Vic Fazio Yolo Bypass Wildlife Area, Jack DeWit and DeWit Farms, Jacob Fleck, Charlie Alpers, Lisamarie Windham-Myers, Mark Marvin-DiPasquale, Mark Stephenson, Phil Bachand, Gary Gill, and the Yolo Basin Foundation for logistical support. The use of trade, product, or firm names in this publication is for descriptive purposes only and does not imply endorsement by the U. S. Government.

Table 1.1. Individuals (alphabetically) and organizations involved in the project

Name	Affiliation	Area of Expertise	Contact Information
Josh Ackerman	U.S. Geological Survey	Biology / Fish and invertebrate Hg analyses	TEL (530) 752-0485 FAX (530) 752-9680 jackerman@usgs.gov
Charlie Alpers	U.S. Geological Survey	Trace metals and aquatic geochemistry	TEL (916) 278-3134 FAX (916) 278-3070 cnalpers@usgs.gov
Phil Bachand	Bachand and Associates	Hydrologic processes and modeling	TEL (530) 758-1336 phil@bachandassociates.com
Ann Brice	Yolo Basin Foundation	Public Outreach	TEL (530) 758-0530 FAX (530) 757-4824 abrice@yolobasin.org
Collin Eagles-Smith	U.S. Geological Survey	Biology / Fish and invertebrate Hg analyses	TEL (541) 750-0949 FAX (541) 750-1069 ceagles-smith@usgs.gov
Dave Feliz	California Dept. Fish and Game	YWMA management	TEL (530) 757-2461 FAX (530) 757-2518 dfeliz@dfg.ca.gov
Jacob Fleck	U.S. Geological Survey	Aquatic chemistry / DOM-Hg interactions	TEL (916) 278-3063 FAX (916) 278-3071 jafleck@usgs.gov
Gary Gill	Batelle Marine Science Laboratories	Aquatic geochemistry / photochemistry	TEL (360) 681-4593 FAX (360)681-3600 gary.gill@pnl.gov
Mark Marvin-DiPasquale	U.S. Geological Survey	Microbial ecology; Hg analysis in sediments	TEL (650) 329-4442 FAX (650)-329-4463 mmarvin@usgs.gov
Mark Stephenson	Moss Landing Marine Laboratories	Hg analyses of water samples; hydrologic measurements	TEL (831) 771-4177 FAX (831) 633-0805 mstephenson@mlml.calstate.edu
Lisamarie Windham-Myers	U.S. Geological Survey	Plant ecology; Hg analysis in plant material	TEL (650) 329-4447 FAX (650) 329-4463 lwindham@usgs.gov

Table 3.1. Study sampling locations and descriptions

[Site coordinates expressed in degrees,minutes,seconds (dd(d)° mm' ss") using World Geodetic System 1984 (WGS84). Field type: 'PW' = 'permanently flooded wetland', 'SW' = 'seasonally flooded wetland'.]

Field Type	Field #	Field Location	Site Code	Latitude (North)	Longitude (West)	Description
White Rice	31	Inlet 1	R31-i1	38 33' 40"	121 37' 11"	check levee weir box on west side of field
White Rice	31	Inlet 2	R31-i2	38 33' 40"	121 36' 45"	check levee weir box in NE corner of field
White Rice	31	Center	R31-c	38 33' 24"	121 36' 59"	center field levee intersection with wind breaks
White Rice	31	Outlet 1	R31-o1	38 33' 11"	121 37' 11"	outlet riser in SW corner of field, W boundary
White Rice	31	Outlet 2	R31-o2	38 33' 09"	121 36' 38"	outlet riser in SE corner of field, S boundary
White Rice	64	Inlet 1	R64-i1	38 33' 07"	121 37' 12"	check levee weir box in NW area of field
White Rice	64	Inlet 2	R64-i2	38 33' 07"	121 37' 04"	check levee weir box in SW area of field
White Rice	64	Center	R64-c	38 33' 01"	121 36' 55"	center field sampling point - levee wall
White Rice	64	Outlet 1	R64-o1	38 33' 06"	121 36' 40"	check levee weir box in NE area of field
White Rice	64	Outlet 2	R64-o2	38 32' 52"	121 36' 41"	check levee weir box in SE area of field
Wild Rice	32	Inlet 1	W32-i1	38 33' 40"	121 36' 38"	screwgate inlet at NW corner of field #32 YWA
Wild Rice	32	Center	W32-c	38 33' 24"	121 36' 32"	center field sampling point - levee wall
Wild Rice	32	Outlet 1	W32-o1	38 33' 10"	121 36' 23"	outlet riser in SE corner of field
Wild Rice	65	Inlet 1	W65-i1	38 33' 07"	121 36' 36"	screwgate inlet at NW corner , 70m E of corner
Wild Rice	65	Center	W65-c	38 32' 48"	121 36' 27"	center field sampling point at levee wall
Wild Rice	65	Outlet 1	W65-o1	38 32' 34"	121 36' 23"	outlet riser at SE corner of field
Fallow	20	Inlet 1	F20-i1	38 33' 10"	121 37' 45"	standpipe inlet in SW corner of YWA #20 lower
Fallow	20	Inlet 2	F20-i2	38 33' 30"	121 37' 45"	screwgate inlet at NW corner of YWAsouth,new structure just put in under new road intersection
Fallow	20	Center	F20-c	38 33' 15"	121 37' 30"	Unkonwn, still being reworked as of 6/20/07
Fallow	20	Outlet 1	F20-o1	38 33' 09"	121 37' 12"	outlet flashboard riser at SE corner of lower unit
Fallow	66	Inlet 1	F66-i1	38 33' 07"	121 36' 09"	screwgate inlet at NE corner of field
Fallow	66	Center	F66-c	38 32' 34"	121 36' 23"	outlet riser at SW corner of field
Fallow	66	Outlet 1	F66-o1	38 32' 34"	121 36' 07"	outlet riser at SE corner of field
PW	5	Inlet 1	PW5-i1	38 33' 08"	121 35' 26"	inlet screwgate culvert for permanent wetland
PW	5	Center	PW5-c	38 32' 57"	121 35' 27"	center openwater site for permanent wetland
PW	5	Outlet 1	PW5-o1	38 32' 34"	121 35' 33"	outlet flashboard riser for permanent wetland
SW	1	Inlet 1	SW1-i1	38 33' 08"	121 36' 05"	inlet screwgate culvert for seasonal wetland
SW	1	Center	SW1-c	38 33' 09"	121 35' 47"	center vegetated site for seasonal wetland
SW	1	Outlet 2	SW1-o1	38 32' 28"	121 36' 04"	outlet flashboard riser for seasonal wetland

Table 4.1. Field size and associated areas for hydrologic units

['Field area' represents the area as measured from the field inflow structure to the field outflow structure. The hydrologic unit (HU) area represents the area encompassed by where the inflow and outflow were actually measured, and is sometimes smaller than the field area due to the location of within-field 'checks' (water control berms). The number of 'checks' is also indicated for both the full field and the HU.]

Field	Field		HU	
	Area, Hectares	# Checks	Area, Hectares	# Checks
F20	47	11	42	9
F66	39	4	35	2
PW	16	3	16	---
R31	78	6	63	4
R64	31	6	25.5	5
SW	52	2	52	---
W32	33	5	30	4
W65	44	5	43	5

Table 4.3. Water budget for agricultural and non-agricultural fields during the summer irrigated period

[Values are in centimeters (water volume normalized to field area). Percentages are based on the measured and calculated fluxes as a percent of total “INs” and “OUTs”. The seasonal wetland (SW) remained dry during this period and the annual imbalance includes the “dry-down” period 5/1/2007 through 9/30/2007. The permanent wetland (PW) was periodically irrigated to maintain a set water level and once in July to flush the system, and includes the period 5/1/2007 through 9/30/2007. The ‘days in season’ are from **Table 4.2** and are operationally defined. The summer period is defined by the period between flood-up and dry down when surface storage equals zero. ‘Seasonal imbalance’ represents the imbalance for the season. ‘Annual imbalance’ represents the cumulative imbalance beginning in spring at the beginning of dry down. Precipitation, evaporation and transpiration vary somewhat between cells because of the different lengths of the seasons. Evapotranspiration is determined utilizing CIMIS data and crop coefficients. Evapotranspiration’s components (evaporation, transpiration) were estimated using a Plug Flow Reactor Model.]

Field ID	F20		F66		R31		R64		W32		W65		SW		PW		
days in season	67		67		136		121		122		131		153		153		
INs	irrigation	50	100%	44	100%	113	100%	137	100%	127	100%	102	97%	0	0%	120	100%
	precipitation	0	0%	0	0%	0	0%	0	0%	0	0%	3	3%	0.5	100%	0.5	0%
OUTs	surface outflow	-6	12%	-6	12%	-31	26%	-43	35%	-39	32%	-15	15%	0	0%	-10	8%
	evaporation	-11	22%	-11	22%	-22	18%	-20	16%	-21	17%	-21	21%	-35	50%	-70	58%
	transpiration	-33	66%	-32	65%	-67	56%	-59	48%	-63	51%	-63	64%	-35	50%	-40	33%
surface storage	0	0%	0	0%	0	0%	0	0%	0	0%	0	0%	0	0%	0	0%	
season imbalance	0	0%	-5	5%	-7	3%	15	6%	4	2%	6	3%	-70	99%	0.5	0%	
annual imbalance	-33	23%	-38	28%	-20	8%	1	0%	-10	4%	-8	4%	-70	99%	0.5	0%	

Table 4.4. Water budget for agricultural and non-agricultural fields during the winter irrigated period

Values are in centimeters (water volume normalized to field area). Percentages are based on the measured and calculated fluxes as a percent of total “INs” and “OUTs”. The ‘days in season’ are from **Table 4.2** and are operationally defined. ‘Surface storage’ is positive for this period for all fields because the regional flooding occurred during flooded conditions. ‘Seasonal imbalance’ represents the imbalance for the season. ‘Annual imbalance’ represents the cumulative imbalance beginning in spring at the beginning of dry down. Evapotranspiration is determined utilizing CIMIS data and crop coefficients. Transpiration is assumed to be equivalent to zero during this period because of vegetation senescence and/or harvest except in the permanent wetland where vegetation is present and active throughout the year.

Field ID	F20		F66		R31		R64		W32		W65		SW		PW		
days in season	101		59		69		69		59		66		115		115		
INs	irrigation	10	28%	18	43%	18	44%	41	64%	12	34%	17	42%	100	78%	17	37%
	precipitation	25	72%	23	57%	23	56%	23	36%	23	66%	23	58%	29	22%	29	63%
OUTs	surface outflow	-24	57%	-24	60%	-6	14%	-20	32%	-0.4	1%	-15	39%	0	0%	-13	27%
	evaporation	-18	43%	-8	20%	-10	24%	-10	16%	-8	23%	-10	25%	-22	17%	-18	40%
	transpiration	0	0%	0	0%	0	0%	0	0%	0	0%	0	0%	0	0%	-9	20%
surface storage	25	72%	25	61%	25	61%	25	39%	25	71%	25	63%	30	23%	0	0%	
season imbalance	-33	32%	-17	17%	1	1%	9	7%	2	2%	-11	12%	77	42%	6	7%	
annual imbalance	-79	30%	-76	29%	-24	7%	2	0%	-18	5%	-28	8%	7	2%	7	2%	

Table 4.6. Water budget for agricultural and non-agricultural fields during the winter drainage period

Values are in centimeters (water volume normalized to field area). Percentages are based on the measured and calculated fluxes as a percent of total “INs” and “OUTs”. The ‘days in season’ are from **Table 4.2** and are operationally defined. ‘Surface storage’ is set equal to zero because the end of the season is defined by the drainage of surface water and the change in storage is captured in the ‘surface outfall’ value. ‘Seasonal imbalance’ represents the imbalance for the season. ‘Annual imbalance’ represents the cumulative imbalance beginning in spring at the beginning of dry down. Evapotranspiration is determined utilizing CIMIS data and crop coefficients. Transpiration is assumed to be equivalent to zero during this period because of vegetation senescence except in the seasonal and permanent wetlands where viable vegetation is present.

Field ID	F20		F66		R31		R64		W32		W65		SW		PW			
days in season	18		18		18		18		18		18		80		80			
INs	irrigation	0	0%	0	0%	0	0%	0	0%	0	0%	0	0%	32	80%	32	80%	
	precipitation	5	100%	5	100%	5	100%	5	100%	5	100%	5	100%	8	20%	8	20%	
OUTs	surface outfall	-25	83%	-25	-12%	-25	-16%	-25	-16%	-25	-14%	-25	-14%	-30	-14%	-3	-1%	
	evaporation	-5	17%	-5	-2%	-5	-3%	-5	-3%	-5	-3%	-5	-3%	-15	-7%	-25	-12%	
	transpiration	0	0%	0	0%	0	0%	0	0%	0	0%	0	0%	-25	-12%	-12	-6%	
surface storage	0	0%	0	0%	0	0%	0	0%	0	0%	0	0%	0	0%	0	0%		
season imbalance	-25	71%	-25	71%	-25	71%	-25	71%	-25	71%	-25	71%	-25	71%	-30	27%	0	0%
annual imbalance	-104	35%	-101	34%	-49	13%	-23	5%	-43	11%	-53	15%	-93	21%	7	2%		

Table 4.7. Water budget for agricultural and non-agricultural fields during the combined winter irrigated and winter drainage periods, excluding the 17-day winter flood period

This budget combines the irrigated and drained periods in winter when water management was possible (Tables 4.4 and 4.6). The period during the regional flood was left out of the budget due to the high uncertainty inherent in the estimates for that period. The ‘seasonal imbalance’ represents the total imbalance for winter. The ‘annual imbalance’ represents the cumulative annual imbalance (March – February for agricultural wetlands and May – April for non-agricultural wetlands). The annual imbalance shows good closure of the water budget (< 10% in most fields) except in F20 and F66 where a larger imbalance suggests subsurface water sources provide additional water to the shallow-flooded fallow fields or a low bias in irrigation volume measurements in these fields.

Field ID	F20	F66	R31	R64	W32	W65	SW	PW	
days in season	119	77	87	87	77	84	195	195	
INs	irrigation	9.5 22%	17.7 36%	18.2 37%	41.1 57%	12 28%	16.7 35%	132 77%	49 55%
	precipitation	33 78%	31 64%	31 63%	31 43%	31 72%	31 65%	39.5 23%	40 45%
OUTs	surface outflow	-49 66%	-49 77%	-31 64%	-45 73%	-25 63%	-40 70%	-30 32%	-16 19%
	evaporation	-25 34%	-15 23%	-17 36%	-17 27%	-15 37%	-17 30%	-39 41%	-45 55%
	transpiration	0 0%	0 0%	0 0%	0 0%	0 0%	0 0%	-25 27%	-21 26%
surface storage	0 0%	0 0%	0 0%	0 0%	0 0%	0 0%	0 0%	0 0%	
season imbalance	-32 27%	-16 14%	1.5 2%	9.9 7%	2.6 3%	-9.6 9%	77.5 29%	7 4%	
annual imbalance	-78 28%	-75 27%	-23 6%	2.9 1%	-17 5%	-27 8%	8 2%	7.5 2%	

Table 4.8. Annual total water budget for agricultural and non-agricultural fields

The annual total water budget is the summation of the seasonal water budgets (including spring and autumn periods). Percentages are based upon the percent of surface water applied from either precipitation or irrigation. The annual imbalance shows good closure of the water budget (< 10% in most fields). The imbalance suggests the water demands for the fallow fields and the seasonal wetland are augmented by subsurface waters or that irrigation measurements are biased low for these fields' managements using the methodologies implemented in this study.

Field ID		F20		F66		R31		R64		W32		W65		SW		PW	
INs	irrigation	60	59%	62	60%	131	76%	178	81%	139	77%	119	75%	132	77%	169	81%
	precipitation	41	41%	41	40%	41	24%	41	19%	41	23%	39	25%	41	23%	40	19%
OUTs	surface outflow	-55	31%	-55	31%	-62	32%	-88	41%	-64	33%	-55	30%	-30	13%	-26	13%
	evaporation	-36	20%	-26	15%	-57	29%	-56	26%	-70	35%	-66	36%	-109	47%	-115	57%
	transpiration	-87	49%	-97	54%	-77	39%	-72	33%	-63	32%	-63	34%	-95	41%	-61	30%
surface storage		0	0%	0	0%	0	0%	0	0%	0	0%	0	0%	0	0%	0	0%
annual imbalance		-78	28%	-75	27%	-23	6%	3	1%	-17	5%	-27	8%	-62	15%	8	2%

Table 5.1. Description of water-quality parameters, Yolo Bypass Wildlife Area mercury study

[ng L⁻¹, nanogram per liter; %, percent; mg L⁻¹, milligram per liter; µg L⁻¹, microgram per liter; nm, nanometer; cm, centimeter]

Parameter Notation	Units	Parameter Name
<u>Water-quality mercury parameters</u>		
u-THg	ng L ⁻¹	total mercury in unfiltered water
f-THg	ng L ⁻¹	total mercury in filtered water
u-MeHg	ng L ⁻¹	methylmercury in unfiltered water
f-MeHg	ng L ⁻¹	methylmercury in filtered water
% u-Me/T	%	percent of total mercury in unfiltered water as methylmercury
% f-Me/T	%	percent of total mercury in filtered water as methylmercury
<u>Water-quality non-mercury parameters</u>		
DOC	mg L ⁻¹	dissolved organic carbon concentration
SUVA	absorbance/(mg L ⁻¹ *100)	specific ultraviolet absorbance at 254 nm
ChlA+Pheophytin	µg L ⁻¹	chlorophyll-a plus pheophytin-a
SPM	mg L ⁻¹	suspended particulate matter
SO ₄	mg L ⁻¹	sulfate in filtered water
Fe	µg L ⁻¹	iron in filtered water
SC	microsiemens cm ⁻¹	specific conductance in unfiltered water
Cl	mg L ⁻¹	chloride in filtered water

Table 5.2. Statistical comparison of selected water-quality parameters for agricultural versus non-agricultural fields

[Analysis includes center field samples for interdisciplinary sampling dates only. The mean, standard error (SE, given in parentheses) and the number of observations (N) are shown, along with all results from all mercury water-quality parameters and selected non-mercury parameters. Significant differences ($p < 0.05$) using the Mann-Whitney test between agricultural and non-agricultural fields are indicated as '****' and non-significant differences are indicated as 'NS'. p-values < 0.10 are indicated in **bold**. See **Table 5.1** for explanations of parameter notation and units]

Parameter	Agricultural Fields		Non-Agricultural Fields			Significance	p-value
	Mean \pm SE	N	Mean \pm	SE	N		
Water-quality mercury parameters							
u-MeHg	2.7 (0.4)	28	1.2 (0.6)		8	****	0.012
f-MeHg	1.3 (0.3)	27	0.6 (0.3)		8	NS	0.135
u-THg	26 (4)	28	7.8 (1.2)		6	****	0.0008
f-THg	7.1 (1.0)	28	1.9 (0.4)		8	****	0.0001
% u-Me/T	16 (4)	27	16 (6)		8	NS	0.666
% f-Me/T	23 (5)	27	24 (5)		8	NS	0.316
dissolved organic carbon concentration							
Water-quality non-mercury parameters							
DOC	15 (1)	28	9.7 (0.9)		8	****	0.011
SUVA	2.2 (0.1)	28	2.4 (0.1)		8	NS	0.171
ChlA+Pheophytin	28 (5)	8	22 (7)		3	NS	0.812
SPM	40 (8)	25	41 (15)		7	NS	0.715
SO ₄	85 (12)	28	49 (8)		8	NS	0.102
Fe	51 (23)	28	92 (43)		8	NS	0.216
SC	990 (73)	28	722 (82)		8	****	0.046
Cl	96 (10)	28	56 (8)		8	NS	0.060

Table 5.3. Statistical comparison of selected water-quality parameters for northern versus southern agricultural fields

[Analysis includes center field samples for interdisciplinary sampling dates only. The mean, standard error (SE, given in parentheses) and the number of observations (N) are shown, along with all results from all mercury water-quality parameters and selected non-mercury parameters. Significant differences ($p < 0.05$) using the Mann-Whitney test between northern and southern agricultural fields are indicated as '****' and non-significant differences are indicated as 'NS'. p-values < 0.10 are indicated in **bold**. See **Table 5.1** for explanations of parameter notation and units]

Parameter	Northern Block Fields		Southern Block Fields		Significance	p-value
	Mean \pm SE	N	Mean \pm SE	N		
<u>Water-quality mercury parameters</u>						
u-MeHg	3.1 (0.5)	14	2.3 (0.7)	14	NS	0.073
f-MeHg	1.4 (0.4)	14	1.1 (0.5)	13	NS	0.627
u-THg	30 (6)	14	23 (4)	14	NS	0.370
f-THg	7.2 (1.4)	14	7.0 (1.3)	14	NS	0.765
% u-Me/T	20 (6)	14	11 (3)	13	NS	0.409
% f-Me/T	28 (7)	14	18 (6)	13	NS	0.716
<u>Water-quality non-mercury</u> dissolved organic carbon concentration						
DOC	16 (2)	14	14 (1)	14	NS	0.395
SUVA	2.2 (0.1)	14	2.2 (0.1)	14	NS	0.730
ChlA+Pheophytin	36 (9)	10	19 (3)	10	NS	0.184
SPM	49 (13)	12	32 (9)	13	NS	0.183
SO ₄	100 (23)	14	70 (9)	14	NS	0.581
Fe	77 (46)	14	26 (7)	14	NS	0.346
SC	1081 (103)	14	898 (99)	14	NS	0.260
Cl	107 (16)	14	85 (12)	14	NS	0.370

Table 5.4. Statistical comparison of selected water-quality parameters from agricultural fields during growing season versus post-harvest season

[Analysis includes center field samples from agricultural fields for interdisciplinary sampling dates only. The mean, standard error (SE, given in parentheses) and the number of observations (N) are shown, along with all results from all mercury water-quality parameters and selected non-mercury parameters. Significant differences ($p < 0.05$) using the Mann-Whitney test between growing season (June through August, 2007) and post-harvest season (December 2007 through February 2008) are indicated as '****' and non-significant differences are indicated as 'NS'. p-values < 0.10 are indicated in **bold**. See **Table 5.1** for explanations of parameter notation and units]

Parameter	Growing Season		Post-Harvest Season		Significance	p-value
	Mean \pm SE	N	Mean \pm SE	N		
Water-quality mercury parameters						
u-MeHg	2.8 (0.47)	16	2.5 (0.7)	12	NS	0.430
f-MeHg	0.9 (0.3)	15	1.7 (0.6)	12	NS	0.143
u-THg	27 (5)	16	25 (5)	12	NS	0.908
f-THg	8.1 (1.6)	16	5.7 (0.5)	12	NS	0.799
% u-Me/T	18 (6)	15	12 (3)	12	NS	0.922
% f-Me/T	21 (7)	15	25 (7)	12	NS	0.213
Water-quality non-mercur dissolved organic carbon concentration						
DOC	16 (1)	16	13 (2)	12	NS	0.109
SUVA	2.0 (0.1)	16	2.5 (0.1)	12	****	0.0032
ChlA+Pheo	24 (4)	14	36 (14)	6	NS	0.321
SPM	31 (10)	13	49 (12)	12	NS	0.092
SO ₄	96 (11)	16	70 (25)	12	****	0.027
Fe	25 (7)	16	86 (53)	12	NS	0.120
SC	1177 (62)	16	740 (115)	12	****	0.0032
Cl	122 (11)	16	62 (14)	12	****	0.0017

Table 5.5. Statistical comparison of selected water-quality parameters for inlet, center and outlet sampling sites on agricultural fields

[The mean, standard error (SE, given in parentheses) and the number of observations (N) are shown, along with all results from all mercury water-quality parameters and selected non-mercury parameters. Significant differences ($p < 0.05$) using the Mann-Whitney test between inlet (I), center (C), and outlet (O) sampling sites on agricultural fields are indicated as '****' and non-significant differences are indicated as 'NS'; p-values < 0.10 are indicated in bold. See **Table 5.1** for explanations of parameter notation and units]

Parameter	Inlet		Center		Outlet		Significance			p-value		
	Mean	SE N	Mean	SE N	Mean	SE N	I vs. C	I vs. O	C vs. O	I vs.. C	I vs. O	C vs. O
Water-quality mercury parameters												
u-MeHg	1.0	(0.2) 23	2.7	(0.4) 28	2.8	(0.6) 29	****	****	NS	0.0002	0.0022	0.539
f-MeHg	0.49	(0.12) 23	1.3	(0.3) 27	1.2	(0.3) 29	****	****	NS	0.0068	0.0096	0.928
u-THg	14	(2) 23	26	(4) 28	31	(5) 29	****	****	NS	0.011	0.0466	0.898
f-THg	2.1	(0.2) 23	7.1	(1.0) 28	9.1	(1.5) 29	****	****	NS	0.0000	0.0000	0.930
% u-Me/T	8.7	(2.2) 23	16	(4) 27	14	(3) 29	NS	NS	NS	0.098	0.173	0.825
% f-Me/T	19	(3) 23	23	(5) 27	20	(4) 29	NS	NS	NS	0.527	0.549	0.670
Water-quality non-merc dissolved organic carbon concentration												
DOC	9.5	(0.4) 23	15	(1) 28	16	(1) 29	****	****	NS	0.0001	0.0001	0.429
SUVA	2.4	(0.00) 23	2.2	(0.1) 28	2.1	(0.1) 29	****	****	NS	0.0019	0.0008	0.962
ChIA+Pheo	47	(5) 18	28	(5) 20	27	(5) 21	****	****	NS	0.0014	0.0053	0.754
SPM	62	(9) 20	40	(8) 25	47	(12) 27	****	****	NS	0.018	0.023	0.927
SO ₄	62	(5) 23	85	(12) 28	92	(13) 29	NS	NS	NS	0.229	0.107	0.702
Fe	32	(7) 22	51	(23) 28	29	(4) 29	NS	NS	NS	0.646	0.849	0.731
SC	831	(39) 23	990	(73) 28	1124	(89) 29	****	****	NS	0.033	0.0033	0.334
Cl	70	(5) 23	96	(10) 28	107	(11) 29	NS	****	NS	0.074	0.0056	0.350

Table 5.6. Non-evaporative (chloride-normalized) changes in concentrations of selected mercury species along flow paths in agricultural and non-agricultural fields during summer and winter sampling periods

[Values represent seasonal averages of ratio of outlet to inlet concentrations of mercury species normalized to aqueous chloride, except as noted. u-MeHg, unfiltered methylmercury; u-THg, unfiltered total mercury; Harvest period for wild rice fields (W32 and W65) not included because harvest activities greatly increased unfiltered methylmercury and total-mercury concentrations at outlet, affecting comparison of outlet to inlet. Fallow fields (F20 and F66) were not completely flooded during July 2007 so water-quality at field centers (rather than outlets) were compared with inlets. At permanent wetland, flow was typically in or out but not both simultaneously; comparisons of outlet to center were used in late July and early August 2007 and comparisons of center to inlet were used in early July and late August, 2007. The seasonal wetland was not flooded during summer 2007.]

field	unit	u-MeHg		u-THg	
		summer	winter	summer	winter
F20	N	0.7	0.5	2.9	2.4
R31	N	0.6	2.8	0.8	0.8
W32	N	1.4	2.8	1.0	1.6
F66	S	5.0	0.4	0.6	0.3
R64	S	5.8	8.3	1.1	1.5
W65	S	2.0	1.3	1.4	1.0
PW	S	1.0	1.0	1.6	1.0
SW	S	NA	8.3	NA	0.6

Table 5.7. Methylmercury loads during the summer irrigation period for agricultural and non-agricultural fields

[Values represent methylmercury loads in units of nanograms per square meter (ng m^{-2}) for the summer irrigation season, which varied in duration among fields, as indicated. Surface imbalance is a comparison of irrigation supply and outlet flows. Precipitation inputs are assumed to be negligible. The net imbalance is the sum of all components (inputs and outputs). Positive values are onto the fields, so a positive imbalance indicates a net loss of MeHg across the field. (Refer to **Table 4.3** for water balance information). 'Days in season' represents the number of days each field was inundated during the summer irrigation period.]

	field ID	F20	F66	R31	R64	W32	W65	SW	PW
	unit/block	North	South	North	South	North	South	South	South
	days in season	67	67	136	121	122	131	0	153
Inflows	irrigation	1429	122	748	377	1312	398	0	360
	precipitation	0	0	0	0	0	0	0	0
Outflows	surface outflow	-124	-331	-237	-642	-1188	-534	0	-50
	transpiration	-660	-640	-1675	-995	-950	-1071	0	-200
S	storage	0	0	0	0	159	80	0	0
	Surface imbalance	1305	-209	511	-265	124	-136	0	310
	Net imbalance	645	-849	-1164	-1259	-985	-1287	0	110

Table 5.8. Methylmercury loads for agricultural and non-agricultural fields during the winter, excluding the 17-day winter flood period

[Values reflect methylmercury loads in units of nanograms per square meter (ng m^{-2}) for the winter, excluding the 17-day winter flood period. Surface imbalance is the comparison of the irrigation supply and outlet flows. Precipitation inputs are assumed to be negligible. The total imbalance is the sum of all Inflows and Outflows. Positive values are onto the fields, and a positive imbalance indicates a net loss of MeHg across the field. See **Section 4** for detailed information on flows and dates included in the season definition. 'Days in season' represents the number of days each field was inundated during winter, excluding the 17-day flood period.]

	field ID	F20	F66	R31	R64	W32	W65	SW	PW
	unit/block	North	South	North	South	North	South	South	South
	days in season	119	77	87	87	77	84	195	195
Inflows	irrigation	207	97	243	213	348	105	529	247
	precipitation	0	0	0	0	0	0	0	0
Outflows	surface outflow	-696	-1167	-1641	-2910	-509	-680	-990	-74
	transpiration	0	0	0	0	0	0	-825	-91
S	storage	0	0	0	0	0	0	0	0
	Surface imbalance	-490	-1070	-1398	-2697	-161	-575	-461	173
	Net imbalance	-490	-1070	-1398	-2697	-161	-575	-1286	82

Table 5.9. Comparison of annual average MeHg loads from Yolo Bypass Wildlife Area loads with other systems

[$\mu\text{g}/\text{ha}/\text{day}$, microgram per hectare per day. Negative values are inputs to the system; positive values are exports from the system to the surrounding environment]

Wetland type	Location	MeHg load ($\mu\text{g}/\text{ha}/\text{day}$)	Source
Mixed managed wetlands	Yolo Bypass, California	-22 to +81	This study
Subsided island drainage	Sacramento – San Joaquin Delta, California	-4 to +6	Heim et al., 2009
Natural tidal marsh	Browns Island, California	+44 to +71	Fleck et al., 2008
Impounded marsh	Twitchell Island, California	+14 to +145	Sassone et al., 2008; Heim et al., 2009
Northern peatlands	Minnesota, Canada, Sweden	+2 to +15	Lee et al. 1995; Jeremiason et al., 2006; St Louis et al., 1994
Upland forest	Wisconsin, New York, Canada	+0.2 to +4.5	Krabbenhoft et al., 1995; St Louis et al., 1995; Driscoll et al., 1998
Duck Ponds	Grizzly Island, California	+5.2	Stephenson et al., 2008b

Table 5.10. Summary of methylmercury loads for summer irrigation season

[Values represent methylmercury loads in units of nanograms per square meter (ng m⁻²). NC, not calculated]

	Field ID		F20	F66	R31	R64	W32	W65	SW	PW
	unit/block	Arrow	North	South	North	South	North	South	South	South
	days in season	in Fig. 5.36	67	67	136	121	122	131	0	153
Inflows	irrigation	Lir	1429	122	748	377	1312	398	0	360
	leaching	Llc	NC							
	soil diffusion	Ld	NC							
	Precipitation / atmospheric deposition	Lad	0	0	0	0	0	0	0	0
Outflows	surface drainage	Lout	-124	-331	-237	-642	-1188	-534	0	-50
	plant biomass	Lpb	NC	NC	NC	NC	NC	NC	NA	NA
	particle settling	Lst	NC							
	photodemethylation	Lph	-268	-161	-408	-194	-683	-419	NC	-107
	transpiration and percolation	dissolved org	-660	-640	-1675	-995	-950	-1071	0	-200
	storage		0	0	0	0	159	80	0	0
	surface imbalance		1305	-209	511	-265	124	-136	0	310
	total imbalance		377	-1010	-1572	-1453	-1668	-1706	0	3

Table 6.1. Description of sediment and pore-water parameters, Yolo Bypass Wildlife Area mercury study

[Unit definitions: dry wt., dry weight; ng g⁻¹, nanogram per gram; d⁻¹, per day; %, percentage; pg g⁻¹ d⁻¹, picogram per gram per day; nmol g⁻¹ d⁻¹, nanomole per gram per day; g cm⁻³, gram per cubic centimeter; wet sed., wet sediment; mL cm⁻³, milliliters per cubic centimeter; μmol g⁻¹, micromole per gram; mg g⁻¹, milligram per gram; mV, millivolt; °C, degrees centigrade; ‰, permil = parts per thousand; mmol L⁻¹, millimole per liter; mg L⁻¹, milligram per liter; μmol L⁻¹, micromole per liter]

Parameter	Notation	Units	Parameter Name
<u>Sediment mercury parameters</u>			
THg		ng g ⁻¹ (dry wt.)	total mercury
k _{meth}		d ⁻¹	MeHg production potential rate constant
Hg(II) _R		ng g ⁻¹ (dry wt.)	inorganic reactive mercury
%Hg(II) _R		%	percent THg as inorganic reactive mercury
MPP		pg g ⁻¹ d ⁻¹ (dry wt.)	MeHg production potential rate (calculated)
MeHg		ng g ⁻¹ (dry wt.)	methylmercury
% MeHg		%	percent THg as methylmercury
<u>Sediment non-mercury parameters</u>			
k _{SR}		d ⁻¹	microbial sulfate reduction rate constant
SR		nmol g ⁻¹ d ⁻¹ (dry wt.)	microbial sulfate reduction rate
%dry wt.		%	percent dry weight
LOI		%	weight loss on ignition
BD		g cm ⁻³ (wet sed.)	bulk density
POR		mL cm ⁻³ (wet sed.)	porosity
AVS		μmol g ⁻¹ (dry wt.)	acid volatile sulfur
TRS		μmol g ⁻¹ (dry wt.)	total reduced sulfur
Fe(II)		mg g ⁻¹ (dry wt.)	acid extractable ferrous iron [Fe(II)]
aFe(III)		mg g ⁻¹ (dry wt.)	amorphous (poorly crystalline) ferric Iron [Fe(III)]
cFe(III)		mg g ⁻¹ (dry wt.)	crystalline ferric Iron [Fe(III)]
Fe _T		mg g ⁻¹ (dry wt.)	total (measured) iron = Fe(II) + aFe(III) + cFe(III)
%Fe(II)/Fe _T		%	percentage of total iron as ferrous iron
GS		%	percent grain size < 63 micron)
E _h laboratory		mV	oxidation-reduction potential: laboratory measurement
E _h field		mV	oxidation-reduction potential: field measurement
pH		pH Units	pH
TEMP		°C	temperature (field)
<u>Pore-water non-mercury parameters</u>			
pw[δ ³⁴ SO ₄ ²⁻]		‰, V-CDT	ratio of ³⁴ S to ³² S in aqueous sulfate relative to the Vienna - Canyon Diablo Troilite (V-CDT) standard
pw[SO ₄ ²⁻]		mmol L ⁻¹	sulfate
pw[Cl ⁻]		mmol L ⁻¹	chloride
pw[SO ₄ /Cl]		(unitless)	sulfate:chloride concentration ratio
pw[Fe(II)]		mg L ⁻¹	ferrous Iron [Fe(II)]
pw[DOC]		mg L ⁻¹	dissolved organic carbon
pw[H ₂ S]		μmol L ⁻¹	sulfide
pw[ALK]		mg L ⁻¹ as HCO ₃ ⁻	bicarbonate alkalinity
pw[Ac]		μmol L ⁻¹	acetate

Table 6.2. Summary statistics for sediment and pore water parameters for individual agricultural fields and non-agricultural wetlands

[First Row = Mean ± (standard error), second row = median and {N}, where N = number of observations. Parameter notation definitions and units are given in **Table 6.1.**]

Parameter	Agricultural fallow field:F20	Agricultural fallow field:F66	Agricultural white rice field:R31	Agricultural white rice field:R64	Agricultural wild rice field:W32	Agricultural wild rice field:W65	Permanent Wetland open water field:PW2	Permanent Wetland open water field:PW5-ow	Permanent Wetland cattail field:PW5-cat	Permanent Wetland tule field:PW5-tule	Seasonal wetland mixed veg. field:SW
TEMP (field)	16.8 (2.5)	17.1 (3.3)	20.3 (2.2)	16.9 (3.5)	21.2 (3.6)	19.9 (3.6)	9.8 (1.8)	18.4 (3.0)	16.9 (3.9)	17.0 (4.4)	12.8 (2.3)
TEMP (field)	17.6 {4}	17.2 {4}	21.0 {5}	13.0 {5}	19.0 {5}	22.0 {5}	9.8 {2}	22.0 {5}	17.7 {4}	16.9 {4}	12.4 {3}
THg	296 (13)	276 (19)	362 (26)	373 (17)	290 (19)	354 (19)	124 (10)	135 (7)	147 (16)	132 (10)	161 (8)
THg	290 {4}	279 {4}	382 {5}	362 {5}	301 {5}	355 {5}	124 {2}	139 {5}	147 {4}	133 {4}	163 {3}
k _{meth}	0.012 (0.007)	0.061 (0.034)	0.090 (0.048)	0.055 (0.034)	0.037 (0.026)	0.077 (0.032)	0.031 (0.020)	0.199 (0.064)	0.634 (0.253)	0.330 (0.102)	0.061 (0.013)
k _{meth}	0.007 {4}	0.057 {4}	0.046 {5}	0.003 {5}	0.012 {5}	0.070 {5}	0.031 {2}	0.141 {5}	0.518 {4}	0.300 {4}	0.073 {3}
Hg(II) _R	5.13 (2.18)	6.31 (2.83)	2.65 (1.39)	4.84 (1.96)	4.24 (1.55)	4.56 (2.09)	0.27 (0.13)	0.27 (0.07)	0.26 (0.04)	0.17 (0.03)	0.16 (0.02)
Hg(II) _R	4.23 {4}	6.36 {4}	1.08 {5}	4.43 {5}	3.93 {5}	4.13 {5}	0.27 {2}	0.24 {5}	0.21 {4}	0.16 {4}	0.14 {3}
%Hg(II) _R	1.72 (0.72)	2.13 (0.89)	0.68 (0.34)	1.33 (0.53)	1.40 (0.48)	1.31 (0.62)	0.21 (0.09)	0.20 (0.04)	0.17 (0.02)	0.12 (0.02)	0.10 (0.01)
%Hg(II) _R	1.43 {4}	2.12 {4}	0.28 {5}	1.35 {5}	1.30 {5}	1.17 {5}	0.21 {2}	0.18 {5}	0.17 {4}	0.13 {4}	0.09 {3}
MPP	38.5 (17.9)	101.0 (44.2)	47.3 (17.3)	125.0 (87.6)	40.1 (17.7)	142.7 (88.7)	5.4 (1.2)	42.2 (13.5)	110.0 (34.2)	38.6 (4.1)	7.3 (1.4)
MPP	30.1 {4}	89.4 {4}	47.4 {5}	6.9 {5}	41.7 {5}	88.7 {5}	5.4 {2}	29.2 {5}	119.8 {4}	39.3 {4}	7.5 {3}
MeHg	2.55 (0.38)	2.31 (0.57)	2.60 (0.79)	3.00 (0.57)	2.68 (0.90)	2.84 (0.53)	0.65 (0.12)	1.27 (0.16)	2.53 (0.50)	1.80 (0.25)	2.03 (0.34)
MeHg	2.64 {4}	2.54 {4}	1.98 {5}	2.43 {5}	2.16 {5}	2.99 {5}	0.65 {2}	1.14 {5}	2.41 {4}	1.58 {4}	1.99 {3}
%MeHg	0.87 (0.12)	0.82 (0.17)	0.82 (0.35)	0.83 (0.18)	1.05 (0.46)	0.80 (0.13)	0.53 (0.14)	0.94 (0.10)	1.77 (0.36)	1.39 (0.21)	1.26 (0.18)
%MeHg	0.97 {4}	0.96 {4}	0.53 {5}	0.65 {5}	0.69 {5}	0.89 {5}	0.53 {2}	0.89 {5}	1.80 {4}	1.28 {4}	1.36 {3}
SR	6.9 (2.8)	48.8 (41.9)	31.2 (9.7)	12.6 (7.2)	303.4 (290.9)	45.7 (18.5)	9.7 (6.1)	98.0 (51.5)	14.4 (3.9)	71.3 (26.5)	11.9 (4.7)
SR	6.9 {4}	10.2 {4}	25.5 {5}	9.4 {5}	18.6 {4}	25.8 {5}	9.7 {2}	37.8 {5}	12.5 {4}	69.4 {4}	16.5 {3}
AVS	0.71 (0.24)	1.78 (1.04)	3.62 (2.10)	1.53 (0.92)	2.16 (0.98)	5.21 (2.06)	1.58 (0.86)	10.29 (2.44)	51.16 (13.80)	30.98 (13.23)	10.11 (1.49)
AVS	0.51 {4}	1.14 {4}	0.82 {5}	0.42 {5}	1.28 {5}	5.32 {5}	1.58 {2}	9.00 {5}	53.85 {4}	29.75 {4}	9.73 {3}

Parameter	Agricultural fallow field:F20	Agricultural fallow field:F66	Agricultural white rice field:R31	Agricultural white rice field:R64	Agricultural wild rice field:W32	Agricultural wild rice field:W65	Permanent Wetland open water field:PW2	Permanent Wetland open water field:PW5-ow	Permanent Wetland cattail field:PW5-cat	Permanent Wetland tule field:PW5-tule	Seasonal wetland mixed veg. field:SW
TRS	2.18 (0.66)	3.45 (1.73)	6.74 (3.33)	2.86 (1.18)	3.34 (1.52)	5.34 (2.28)	4.59 (1.09)	16.82 (4.13)	83.59 (18.76)	36.11 (8.84)	19.58 (1.68)
TRS	1.81 {4}	2.13 {4}	5.13 {5}	1.21 {5}	2.55 {5}	4.80 {5}	4.59 {2}	14.95 {5}	93.39 {4}	39.23 {4}	19.66 {3}
Fe(II)	4.05 (0.76)	4.17 (1.36)	5.34 (1.02)	3.30 (1.12)	4.08 (0.84)	5.03 (1.40)	4.07 (1.62)	6.36 (0.49)	7.16 (0.97)	7.33 (0.57)	7.53 (0.11)
Fe(II)	3.77 {4}	4.04 {4}	6.55 {5}	2.36 {5}	3.94 {5}	5.25 {5}	4.07 {2}	6.39 {5}	6.85 {4}	7.55 {4}	7.47 {3}
aFe(III)	0.55 (0.09)	0.61 (0.16)	0.55 (0.16)	0.65 (0.11)	0.59 (0.10)	0.35 (0.11)	0.28 (0.15)	0.03 (0.01)	0.05 (0.00)	0.09 (0.04)	0.01 (0.00)
aFe(III)	0.52 {4}	0.66 {4}	0.49 {5}	0.50 {5}	0.72 {5}	0.33 {5}	0.28 {2}	0.03 {5}	0.05 {4}	0.07 {4}	0.00 {3}
cFe(III)	11.71 (1.26)	12.00 (1.97)	11.53 (0.99)	14.69 (0.94)	13.26 (1.48)	12.34 (2.24)	9.08 (2.40)	5.85 (0.84)	3.97 (0.15)	8.53 (2.73)	5.92 (1.26)
cFe(III)	12.07 {4}	11.34 {4}	10.90 {5}	15.75 {5}	14.30 {5}	13.36 {5}	9.08 {2}	4.87 {5}	4.06 {4}	5.89 {4}	6.09 {3}
%Fe(II)/Fe _T	25.39 (5.66)	25.64 (8.50)	30.76 (5.90)	17.51 (5.86)	23.52 (5.71)	30.38 (9.63)	31.31 (14.21)	52.58 (5.26)	63.24 (3.65)	49.25 (7.83)	56.94 (5.81)
%Fe(II)/Fe _T	22.88 {4}	25.22 {4}	38.65 {5}	12.29 {5}	21.11 {5}	27.26 {5}	31.31 {2}	59.40 {5}	61.84 {4}	55.88 {4}	55.08 {3}
E _h laboratory	38 (43)	49 (72)	32 (57)	69 (48)	57 (65)	36 (40)	89 (46)	-20 (25)	-68 (39)	-44 (42)	-27 (37)
E _h laboratory	50 {4}	18 {4}	5 {5}	57 {5}	102 {5}	1 {5}	89 {2}	6 {5}	-65 {4}	-50 {4}	-3 {3}
E _h field	128 (10)	142 (82)	97 (38)	209 (48)	115 (46)	127 (35)	186 (73)	40 (24)	0 (23)	20 (42)	17 (12)
E _h field	131 {4}	123 {4}	69 {5}	195 {5}	76 {5}	149 {5}	186 {2}	47 {5}	9 {4}	28 {4}	12 {3}
pH	7.03 (0.10)	6.82 (0.05)	6.92 (0.09)	6.86 (0.04)	7.10 (0.07)	6.95 (0.07)	7.31 (0.15)	7.03 (0.08)	6.91 (0.10)	6.94 (0.05)	6.77 (0.16)
pH	6.96 {4}	6.83 {4}	6.88 {5}	6.84 {5}	7.05 {5}	6.96 {5}	7.31 {2}	7.06 {5}	7.00 {4}	6.91 {4}	6.79 {3}
GS	76.9 (7.4)	81.8 (6.0)	81.7 (5.3)	76.3 (7.4)	77.3 (2.5)	79.9 (4.0)	65.2 (8.4)	62.4 (6.9)	68.6 (6.8)	51.4 (6.5)	81.7 (2.7)
GS	77.9 {4}	83.5 {4}	81.6 {5}	72.1 {5}	77.6 {5}	78.9 {5}	65.2 {2}	54.2 {5}	63.1 {4}	51.9 {4}	80.1 {3}
%dry wt.	59.3 (1.0)	63.6 (1.7)	56.8 (2.6)	57.5 (1.5)	59.4 (0.3)	56.3 (1.2)	62.4 (0.9)	49.1 (2.3)	31.9 (2.1)	48.8 (4.8)	56.4 (1.7)
%dry wt.	59.3 {4}	65.0 {4}	59.1 {5}	57.6 {5}	59.4 {5}	56.9 {5}	62.4 {2}	46.1 {5}	30.6 {4}	48.9 {4}	55.0 {3}
LOI	6.66 (0.34)	6.80 (0.45)	6.85 (0.38)	7.31 (0.29)	6.55 (0.20)	7.01 (0.29)	4.44 (0.27)	6.71 (0.24)	10.22 (0.29)	8.60 (0.74)	8.94 (0.40)
LOI	6.55 {4}	6.72 {4}	6.76 {5}	7.27 {5}	6.64 {5}	6.91 {5}	4.44 {2}	6.87 {5}	10.14 {4}	8.23 {4}	8.83 {3}

Parameter	Agricultural fallow field:F20	Agricultural fallow field:F66	Agricultural white rice field:R31	Agricultural white rice field:R64	Agricultural wild rice field:W32	Agricultural wild rice field:W65	Permanent Wetland open water field:PW2	Permanent Wetland open water field:PW5-ow	Permanent Wetland cattail field:PW5-cat	Permanent Wetland tulle field:PW5-tule	Seasonal wetland mixed veg. field:SW
BD	1.51 (0.02)	1.53 (0.02)	1.47 (0.05)	1.46 (0.03)	1.52 (0.01)	1.46 (0.04)	1.61 (0.08)	1.40 (0.04)	1.19 (0.02)	1.39 (0.05)	1.42 (0.02)
BD	1.52 {4}	1.52 {4}	1.51 {5}	1.44 {5}	1.52 {5}	1.47 {5}	1.61 {2}	1.41 {5}	1.18 {4}	1.37 {4}	1.43 {3}
POR	0.61 (0.02)	0.56 (0.03)	0.63 (0.02)	0.62 (0.02)	0.62 (0.01)	0.64 (0.00)	0.60 (0.02)	0.71 (0.02)	0.81 (0.01)	0.71 (0.04)	0.62 (0.02)
POR	0.61 {4}	0.54 {4}	0.63 {5}	0.62 {5}	0.62 {5}	0.64 {5}	0.60 {2}	0.70 {5}	0.82 {4}	0.70 {4}	0.63 {3}
pw[Cl ⁻]	2.59 (0.68)	2.76 (0.68)	3.79 (0.82)	3.17 (0.52)	4.66 (1.44)	5.68 (1.99)	1.80 (0.46)	2.46 (0.51)	2.01 (0.38)	1.95 (0.34)	1.32 (0.18)
pw[Cl ⁻]	2.76 {4}	2.89 {4}	4.40 {5}	3.72 {5}	3.99 {5}	4.21 {5}	1.80 {2}	2.56 {5}	2.08 {4}	2.07 {4}	1.35 {3}
pw[SO ₄ ²⁻]	0.52 (0.19)	0.92 (0.40)	1.09 (0.36)	1.10 (0.46)	1.49 (0.74)	1.48 (0.56)	0.50 (0.12)	0.43 (0.10)	0.01 (0.00)	0.10 (0.04)	0.00 (0.00)
pw[SO ₄ ²⁻]	0.52 {4}	0.81 {4}	1.19 {5}	0.71 {5}	0.99 {5}	1.35 {5}	0.50 {2}	0.34 {5}	0.01 {4}	0.10 {4}	0.00 {3}
pw[SO ₄ ²⁻ /Cl ⁻]	0.21 (0.05)	0.38 (0.15)	0.24 (0.07)	0.30 (0.11)	0.30 (0.06)	0.24 (0.06)	0.28 (0.00)	0.19 (0.04)	0.004 (0.001)	0.05 (0.02)	0.003 (0.001)
pw[SO ₄ ²⁻ /Cl ⁻]	0.23 {4}	0.34 {4}	0.27 {5}	0.25 {5}	0.32 {5}	0.25 {5}	0.28 {2}	0.19 {5}	0.004 {4}	0.06 {4}	0.003 {3}
pw[H ₂ S]	0.49 (0.13)	0.56 (0.21)	0.76 (0.22)	2.27 (1.34)	0.43 (0.15)	0.91 (0.22)	0.22 (0.07)	0.45 (0.07)	0.93 (0.27)	0.89 (0.21)	1.54 (0.19)
pw[H ₂ S]	0.49 {4}	0.43 {4}	0.85 {5}	1.35 {5}	0.25 {5}	1.08 {5}	0.22 {2}	0.49 {5}	1.04 {4}	0.78 {4}	1.62 {3}
pw[Fe(II)]	0.10 (0.04)	0.20 (0.08)	0.62 (0.50)	0.85 (0.69)	0.20 (0.13)	0.55 (0.29)	0.06 (0.02)	0.24 (0.08)	0.68 (0.20)	0.55 (0.08)	8.83 (4.51)
pw[Fe(II)]	0.08 {4}	0.19 {4}	0.13 {5}	0.05 {5}	0.03 {5}	0.10 {5}	0.06 {2}	0.23 {5}	0.73 {4}	0.52 {4}	4.45 {3}
pw[ALK]	526 (71)	518 (81)	696 (92)	652 (97)	573 (40)	725 (196)	375 (78)	460 (46)	458 (60)	467 (61)	391 (57)
pw[ALK]	549 {4}	471 {4}	678 {5}	638 {4}	529 {5}	523 {5}	375 {2}	408 {5}	494 {4}	471 {4}	407 {3}
pw[DOC]	16.7 (4.6)	18.1 (4.6)	24.4 (5.8)	22.8 (4.3)	19.2 (3.8)	26.6 (7.4)	9.8 (0.2)	10.0 (0.7)	13.2 (0.5)	17.8 (6.1)	41.3 (19.2)
pw[DOC]	13.4 {4}	15.5 {4}	22.8 {5}	22.7 {5}	16.5 {5}	22.1 {5}	9.8 {2}	10.7 {5}	13.1 {4}	12.1 {4}	24.5 {3}
pw[Ac]	5.4 (4.4)	166.2 (81.9)	163.7 (123.6)	548.3 (413.4)	83.7 (73.8)	175.8 (145.2)	1.0 (0.0)	1.0 (0.0)	138.0 (46.3)	245.6 (182.2)	347.5 (155.6)
pw[Ac]	1.0 {4}	156.1 {4}	34.5 {5}	79.8 {5}	16.1 {5}	51.8 {5}	1.0 {2}	1.0 {5}	173.0 {4}	96.8 {4}	220.8 {3}

Table 6.3. ANOVA results comparing sediment and pore water data grouped as agricultural versus non-agricultural fields

[Analysis includes all sampling dates and excludes experimental devegetation plots. The mean, standard error (SE), and the number of observations (N) is shown, along with all results from all mercury metric comparisons. Only significant results for non-mercury metrics are shown. Significant differences between groupings ($p < 0.05$) are indicated as '****' and non-significant differences are indicated as 'NS'. Parameter notation definitions and units are given in **Table 6.1.**]

Parameter	Agricultural Fields		Non-Agricultural Fields		Significant
	Mean \pm SE	N	Mean \pm SE	N	
THg	328 (10)	28	140 (5)	18	****
k_{meth}	0.057 (0.013)	28	0.283 (0.077)	18	****
Hg(II) _R	4.54 (0.76)	28	0.22 (0.03)	18	****
%Hg(II) _R	1.39 (0.23)	28	0.16 (0.02)	18	****
MPP	83.3 (23.0)	28	46.6 (11.8)	18	NS
MeHg	2.68 (0.25)	28	1.73 (0.19)	18	****
%MeHg	0.86 (0.11)	28	1.23 (0.13)	18	****
Fe(II)	4.34 (0.43)	28	6.69 (0.38)	18	****
aFe(III)	0.55 (0.05)	28	0.07 (0.02)	18	****
cFe(III)	12.6 (0.6)	28	6.4 (0.8)	18	****
%Fe(II)/Fe _T	25.5 (2.8)	28	52.6 (3.4)	18	****
pw[SO ₄ ²⁻]	1.13 (0.20)	28	0.20 (0.06)	18	****
pw[$\delta^{34}\text{SO}_4^{2-}$]	5.0 (1.7)	24	14.3 (3.4)	6	****
AVS	2.6 (0.6)	28	23.0 (5.8)	18	****
TRS	4.07 (0.82)	28	35.04 (7.92)	18	****
pw[ALK]	621 (45)	27	440 (24)	18	****
%LOI	6.87 (0.13)	28	8.03 (0.47)	18	****
pw[Cl ⁻]	3.85 (0.49)	28	1.98 (0.19)	18	****
E _h Field	136 (19)	28	39 (18)	18	****
E _h Lab	47 (21)	28	-25 (18)	18	****
GS	79 (2)	28	65 (4)	18	****

Table 6.4. ANOVA results comparing northern versus southern agricultural fields

[Analysis includes all sampling dates and excludes experimental devegetation plots. The mean, standard error (SE), and the number of observations (N) is shown, along with all results from all mercury metric comparisons. Only significant results for non-mercury metrics are shown. Significant differences between groupings ($p < 0.05$) are indicated as '****' and non-significant differences are indicated as 'NS'. Parameter notation definitions and units are given in **Table 6.1.**]

Parameter	Northern Block Fields		Southern Block Fields		Significant
	Mean \pm SE	N	Mean \pm SE	N	
THg	318 (15)	14	338 (15)	14	NS
k_{meth}	0.049 (0.020)	14	0.065 (0.018)	14	NS
Hg(II) _R	3.93 (0.93)	14	5.16 (1.21)	14	NS
%Hg(II) _R	1.24 (0.29)	14	1.55 (0.37)	14	NS
MPP	42.2 (9.5)	14	124.4 (43.1)	14	NS
MeHg	2.61 (0.41)	14	2.75 (0.31)	14	NS
%MeHg	0.91 (0.20)	14	0.81 (0.09)	14	NS
pH	7.01 (0.05)	14	6.88 (0.03)	14	****

Table 6.5. ANOVA results comparing growing season versus post-harvest season sediment and pore water data from agricultural fields

[Analysis conducted for growing season (June through August, 2007) and post-harvest season (December 2007 through February 2008) excludes experimental devegetation plots. The mean, standard error (SE), and the number of observations (N) is shown, along with all results from all mercury metric comparisons. Only significant results for non-mercury metrics are shown. Significant differences between groupings ($p < 0.05$) are indicated as '****' and non-significant differences are indicated as 'NS'. Parameter notation definitions and units are given in **Table 6.1.**]

Parameter	growing season		post-harvest season		Significant
	Mean \pm SE	N	Mean \pm SE	N	
THg	332 (14)	16	323 (16)	12	NS
k_{meth}	0.053 (0.015)	16	0.061 (0.025)	12	NS
Hg(II) _R	3.90 (1.02)	16	5.40 (1.15)	12	NS
%Hg(II) _R	1.18 (0.30)	16	1.68 (0.36)	12	NS
MPP	59.5 (15.9)	16	115.1 (49.2)	12	NS
MeHg	1.91 (0.17)	16	3.70 (0.38)	12	****
%MeHg	0.59 (0.05)	16	1.23 (0.19)	12	****
pw[$\delta^{34}\text{SO}_4^{2-}$]	7.78 (1.76)	16	-0.62 (2.78)	8	****
pw[ALK]	706 (64)	16	497 (33)	11	****
pw[Cl ⁻]	4.73 (0.63)	16	2.67 (0.68)	12	****
E_h Lab	3 (27)	16	106 (24)	12	****
GS	73 (2)	16	88 (2)	12	****
pw[DOC]	25.8 (3.1)	16	16.0 (1.7)	12	****

Table 6.6. Linear regression results for longitude versus individual mercury metrics

[The linear regression slope \pm standard error (SE) and Y-intercept (Y-int.) is shown, along with the number of observations (N), the regression R^2 , and the statistical Type II Error probability (p) that the slope is not significantly different from zero. Model regressions were deemed significant (****) or non-significant (NS) based on a criteria of $p < 0.05$. Y_Variable parameter notation definitions and units are given in **Table 6.1.**]

X_Variable	Y_Variable	slope \pm SE	Y-int.	N	R^2	p	Significant
Longitude	THg	-7531 (751)	-915508	57	0.65	< 0.0001	****
Longitude	k_{meth}	9.87 (2.33)	1201	55	0.25	< 0.0001	****
Longitude	Hg(II) _R	-161 (44)	-19627	55	0.20	0.0006	****
Longitude	%Hg(II) _R	-44.0 (13.3)	-5349	55	0.17	0.002	****
Longitude	MPP	-161 (1157)	-19560	55	< 0.001	0.88	NS
Longitude	MeHg	-30.3 (13.7)	-3688	55	0.08	0.031	****
Longitude	%MeHg	17.5 (6.4)	2129	55	0.12	0.009	****

Table 7.1. Field descriptions of dominant plant species, yield, and leaf area during the 2007–2008 study period

[Key characteristics of plant community structure during summer growing season for crops and extant vegetation in each field and during winter in permanent wetland. Field Type designations: Ag, agricultural (rice production); Non-Ag, non-agricultural (managed wetland for wildlife). Root depth measured by in-field live root presence during June and August 2007. Rice yield values provided by the farmer (Jack DeWit). Average and standard deviation (in parentheses) for leaf area was calculated by assessment of leaf area on replicate harvested leaf material (n=3) and stem density (n=3). cm, centimeter; kg ha⁻¹, kilogram per hectare; leaf area is unitless as m² of leaf tissue divided by m² of planar surface cancels the units; na, not applicable; ND; not determined]

Field Code	Field Type	Status during study period	Dominant Plant (Common Name)	Dominant Plant (Genus species)	Maximum root depth (cm)	Rice Yield (kg ha ⁻¹)	Leaf Area (m ² _{leaf} m ⁻² _{planar surface})				
							June 2007	July 2007	August 2007	December 2007	February 2008
R31	Ag	vegetated	white rice	<i>Oryza sativa</i> S-102	24	1272	0	1.5 (0.1)	2.6 (0.1)	3.0 (0.1)	0
R64	Ag	vegetated	white rice	<i>Oryza sativa</i> Akita	20	704	0	1.2 (0.1)	2.5 (0.2)	2.5 (0.2)	0
W32	Ag	vegetated	wild rice	<i>Zizania palustris</i> -Franklin	30	253	0	2.0 (0.3)	2.6 (0.4)	2.7 (0.4)	0
W65	Ag	vegetated	wild rice	<i>Zizania palustris</i> -Franklin	30	226	0	0.6 (0.1)	1.9 (0.2)	1.6 (0.2)	0
F20	Ag	barren	plantain / algal	<i>Alisma</i> spp.	0	na	0	0	0	0	0
F66	Ag	vegetated	sedge	<i>Cyperus difformis</i>	14	na	0	0	0.8 (0.3)	0.8 (0.3)	0
PW5	Non-Ag	vegetated	cattail	<i>Typha dominguensis</i>	>50	na	1.5 (0.5)	1.6 (0.3)	1.8 (0.2)	1.8 (0.2)	0.6 (0.5)
PW5	Non-Ag	vegetated	tule	<i>Schoenolpectus acutus</i>	>50	na	2.0 (0.4)	2.5 (0.4)	2.6 (0.3)	2.6 (0.3)	1.0 (0.4)

Table 7.2. Concentrations of carbon, nitrogen, mercury, and methylmercury and biomass of plant tissue in individual fields

[Data for biomass and concentrations represent peak biomass conditions for all fields. Averages and standard deviations (reported in parentheses) represent a minimum of n=3 field samples. All pools and concentrations for individual tissues are provided on a dry weight basis. Ratios of C:N and MeHg/THg in plant tissues are calculated from average concentrations. No assessment of these parameters were made for vegetation associated with the seasonal wetland site. C, carbon; N, nitrogen; %, percent; THg, total mercury; MeHg, methylmercury; ng g⁻¹, nanogram per gram; g m⁻², gram per square meter; µg m⁻², microgram per

Field Code	Dominant plant type	Plant Biomass (g m ⁻²)	Carbon (%)	Nitrogen (%)	C:N Ratio	THg (ng g ⁻¹)	MeHg (ng g ⁻¹)	MeHg/THg Ratio	Carbon (g m ⁻²)	Nitrogen (g m ⁻²)	THg (µg m ⁻²)	MeHg (µg m ⁻²)
LEAF DATA												
R31	white rice	1139 (27)	36.9 (1.2)	1.8 (0.6)	20	14 (4)	2.6 (0.2)	19%	420 (12)	20.7 (3.7)	16 (2)	3.0 (0.1)
R64	white rice	984 (12)	36.7 (0.8)	1.0 (0.2)	37	15 (9)	1.3 (0.4)	9%	361 (6)	9.8 (1.0)	15 (5)	1.3 (0.2)
W32	wild rice	1027 (10)	40.4 (1.1)	0.4 (0.1)	107	107 (11)	4.4 (0.5)	4%	415 (8)	3.9 (0.5)	110 (6)	4.5 (0.3)
W65	wild rice	942 (30)	38.6 (2.4)	0.5 (0.1)	77	101 (8)	1.7 (0.1)	2%	364 (17)	4.7 (0.5)	95 (5)	1.6 (0.1)
F20	plantain / algae	10 (9)	40.6 (0.1)	2.9 (0.4)	14	37 (4)	3.1 (0.9)	8%	4.1 (1.8)	0.3 (0.2)	0.4 (0.2)	0.03 (0.02)
F66	sedge	330 (34)	34.5 (1.1)	1.7 (0.2)	20	31 (5)	5.6 (0.4)	18%	114 (8)	5.6 (0.6)	10 (1)	1.8 (0.2)
PW5	tule	1404 (50)	41.0 (1.8)	0.7 (0.0)	59	50 (6)	0.5 (0.1)	1%	576 (23)	9.8 (0.2)	70 (5)	0.7 (0.1)
PW5	cattail	1188 (36)	40.3 (2.2)	0.8 (0.1)	50	55 (11)	0.4 (0.1)	1%	479 (18)	9.5 (11)	65 4	0.5 (0.1)
ROOT DATA												
R31	white rice	424 (83)	12.2 (0.2)	0.7 (0.2)	17	273 (25)	3.1 (2.4)	1%	52 (5)	3.0 (0.7)	116 (17)	1.3 (0.6)
R64	white rice	395 (19)	16.7 (0.2)	0.8 (0.1)	21	295 (36)	10 (2.1)	3%	66 (2)	3.2 (0.2)	117 (10)	4.0 (0.5)
W32	wild rice	308 (101)	32.6 (0.8)	0.7 (0.0)	47	279 (22)	12 (1.9)	4%	100 (18)	2.2 (0.4)	86 (17)	3.8 (0.9)
W65	wild rice	107 (12)	28.3 (0.1)	0.5 (0.0)	57	105 (41)	11 (2.5)	10%	30 (2)	0.5 (0.0)	11 (3)	1.2 (0.2)
F20	plantain / algae	1.0 (3.0)	22.4 (0.2)	1.0 (0.0)	22	214 (77)	12 (1.1)	6%	0.2 (0.3)	0.01 (0.02)	0.2 (0.4)	0.01 (0.02)
F66	sedge	74 (27)	27.6 (0.1)	0.9 (0.0)	31	247 (12)	11 (0.4)	4%	20 (4)	0.7 (0.1)	18 (4)	0.8 (0.2)
PW5	tule	563 (88)	36.3 (0.1)	1.4 (0.0)	26	150 (26)	1.2 (0.6)	1%	204 (16)	7.9 (0.6)	84 (14)	0.7 (0.2)
PW5	cattail	143 (49)	38.3 (0.2)	1.2 (0.0)	32	104 (18)	1.9 (0.8)	2%	55 (10)	1.7 (0.3)	15 (4)	0.3 (0.1)
SEED DATA												
R31	white rice	16 (11)	41.5 (0.2)	1.6 (0.1)	26	54 (12)	4.1 (1.1)	8%	6.6 (2.3)	0.3 (0.1)	0.9 (0.4)	0.1 (0.0)
R64	white rice	28 (13)	39.4 (0.1)	1.2 (0.3)	33	46 (6)	4.2 (0.6)	9%	11 (3)	0.3 (0.1)	1.3 (0.4)	0.1 (0.0)
W32	wild rice	12 (6)	44.1 (2.1)	1.6 (0.1)	28	11 (2)	6.6 (1.4)	60%	5.3 (1.4)	0.2 (0.1)	0.1 (0.0)	0.1 (0.0)
W65	wild rice	10 (8)	42.5 (0.1)	2.3 (0.2)	18	16 (12)	5.9 (1.6)	37%	4.3 (1.7)	0.2 (0.1)	0.2 (0.1)	0.1 (0.0)
F20	plantain / algae	0 (0)	ND	ND	ND	ND	ND	ND	ND	ND	ND	ND
F66	sedge	0 (0)	ND	ND	ND	ND	ND	ND	ND	ND	ND	ND
PW5	tule	4 (9)	41.0 (0.1)	1.1 (0.1)	37	150 (26)	1.2 (0.2)	1%	1.6 (1.8)	0.04 (0.05)	0.6 (0.7)	0.005 (0.006)
PW5	cattail	21 (15)	44.2 (0.5)	1.0 (0.1)	44	104 (18)	1 (0.4)	1%	9.3 (3.4)	0.2 (0.1)	2.2 (1.0)	0.02 (0.01)

Table 7.3. Devegetation effect on sediment and pore-water parameters during the period of peak plant biomass, by habitat type

[Values represent the percentage (%) decrease (-) or increase (+) for each parameter listed in devegetated plots compared to vegetated plots, as calculated by: %DevegEffect = $(X_{\text{vegetated plot}} - X_{\text{devegetated plot}}) / X_{\text{vegetated plot}} \times 100$, during August 2007 for agricultural fields (Ag Management) and during December 2007 for non-agricultural fields (Non-Ag Management), where 'X' is the particular parameter of interest. Statistically significant differences between vegetated and devegetated sites for a given sub-habitat parameter (X), as assessed using pairwise t-tests ($p \leq 0.05$) on normalized data. Abbreviations: sed, sediment; pw, sediment porewater; k_{meth} , mercury-methylation rate constant; Hg(II)_{R} , inorganic "reactive" mercury; MP, microbial methylmercury production rate; MeHg, methylmercury; SR, microbial sulfate reduction rate; S^{2-} , sulfide; Fe(II), ferrous iron; aFe(III), amorphous ferric iron; DOC, dissolved organic carbon; TRS, total reduced sulfur; AVS, acid volatile sulfur; Cl, chloride; Root Density, volume of soil occupied by live root material; ns, not significant]

Field Type (dominant vegetation)	Management	sed k_{meth}	sed Hg(II)_{R}	sed MP	sed MeHg	sed %MeHg	sed SR	pw acetate	pw S^{2-}	pw Fe(II)	sed Fe(II)	sed aFe(III)	pw DOC	sed TRS	sed AVS	pw Cl	Root Density
White rice	Ag	-48	ns	-64	-38	-16	ns	-63	ns	ns	+17	-24	-47	ns	ns	-28	-99
Wild rice	Ag	-67	ns	-67	ns	ns	ns	-93	ns	ns	+16	-23	ns	ns	ns	-37	-99
Fallow-mixed (sedge)	Ag	-56	-82	-92	-55	-42	-81	-63	+68	+87	ns	-93	ns	+26	ns	-13	-95
Fallow-barren (plantain / algal)	Ag	-67	+81	ns	-49	-19	-49	-93	-72	-50	ns	+21	ns	-58	ns	ns	ns
Seasonal wetland (swamp timothy)	Non-Ag	-17	ns	ns	-35	-21	ns	-79	ns	+30	ns	ns	ns	ns	ns	ns	-87
Permanent wetland (tule)	Non-Ag	-87	+83	ns	-41	-23	-80	-98	ns	-38	ns	ns	ns	-71	-80	ns	-93
Permanent wetland (cattail)	Non-Ag	ns	+24	ns	-14	ns	ns	-99	-45	-30	ns	ns	ns	-10	-26	ns	-99

Table 7.4. Plant litter decomposition rates and areal pool sizes

[Plant litter on the sediment surface during February 2008 was calculated based on growing season biomass (field measurements), date of litterfall via harvest (rice crop) or senescence (native wetland plants), and the decomposition rate constants (k) at 30 °C determined in the laboratory for each plant species. The temperature-dependent k value was then adjusted for mean monthly in-field air temperature (in °C) as reported by the Calif. Dept. of Fish and Game at El Macero Station, Calif., and was assumed to follow Q₁₀ kinetics (increasing by a factor of 2.4 for every 10 °C change in temperature, as per **Gu et al. (2004)**). Averages and standard deviations (reported in parentheses) represent a minimum of n=3 field samples. %, percentage; °C, degree Celsius; g m⁻², gram per square meter, on a dry weight basis]

Field Code	Plant Species	Decomposition	Litterfall Date (Estimated)	Initial	Surface Litter for
		rate constant (k) at 30 °C % per day		Biomass at Litterfall (g m ⁻²)	February 2008 (g m ⁻²)
R31	<i>Oryza sativa</i>	-4.2 (0.8)	10/1/07	1139	391 (31)
R64	<i>Oryza sativa</i>	-4.7 (1.2)	10/1/07	984	288 (16)
W32	<i>Zizania palustris</i>	-2.3 (1.6)	9/1/07	1027	253 (14)
W65	<i>Zizania palustris</i>	-2.8 (0.8)	9/1/07	942	163 (17)
F66	<i>Cyperus difformis</i>	-7.1 (1.0)	10/1/07	330	18 (2)
PW5	<i>Schoenolpectus acutus</i>	-2.2 (0.5)	12/15/07	1404	952 (72)
PW5	<i>Typha dominguensis</i>	-2.0 (0.8)	12/15/07	1188	836 (109)

Table 8.1. Western mosquitofish whole body total mercury concentration and body burden immediately prior to and after 60 days of caged exposure in agricultural and non-agricultural wetlands within the Yolo Bypass Wildlife Area, California

[Statistical analysis using the two-sample t-test to examine temporal changes in fish total mercury concentrations (whole body) and total mercury body burden, at the time the fish were first caged (Introduction) compared to after 60 days of in-situ exposure, for individual fields and within-field locations (inlets, center and outlet). Non-agricultural wetlands are represented by permanent wetland sites PW-2 and PW-5. Agricultural wetlands are represented by sites R31, R64, W32 and W65. Where: THg, total mercury; $\mu\text{g g}^{-1}\text{ dw}$; microgram per gram fish (whole body) on a dry weight basis; $\mu\text{g fish}^{-1}\text{ dw}$, microgram per fish on a dry weight basis; N, number of observations; SE, standard error of the mean; DF, degrees of freedom; t, t-test statistic; P, probability of a Type II error; %, percentage; <, less than. Statistical significance found after a sequential Bonferroni correction was applied is indicated by an asterisk (*). No fish were present in the cages after 60 days, indicated as 'na'.]

Field / Location	Introduction			After 60 days			t-test			Difference	
	N	Mean	SE	N	Mean	SE	DF	t	P	Mean	%
Whole body THg concentration ($\mu\text{g g}^{-1}\text{ dw}$)											
PW-2 (permanent wetlands)											
Inlet	37	0.14	0.01	6	0.49	0.08	41	8.41	<.0001*	0.35	246%
Center	37	0.14	0.01	14	0.40	0.02	49	10.62	<.0001*	0.25	176%
Outlet	37	0.14	0.01	20	0.44	0.02	55	13.77	<.0001*	0.29	204%
PW-5 (permanent wetlands)											
Inlet	37	0.14	0.01	16	0.34	0.02	51	9.08	<.0001*	0.19	135%
Center	37	0.14	0.01	14	0.34	0.02	49	9.16	<.0001*	0.19	136%
Outlet	37	0.14	0.01	15	0.34	0.02	50	9.26	<.0001*	0.20	140%
R31 (white rice)											
Inlet	37	0.14	0.01	6	0.48	0.06	41	8.58	<.0001*	0.34	237%
Center	37	0.14	0.01	24	1.57	0.05	59	33.33	<.0001*	1.42	995%
Outlet	37	0.14	0.01	14	1.64	0.05	49	27.10	<.0001*	1.50	1046%
R64 (white rice)											
Inlet	37	0.14	0.01	6	0.40	0.03	41	7.49	<.0001*	0.26	180%
Center	37	0.14	0.01	26	1.53	0.03	61	35.88	<.0001*	1.39	969%
Outlet	37	0.14	0.01	26	1.86	0.05	61	37.47	<.0001*	1.71	1197%
W32 (wild rice)											
Inlet	37	0.14	0.01	0	na	na	na	na	na	na	na
Center	37	0.14	0.01	26	0.97	0.02	61	28.56	<.0001*	0.83	579%
Outlet	37	0.14	0.01	21	0.75	0.05	56	19.30	<.0001*	0.60	422%
W65 (wild rice)											
Inlet	37	0.14	0.01	21	1.79	0.13	56	27.76	<.0001*	1.65	1153%
Center	37	0.14	0.01	24	0.92	0.02	59	27.32	<.0001*	0.78	546%
Outlet	37	0.14	0.01	25	1.02	0.04	60	26.97	<.0001*	0.88	615%
THg body burden ($\mu\text{g fish}^{-1}\text{ dw}$)											
PW-2 (permanent wetlands)											
Inlet	37	0.05	0.01	6	0.11	0.02	41	2.52	0.02	0.06	117%
Center	37	0.05	0.01	14	0.08	0.01	49	2.01	0.05	0.03	51%
Outlet	37	0.05	0.01	20	0.07	0.01	55	1.44	0.16	0.01	29%
PW-5 (permanent wetlands)											
Inlet	37	0.05	0.01	16	0.11	0.01	51	3.52	0.001*	0.05	106%
Center	37	0.05	0.01	14	0.09	0.01	49	2.81	0.01	0.04	78%
Outlet	37	0.05	0.01	15	0.09	0.02	50	2.72	0.01	0.04	80%
R31 (white rice)											
Inlet	37	0.05	0.01	6	0.11	0.01	41	2.42	0.02	0.06	110%
Center	37	0.05	0.01	24	0.63	0.03	59	16.06	<.0001*	0.58	1118%
Outlet	37	0.05	0.01	14	0.71	0.03	49	13.07	<.0001*	0.65	1265%
R64 (white rice)											
Inlet	37	0.05	0.01	6	0.10	0.01	41	2.16	0.04	0.05	93%
Center	37	0.05	0.01	26	0.65	0.03	61	17.05	<.0001*	0.60	1162%
Outlet	37	0.05	0.01	26	0.86	0.03	61	19.04	<.0001*	0.81	1566%
W32 (wild rice)											

Field / Location	Introduction			After 60 days			<i>t</i> -test			Difference	
	<i>N</i>	Mean	SE	<i>N</i>	Mean	SE	<i>DF</i>	<i>t</i>	<i>P</i>	Mean	%
Inlet	37	0.05	0.01	0	na	na	na	na	na	na	na
Center	37	0.05	0.01	26	0.39	0.03	61	12.76	<.0001*	0.34	656%
Outlet	37	0.05	0.01	21	0.32	0.03	56	10.18	<.0001*	0.27	527%
W65 (wild rice)											
Inlet	37	0.05	0.01	21	0.38	0.03	56	11.67	<.0001*	0.33	640%
Center	37	0.05	0.01	24	0.45	0.03	59	13.62	<.0001*	0.40	779%
Outlet	37	0.05	0.01	25	0.49	0.04	60	13.96	<.0001*	0.44	850%

Table 8.2. Western mosquitofish size and body condition immediately prior to and after 60 days of caged exposure in agricultural and non-agricultural wetlands within the Yolo Bypass Wildlife Area, California

[Statistical analysis using the two-sample t-test to examine temporal changes in fish standard length, wet mass and relative condition factor, at the time the fish were first caged (Introduction) compared to after 60 days of in-situ exposure, for individual fields and within-field locations (inlets, center and outlet). Non-agricultural wetlands are represented by Permanent Wetland sites 2 and 5. Agricultural wetlands are represented by sites R31, R64, W32 and W65. Where: mm, millimeters; g, gram; N, number of observations; SE, standard error of the mean; DF, degrees of freedom; t, t-test statistic; P, probability of a Type II error; %, percentage; <, less than. Statistical significance found after a sequential Bonferroni correction was applied is indicated by an asterisk (*). No fish were present in the cages after 60 days, indicated as 'na'.]

Location	Introduction			After 60 days			t-test			Difference	
	N	Mean	SE	N	Mean	SE	DF	t	P	Mean	%
<u>Fish standard length (mm)</u>											
PW-2 (permanent wetlands)											
Inlet	30	39.13	0.78	6	38.32	0.42	34	-0.46	0.65	-0.81	-2%
Center	30	35.91	0.40	14	37.08	0.67	42	1.54	0.13	1.17	3%
Outlet	30	38.24	0.38	20	35.80	0.64	48	-3.41	0.001*	-2.44	-6%
PW-5 (permanent wetlands)											
Inlet	30	40.37	0.93	16	41.43	1.16	44	0.69	0.49	1.06	3%
Center	30	38.02	0.46	14	38.67	0.54	42	0.83	0.41	0.65	2%
Outlet	30	40.85	0.94	16	40.57	1.30	44	-0.20	0.84	-0.28	-1%
R31 (white rice)											
Inlet	30	37.11	0.63	6	38.59	0.96	34	0.95	0.35	1.48	4%
Center	30	35.95	0.61	24	43.51	0.61	52	8.47	<.0001*	7.57	21%
Outlet	30	35.41	0.46	14	44.66	0.67	42	11.01	<.0001*	9.25	26%
R64 (white rice)											
Inlet	30	39.10	0.66	6	38.24	1.11	34	-0.55	0.59	-0.85	-2%
Center	30	39.33	0.79	26	44.26	0.62	54	4.67	<.0001*	4.93	13%
Outlet	30	39.02	0.66	26	45.29	0.54	54	6.83	<.0001*	6.27	16%
W32 (wild rice)											
Inlet	30	41.14	0.78	0	na	na	na	na	na	na	na
Center	30	40.85	0.61	26	45.06	0.68	54	4.48	<.0001*	4.21	10%
Outlet	30	37.68	0.83	21	45.15	0.81	49	6.04	<.0001*	7.48	20%
W65 (wild rice)											
Inlet	30	37.37	0.78	21	37.79	0.38	49	0.37	0.71	0.41	1%
Center	30	38.78	0.70	24	45.60	0.78	52	6.35	<.0001*	6.82	18%
Outlet	30	38.51	0.85	25	47.23	0.76	53	7.29	<.0001*	8.72	23%
<u>Fish wet mass (g)</u>											
PW-2 (permanent wetlands)											
Inlet	30	1.48	0.10	6	1.26	0.05	34	-0.99	0.33	-0.22	-15%
Center	30	1.40	0.06	14	1.15	0.06	42	-2.71	0.01	-0.25	-18%
Outlet	30	1.69	0.09	20	0.93	0.04	48	-7.77	<.0001*	-0.76	-45%
PW-5 (permanent wetlands)											
Inlet	30	1.80	0.14	16	1.70	0.14	44	-0.46	0.65	-0.10	-6%
Center	30	1.47	0.07	14	1.48	0.06	42	0.04	0.97	0.00	0%
Outlet	30	1.79	0.13	16	1.55	0.14	43	-1.18	0.24	-0.24	-13%
R31 (white rice)											

Location	Introduction			After 60 days			<i>t</i> -test			Difference	
	<i>N</i>	Mean	SE	<i>N</i>	Mean	SE	<i>DF</i>	<i>t</i>	<i>P</i>	Mean	%
Inlet	30	1.40	0.07	6	1.20	0.04	34	-1.31	0.20	-0.20	-14%
Center	30	1.31	0.09	24	2.02	0.08	52	5.24	<.0001*	0.71	54%
Outlet	30	1.25	0.05	14	2.13	0.09	42	7.55	<.0001*	0.87	70%
R64 (white rice)											
Inlet	30	1.64	0.08	6	1.27	0.13	34	-2.10	0.04	-0.37	-23%
Center	30	1.63	0.12	26	2.18	0.08	54	3.48	0.001*	0.55	34%
Outlet	30	1.56	0.09	26	2.19	0.11	54	4.34	<.0001*	0.63	40%
W32 (wild rice)											
Inlet	30	1.87	0.13	0	na	na	na	na	na	na	na
Center	30	1.80	0.09	26	2.02	0.11	54	1.56	0.13	0.22	12%
Outlet	30	1.54	0.10	21	2.19	0.12	49	3.86	0.0003*	0.65	43%
W65 (wild rice)											
Inlet	30	1.37	0.10	21	1.11	0.04	49	-2.15	0.04	-0.25	-19%
Center	30	1.56	0.10	24	2.43	0.14	52	5.02	<.0001*	0.86	55%
Outlet	30	1.58	0.10	25	2.38	0.12	53	4.96	<.0001*	0.81	51%
<u>Relative condition factor</u>											
PW-2 (permanent wetlands)											
Inlet	30	0.91	0.02	6	0.83	0.04	34	-1.80	0.08	-0.08	-9%
Center	30	1.11	0.04	14	0.83	0.04	42	-4.74	<.0001*	-0.28	-25%
Outlet	30	1.16	0.07	20	0.74	0.02	48	-4.88	<.0001*	-0.42	-36%
PW-5 (permanent wetlands)											
Inlet	30	1.01	0.02	16	0.89	0.02	44	-3.44	0.001*	-0.13	-13%
Center	30	0.99	0.03	14	0.94	0.02	42	-1.12	0.27	-0.06	-6%
Outlet	30	0.97	0.03	16	0.86	0.02	43	-2.32	0.03	-0.11	-11%
R31 (white rice)											
Inlet	30	1.00	0.03	6	0.77	0.05	34	-3.78	0.001*	-0.23	-23%
Center	30	1.03	0.03	24	0.91	0.02	52	-2.89	0.01	-0.12	-11%
Outlet	30	1.05	0.06	14	0.90	0.04	42	-1.71	0.09	-0.15	-14%
R64 (white rice)											
Inlet	30	1.01	0.03	6	0.83	0.04	34	-2.86	0.01	-0.18	-18%
Center	30	0.99	0.02	26	0.94	0.02	54	-1.36	0.18	-0.05	-5%
Outlet	30	0.97	0.02	26	0.89	0.02	54	-2.55	0.01	-0.08	-9%
W32 (wild rice)											
Inlet	30	1.00	0.03	0	na	na	na	na	na	na	na
Center	30	0.98	0.03	26	0.83	0.02	54	-4.02	0.0002*	-0.15	-16%
Outlet	30	1.05	0.02	21	0.90	0.03	49	-4.35	<.0001*	-0.15	-15%
W65 (wild rice)											
Inlet	30	0.96	0.02	21	0.76	0.02	49	-6.37	<.0001*	-0.20	-21%
Center	30	0.99	0.02	24	0.97	0.03	52	-0.51	0.62	-0.02	-2%
Outlet	30	1.01	0.02	25	0.86	0.02	53	-5.51	<.0001*	-0.16	-15%

Table 9.1 Sampling dates and locations for photodemethylation experiments

[Coordinates for water sampling, light meter, and incubation locations are given in datum WGS84 and in degrees decimal minutes (ddd mm.mmm). See **Figure 3.5** for corresponding map. Field codes varied between years based on crop rotation.]

Sampling Period	Field Number	Field Code	Field type	Latitude [dd mm.mmm]	Longitude [ddd mm.mmm]
Dec 3-7, 2007	20	F20	Fallow	38° 33.150' N	121° 37.200' W
Jul 29 - Aug 1, 2008	20	R20	White rice	38° 33.150' N	121° 37.200' W
Dec 3-7, 2007	31	R31	White rice	38° 33.150' N	121° 36.628' W
Jul 29 - Aug 1, 2008	31	W31	Wild rice	38° 33.150' N	121° 36.628' W
Dec 3-7, 2007	32	W32	Wild rice	38° 33.163' N	121° 36.387' W
Dec 3-7, 2007	64	R64	White rice	38° 32.867' N	121° 36.683' W
Jul 29 - Aug 1, 2008	64	W64	Wild rice	38° 32.867' N	121° 36.683' W
Dec 3-7, 2007	65	W65	Wild rice	38° 32.567' N	121° 36.450' W
Dec 3-7, 2007	66	F66	Fallow	38° 32.567' N	121° 36.108' W
Jul 29 - Aug 1, 2008	66	R66	White rice	38° 32.567' N	121° 36.108' W
Dec 3-7, 2007	1	SW1	Seasonal Wetland	38° 32.474' N	121° 36.068' W
Dec 3-7, 2007	5	PW5	Permanent Wetland	38° 32.567' N	121° 35.550' W
Jul 29 - Aug 1, 2008	5	PW5	Permanent Wetland	38° 32.567' N	121° 35.550' W
Dec 3-7, 2007	Light Meter Location			38° 33.177' N	121° 40.312' W
Jul 29 - Aug 1, 2008	Light Meter Location			38° 33.177' N	121° 40.312' W
Dec 3-7, 2007	Incubation Location			38° 33.070' N	121° 37.665' W
Jul 29 - Aug 1, 2008	Incubation Location			38° 33.052' N	121° 37.600' W

Table 9.2. Summary of the linear regression slopes associated with the change in methylmercury concentration as a function of cumulative solar photosynthetically available radiation and ultraviolet radiation measured during the winter and summer photodemethylation experiments

[Linear least-squares regression slopes for methylmercury (MeHg) degradation were calculated as the change in MeHg concentration as a function of the cumulative PAR or UV solar radiation exposure over a 2-3 day incubation (5 time points) of sample bottles exposed to light or dark conditions. The difference represents the dark-corrected light-induced slope for MeHg degradation. PAR, photosynthetically available radiation; UV, ultraviolet; ng L⁻¹, nanogram per liter; ng L⁻¹ mol⁻¹ m⁻², nanogram per liter per mole per square meter]

Field Code	Sampling Period	Initial MeHg Concentration (ng L ⁻¹)	PAR Regression Slope (ng L ⁻¹ mol ⁻¹ m ⁻²)			UV Regression Slope (ng L ⁻¹ mol ⁻¹ m ⁻²)		
			Light	Dark	Difference	Light	Dark	Difference
F20	Dec 3-7, 2007	0.7	-0.0086	-0.0032	-0.0054	-0.216	-0.078	-0.138
R31	Dec 3-7, 2007	1.75	-0.0148	0.0002	-0.0150	-0.372	0.040	-0.412
F66	Dec 3-7, 2007	0.84	-0.0047	0.0001	-0.0048	-0.124	0.004	-0.128
SW1	Dec 3-7, 2007	1	-0.0068	-0.0043	-0.0025	-0.172	-0.114	-0.058
R64	Dec 3-7, 2007	0.83	-0.0037	-0.0004	-0.0033	-0.094	-0.009	-0.084
W65	Dec 3-7, 2007	0.93	-0.0046	-0.0005	-0.0041	-0.116	0.017	-0.130
PW5	Dec 3-7, 2007	0.37	-0.0038	-0.0003	-0.0035	-0.010	-0.006	-0.094
PW32	Dec 3-7, 2007	1.06	-0.0057	0.0024	-0.0081	-0.015	0.062	-0.210
W31	Jul 29 - Aug 1, 2008	0.65	-0.0029	-0.0018	-0.0012	-0.071	-0.047	-0.024
PW5	Jul 29 - Aug 1, 2008	0.21	-0.0008	-0.0003	-0.0005	-0.020	-0.008	-0.012
W64	Jul 29 - Aug 1, 2008	3.75	-0.0165	0.0036	-0.0201	-0.397	0.086	-0.483
W66	Jul 29 - Aug 1, 2008	0.5	-0.0025	-0.0003	-0.0022	-0.064	-0.008	-0.056
W20	Jul 29 - Aug 1, 2008	1.5	-0.0079	-0.0003	-0.0076	-0.191	-0.006	-0.185

Table 9.3. Average daily percent loss of methylmercury as a function of daily integrated photosynthetically available radiation or ultraviolet radiation intensity and light attenuation with water-column depth

[Values represent the percentage (%) of methylmercury lost per day though photodecomposition. The extinction coefficient (unitless) is a measure of light attenuation with water depth, and is given for a maximum water-column depth of 30 centimeters. PAR, photosynthetically available radiation; UV, ultraviolet radiation; mol m⁻², moles of photons per square meter]

Extinction Coefficient	Daily Integrated PAR (mol m ⁻²)							
	3	5	10	15	20	30	40	50
-0.01	1.2	2.1	4.2	6.2	8.3	12	17	21
-0.02	1.1	1.8	3.6	5.4	7.2	11	14	18
-0.03	0.95	1.6	3.2	4.8	6.3	9.5	13	16
-0.04	0.84	1.4	2.8	4.2	5.6	8.4	11	14
-0.05	0.75	1.2	2.5	3.7	5.0	7.5	9.0	12
-0.06	0.67	1.1	2.2	3.3	4.5	6.7	8.9	11
-0.07	0.60	1.0	2.0	3.0	4.0	6.0	8.0	10
-0.08	0.55	0.91	1.8	2.7	3.6	5.5	7.3	9.1
-0.09	0.50	0.83	1.7	2.5	3.3	5.0	6.6	8.3
-0.10	0.46	0.76	1.5	2.3	3.0	4.6	6.1	7.6

Extinction Coefficient	Daily Integrated UV (mol m ⁻²)							
	0.3	0.5	1	1.5	2	3	4	5
-0.01	3.1	5.1	10	15	20	31	41	51
-0.02	2.7	4.4	8.9	13	18	27	35	44
-0.03	2.3	3.9	7.8	12	16	23	31	39
-0.04	2.1	3.4	6.9	10	14	21	27	34
-0.05	1.8	3.1	6.1	9.2	12	18	24	31
-0.06	1.6	2.7	5.5	8.2	11	16	22	27
-0.07	1.5	2.5	4.9	7.4	9.9	15	20	25
-0.08	1.3	2.2	4.5	6.7	8.9	13	18	22
-0.09	1.2	2.0	4.1	6.1	8.2	12	16	20
-0.10	1.1	1.9	3.7	5.6	7.5	11	15	19

Table 9.4. Average daily percent loss of methylmercury as a function of daily integrated photosynthetically available radiation or ultraviolet radiation intensity and initial methylmercury concentration.

[Values represent the mass loss of methylmercury (in units of $\text{ng m}^{-2} \text{d}^{-1}$, nanograms per square meter per day) via photodecomposition, assuming an extinction coefficient of -0.029 and water-column depth of 30 centimeters. MeHg, methylmercury; PAR, photosynthetically available radiation; UV, ultra-violet radiation; mol m^{-2} , moles of photons per square meter]

Initial MeHg Concentration ng L^{-1}	Daily Integrated PAR (mol m^{-2})							
	3	5	10	15	20	30	40	50
0.5	0.05	0.08	0.16	0.24	0.32	0.48	0.64	0.80
1.0	0.10	0.16	0.32	0.48	0.64	0.96	1.3	1.6
1.5	0.14	0.24	0.48	0.72	0.96	1.4	1.9	2.4
2.0	0.19	0.32	0.64	0.96	1.3	1.9	2.6	3.2
2.5	0.24	0.40	0.80	1.2	1.6	2.4	3.2	4.0
3.0	0.29	0.48	0.96	1.4	1.9	2.9	3.8	4.8
4.0	0.39	0.64	1.3	1.9	2.6	3.8	5.1	6.4
5.0	0.48	0.80	1.6	2.4	3.2	4.8	6.4	8.0
6.0	0.58	0.96	1.9	2.9	3.8	5.8	7.7	9.6
8.0	0.77	1.3	2.6	3.8	5.1	7.7	10	13
10.0	0.96	1.6	3.2	4.8	6.4	9.6	13	16

	Daily Integrated UV (mol m^{-2})							
	0.3	0.5	1	1.5	2	3	4	5
0.5	0.02	0.04	0.08	0.12	0.16	0.24	0.32	0.39
1.0	0.07	0.12	0.24	0.36	0.47	0.71	1.0	1.2
1.5	0.12	0.20	0.39	0.59	0.79	1.2	1.6	2.0
2.0	0.24	0.39	0.79	1.2	1.6	2.4	3.2	3.9
2.5	0.36	0.59	1.2	1.8	2.4	3.6	4.7	5.9
3.0	0.47	0.79	1.6	2.4	3.2	4.7	6.3	7.9
4.0	0.59	1.0	2.0	3.0	3.9	5.9	7.9	9.9
5.0	0.71	1.2	2.4	3.6	4.7	7.1	9.5	12
6.0	1.0	1.6	3.2	4.7	6.3	9.5	13	16
8.0	1.2	2.0	3.9	5.9	7.9	12	16	20
10.0	1.4	2.4	4.7	7.1	9.5	14	19	24

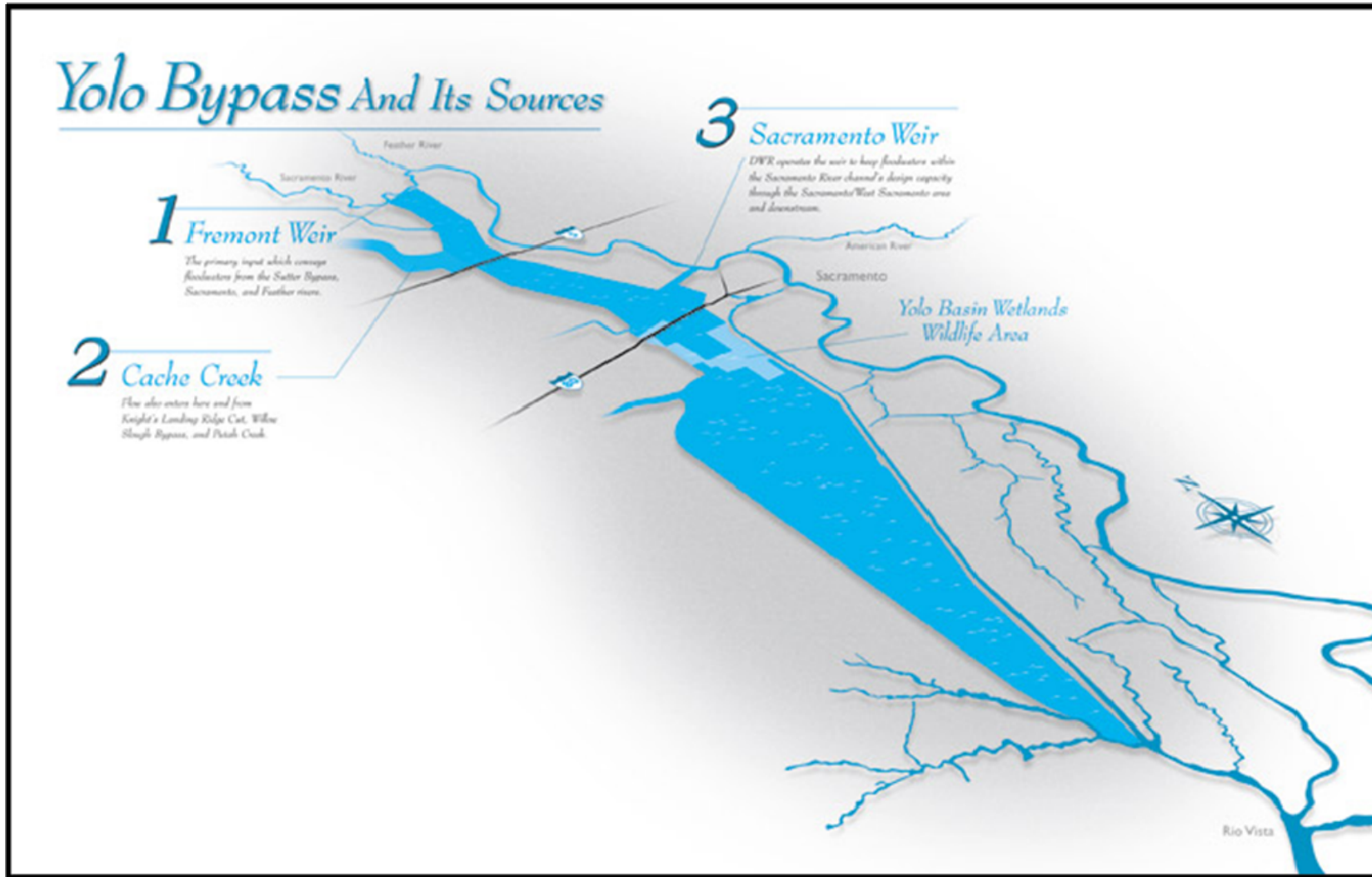
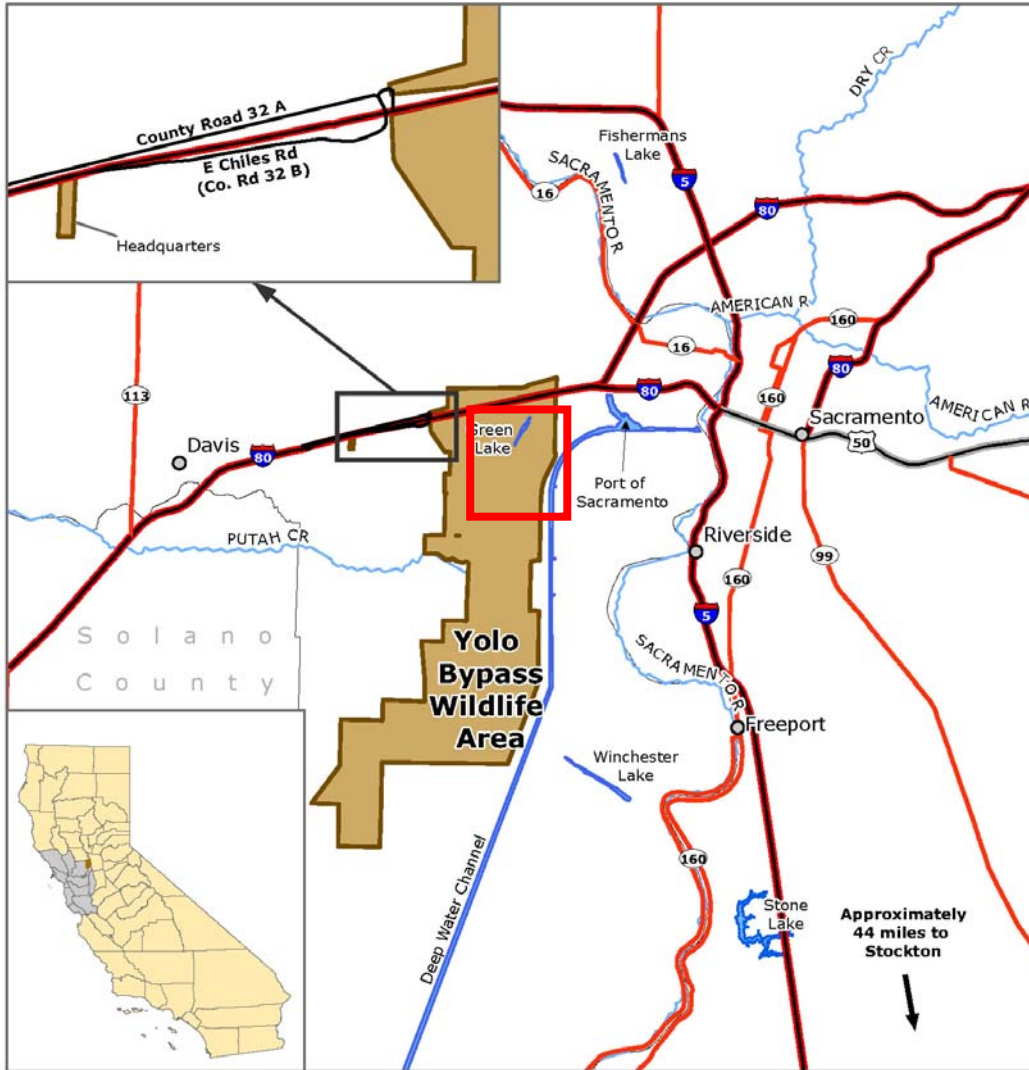


Figure 3.1. Northern-looking oblique graphic illustration of the hydrologic contribution of the Yolo Basin Wildlife Area (YBWA) to the Yolo ByPass hydrologic unit. Image taken from California Department of Water Resources news: http://geography.sierra.cc.ca.us/booth/california/9_water/Yolo_Bypass.jpg

California Department of Fish and Game
Bay Delta Region
YOLO BYPASS WILDLIFE AREA
Yolo County



June 2008 - Greg Ewing, DFG - WB / BDB
Prepared by BDB for WB

Figure 3.2. Map illustrating the location of the study area within the Yolo Bypass Wildlife Area, Yolo County, CA. The red square depicts the study area. Taken from the California Department of Fish and Game Web Site:

http://www.dfg.ca.gov/lands/wa/region3/yolo/docs/YoloBypass_WA_Web.pdf.

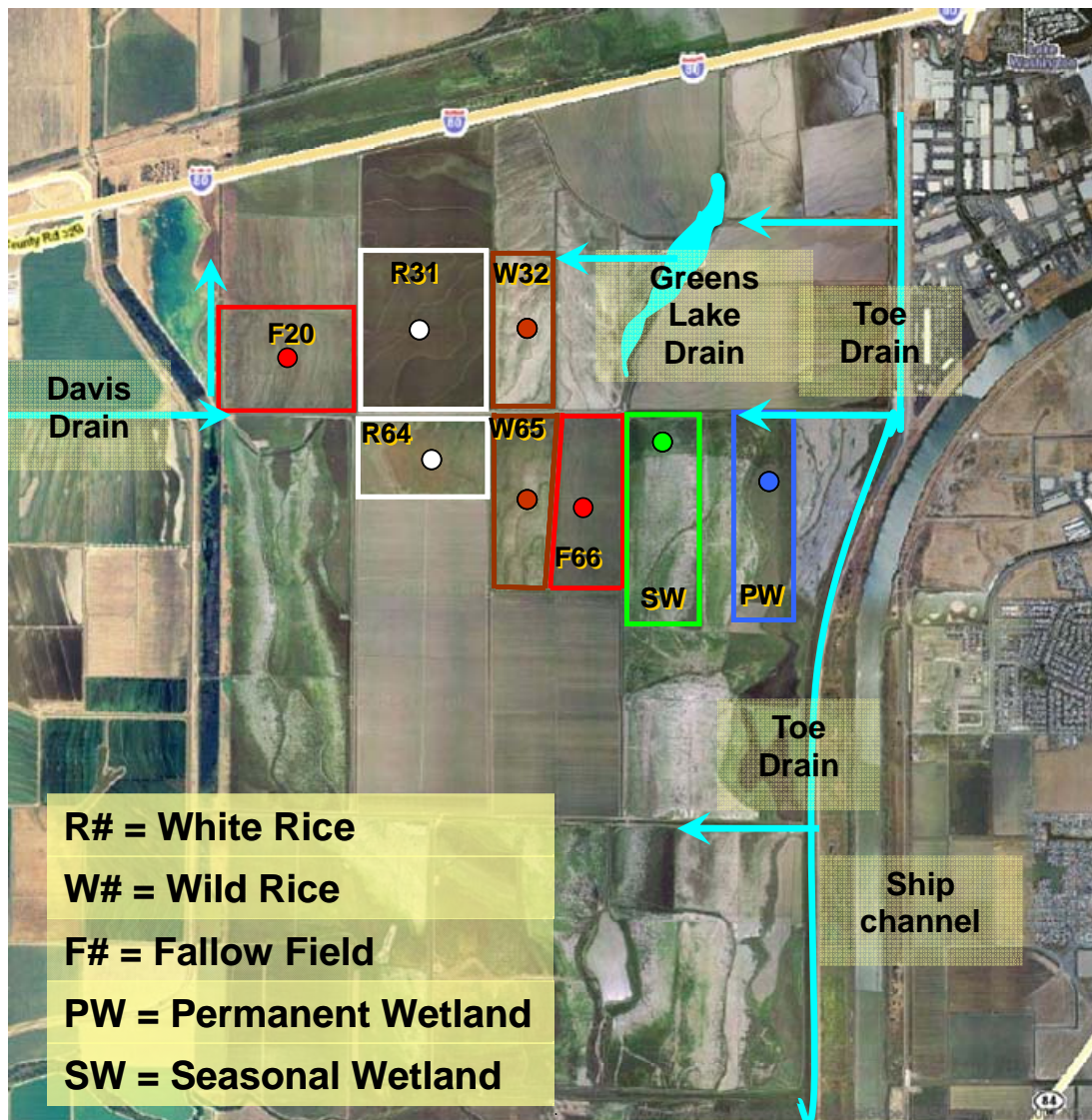


Figure 3.3 Satellite image (GoogleEarth™) of the study area depicting the five wetland types studied. Similar field types share the same color border. The circles in each field indicate the location of the primary sediment sampling sites. GPS coordinates are listed in **Table 3.1**. The turquoise lines and arrows indicate the major water flows in and around the study area.



Figure 3.4. Satellite image (GoogleEarth™) depicting sampling locations for specific matrices. Where: inlet (blue), outlet (red) and centerfield (green) sites were sampled for water (blue, red and green), sediment (green only), plant (green only) and biota (red and blue only). GPS coordinates are listed in **Table 3.1**.



Figure 3.5. Satellite image (GoogleEarth™) depicting photodemethylation study sampling locations. The red dot indicates the location of the light meter. The blue dots indicate the locations where water samples were collected, and the yellow dots indicate the locations of sample deployment (photo-incubations).

A) Continuous Flow Stirred Tank Reactor (CFSTR)

B) Plug Flow Reactor (PFR)

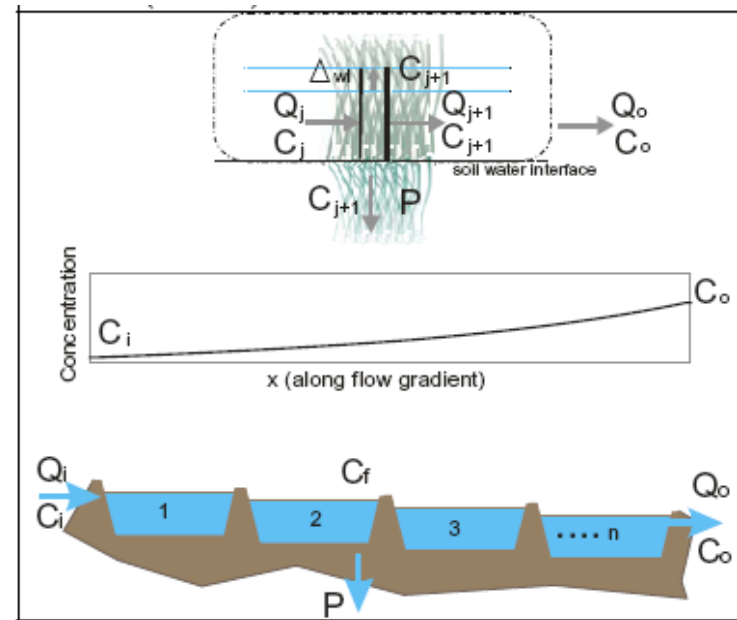
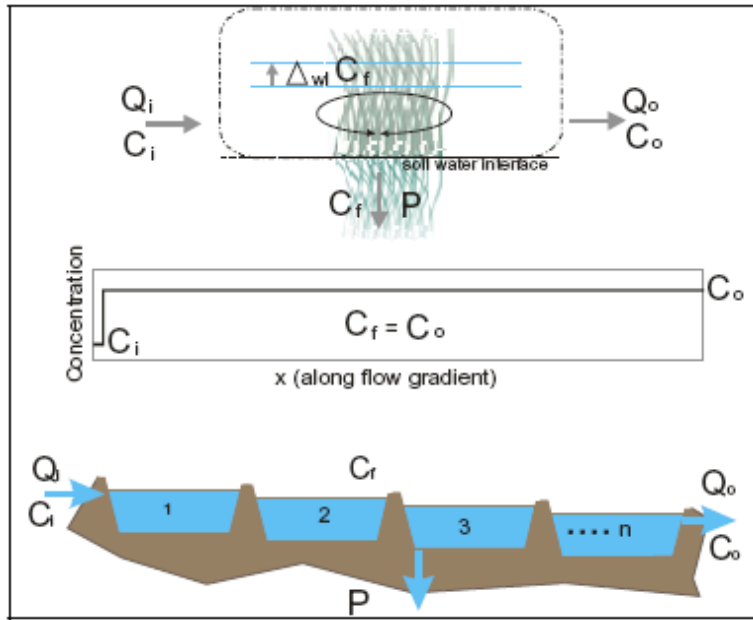


Figure 4.1. Schematics for water flow and concentration trends across the fields based on A) the Continuous Flow Stirred Tank Reactor model and B) the Plug Flow Reactor model. Where: Q_i = flow in, Q_o = flow out, C_i = concentration in, C_o = concentration out, P = percolation.

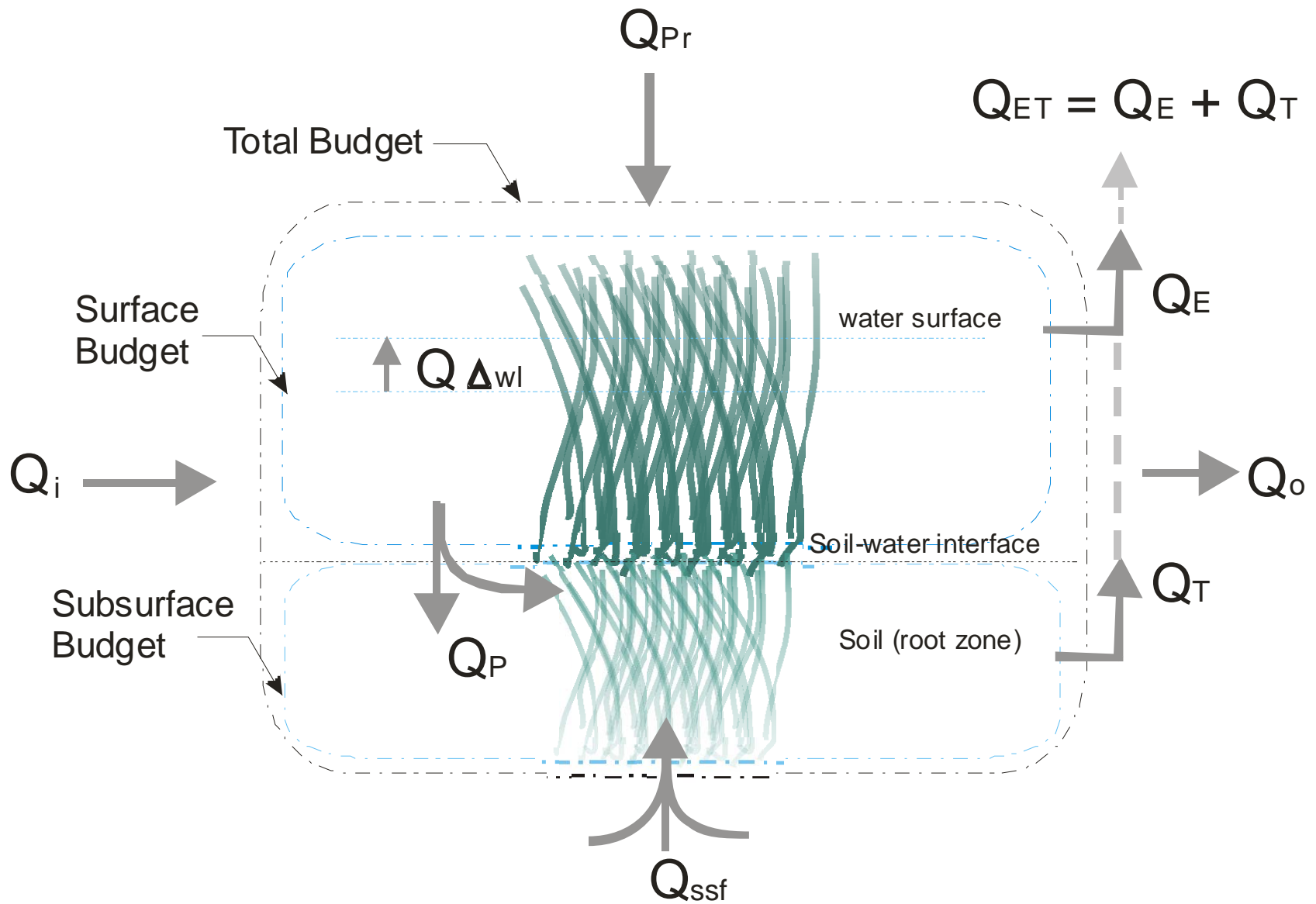


Figure 4.2. Water budget model. See Section 4.2 for model parameter definitions.

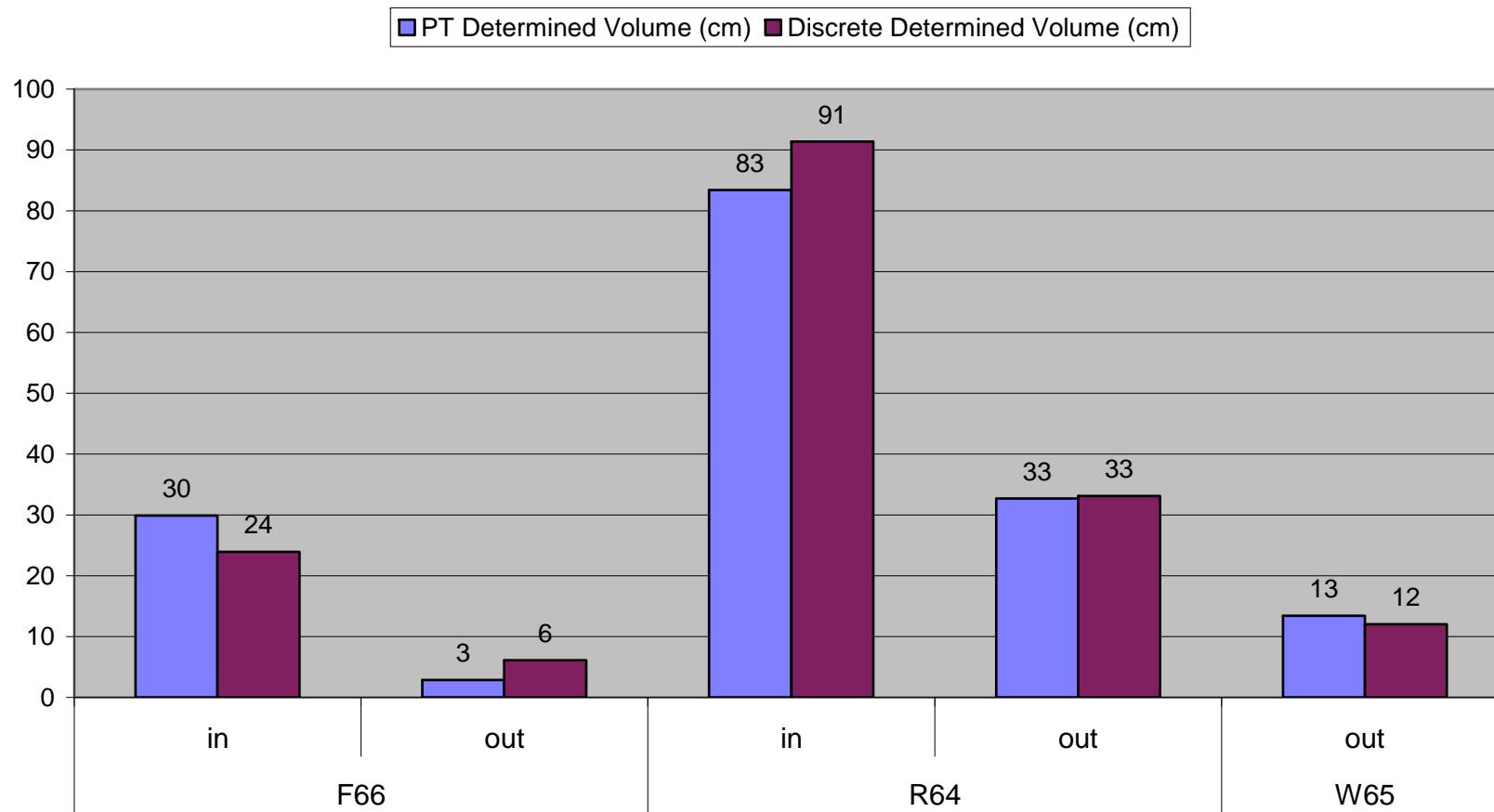


Figure 4.3. Comparison of water flux calculations using pressure transducer and manual measurements for the fields where both data were collected.

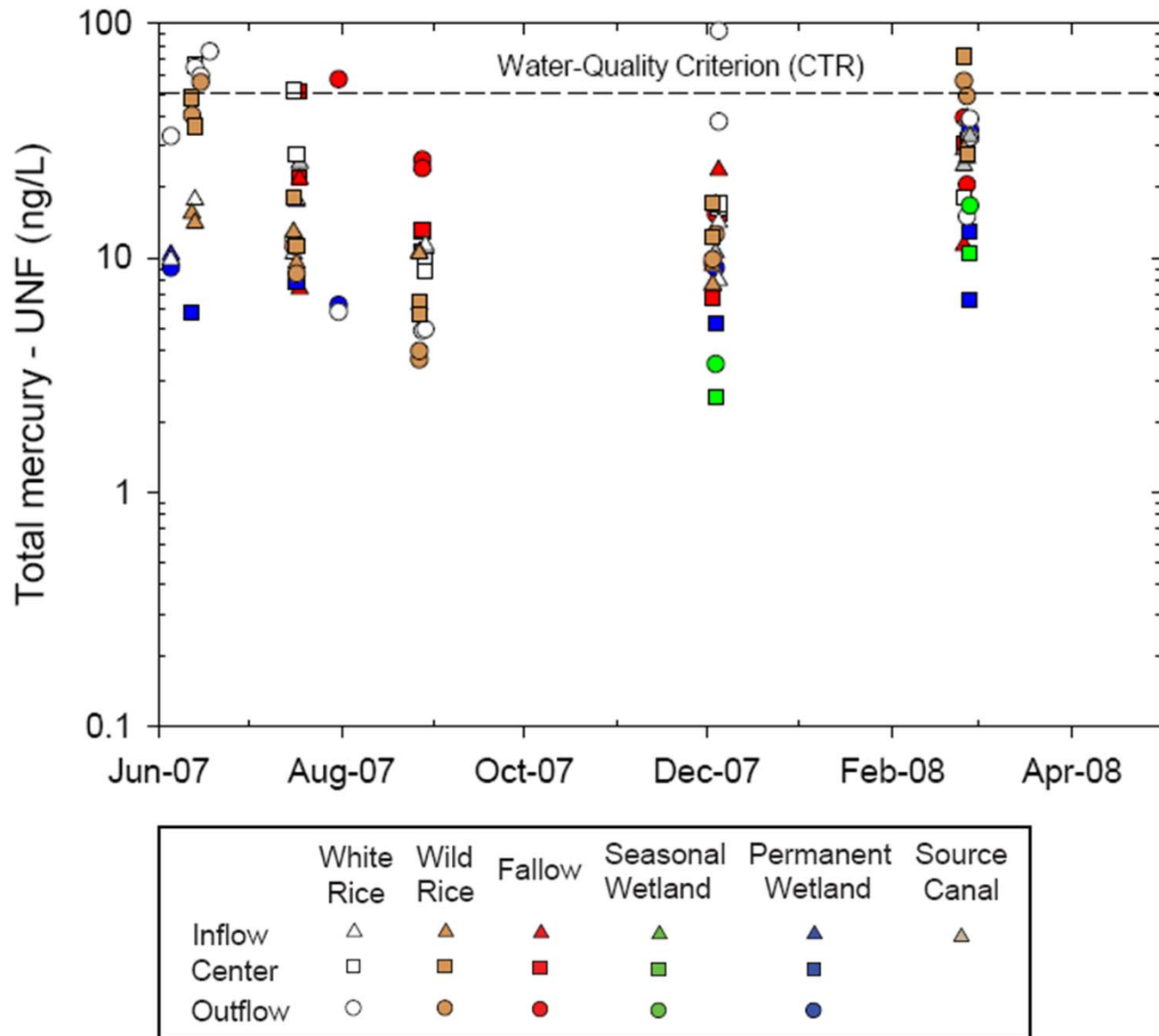


Figure 5.1. Time series plot of total mercury concentration in unfiltered surface water. The dashed line indicates the 50 ng/L water-quality criterion for unfiltered total mercury in the California Toxics Rule (CTR) (U.S. Environmental Protection Agency, 2000b).

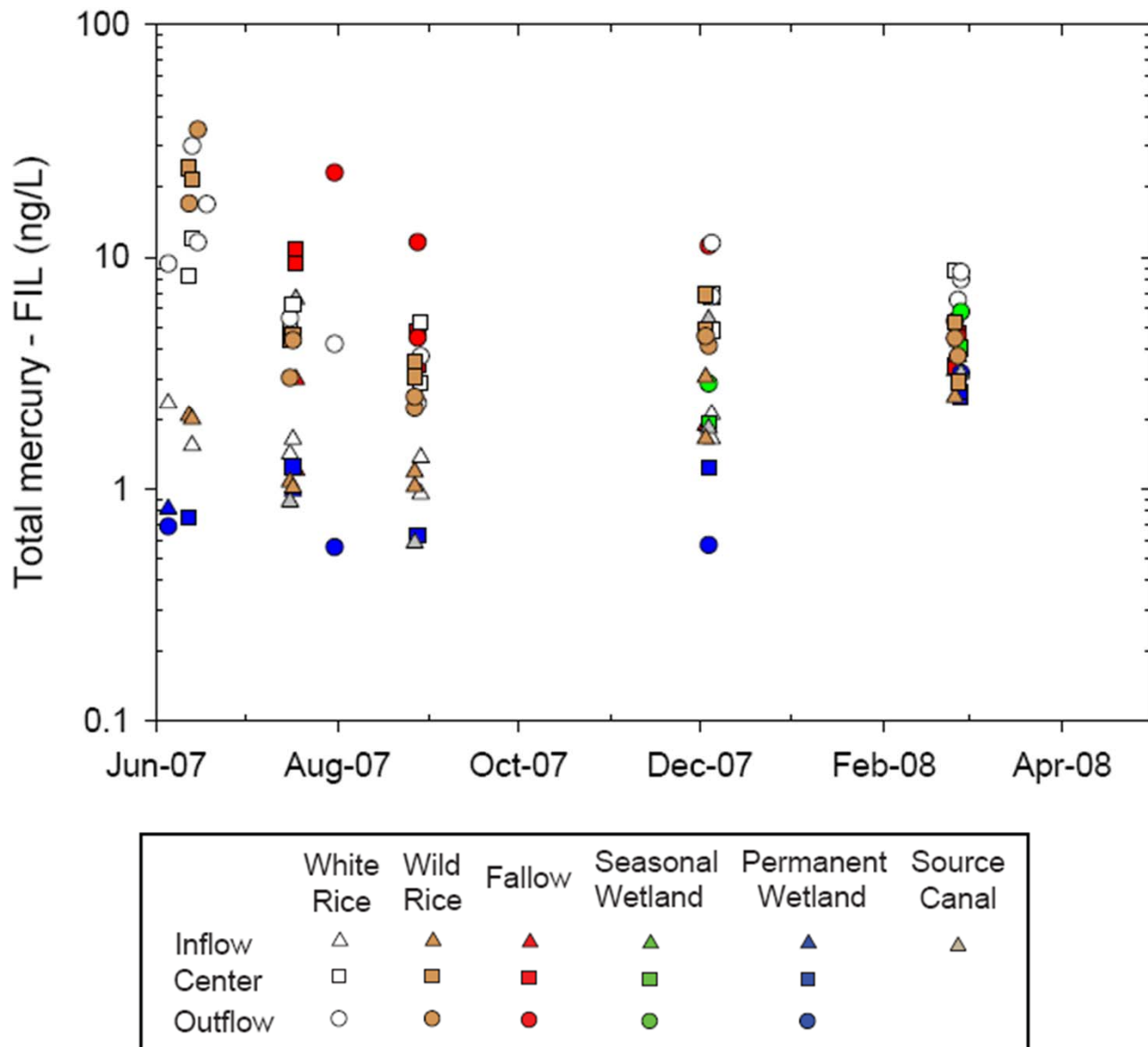


Figure 5.2. Time series plot of total mercury concentration in filtered surface water.

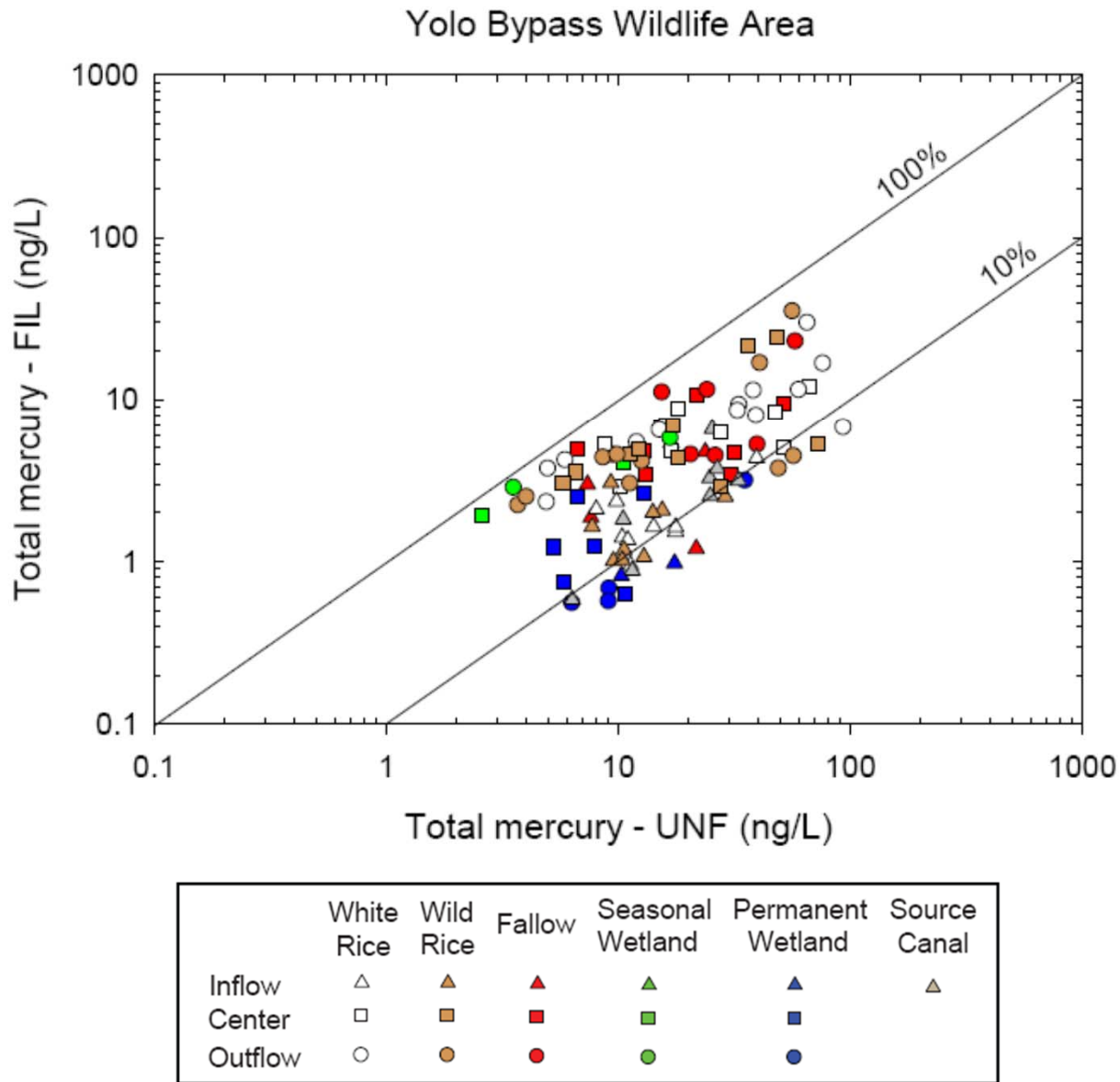


Figure 5.3. Log-log plot of total mercury concentration in unfiltered versus filtered surface water. Diagonal lines represent lines of equal proportions of mercury passing through the filter, as indicated.

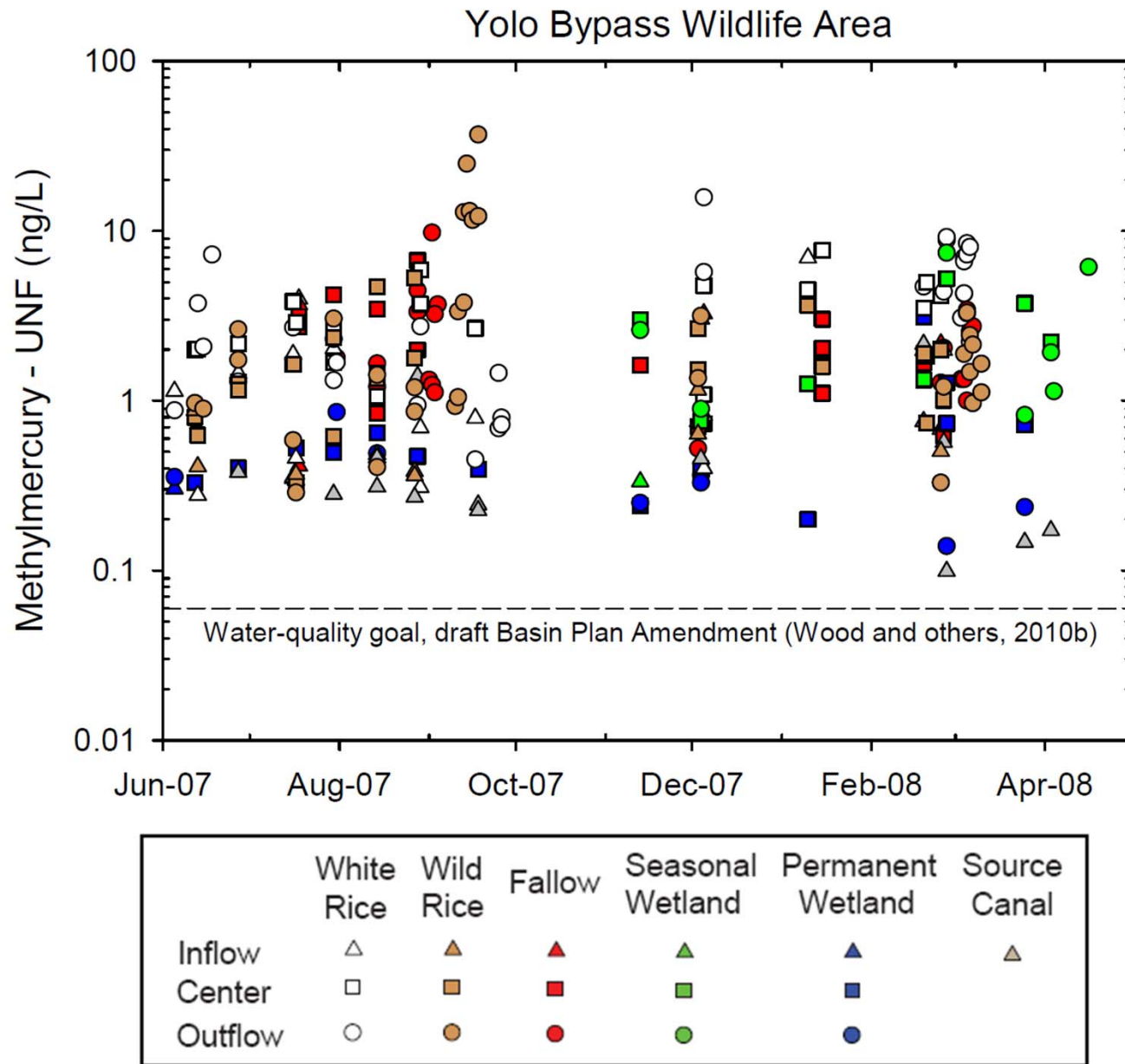


Figure 5.4. Time series plot of methylmercury concentration in unfiltered surface water. The dashed horizontal line reflects the 0.06 ng/L proposed water -quality goal for unfiltered methylmercury (Wood et al., 2010b) .

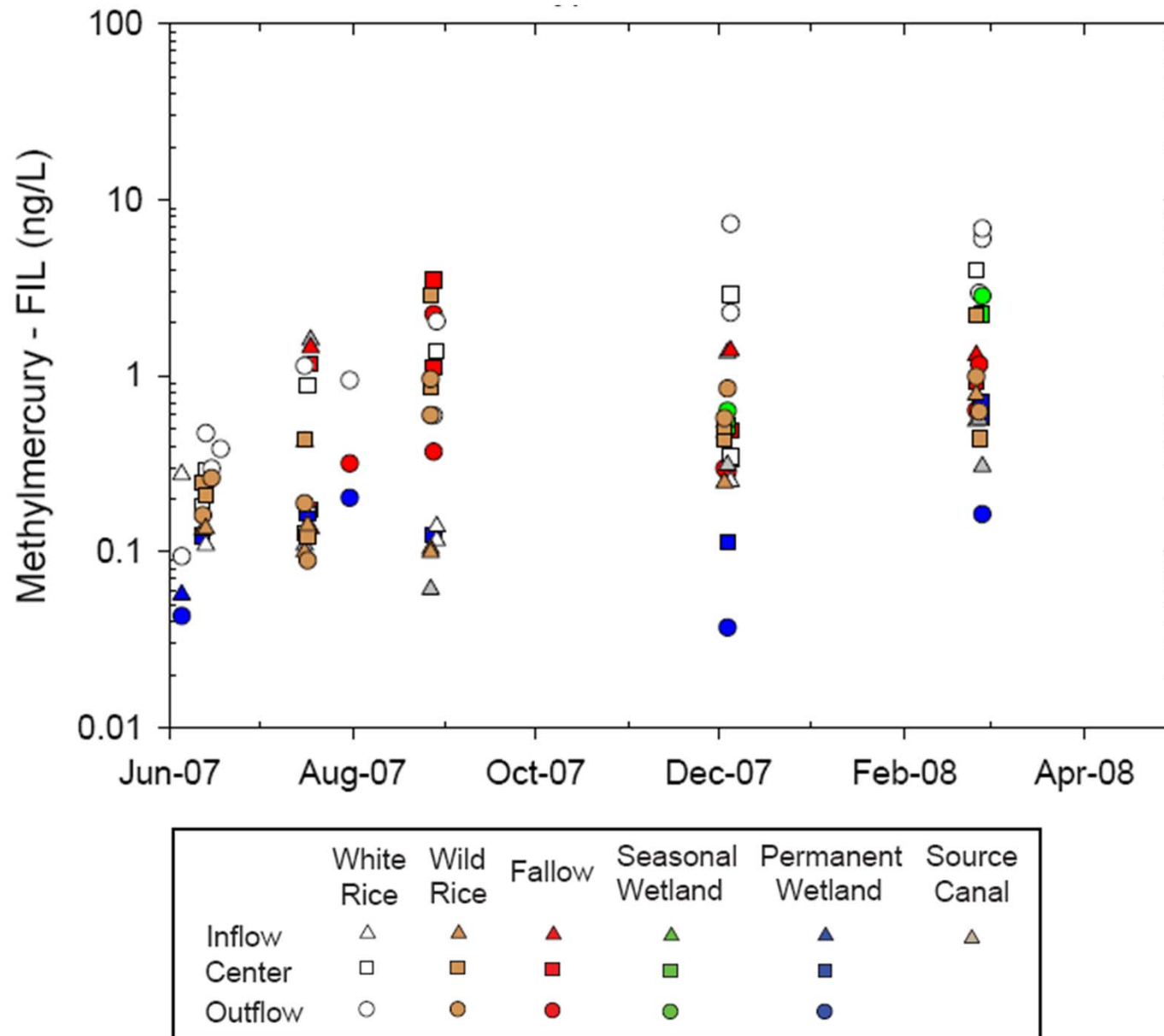


Figure 5.5. Time series plot of methylmercury concentration in filtered surface water.

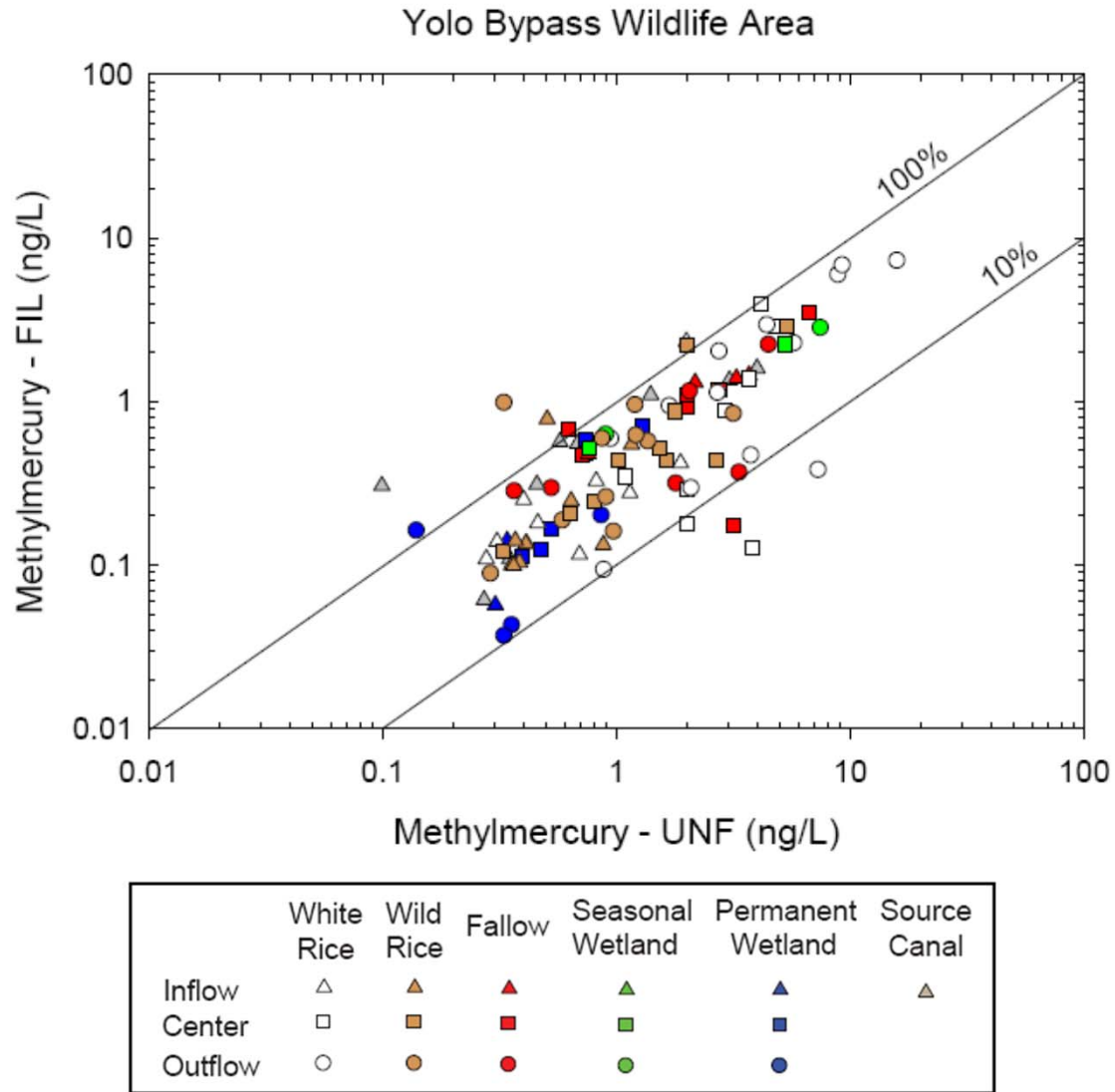


Figure 5.6. Log-log plot of methylmercury concentration in unfiltered versus filtered surface water. Diagonal lines represent lines of equal proportions of mercury passing through the filter, as indicated.

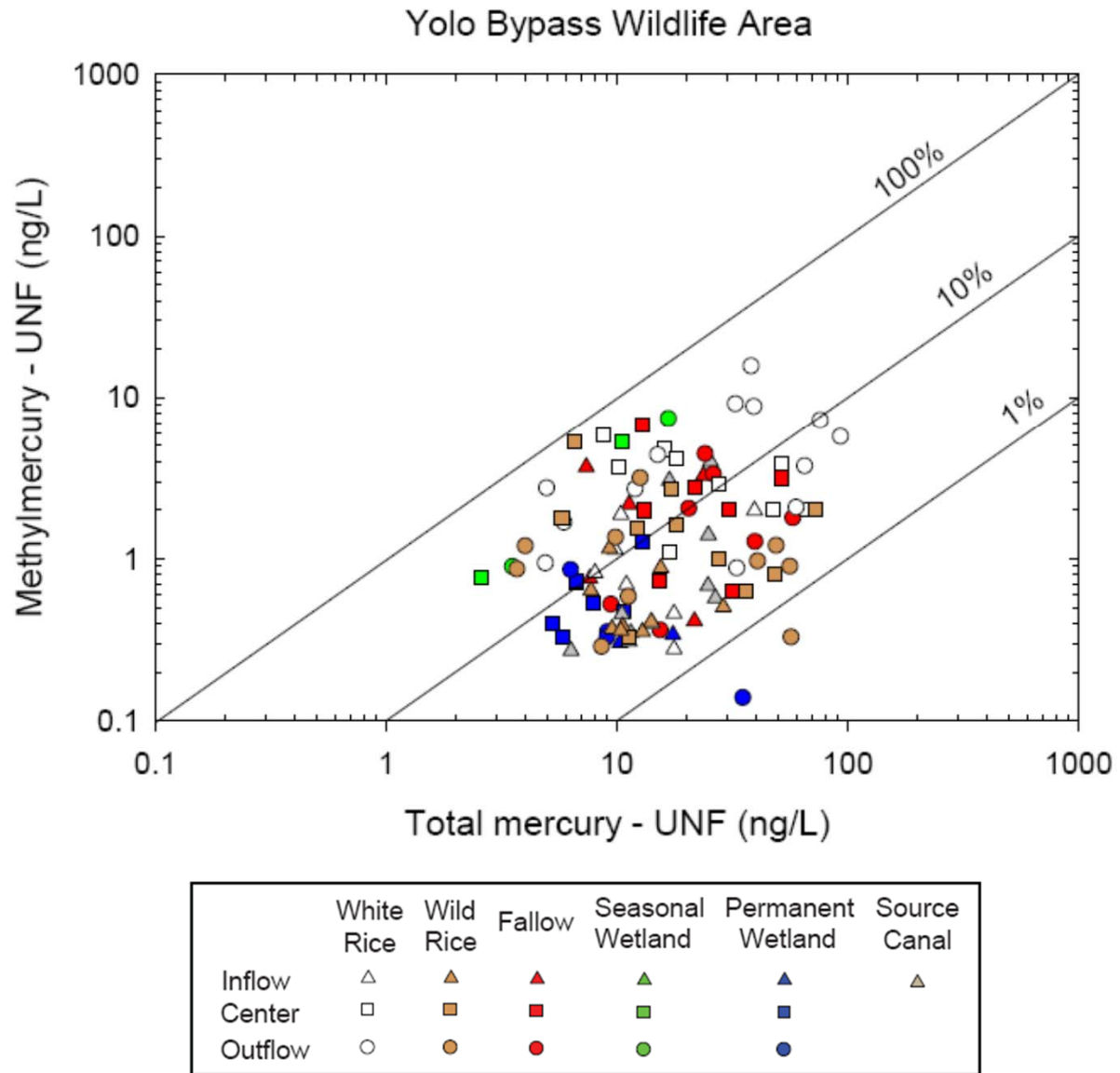


Figure 5.7. Log-log plot of total mercury concentration versus methylmercury concentration in unfiltered surface water. Diagonal lines represent lines of equal values of the ratio of methylmercury to total mercury.

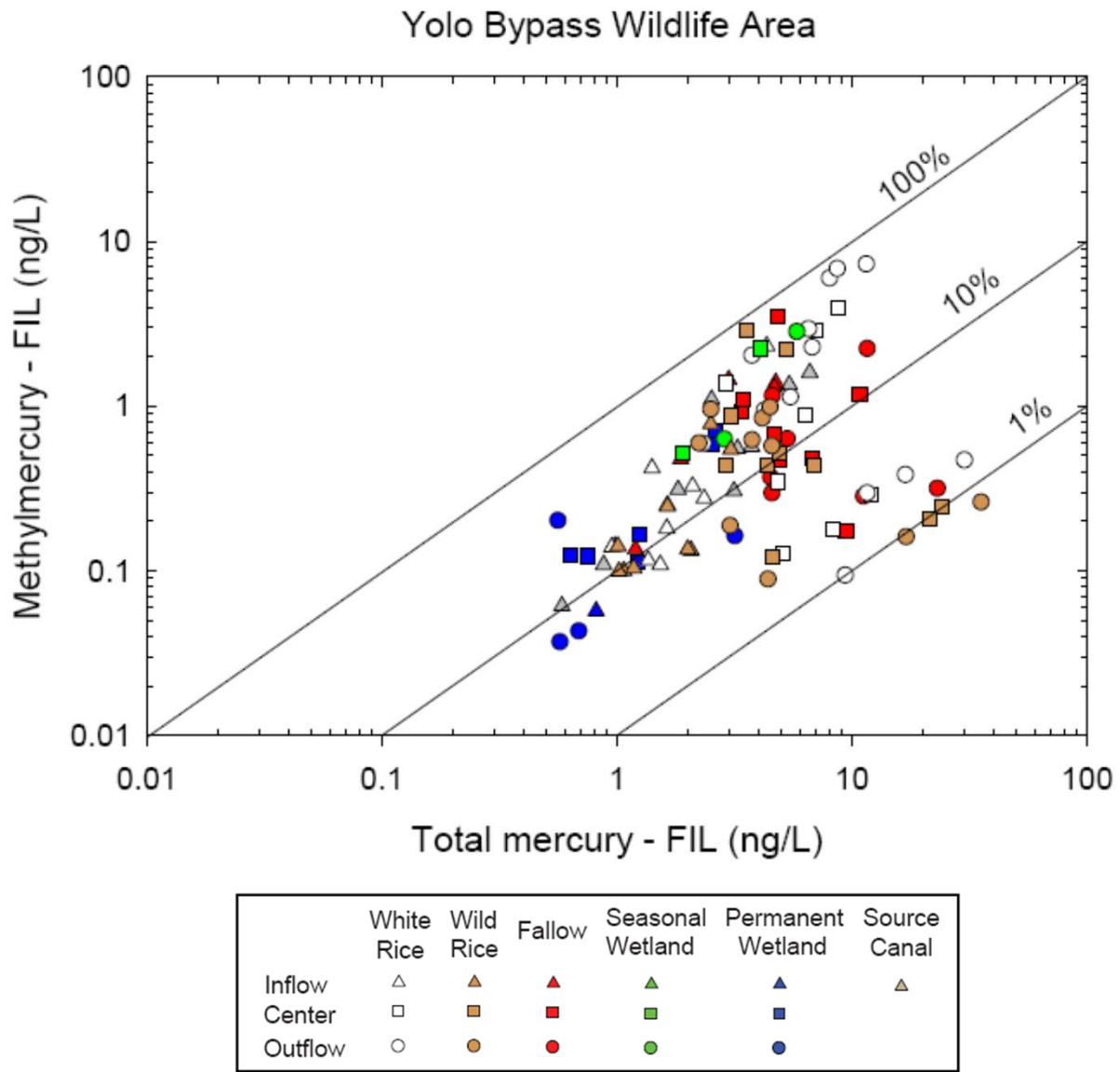


Figure 5.8. Log-log plot of total mercury concentration versus methylmercury concentration in filtered surface water. Diagonal lines represent lines of equal values of the ratio of methylmercury to total mercury.

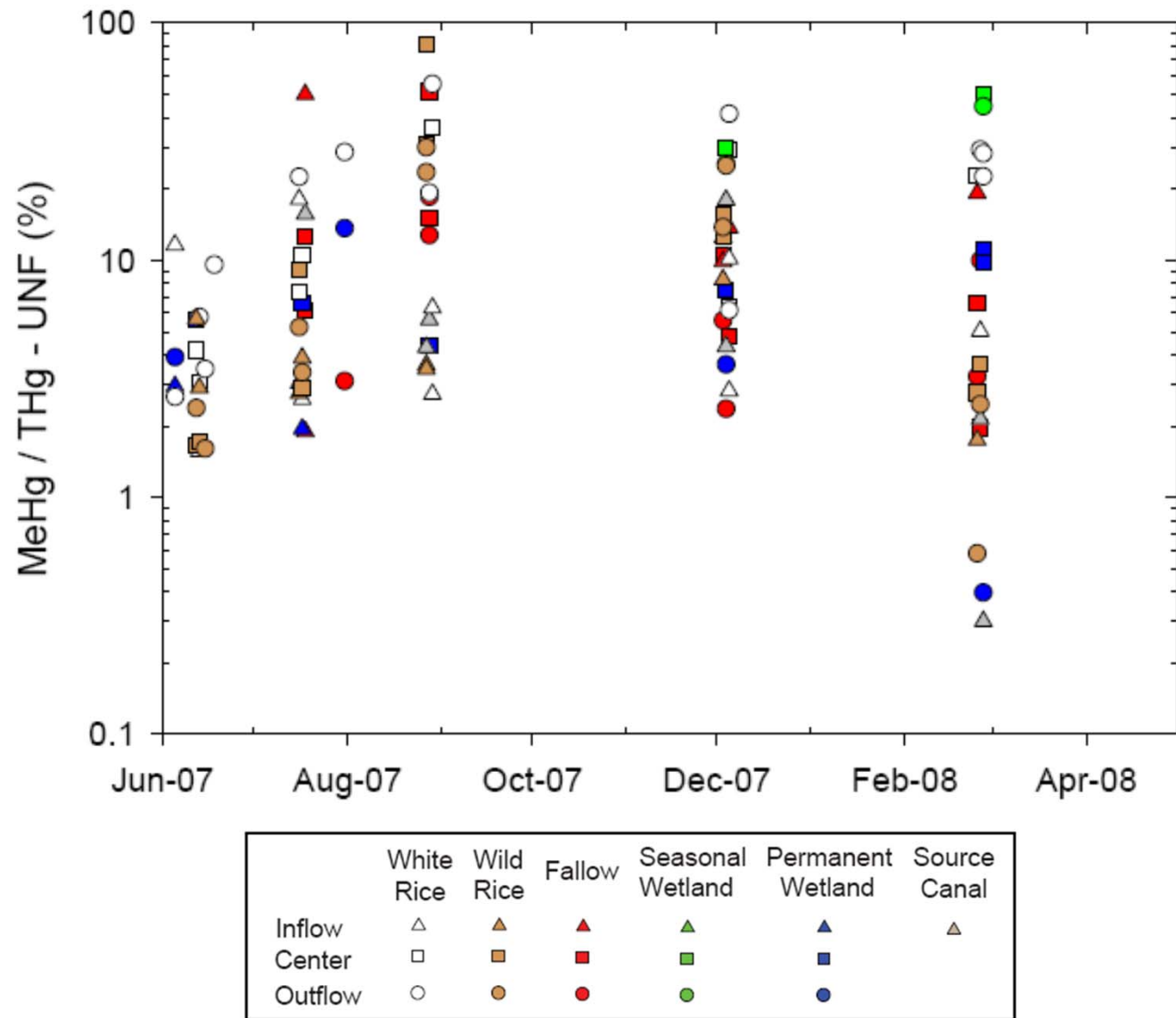


Figure 5.9. Time series plot of the methylmercury-to-total-mercury ratio (MeHg/THg) in unfiltered surface water. The ratio is expressed as a percentage (%THg as MeHg).

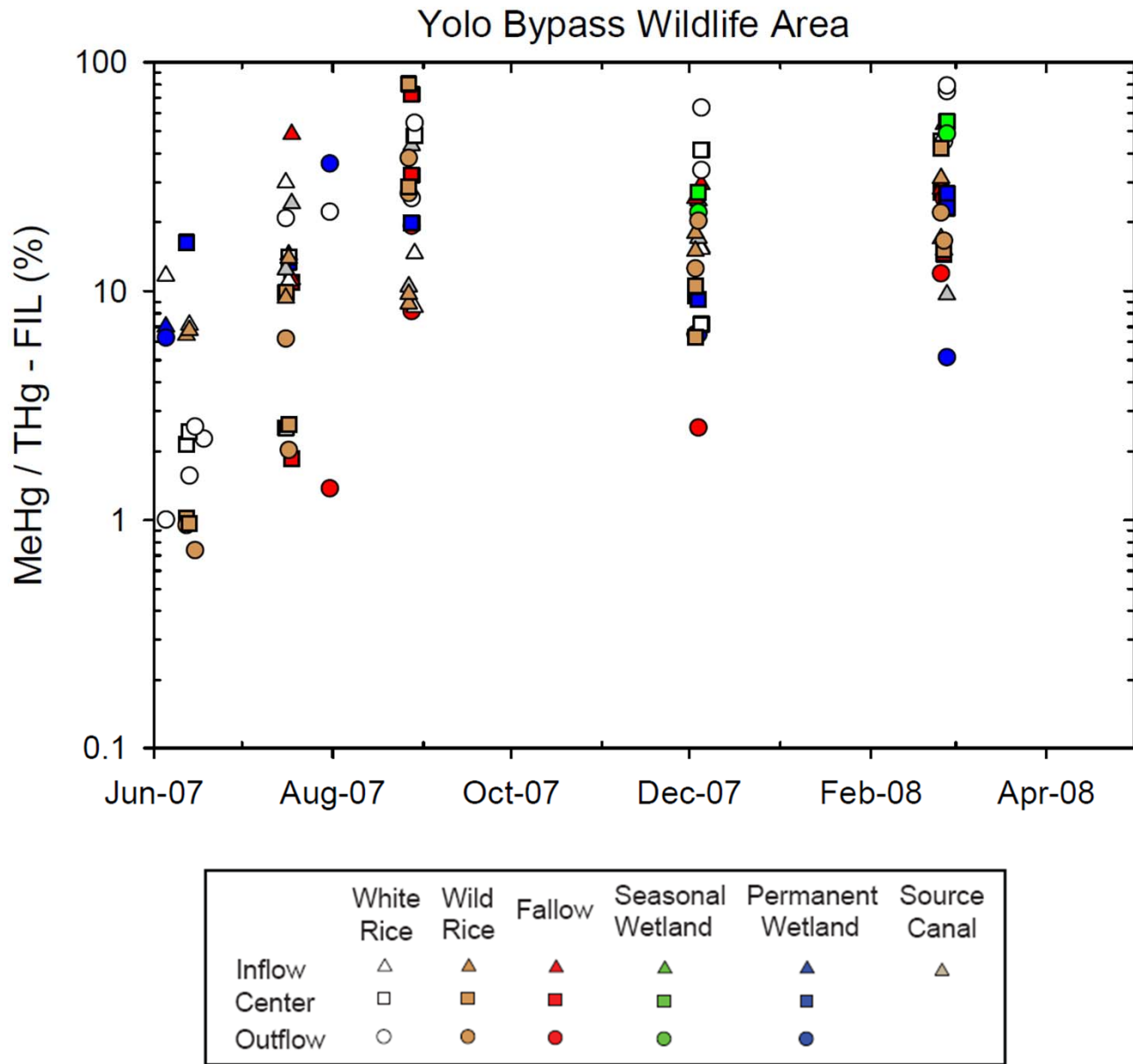


Figure 5.10. Time series plot of the methylmercury to total mercury ratio (MeHg/THg) in filtered surface water. Ratio expressed as a percentage (%THg as MeHg).

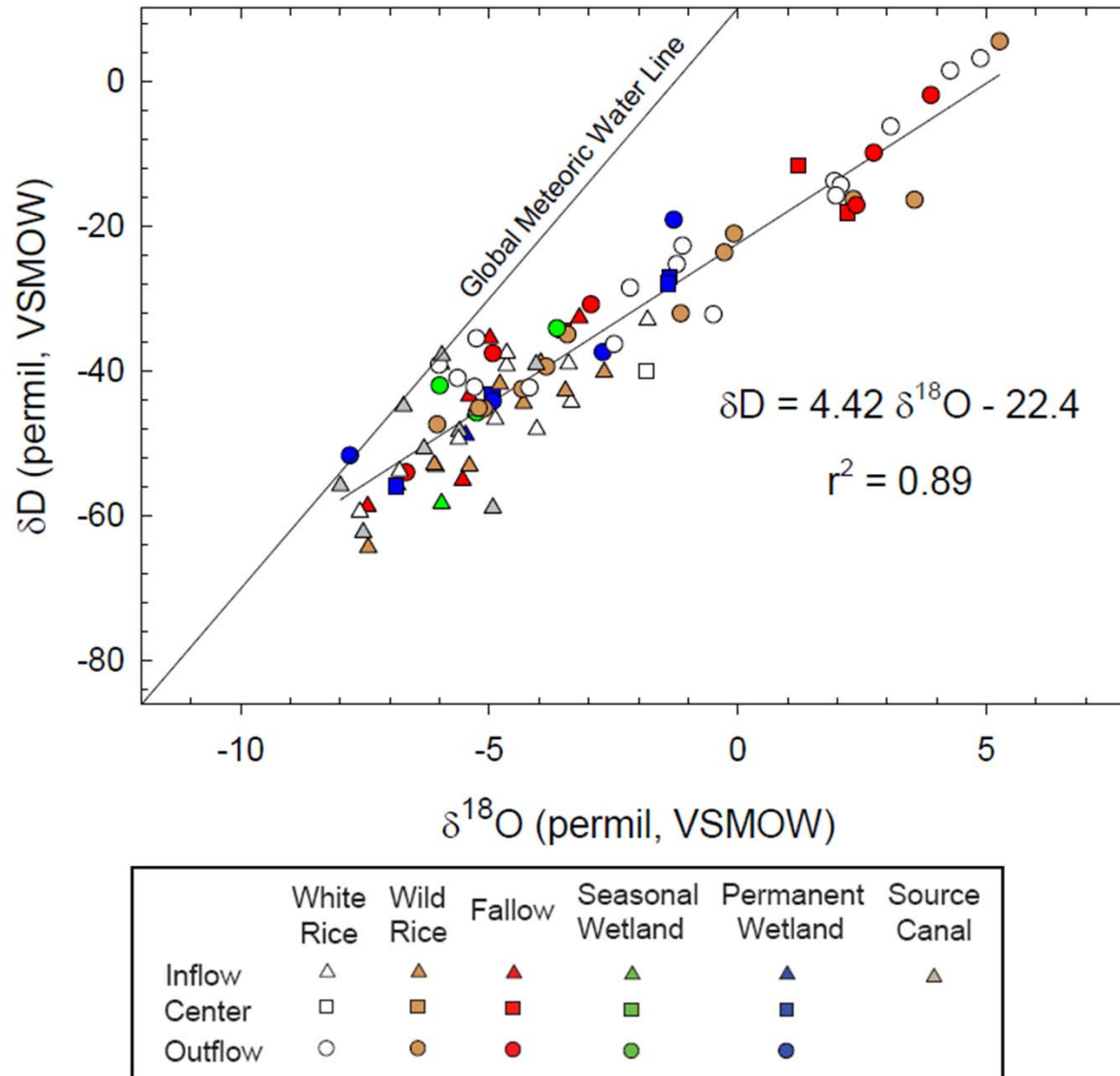


Figure 5.11. Scatter plot of oxygen isotope ratio in water versus hydrogen isotope ratio in water. Oxygen stable isotope ratio $^{18}\text{O}/^{16}\text{O}$ expressed as $\delta^{18}\text{O}$ and hydrogen isotope ratio $^2\text{H}/^1\text{H}$ expressed as δD as explained in text. Ratios are in units of permil (parts per thousand) relative to Vienna Standard Mean Ocean Water (VSMOW). Linear least-squares regression equation and correlation coefficient are indicated. Global Meteoric Water Line [$\delta\text{D} = 8 \delta^{18}\text{O} + 10$], from Clark and Fritz (1997).

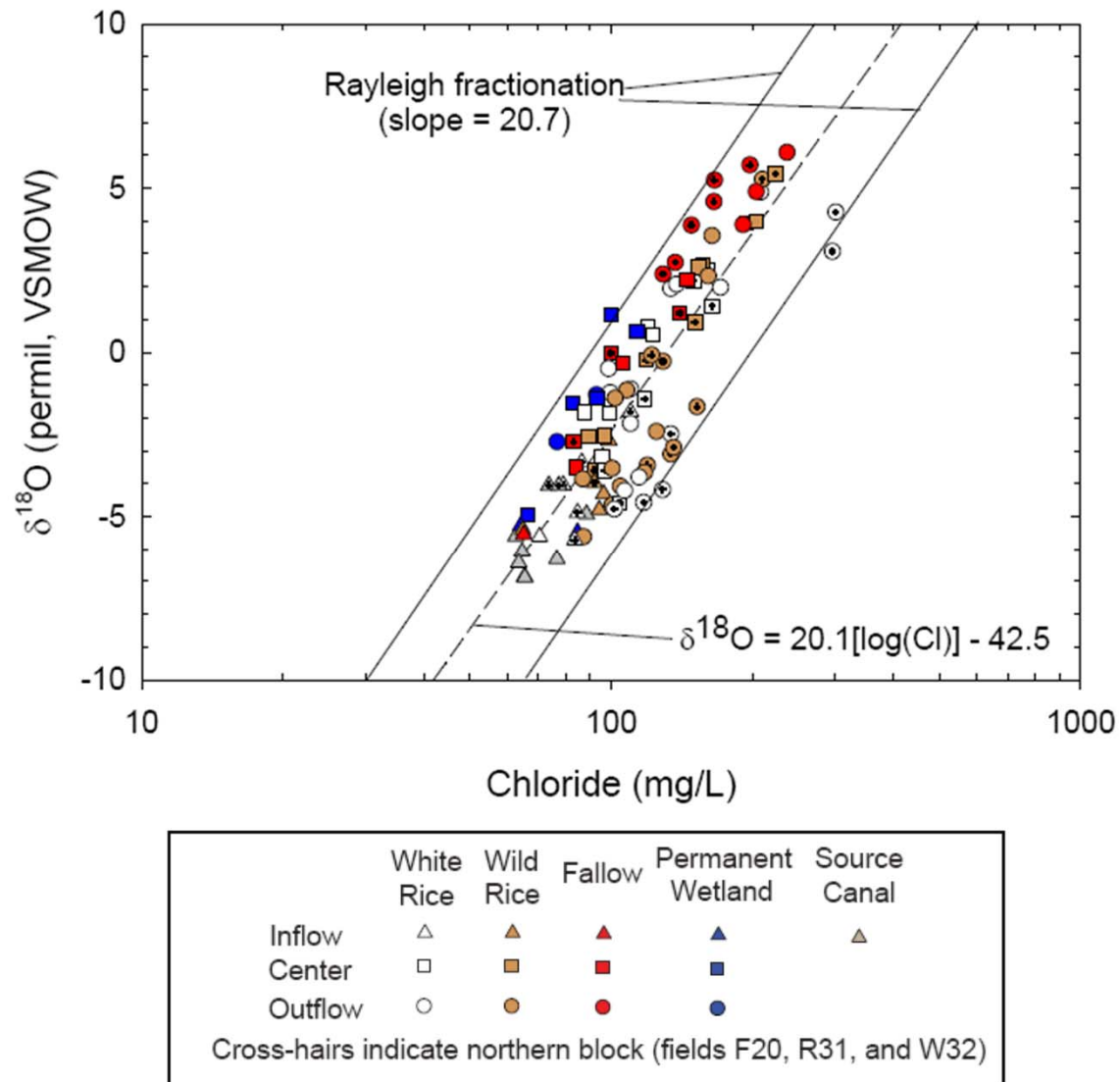


Figure 5.12. Log-linear plot showing relation between chloride concentration and $\delta^{18}\text{O}$ in water for summer irrigation season (June – September, 2007). Linear least-squares regression ($r^2 = 0.76$) compared with theoretical lines indicating Rayleigh fractionation ($\alpha = 1.009$) (Clark and Fritz, 1997).

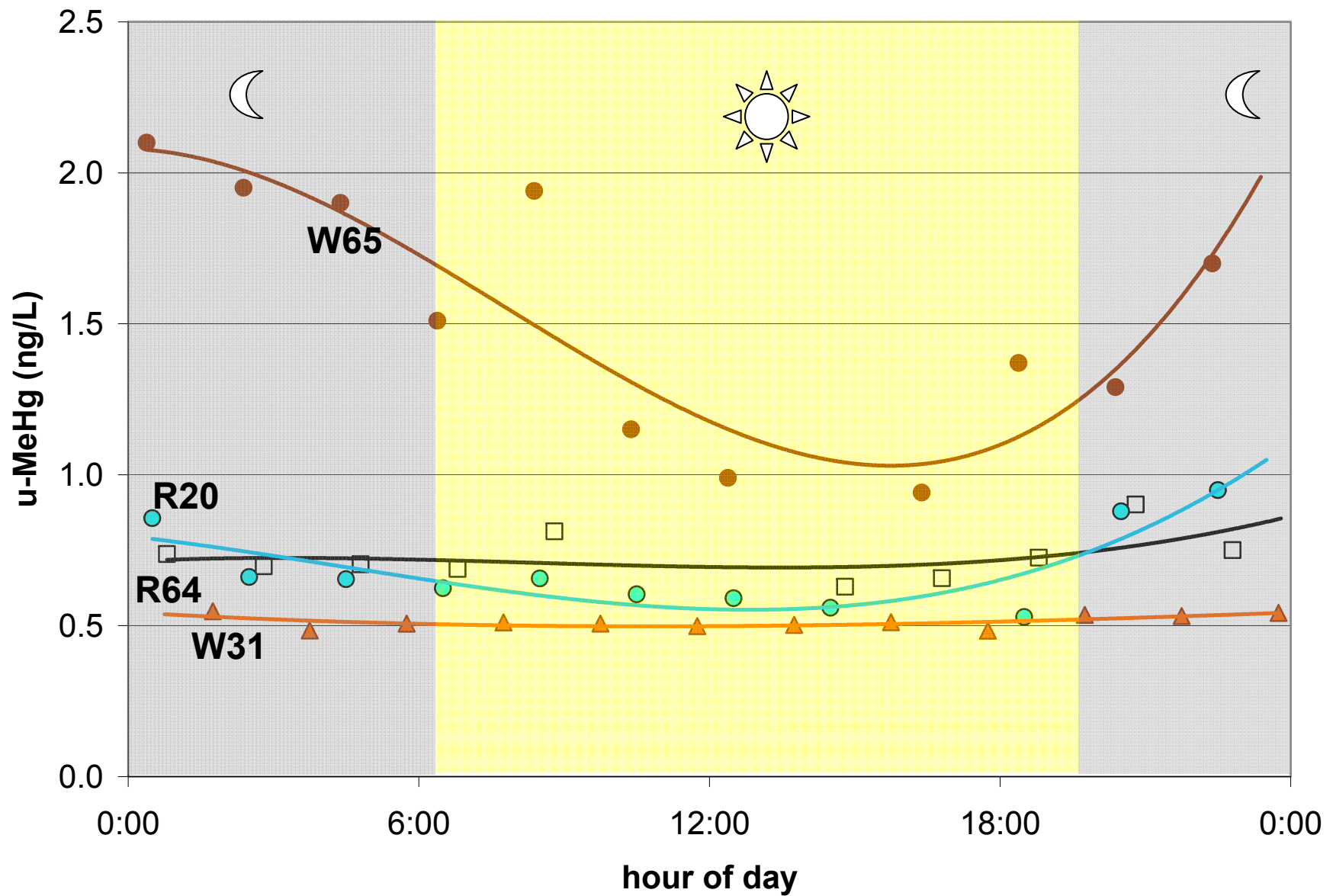


Figure 5.13. Diel time series plot of surface water unfiltered methylmercury concentration (u-MeHg) in four agricultural fields. W65 and R64 measured in summer, 2007; W31 and R20 measured in summer, 2008.

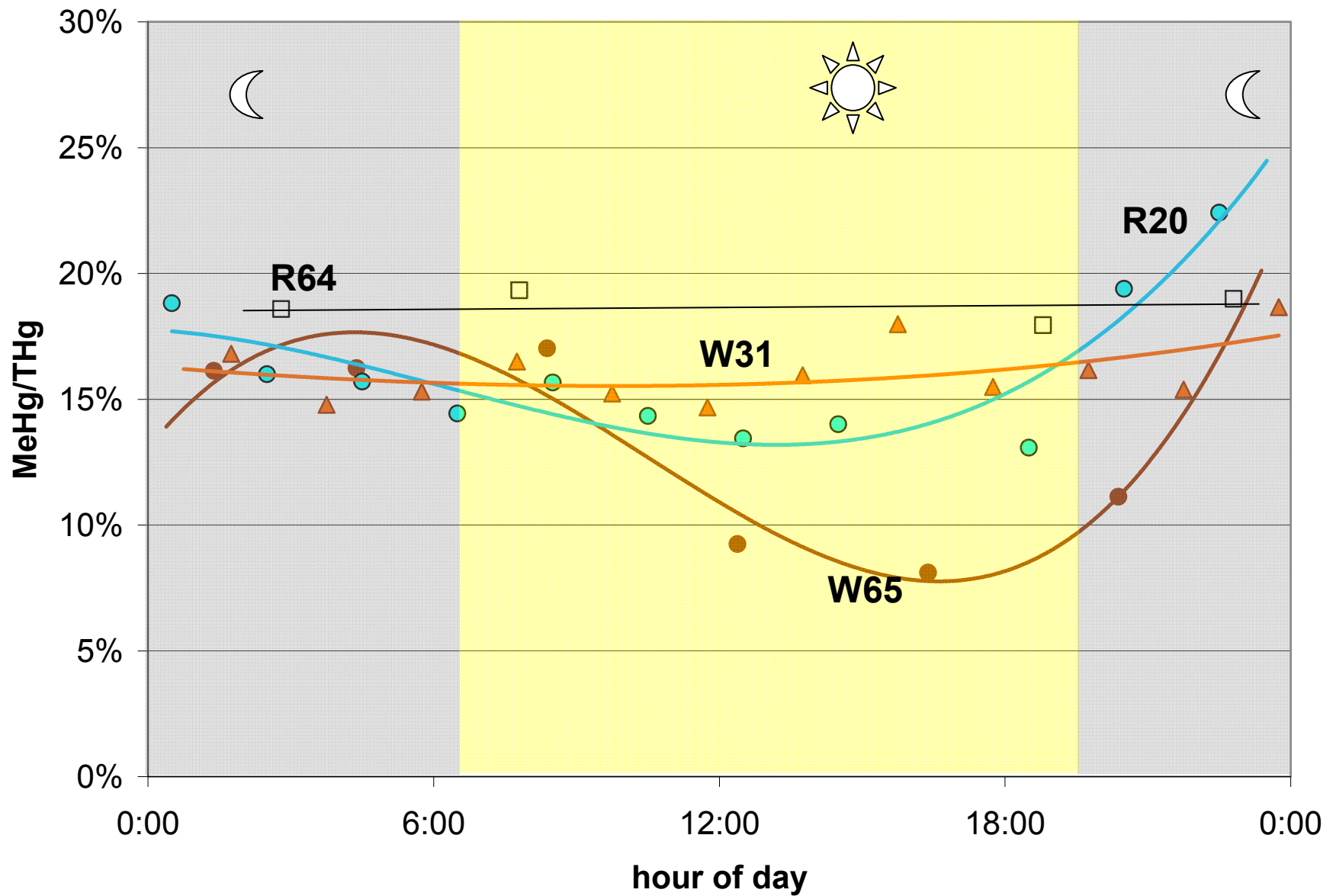


Figure 5.14. Diel time series plot of methylmercury to total mercury ratio (MeHg/THg) in unfiltered surface water from four fields of the Yolo Bypass Wildlife Area. W65 and R64 measured in summer 2007; W31 and R20 measured in summer 2008. The ratio is expressed as a percentage (%THg as MeHg).

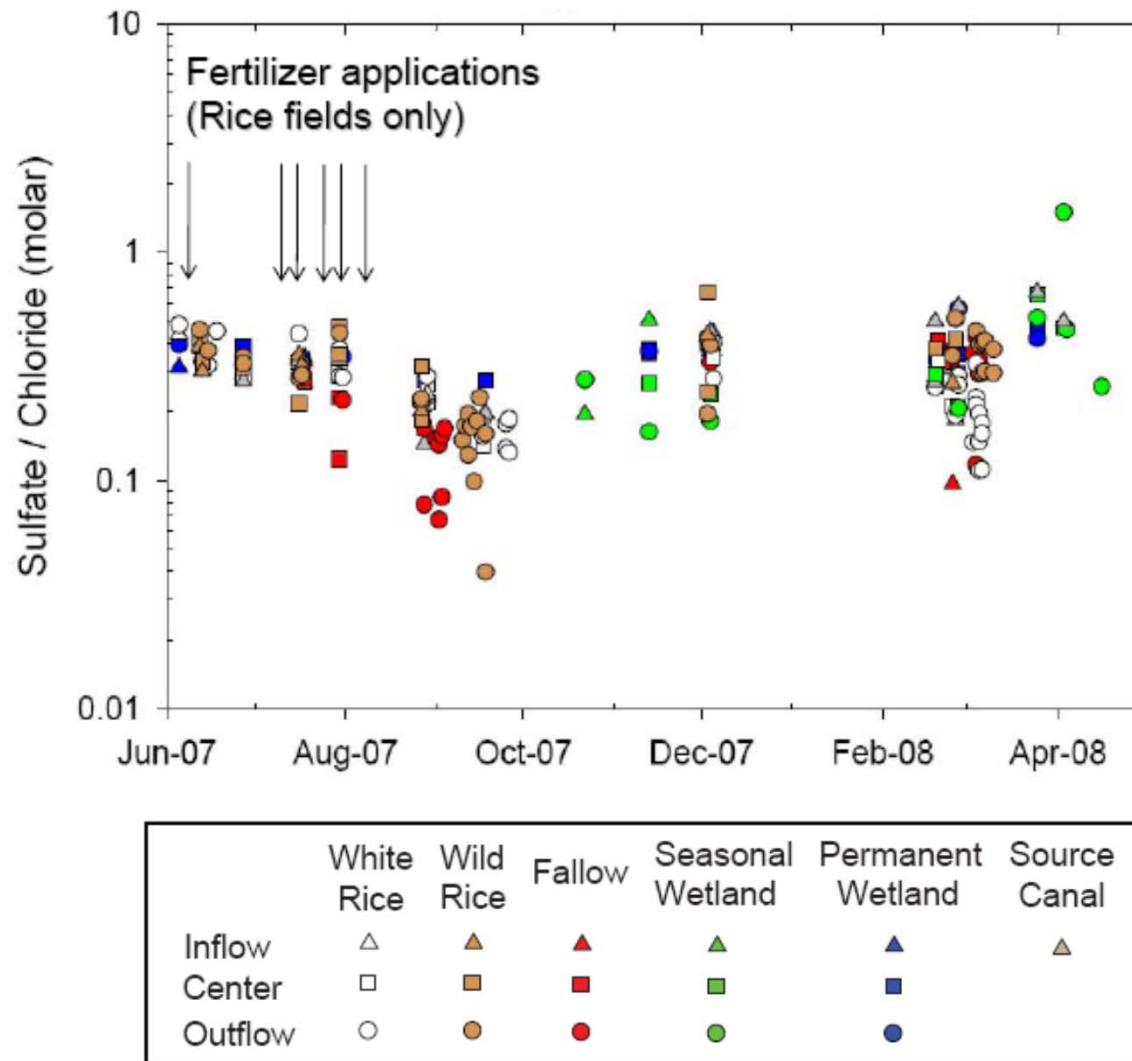


Figure 5.15. Time series plot of the sulfate-to-chloride molar ratio in filtered surface water. The timing of the application of sulfate-bearing fertilizer to white rice and wild rice fields is indicated by the arrows.

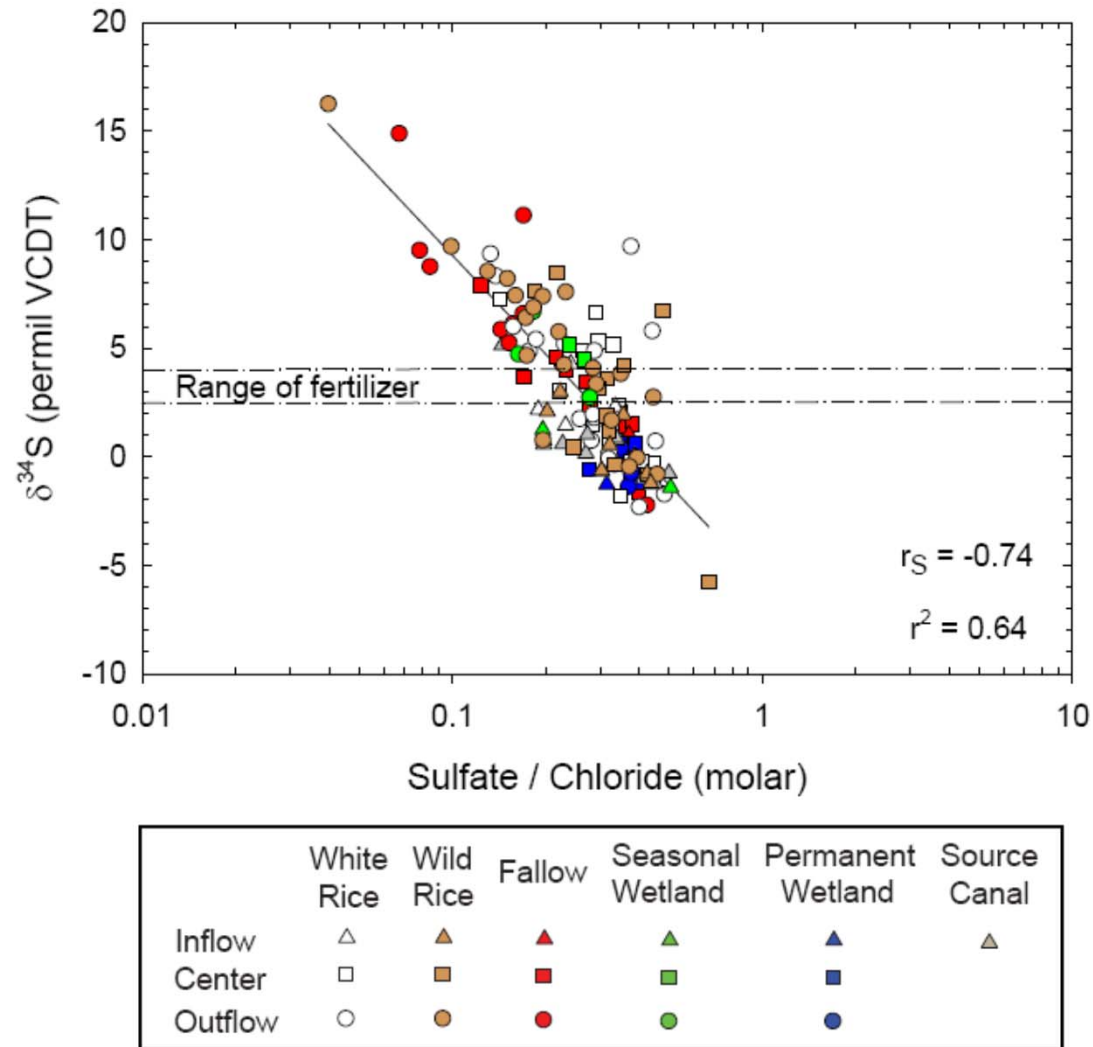


Figure 5.16. Log-log plot of sulfate-to-chloride molar ratio versus sulfur stable isotope ratio in aqueous sulfate in filtered surface water. Sulfur stable isotope ratio $^{34}\text{S}/^{32}\text{S}$ expressed as $\delta^{34}\text{S}$ as explained in text. Range of sulfur isotope values of fertilizer shown by the horizontal dashed lines. Sulfur isotope values above 4 permil indicate isotopic enrichment in pool of residual sulfate after microbial sulfate reduction has preferentially removed ^{32}S relative to ^{34}S . Linear least-squares regression coefficient (r^2) and Spearman rank order correlation coefficient (r_s) are shown.

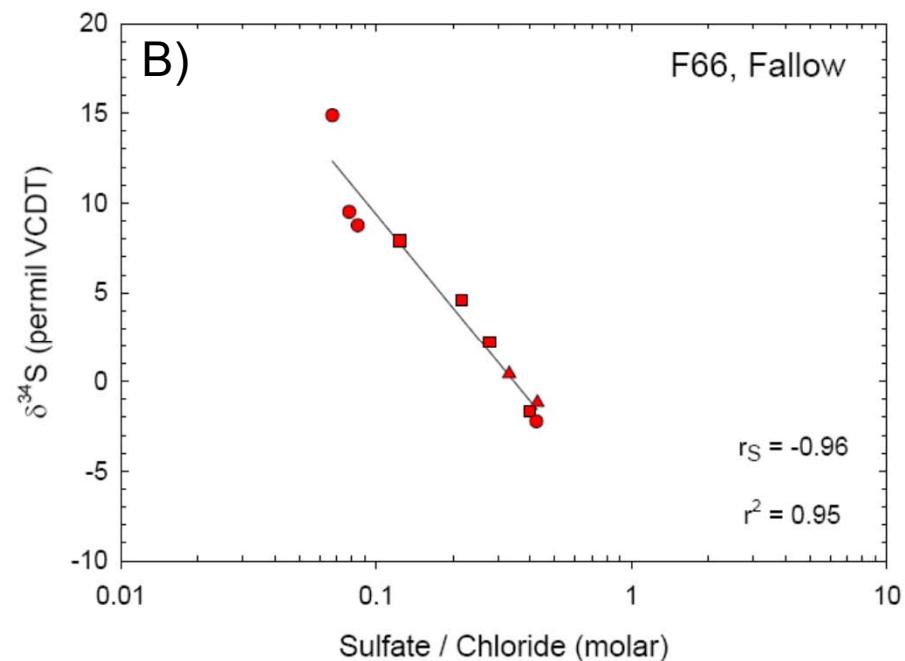
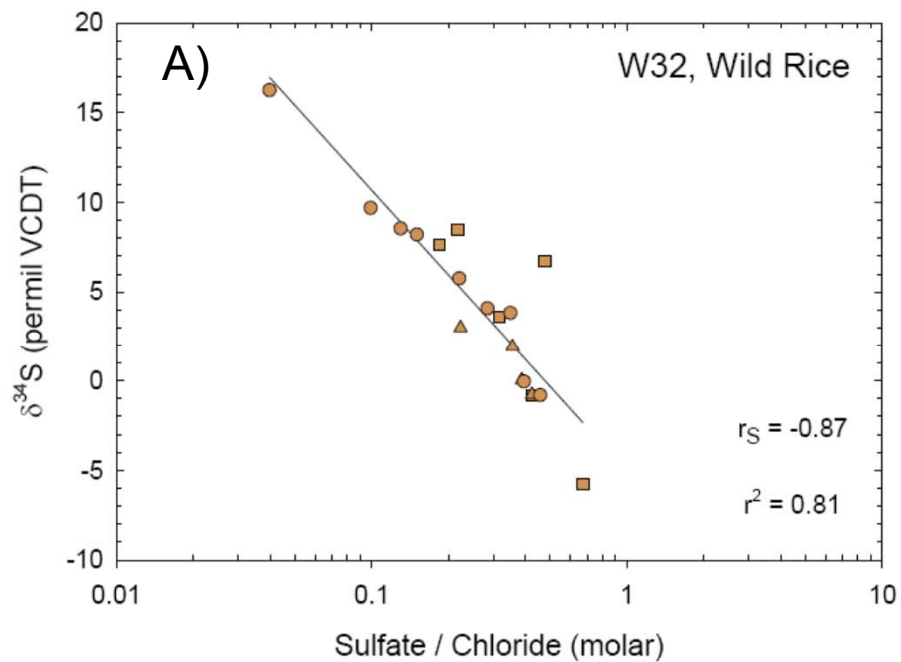


Figure 5.17. Log-linear plots of sulfate-to-chloride molar ratio versus sulfur stable isotope ratio in filtered surface water for (A) wild rice field W32, and (B) fallow field F66. Linear least-squares regression coefficients (r^2) and Spearman rank order correlation coefficients (r_S) are shown.

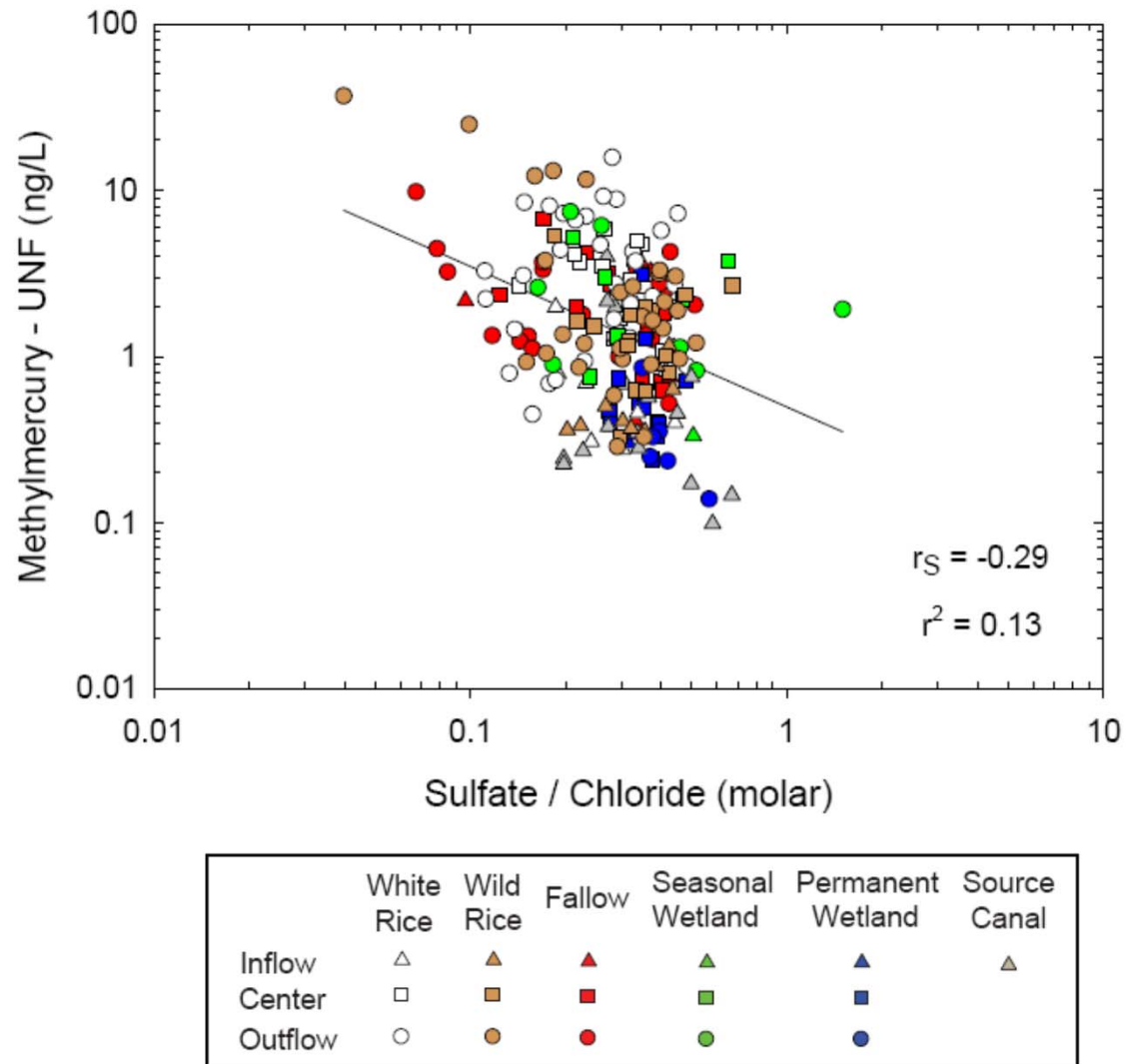


Figure 5.18. Log-log plot of sulfate-to-chloride molar ratio in filtered surface water versus methylmercury concentration in unfiltered surface water. Linear least-squares regression coefficient (r^2) and Spearman rank order correlation coefficient (r_s) are shown.

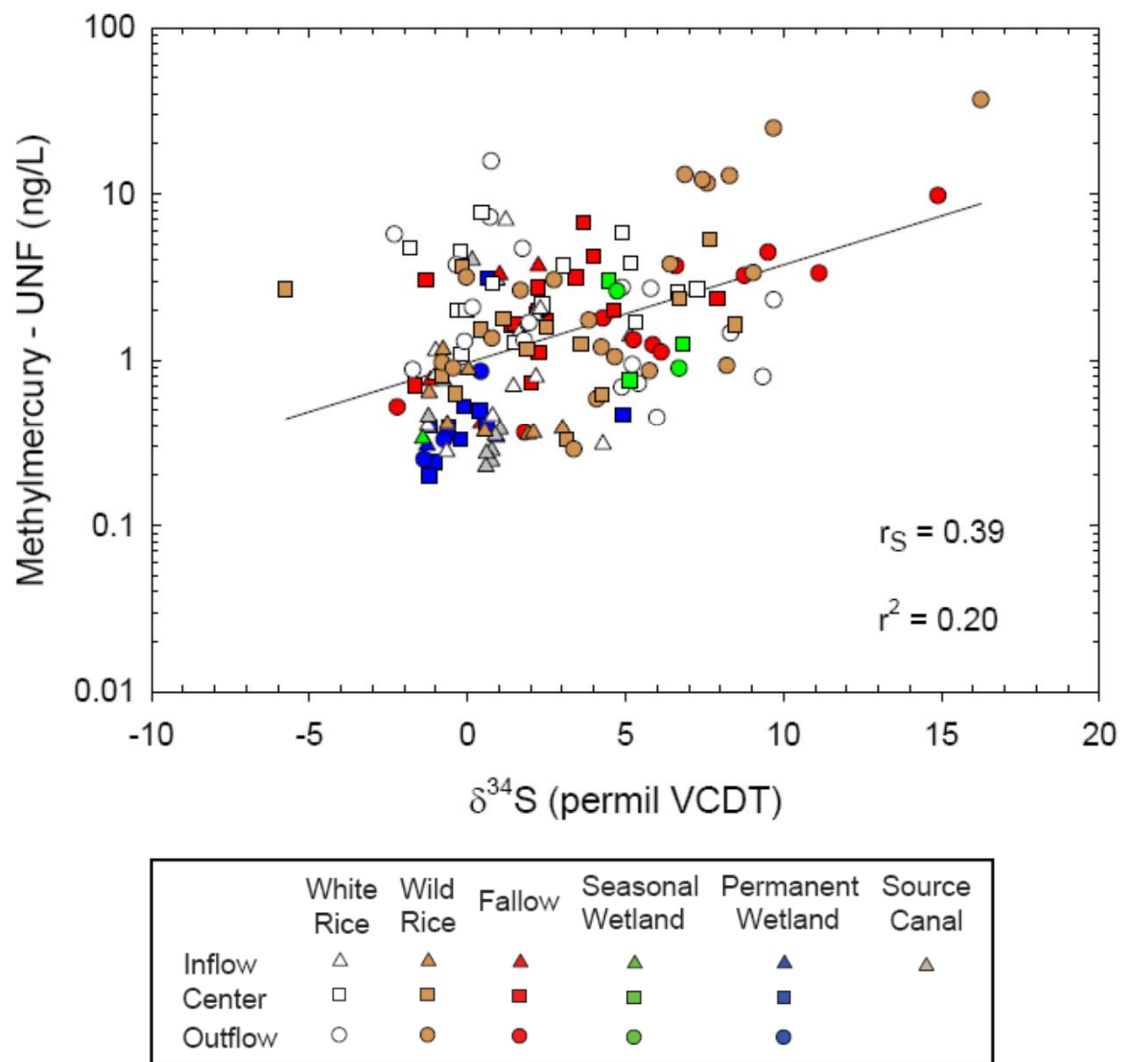


Figure 5.19. Linear-log plot of sulfur stable isotope ratio in aqueous sulfate versus unfiltered methylmercury concentration in surface water. Linear least-squares regression coefficient (r^2) and Spearman rank correlation coefficient (r_s) are shown.

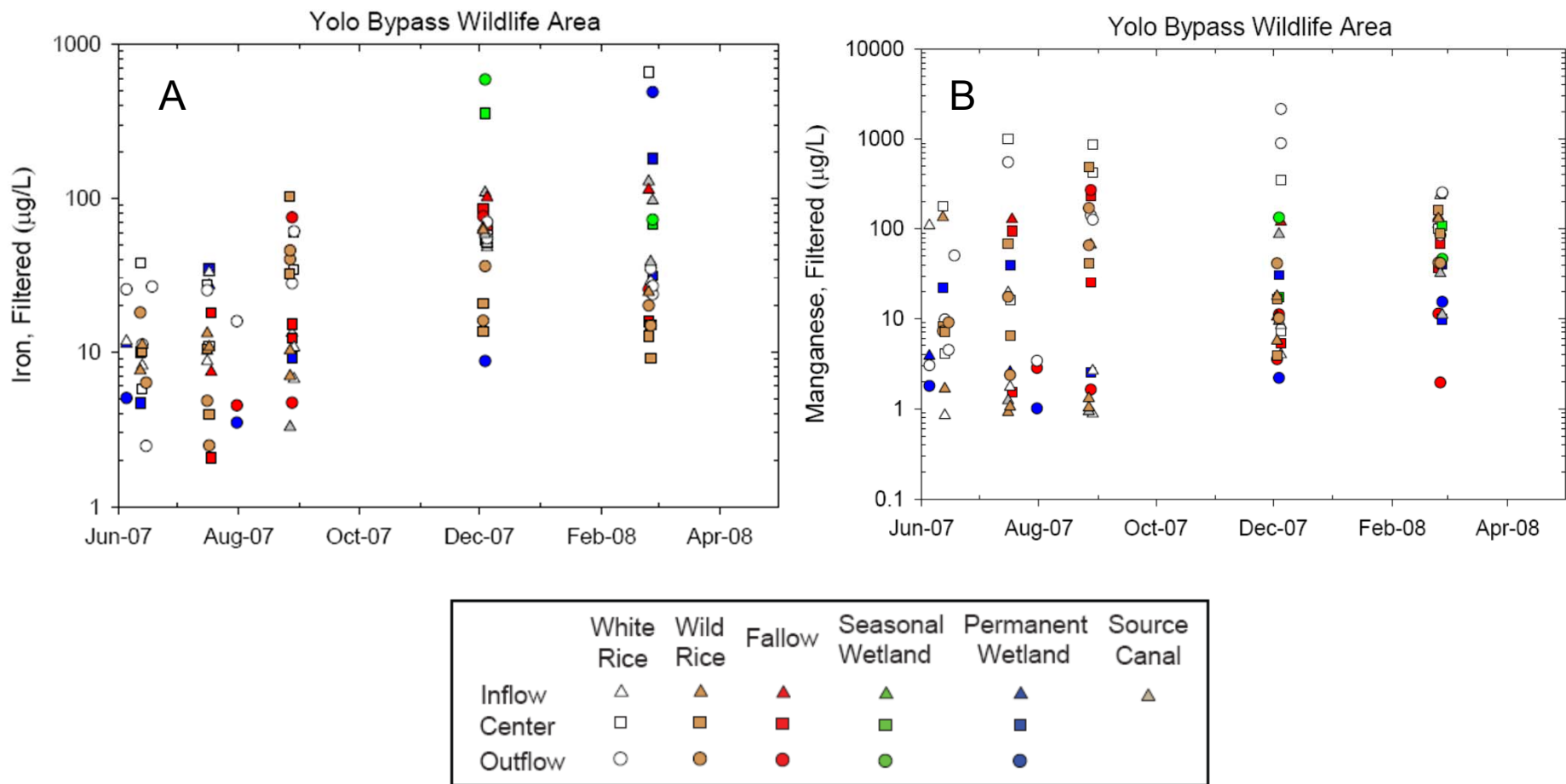


Figure 5.20. Time series plots of (A) iron concentration and (B) manganese concentration in filtered surface water. Note different logarithmic scales in A and B.

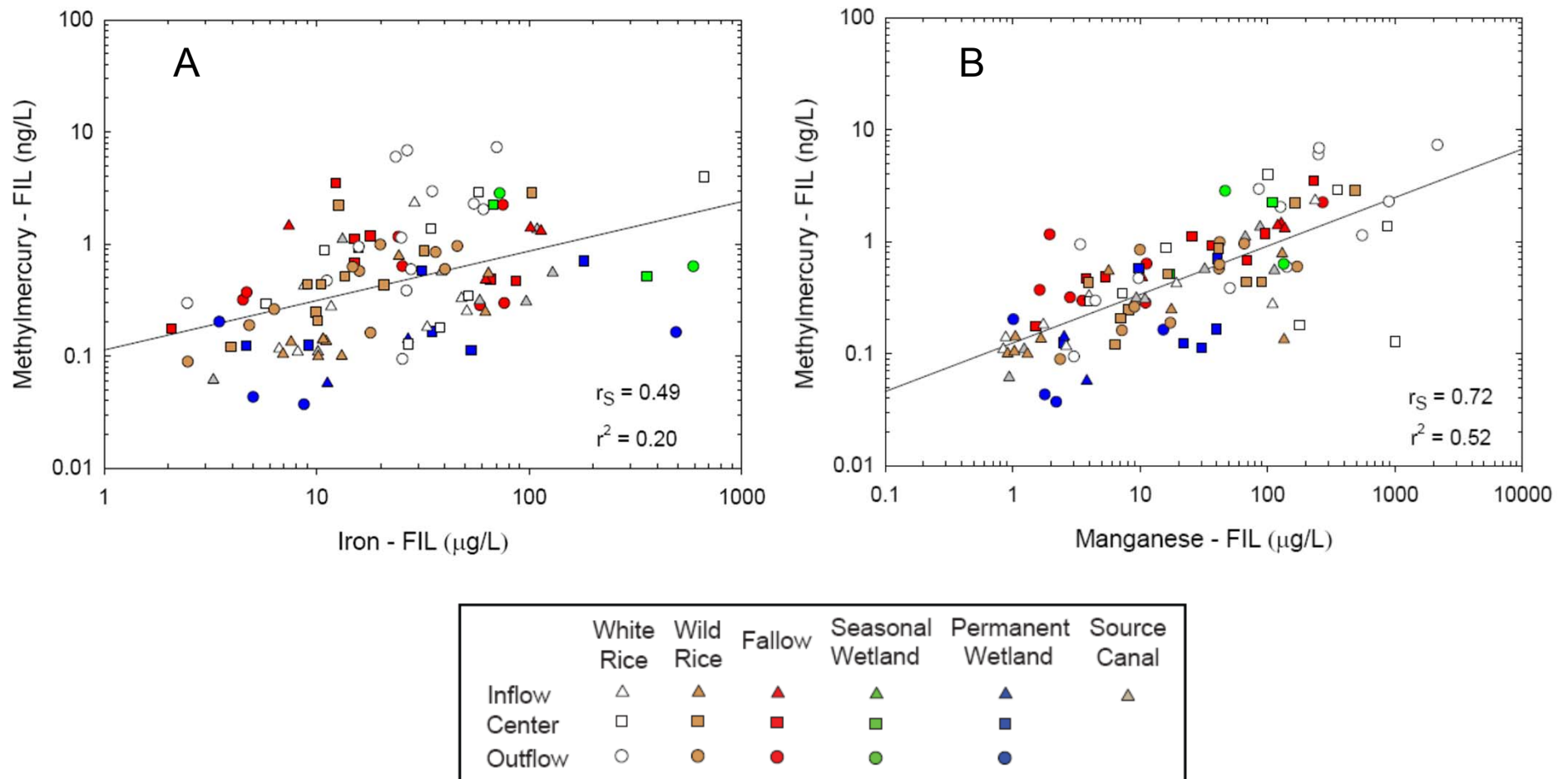
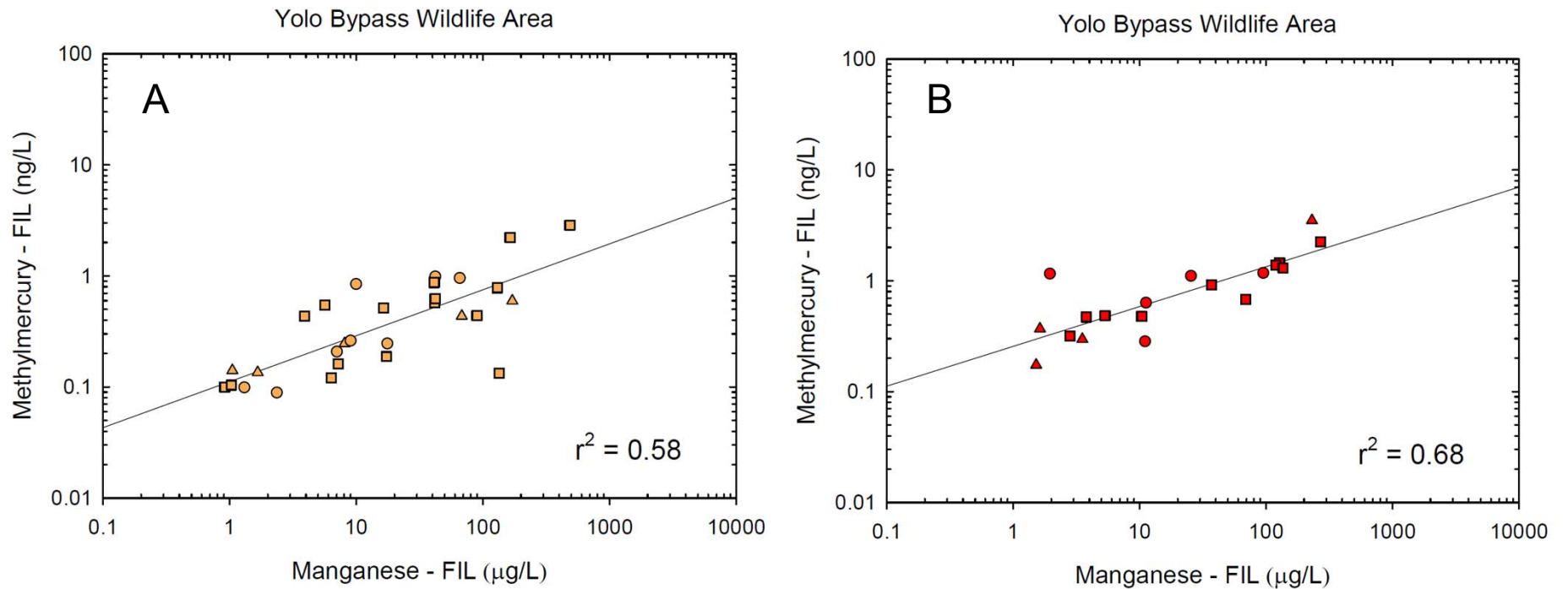


Figure 5.21. Log-log plots of (A) iron concentration and (B) manganese concentration versus methylmercury concentration in filtered surface water. Linear least-squares regression coefficients (r^2) and Spearman rank correlation coefficients (r_s) are shown.



	White Rice	Wild Rice	Fallow	Seasonal Wetland	Permanent Wetland	Source Canal
Inflow	△	▲	▲	▲	▲	▲
Center	□	■	■	■	■	▲
Outflow	○	●	●	●	●	

Figure 5.22. Log-log plots of manganese concentration versus methylmercury concentration in filtered surface water from (A) wild rice fields and (B) fallow fields. Linear least-squares regression coefficients are shown.

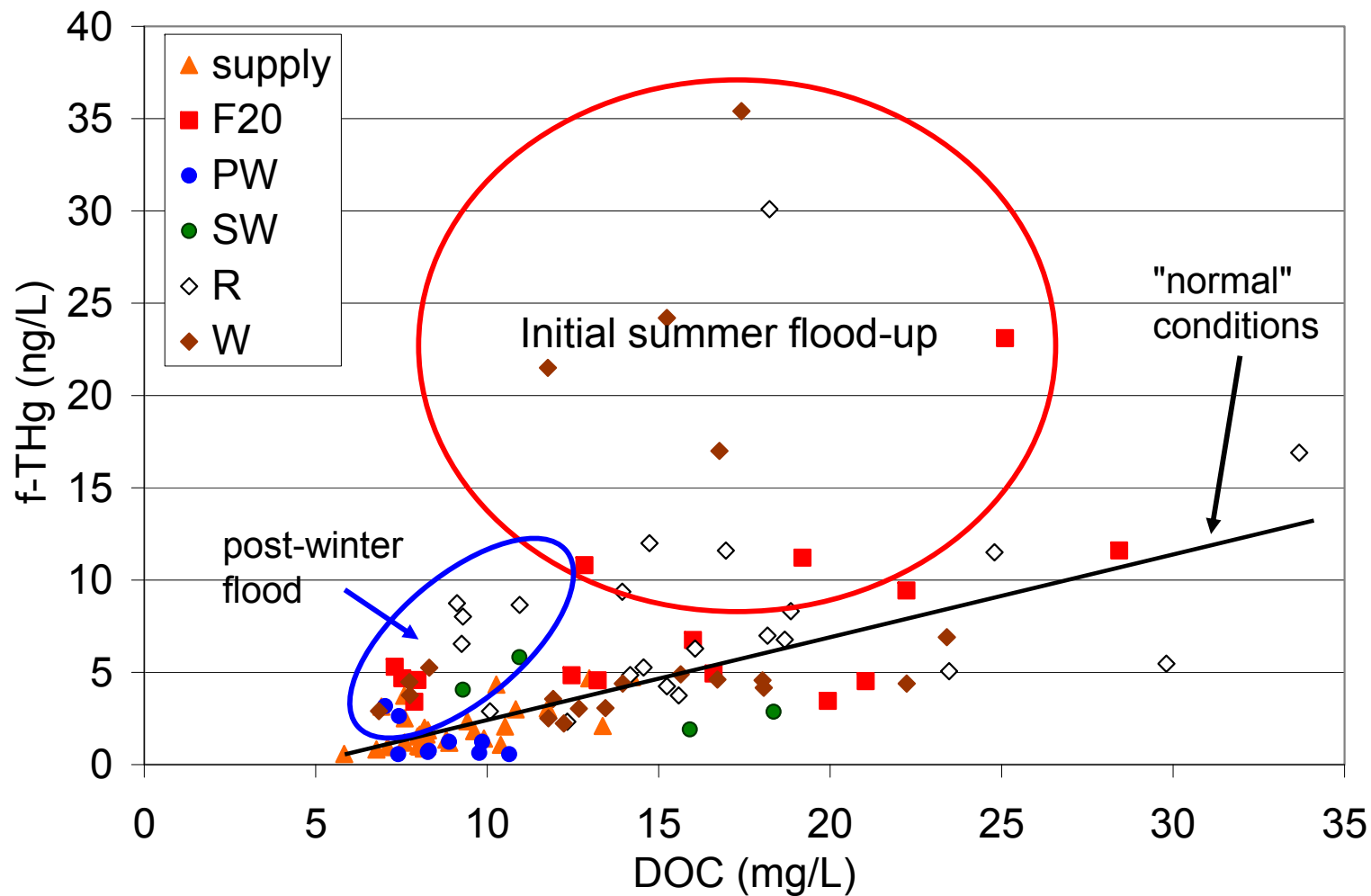


Figure 5.23. Scatter plot of surface water dissolved organic carbon (DOC) versus filtered total mercury (f-THg). This relationship varies across three conditions: initial summer irrigation, normal flow-through conditions and post-winter flood.

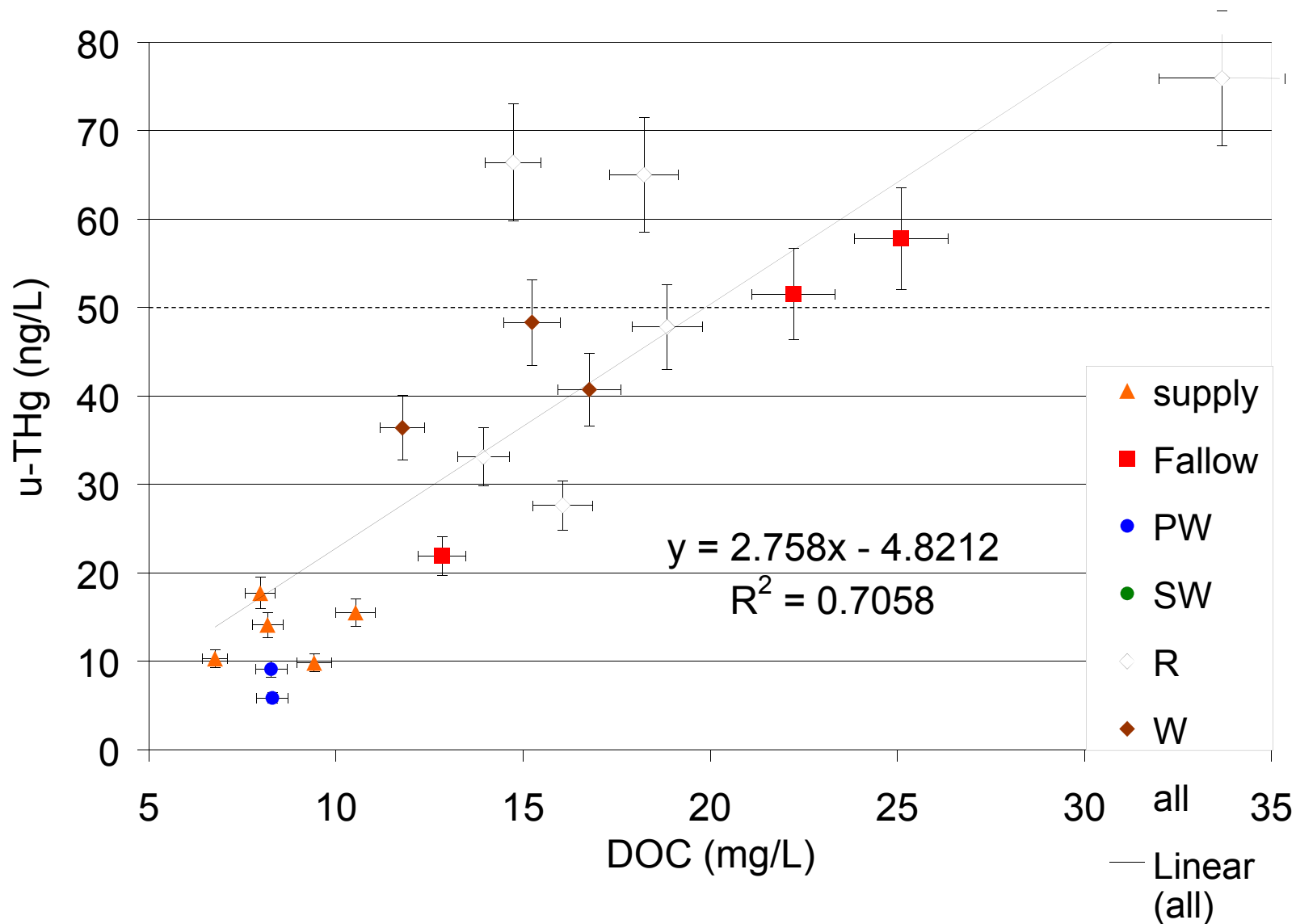


Figure 5.24. Scatter plot of surface water dissolved organic carbon (DOC) versus unfiltered total mercury (u-THg) within 30 days of the initial irrigation of the agricultural fields during early summer. During this period, DOC and filtered total mercury (f-THg) are poorly correlated (see **Figure 5.21**). Dotted line indicates concentrations of u-THg above the 50 ng/L water-quality criterion for the California Toxics Rule (CTR, U.S. Environmental Protection Agency, 2000b). Linear least-squares regression equation and coefficient are shown.

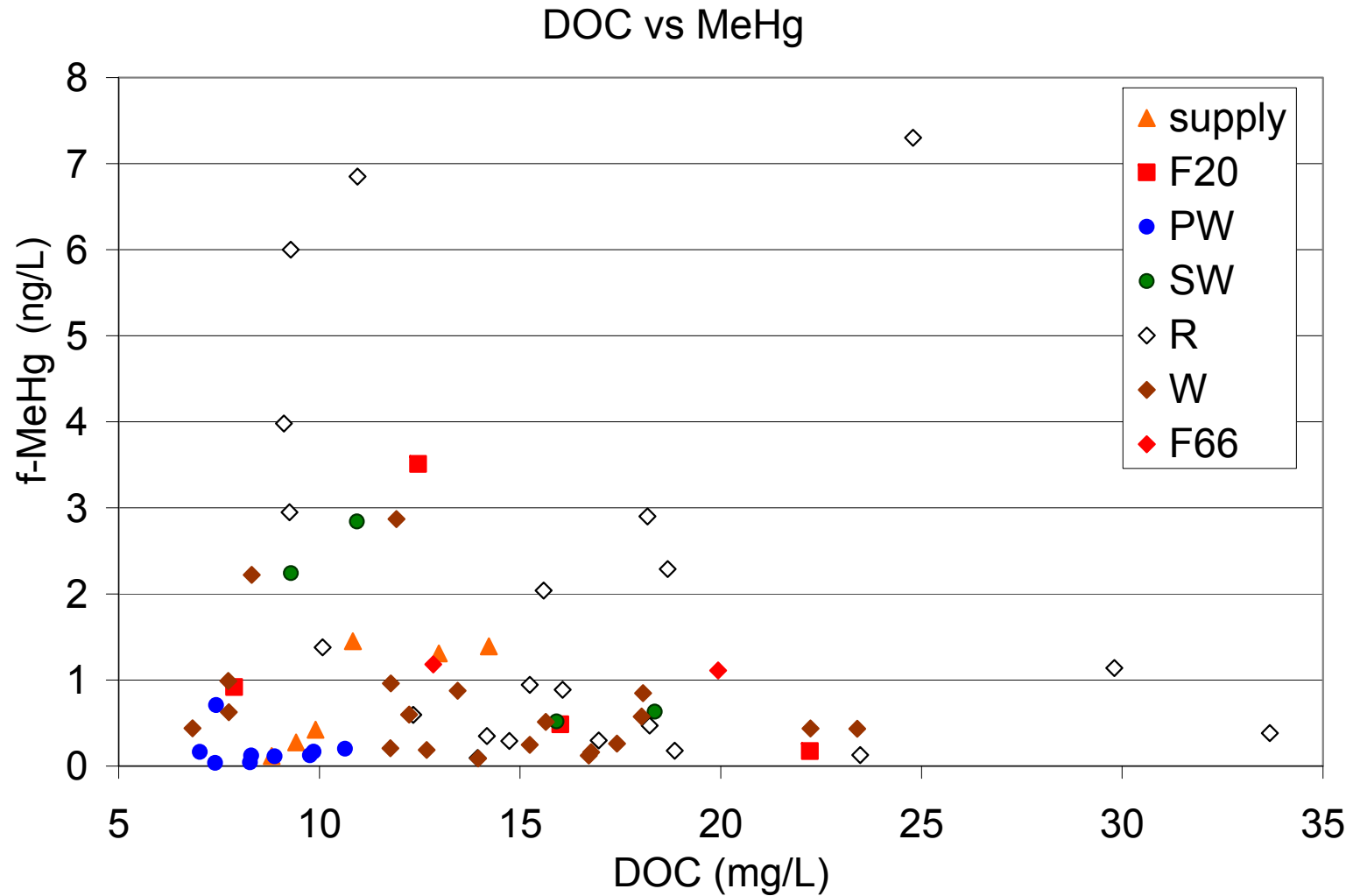


Figure 5.25. Scatter plot of surface water dissolved organic carbon (DOC) versus filtered methylmercury (f-MeHg). This relation was highly variable in agricultural fields (F20 and F66, fallow; R, white rice; W, wild rice) compared with non-agricultural wetlands (PW, permanent wetland; SW, seasonal wetland).

"natural" wetlands

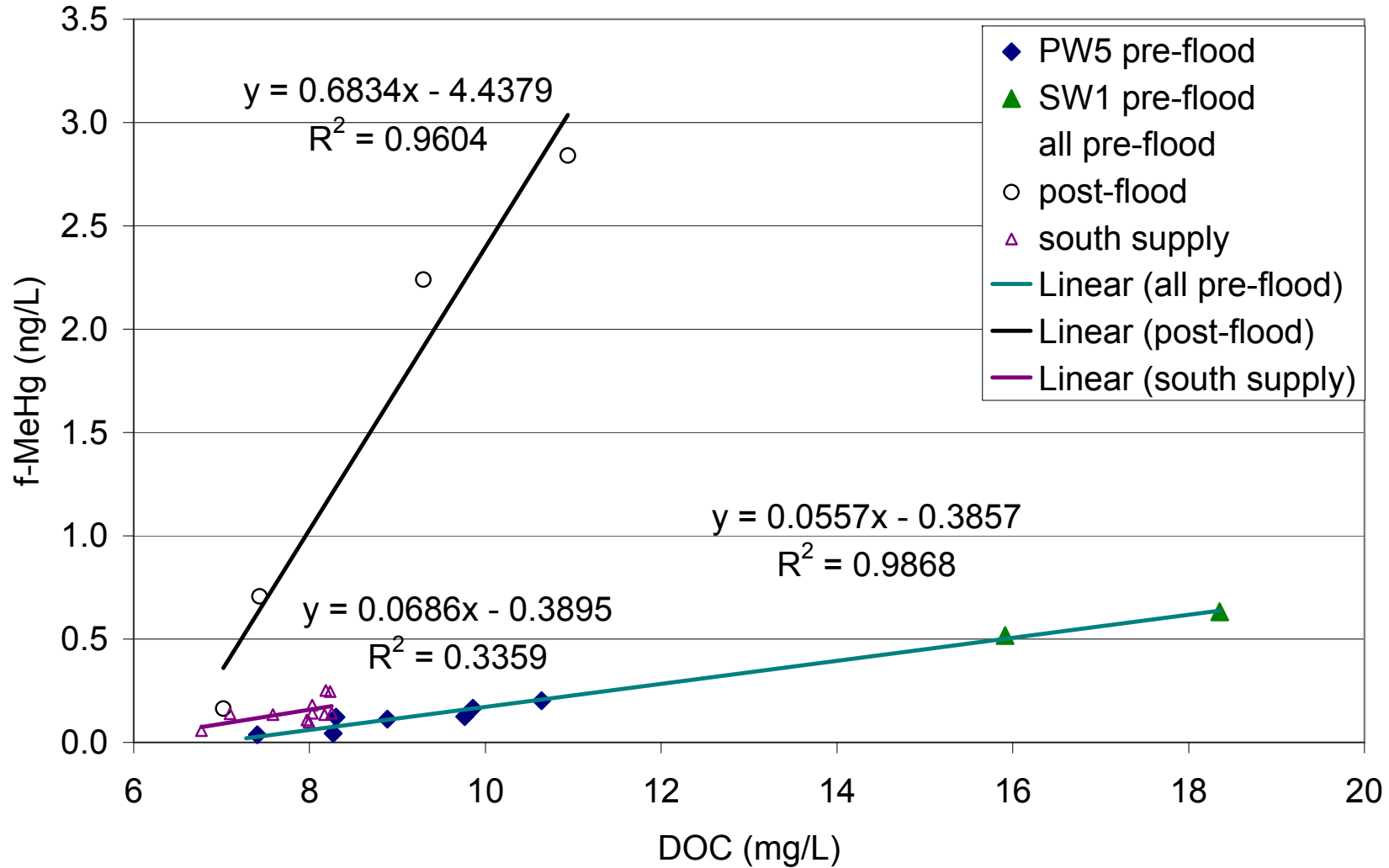


Figure 5.26. Scatter plot of surface water dissolved organic carbon (DOC) versus filtered methylmercury (f-MeHg) in the non-agricultural wetlands. The high slope of the post-flood samples shows markedly different relationship during the winter 2008 flood compared to the rest of the water year. (PW5, permanent wetland; SW1, seasonal wetland)

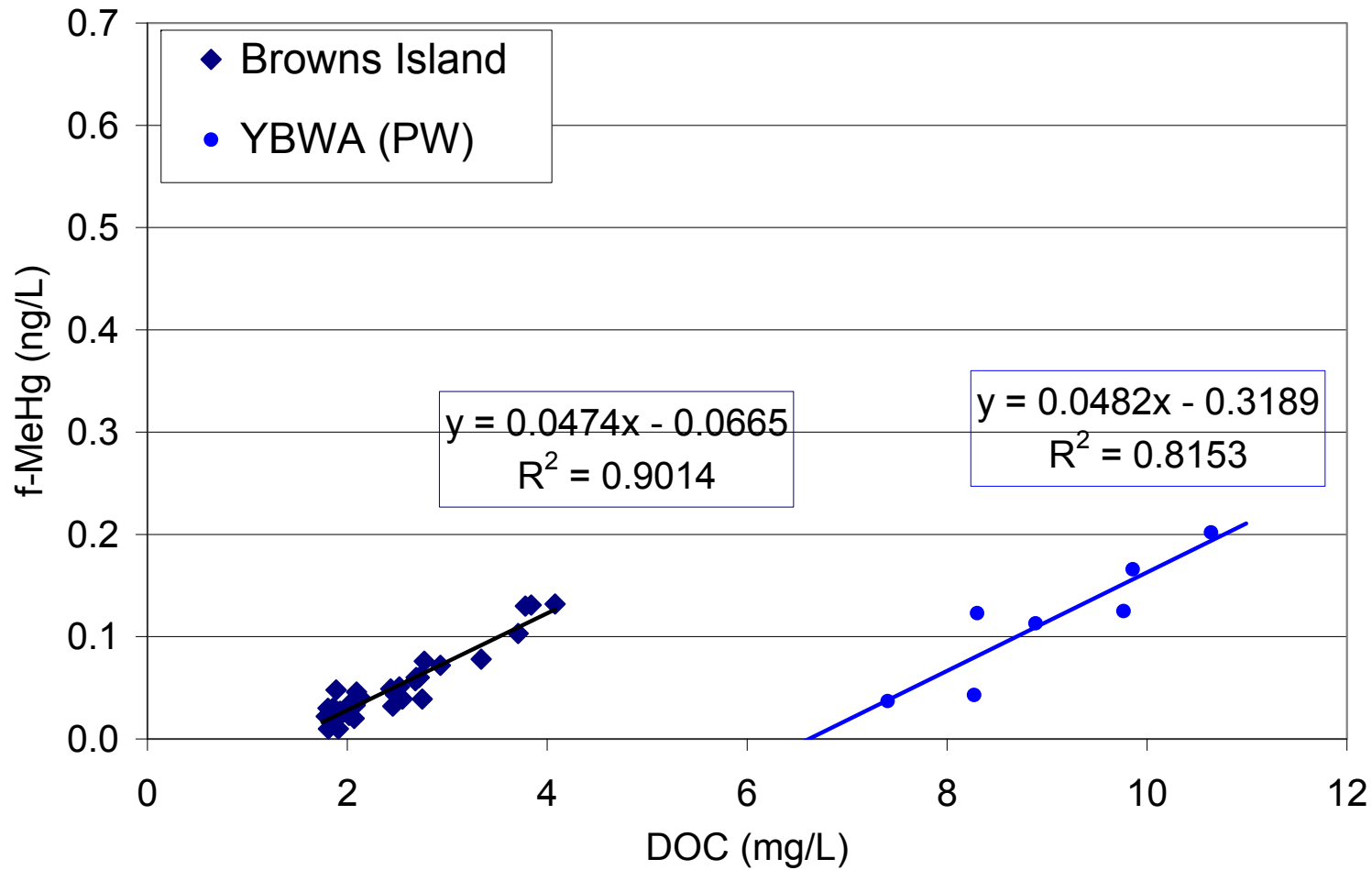


Figure 5.27. Scatter plot of surface water dissolved organic carbon (DOC) versus filtered methylmercury (f-MeHg) for the permanent wetland (PW) site in the Yolo Bypass Wildlife Area and for Browns Island, a tidal wetland in the San Francisco Bay-Delta.

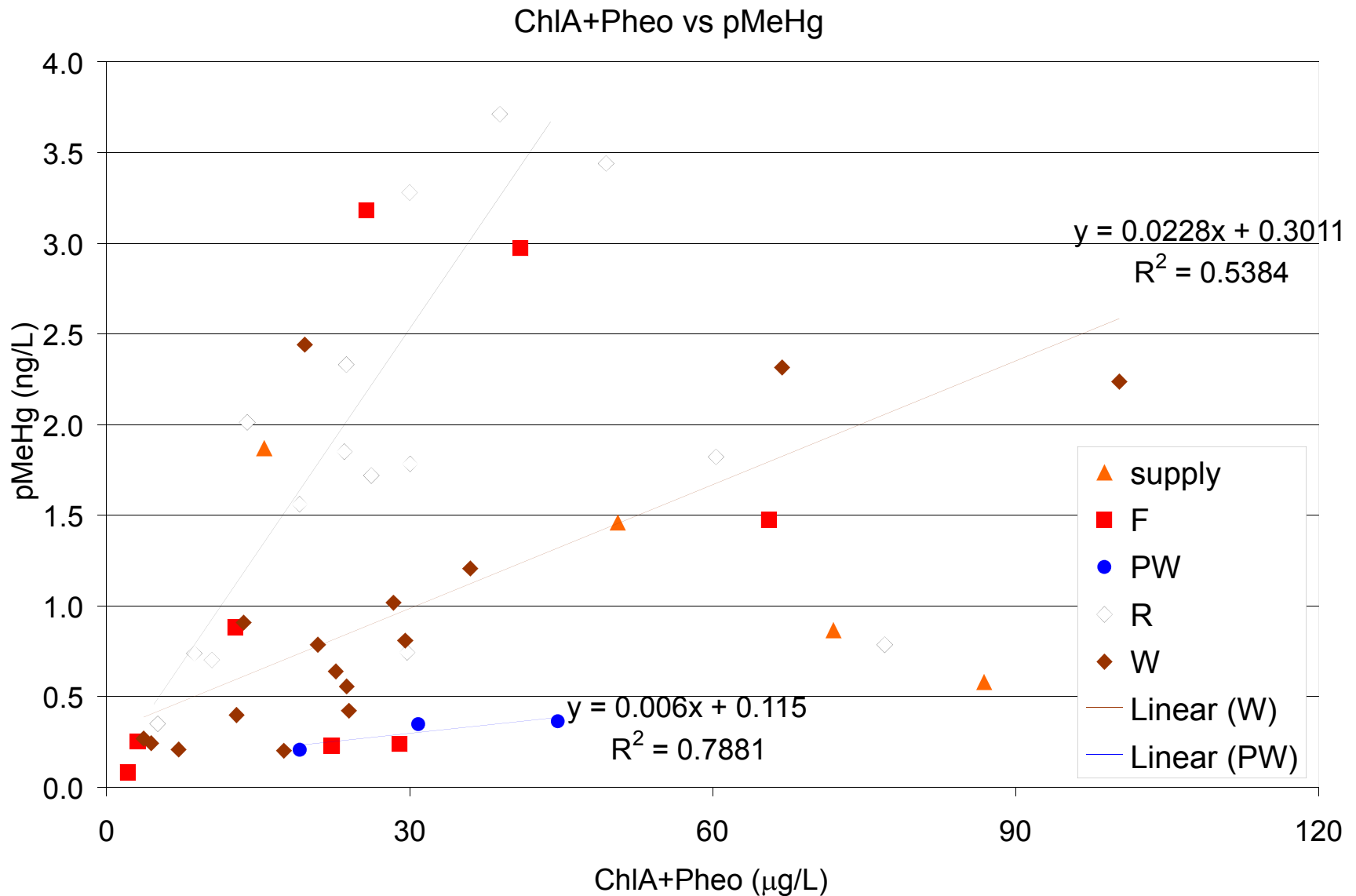


Figure 5.28. Scatter plot of surface water particulate algal concentration (as chlorophyll-a plus pheophytin; Chl-a+Pheo) versus particulate methylmercury (pMeHg) concentration. The relationship differs among field types -- fallow (F) and white rice (R) fields possess high slopes, permanent wetlands (PW) possess the lowest slope, and wild rice (W) fields fall in between. Linear least-squares regression equations and coefficients are shown for wild rice fields and the permanent wetland.

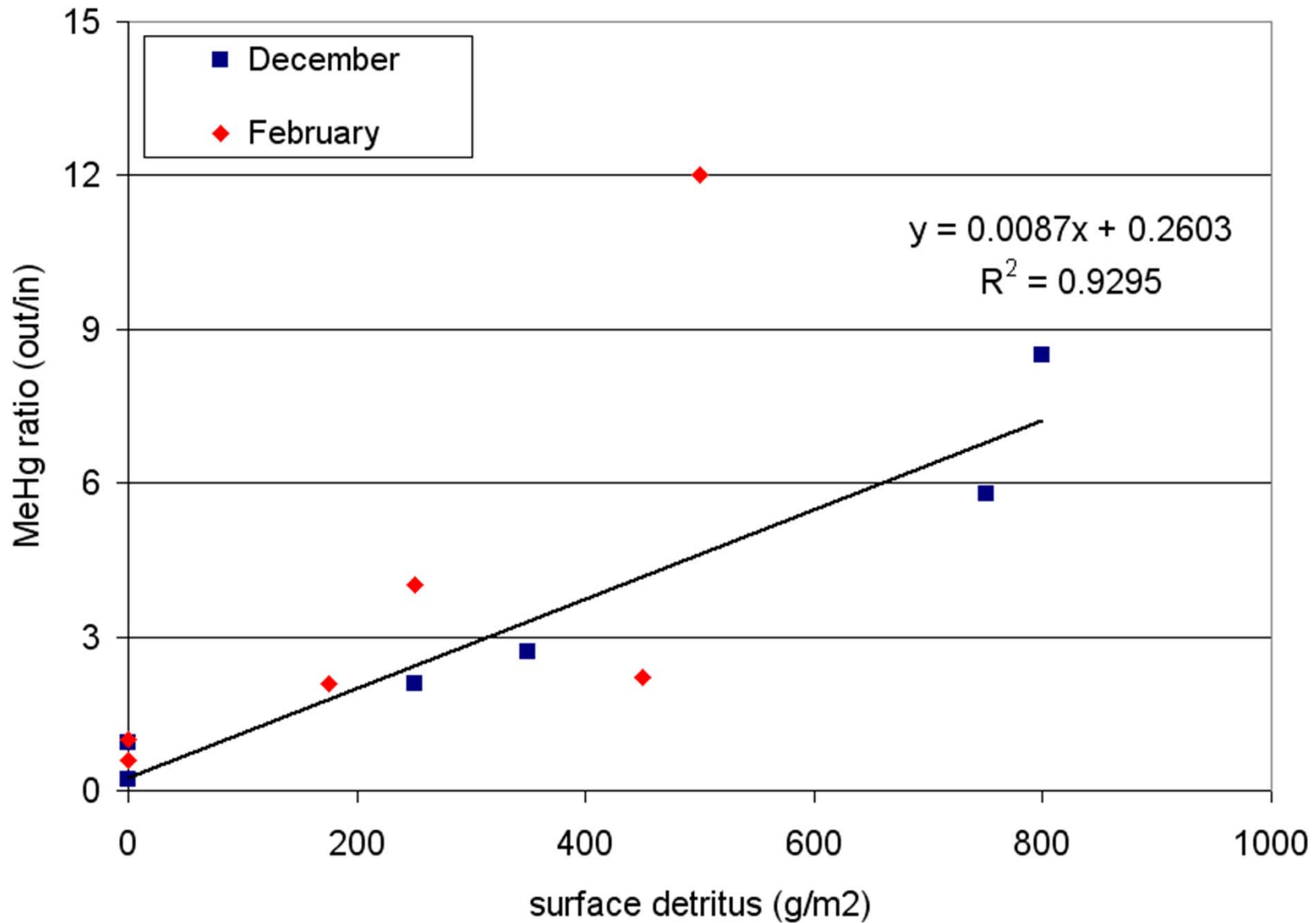


Figure 5.29. Scatter plot of surface water particulate detritus (plant residue) concentration versus the [Out/In] ratio of unfiltered methylmercury concentration along a flow path across agricultural and non-agricultural wetlands during winter (December 2007 and February 2008). Linear least-squares regression equation and coefficient are shown.

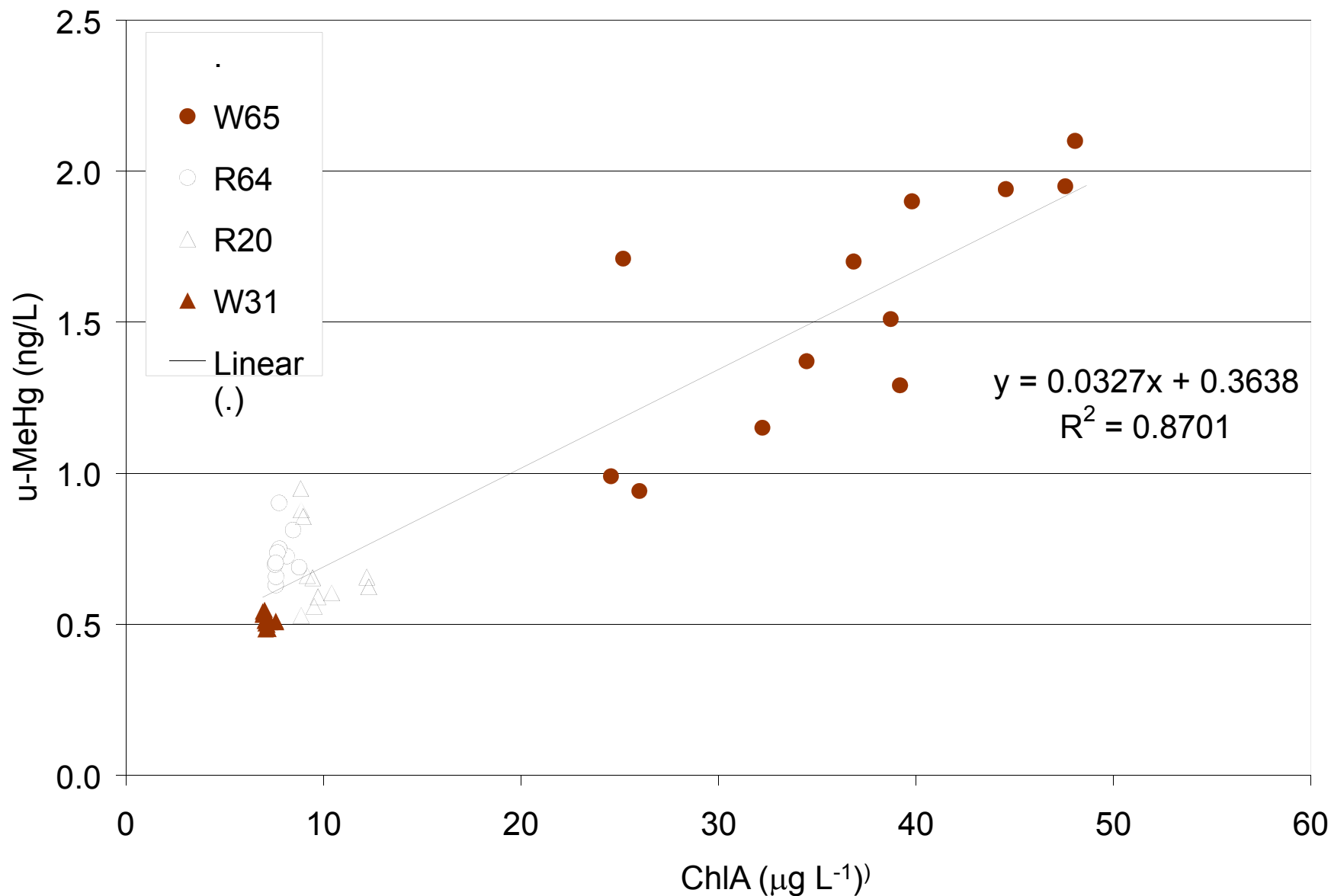


Figure 5.30. Scatter plot of surface water chlorophyll-a (ChlA) fluorescence versus unfiltered methylmercury (u-MeHg) concentration across white rice (R) and wild rice (W) fields during the diel measurements of summer 2007 (fields W65 and R64) and summer 2008 (fields R20 and W31). Linear least-squares regression equation and coefficient are shown.

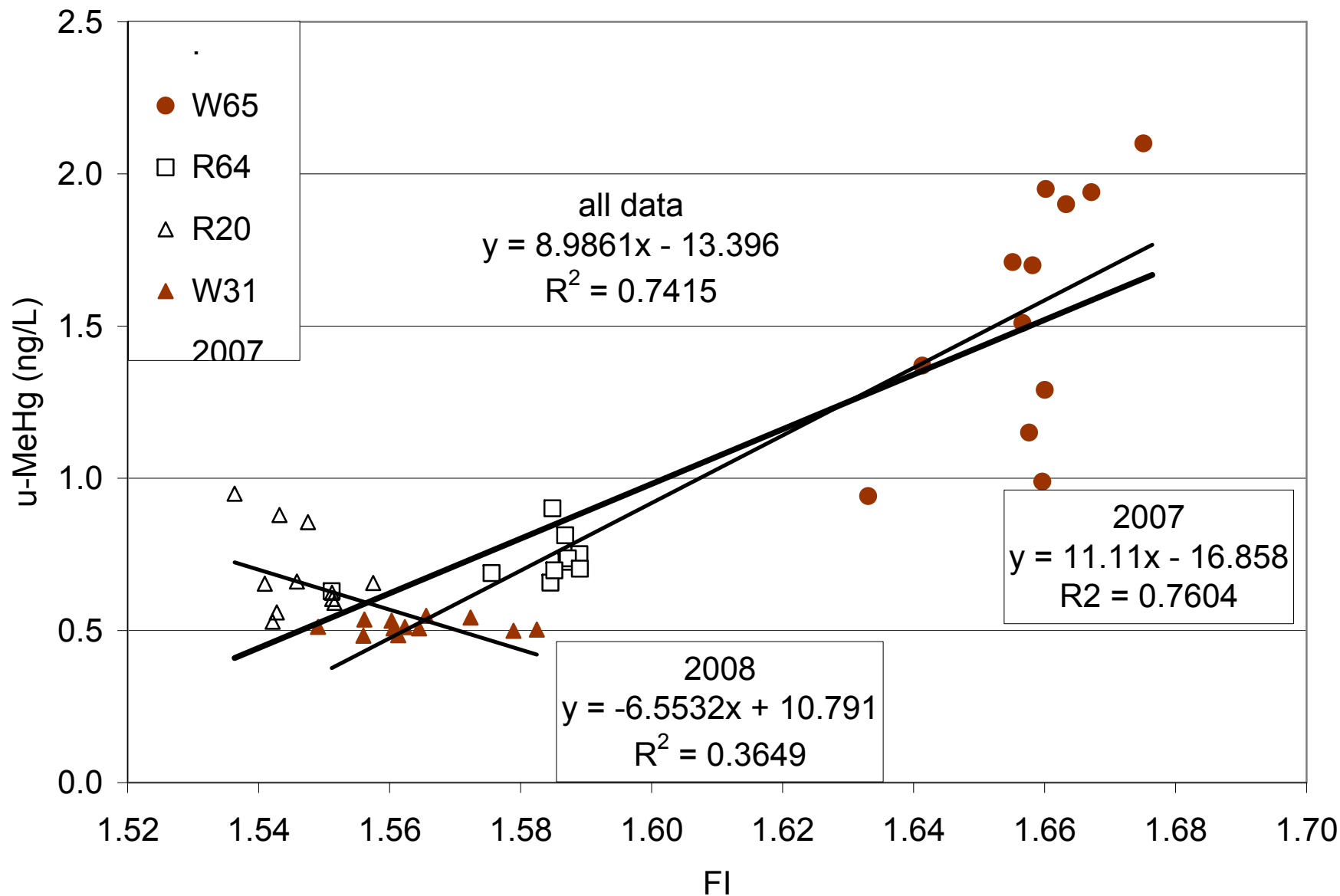


Figure 5.31. Scatter plot of fluorescence index (FI) versus unfiltered methylmercury (u-MeHg) concentration in surface water across white rice (R) and wild rice (W) fields during the diel measurements of summer 2007 (fields W65 and R64) and summer 2008 (fields R20 and W31). Linear least-squares regression equations and coefficients are shown for the 2007 data, the 2008, and all data combined.

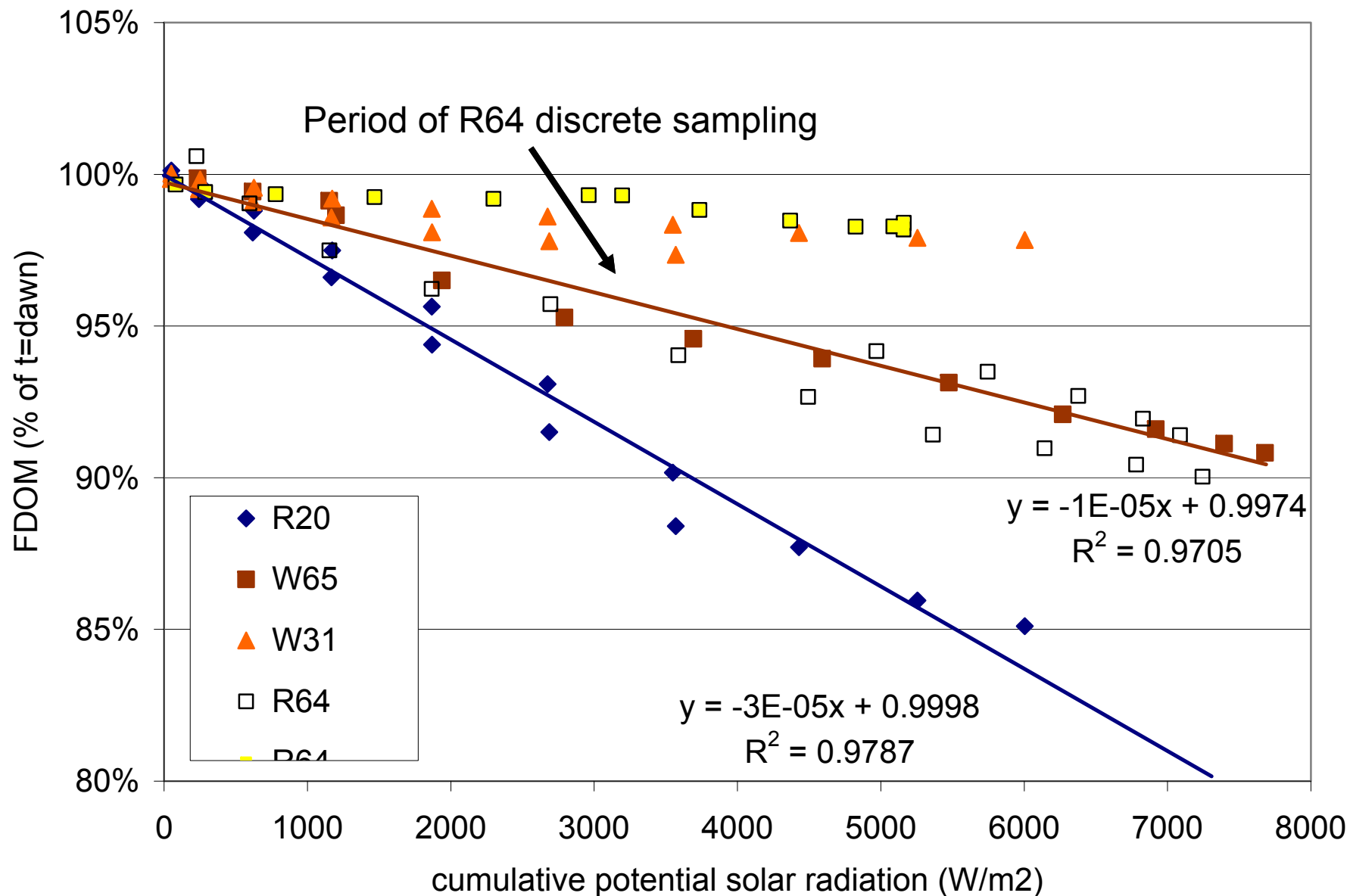


Figure 5.32. Scatter plot of cumulative potential solar radiation versus fluorescent dissolved organic matter (FDOM) in surface water during the *in situ* deployments of summer 2007 (fields W65 and R64) and summer 2008 (fields R20 and W31). Linear least-squares regression equations and coefficients are shown for fields W65 and R64..

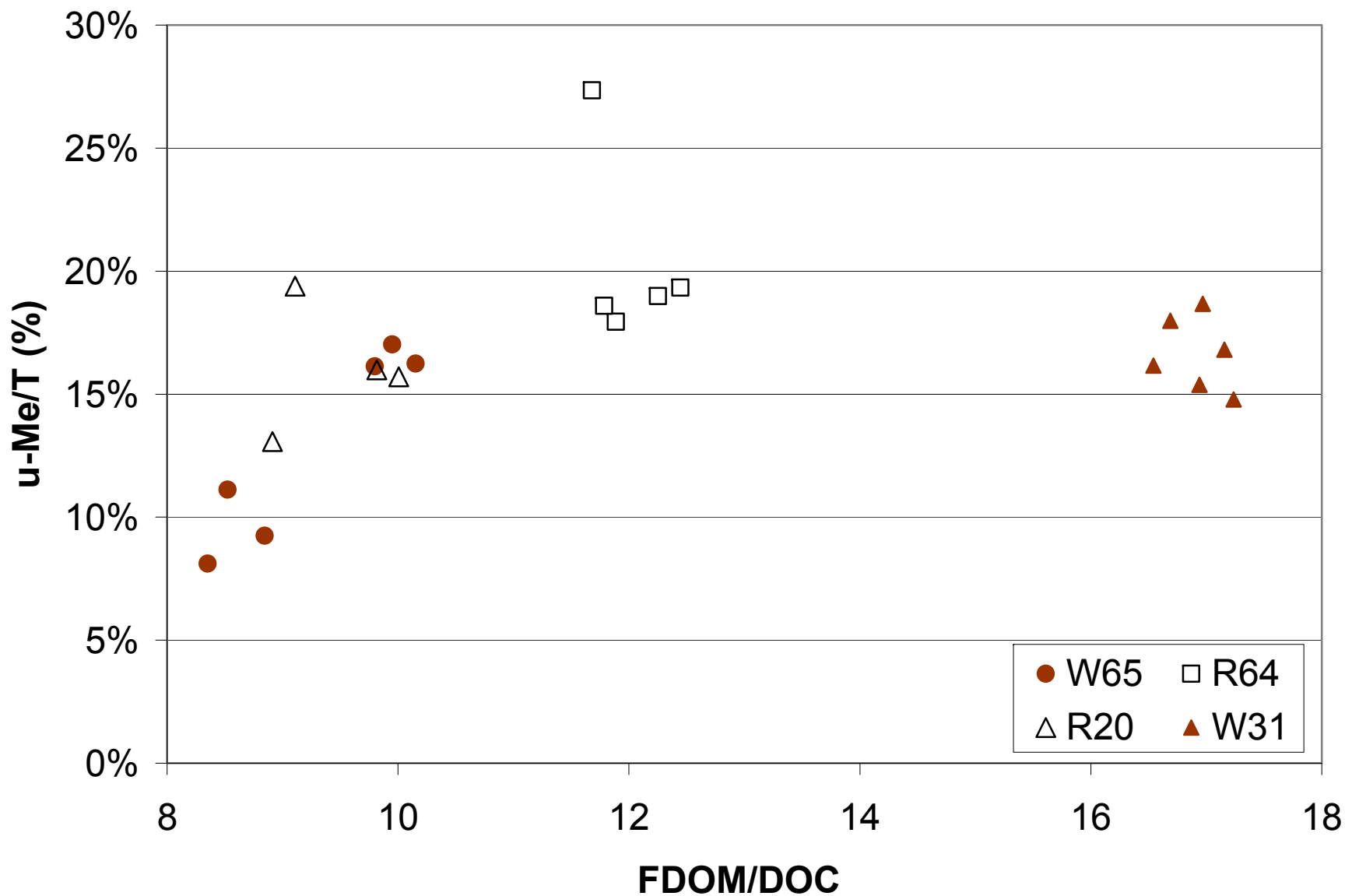


Figure 5.33. Scatter plot of the ratio of fluorescent dissolved organic matter (FDOM) to dissolved organic carbon (DOC) (FDOM/DOC) versus the ratio of unfiltered methylmercury to total mercury u-MeHg/THg) in surface water during the 2007 and 2008 diel studies. The u-MeHg/THg ratio is expressed as a percentage (% THg as MeHg).

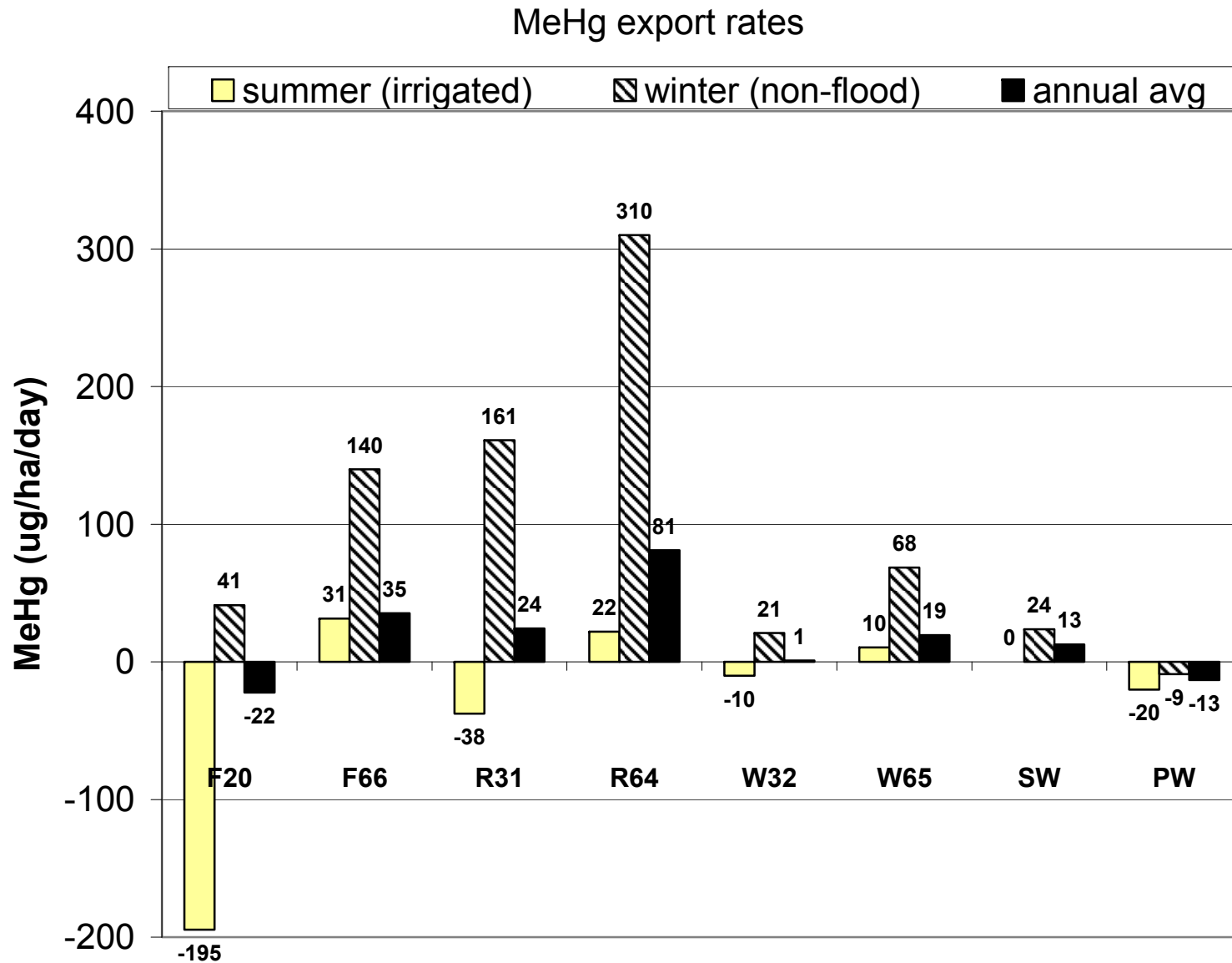


Figure 5.34. Bar graph showing methylmercury (MeHg) loads from individual fields during the summer irrigation period, the winter period (excluding the 17-day flood), and the annual average. Loads in micrograms per hectare per day ($\mu\text{g}/\text{ha}/\text{day}$). Positive values represent net export, whereas negative values represent net import.

Net area-normalized MeHg loads

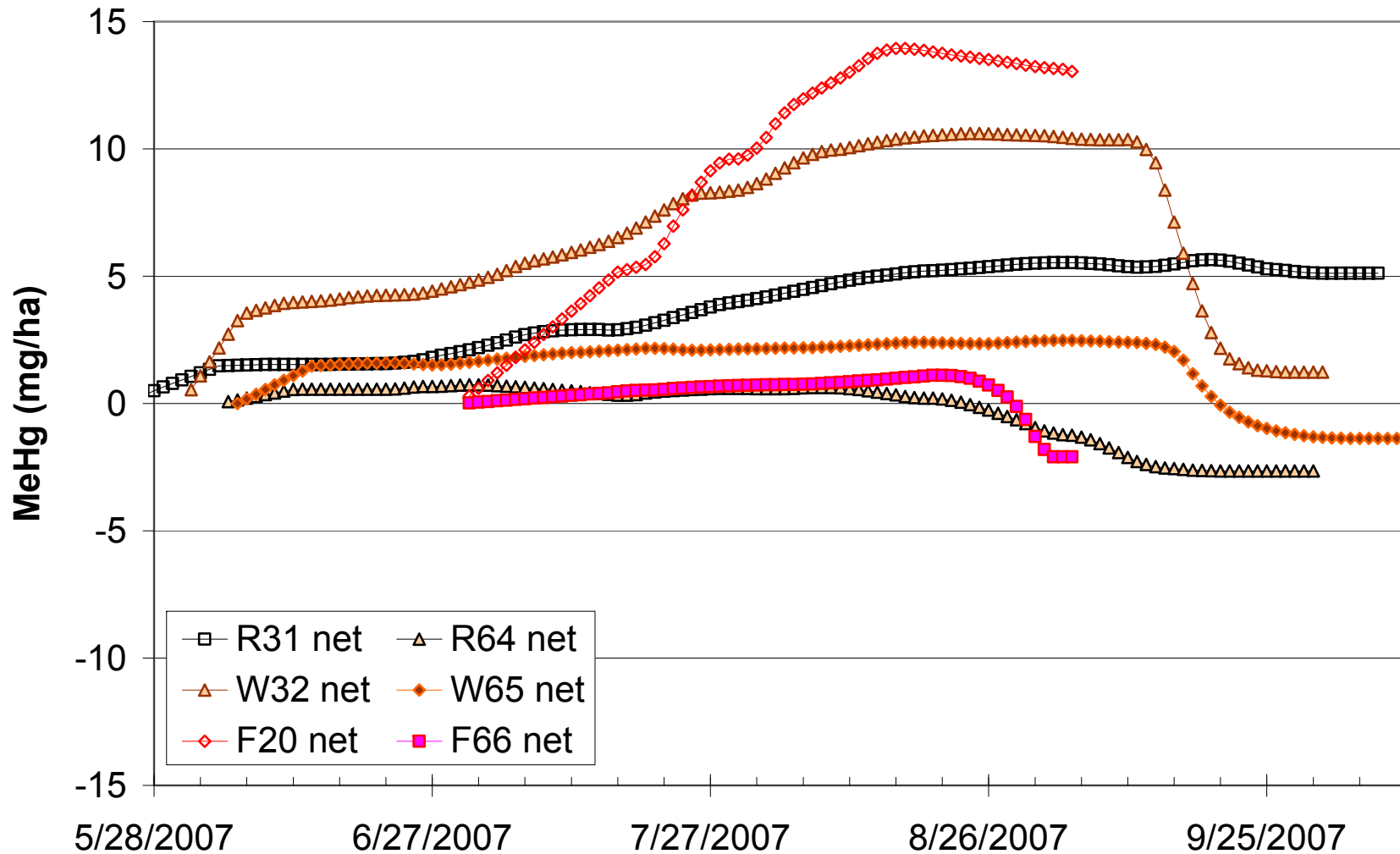


Figure 5.35. Time series plot of area-normalized, cumulative methylmercury (MeHg) mass net loading for individual fields in the Yolo Bypass Wildlife Area. Positive values represent net import, whereas negative values represent net export.

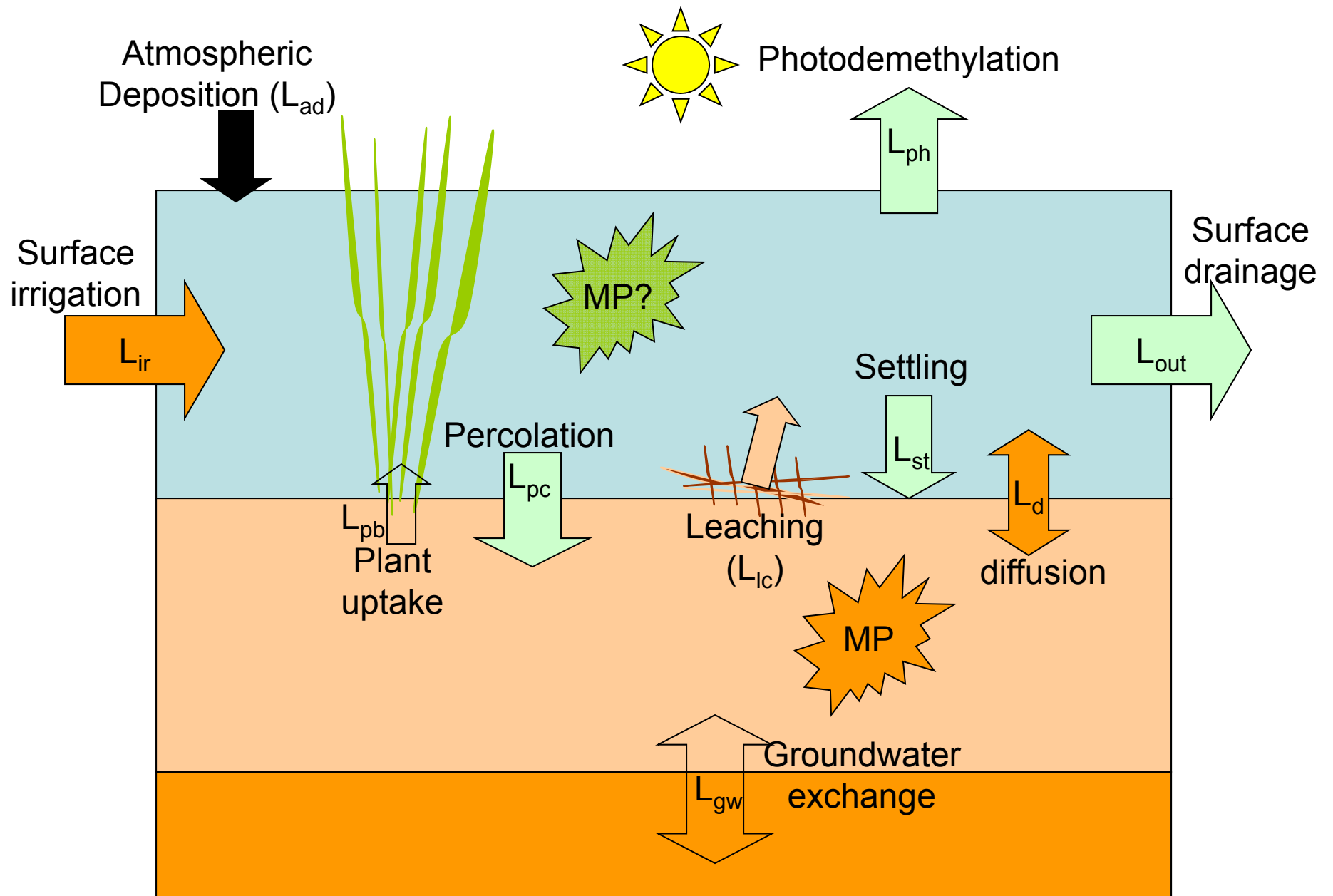


Figure 5.36. Schematic diagram showing methylmercury inputs and outputs from a generic managed wetland. See Table 5.10 for explanation of diagram notation. (MP, methylmercury production)

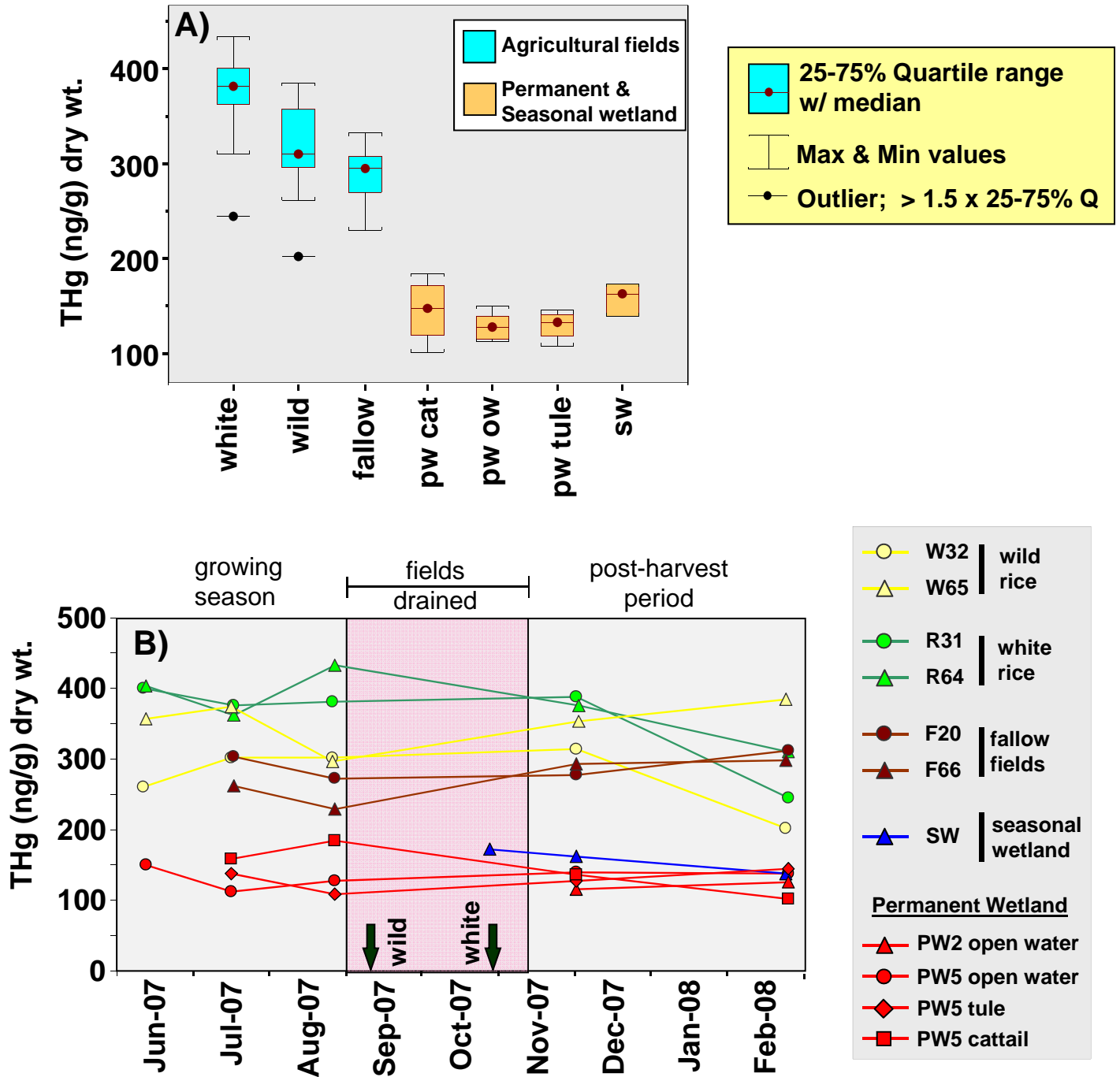


Figure 6.1. Sediment total mercury (THg) concentration data depicted as (A) a box and whisker plot by habitat type and (B) in time series for each field. (A) includes all sampling events and include replicate white rice (white), wild rice (wild) and fallow agricultural fields. Permanent wetland (pw) open water (ow) shown in (A) included data from PW5 and PW2, while cattail and tule dominated sites (pw cat and pw tule, respectively) are from PW5 only. Arrows on (B) indicate when white and wild rice fields were harvested. Temporal data groupings (growing season and post-harvest period) for agricultural field statistical comparisons (Table 6.4**) are indicated in the grey shaded areas, and are separated by the period during which agricultural fields were drained (pink background).**

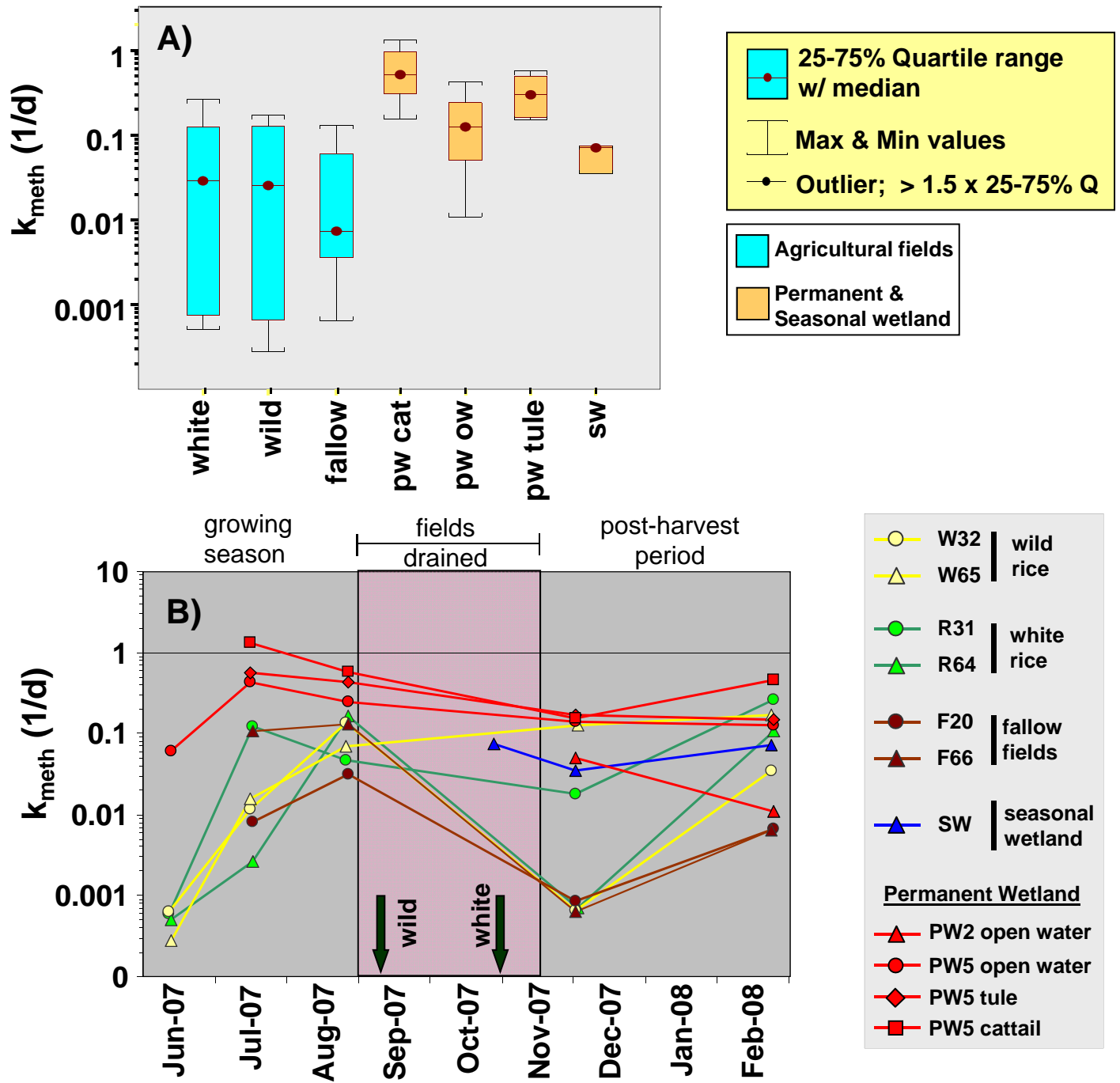


Figure 6.2. Sediment $^{203}\text{Hg(II)}$ -methylation rate constant (k_{meth}) data depicted as (A) a box-and-whisker plot by habitat type and (B) in time series for each field. (A) includes all sampling events and include replicate white rice (white), wild rice (wild) and fallow agricultural fields. Permanent wetland (pw) open water (ow) shown in (A) included data from PW5 and PW2, while cattail and tule dominated sites (pw cat and pw tule, respectively) are from PW5 only. Arrows and seasonal groupings on (B) are described in **Figure 6.1.**

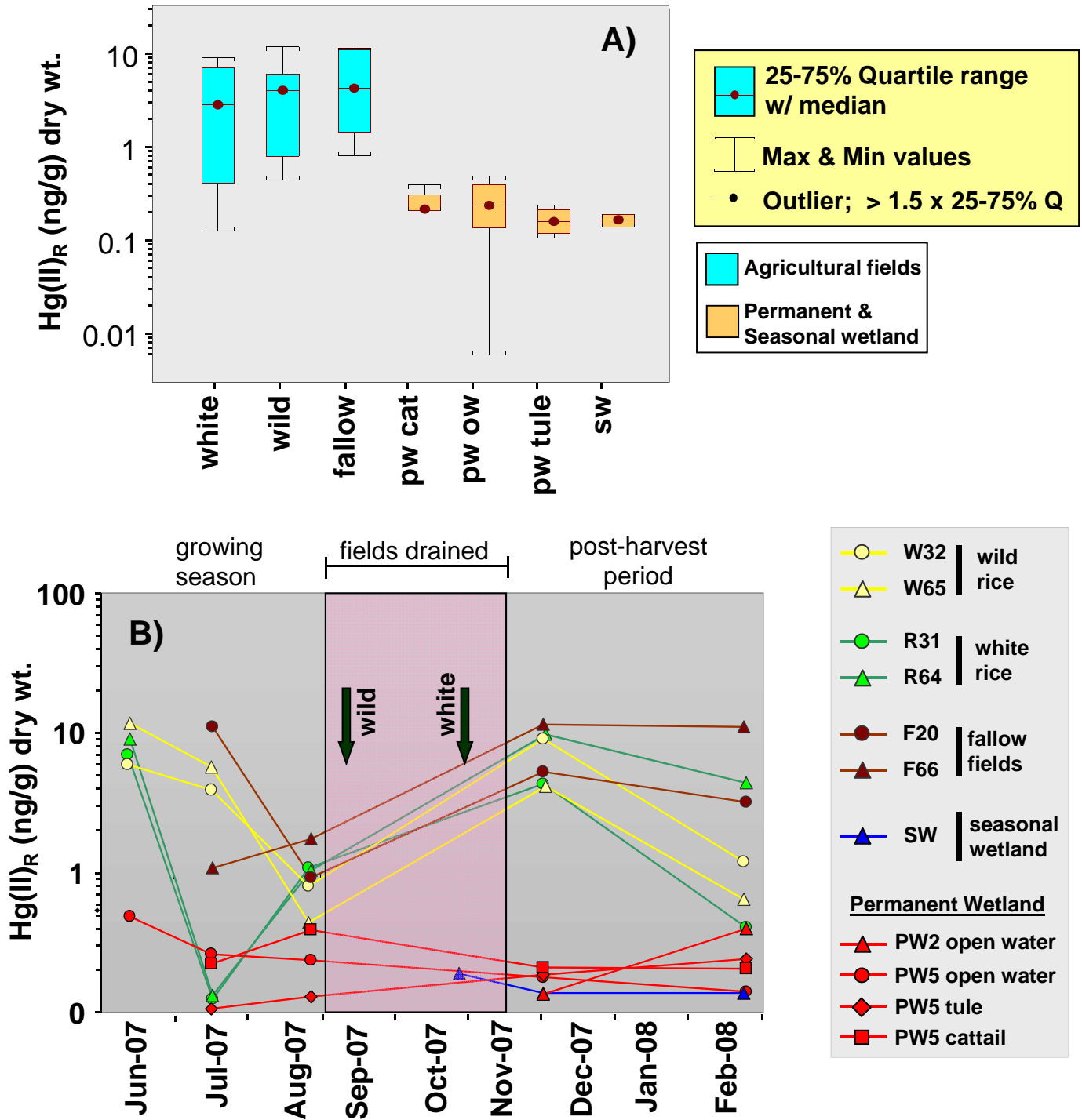


Figure 6.3. Sediment inorganic reactive mercury ($Hg(II)_R$) concentration data depicted as (A) a box-and-whisker plot by habitat type and (B) in time series for each field. (A) includes all sampling events and include replicate white rice (white), wild rice (wild) and fallow agricultural fields. Permanent wetland (pw) open water (ow) shown in (A) included data from PW5 and PW2, while cattail and tulle dominated sites (pw tulle, respectively) are from PW5 only. Arrows and seasonal groupings on (B) are described in Figure 6.1.

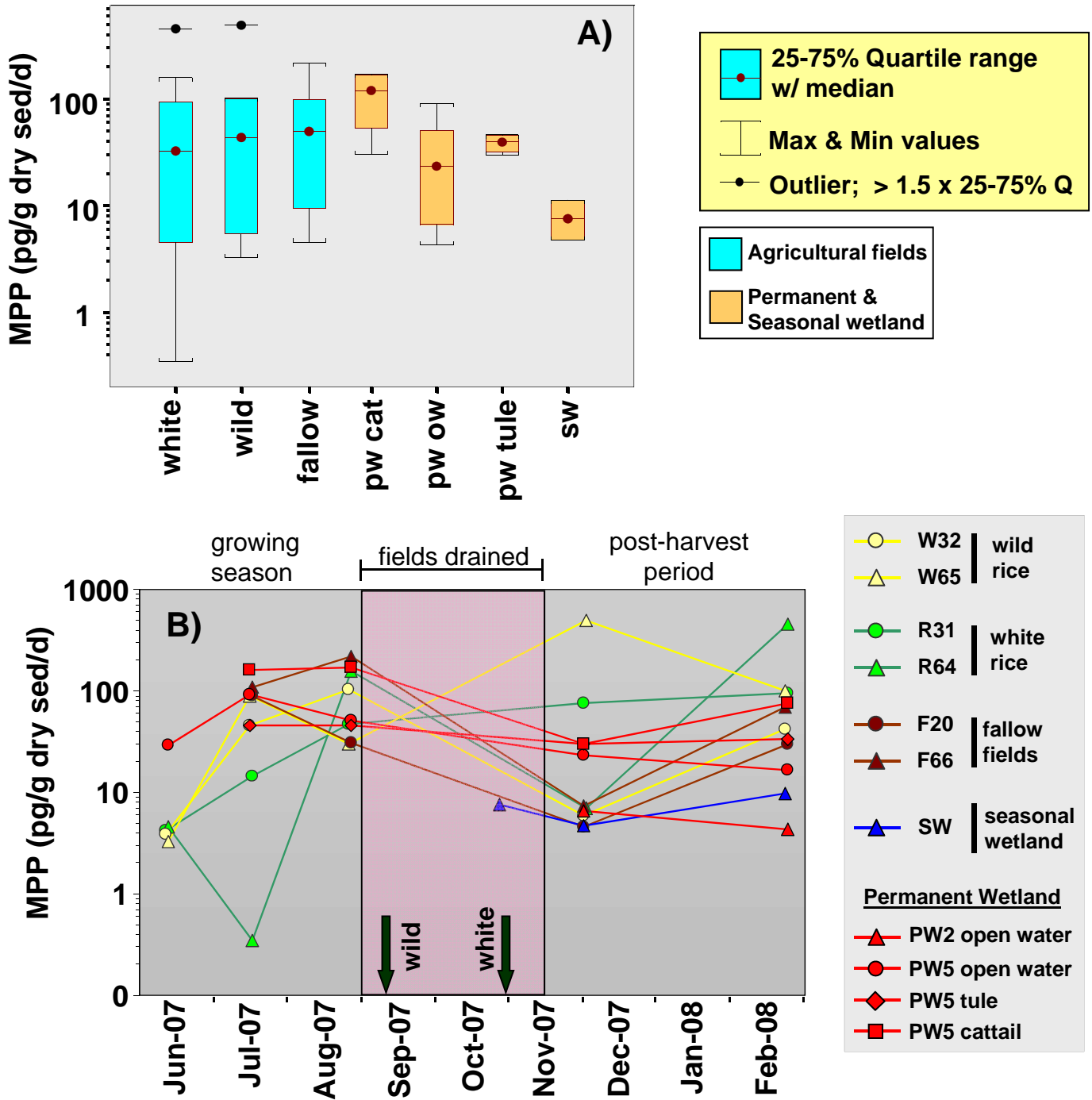


Figure 6.4. Sediment methylmercury production potential (MPP) rate data depicted as (A) a box-and-whisker plot by habitat type and (B) in time series for each field. (A) includes all sampling events and include replicate white rice (white), wild rice (wild) and fallow agricultural fields. Permanent wetland (pw) open water (ow) shown in (A) included data from PW5 and PW2, while cattail and tulle dominated sites (pw cat and pw tule, respectively) are from PW5 only. Arrows and seasonal groupings on (B) are described in Figure 6.1.

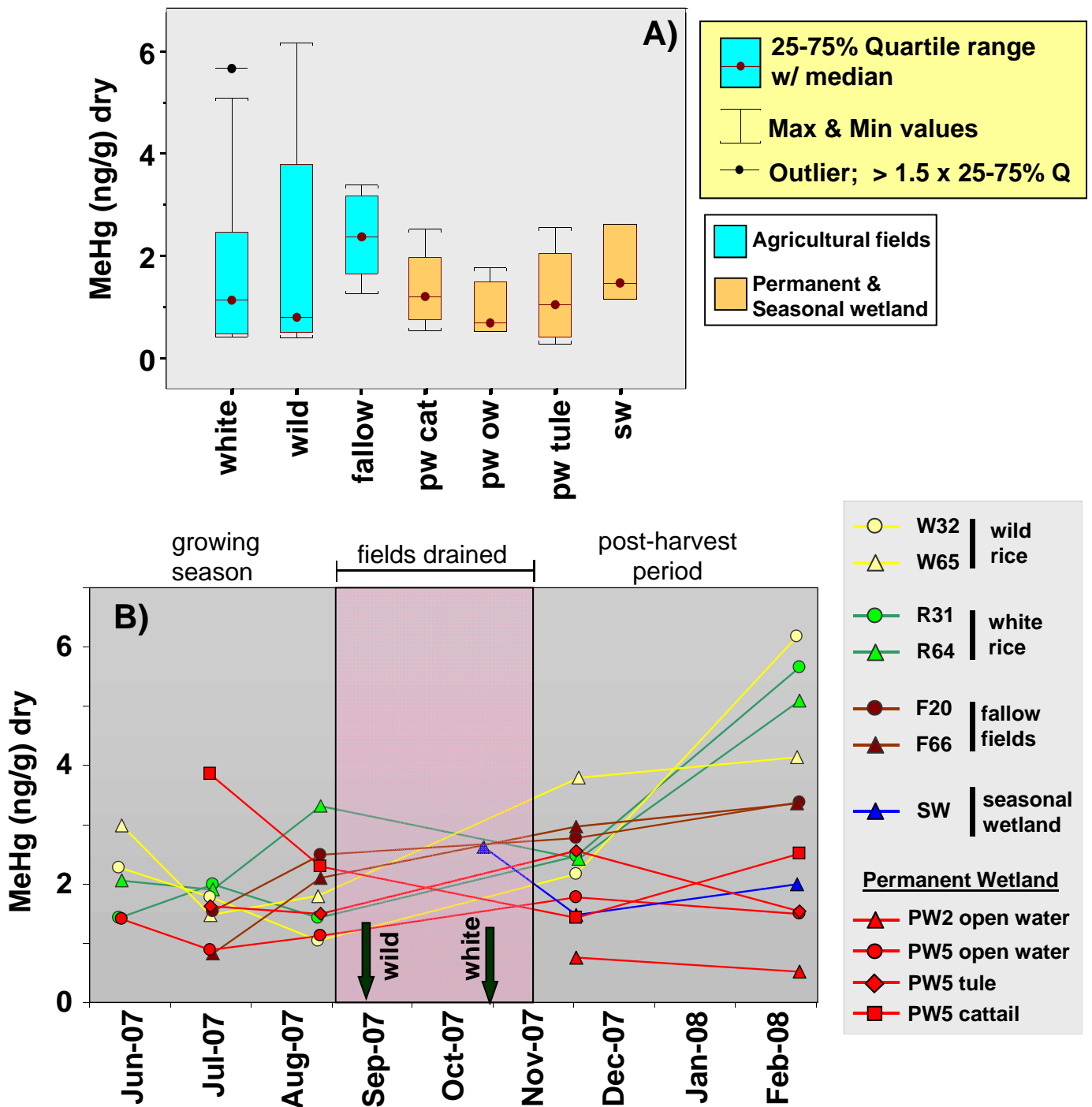


Figure 6.5. Sediment methylmercury (MeHg) concentration data depicted as (A) a box-and-whisker plot by habitat type and (B) in time series for each field. (A) includes all sampling events and include replicate white rice (white), wild rice (wild) and fallow agricultural fields. Permanent wetland (pw) open water (ow) shown in (A) included data from PW5 and PW2, while cattail and tulle dominated sites (pw cat and pw tule, respectively) are from PW5 only. Arrows and seasonal groupings on (B) are described in Figure 6.1.

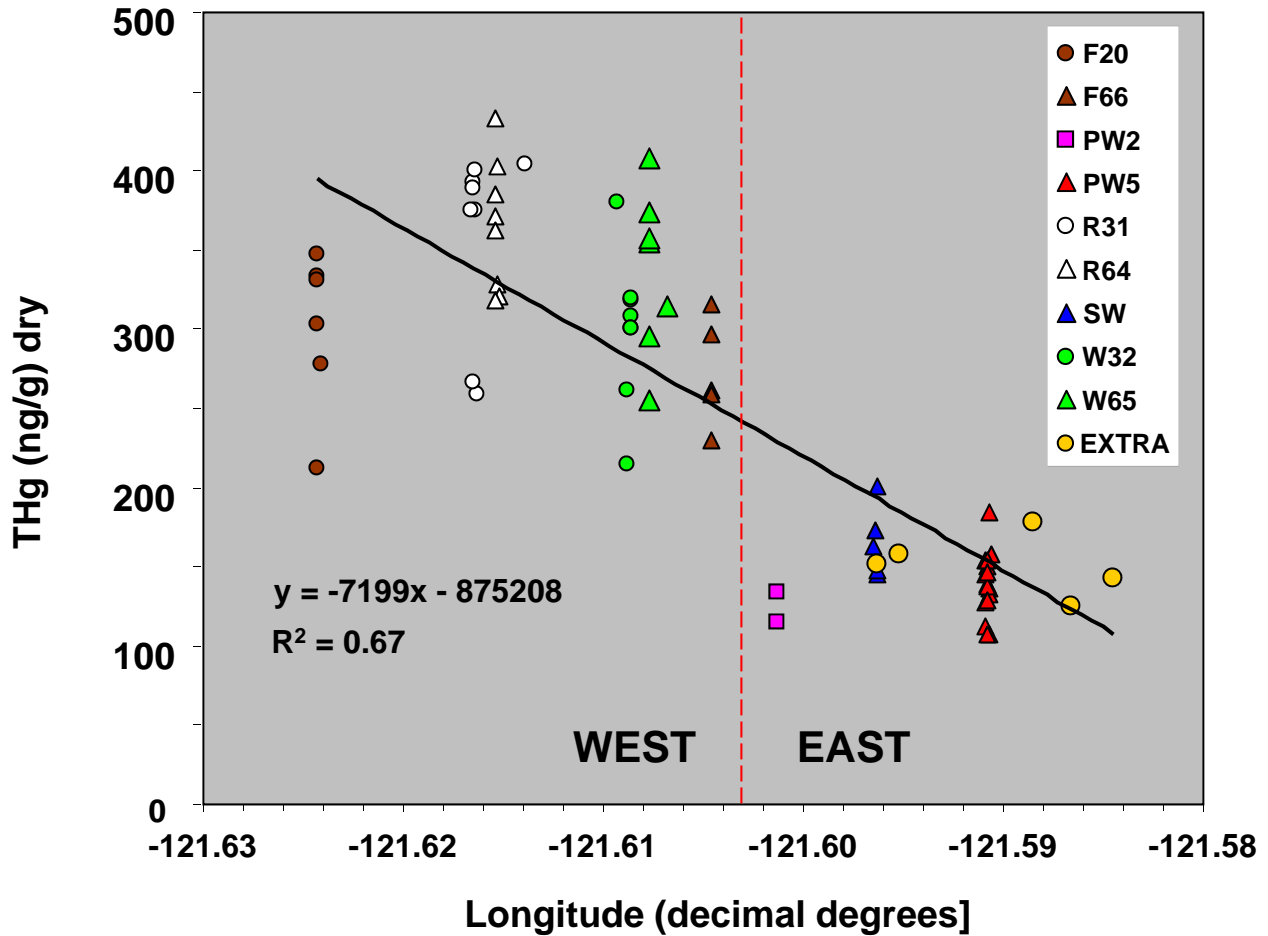


Figure 6.6. Scatter plot of sediment total mercury (THg) concentration versus longitude showing least-squares linear regression. The solid line represents the least-squares linear fit to the data, with the linear equation and R^2 value inset. The dashed red vertical line represents -121.603° longitude, and represents a visual demarkation where THg concentrations appear to abruptly shift concentration from east to west. Of the primary sampling sites in the current study, all agricultural fields were located west of this longitude, while all non-agricultural fields sampled were located to the east. Additional samples 'EXTRA' were collected during May 2008 and submitted by J. Holloway (USGS, Denver, CO) as part of the California Geochemical Landscapes project (Marty Goldhaber, USGS, Denver, CO; Project Chief).

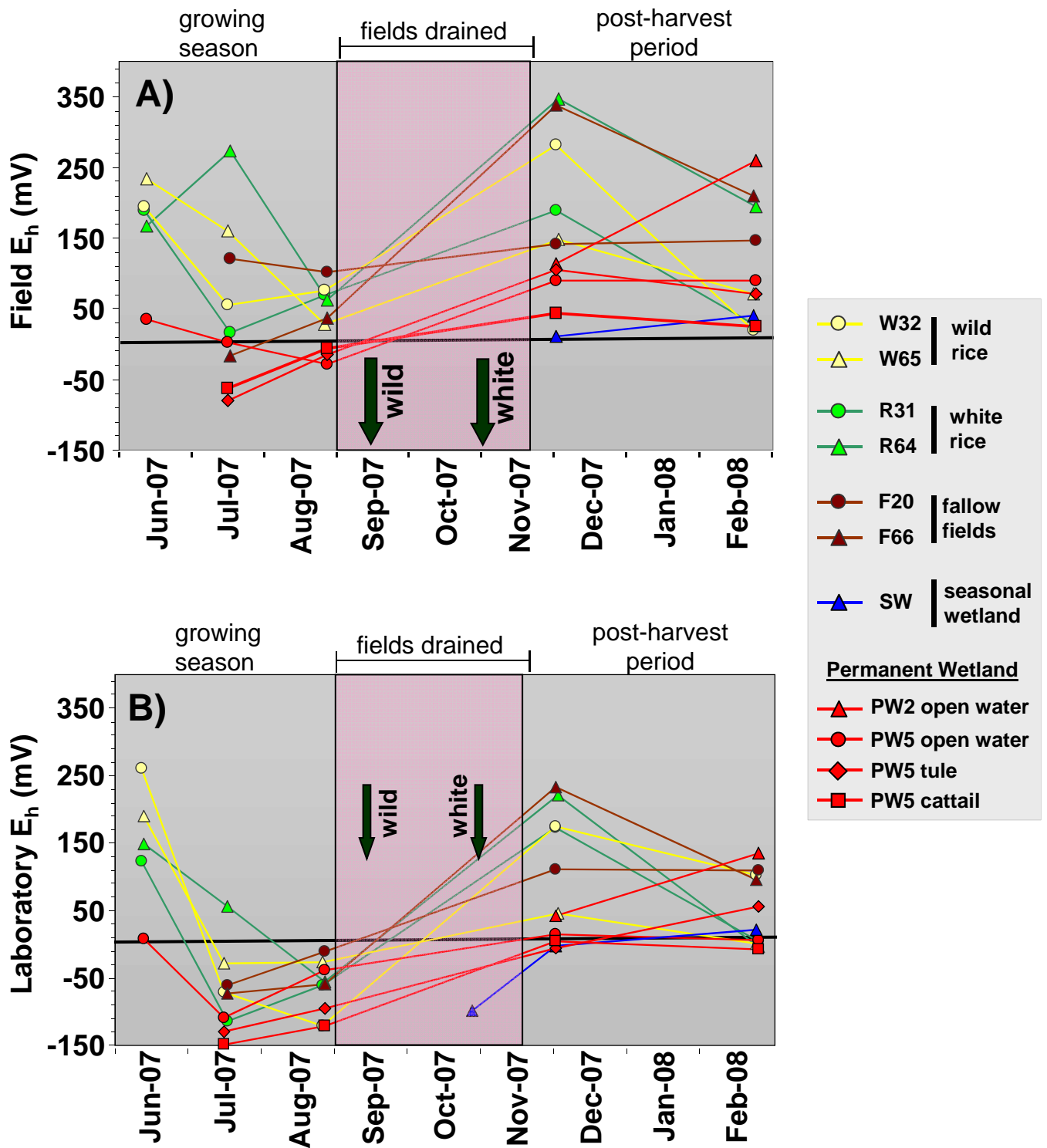


Figure 6.7. Time series plots of sediment oxidation-reduction potential (E_h) as measured in the (A) field and (B) laboratory at the time of sediment sub-sampling, by field. Sub-sampling occurred 1-4 days after field collection. Arrows and seasonal groupings on are described in Figure 6.1.

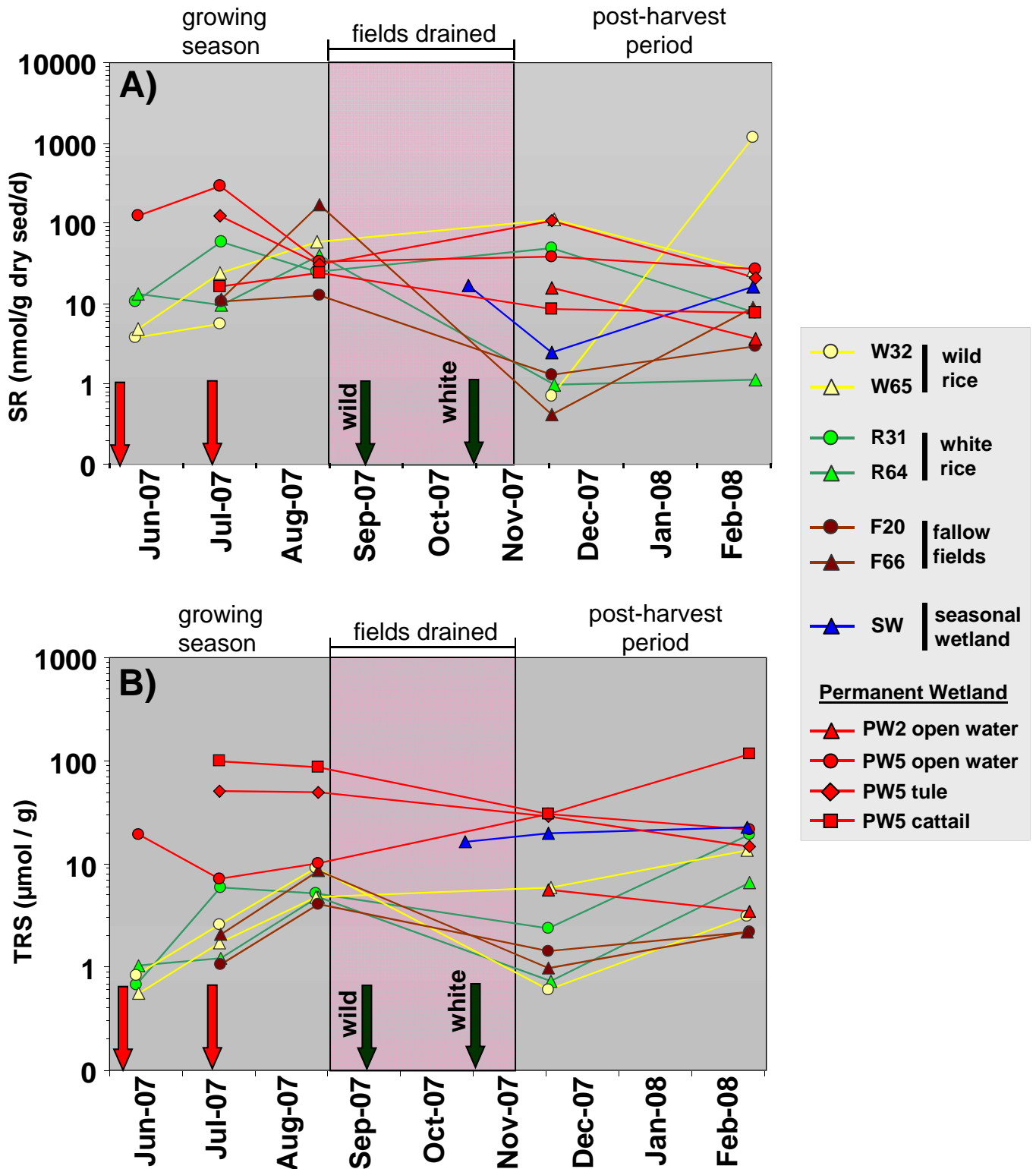


Figure 6.8. Time series plots of sediment A) microbial sulfate reduction (SR) rate and B) total reduced sulfur (TRS), by field. Red arrows and green arrows indicate when fertilizer was applied to rice fields and when rice fields were harvested, respectively. Seasonal groupings are described in **Figure 6.1**. Note: the August SR rate data for field W32 was lost during analysis.

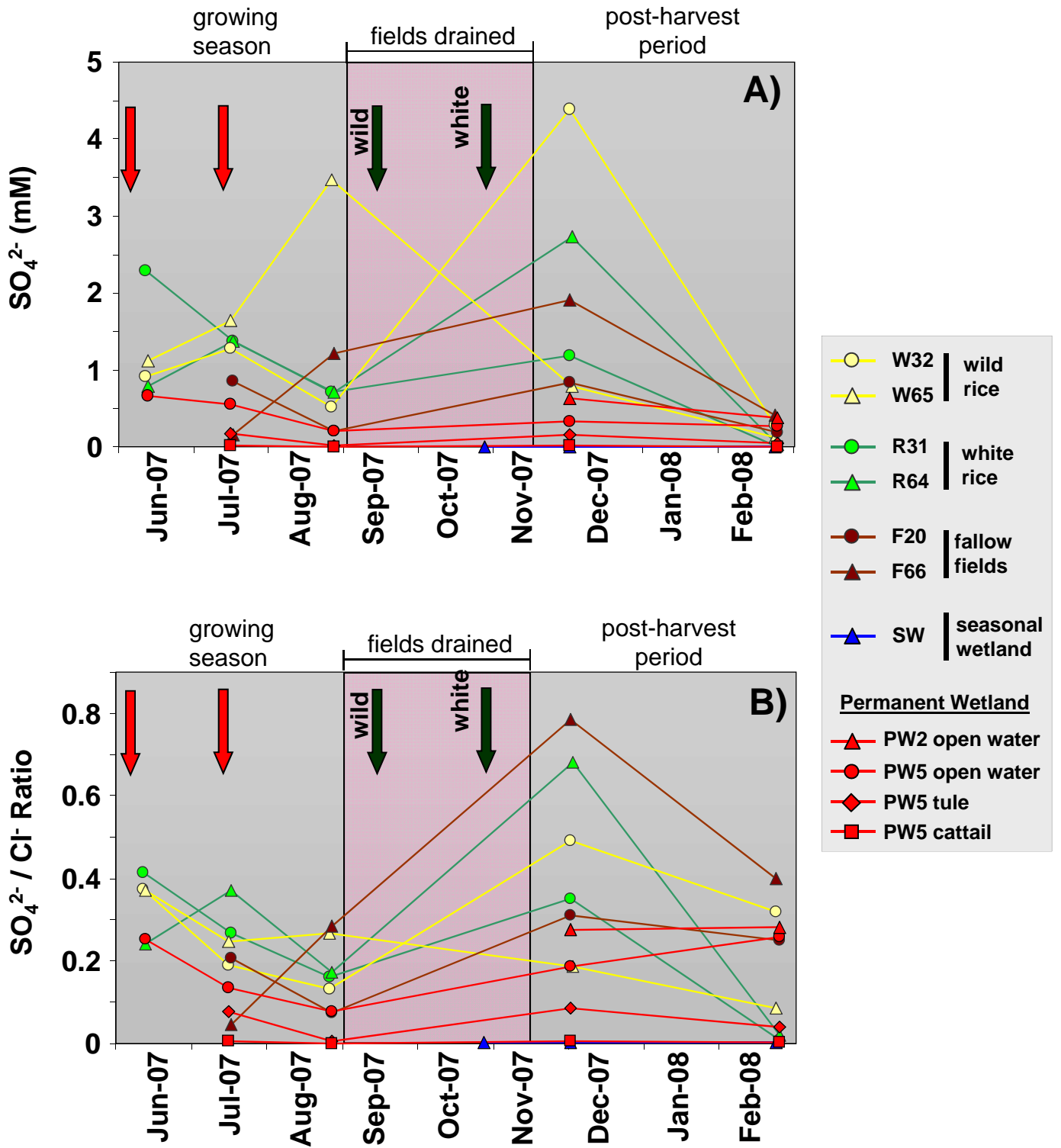


Figure 6.9. Time series plots of pore water A) sulfate (SO_4^{2-}) concentration and B) the sulfate to chloride (SO_4^{2-} / Cl^-) molar ratio, by field. Red arrows and green arrows indicate when fertilizer was applied to rice fields and when rice fields were harvested, respectively. Seasonal groupings are described in **Figure 6.1**.

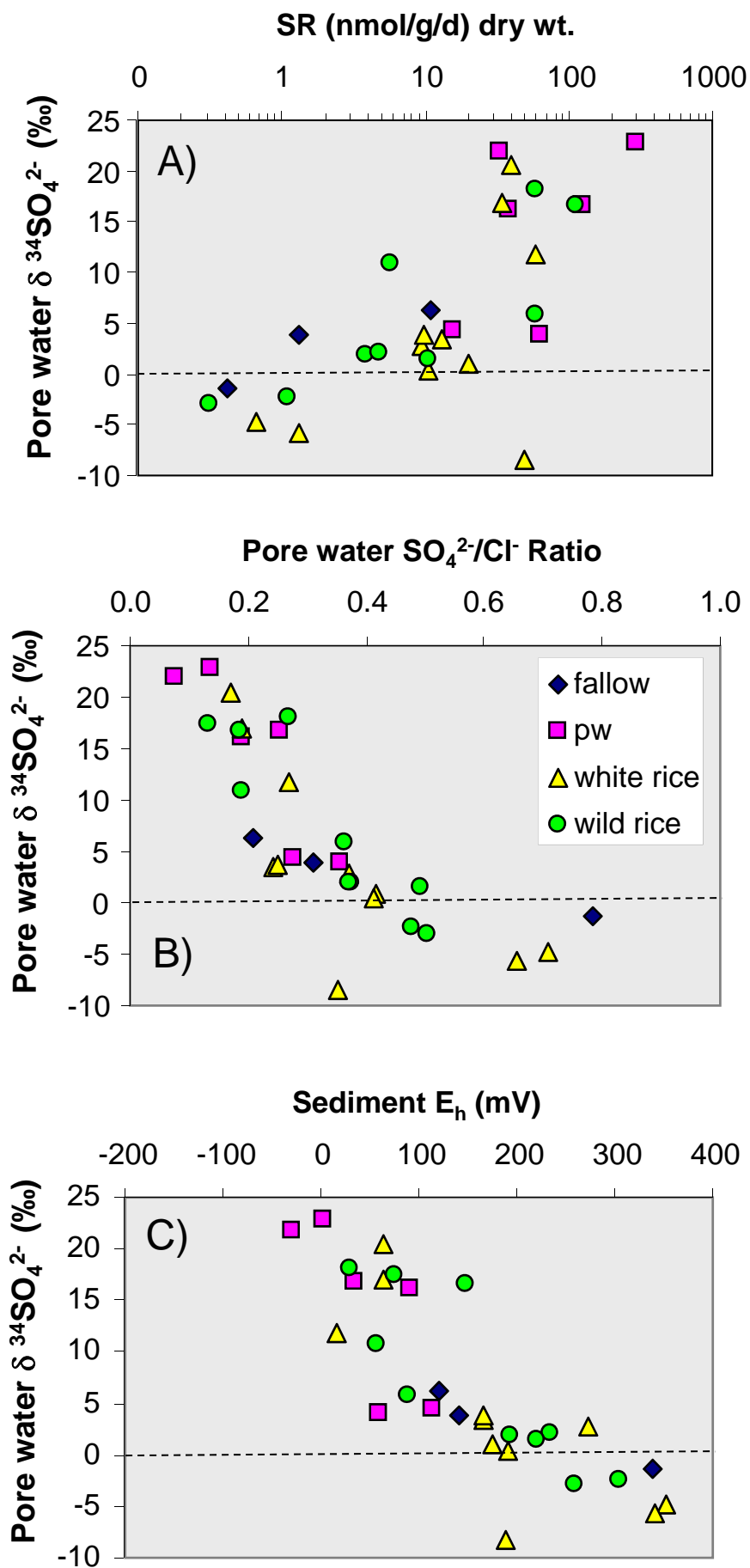


Figure 6.10. Scatter plots of pore water sulfate-sulfur stable isotope data ($\delta^{34}\text{SO}_4^{2-}$) as a function of (A) sediment microbial sulfate reduction (SR) rate, (B) pore water sulfate-to-chloride concentration ratio, and (C) sediment redox (E_h). Data from the June through December (2007) sampling period. Data organized by habitat type (legend inset). Dashed line indicates the $\delta^{34}\text{SO}_4^{2-}$ zero value.

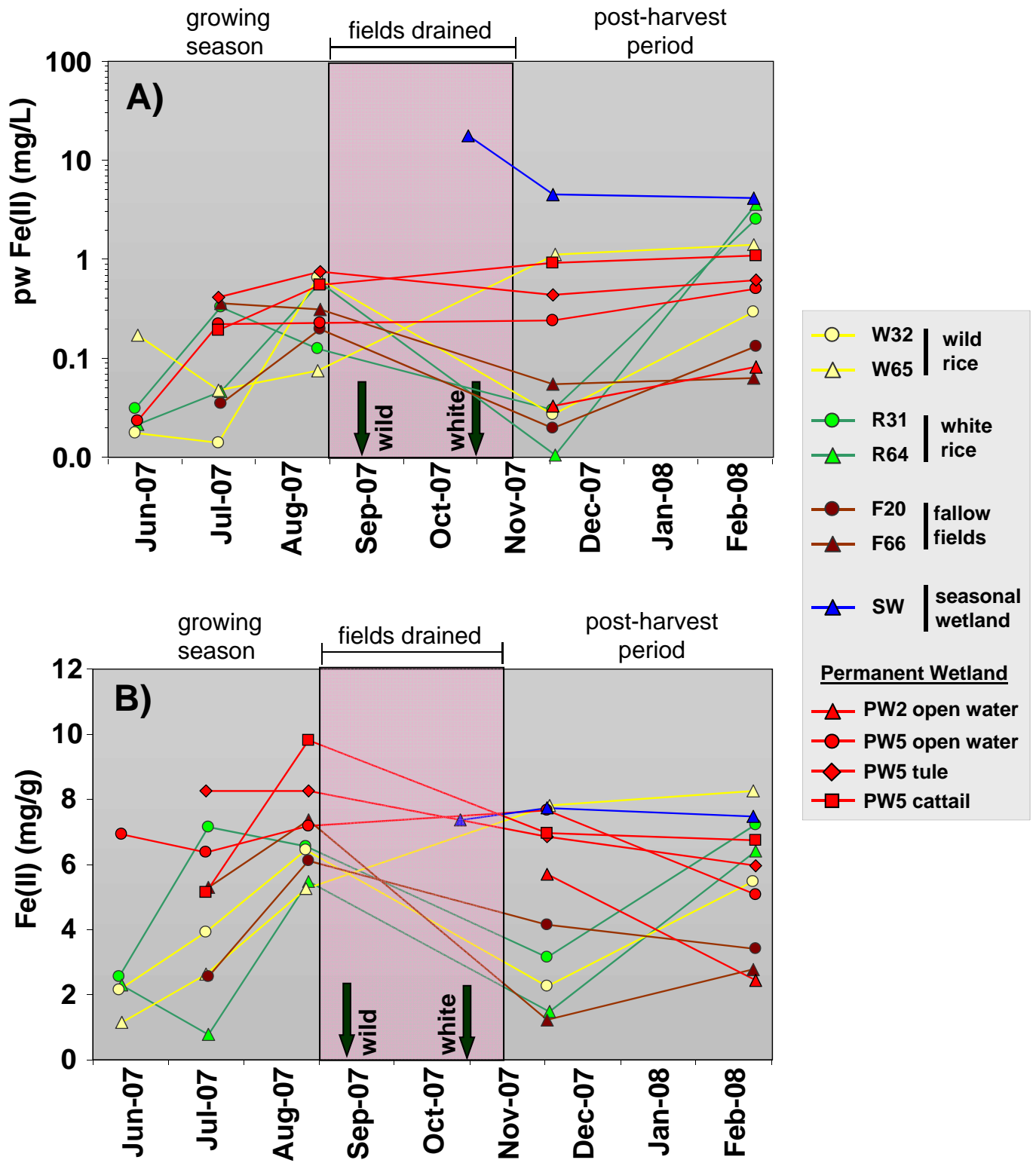


Figure 6.11. Time series plots of ferrous iron (Fe(II)) concentration in (A) pore water and (B) sediment, by field. Arrows and seasonal groupings are described in Figure 6.1.

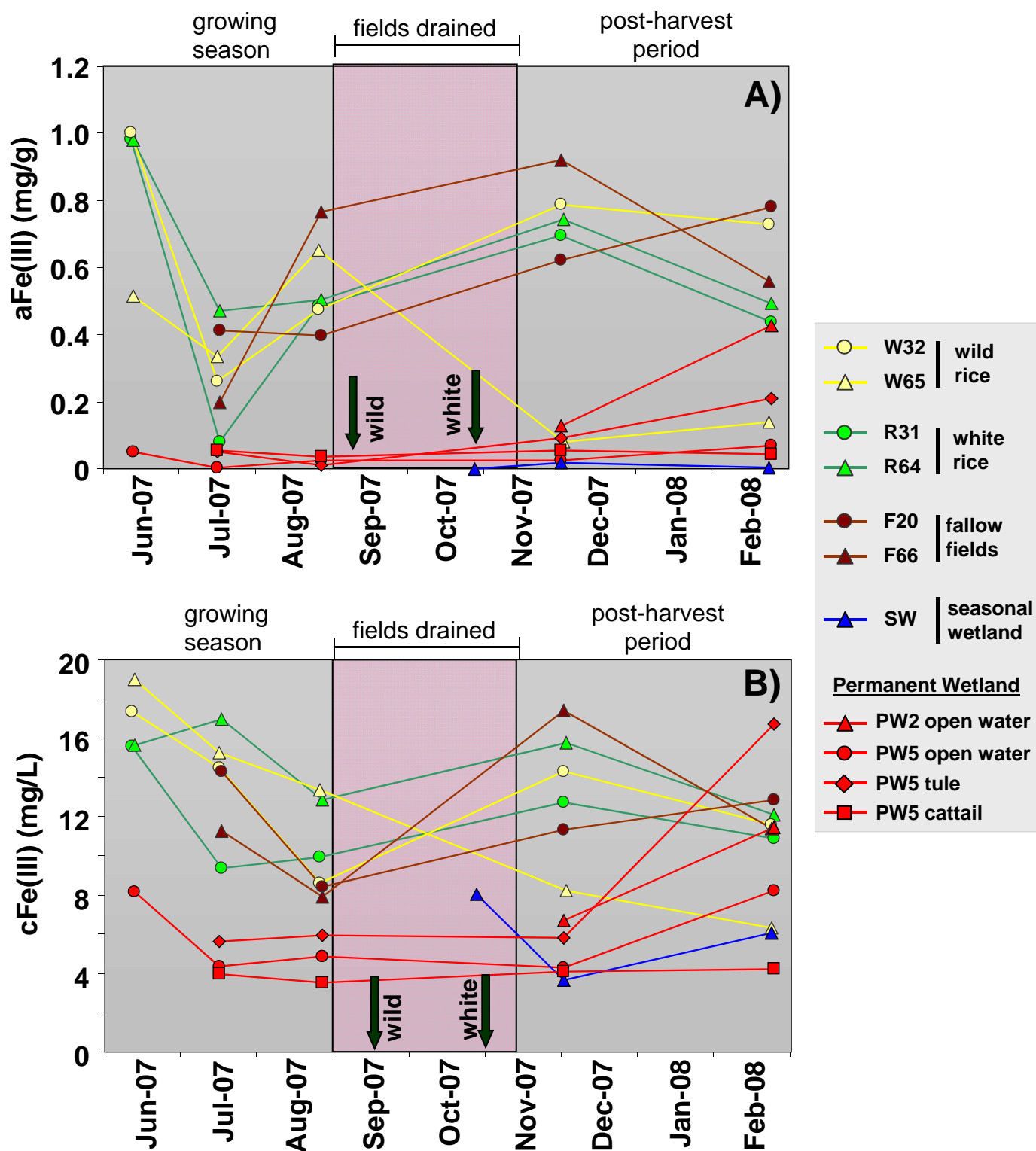


Figure 6.12. Time series plots of sediment (A) amorphous / poorly-crystalline ferric iron (aFe(III)) and (B) crystalline ferric iron (cFe(III)), by field. Arrows and seasonal groupings are described in Figure 6.1.

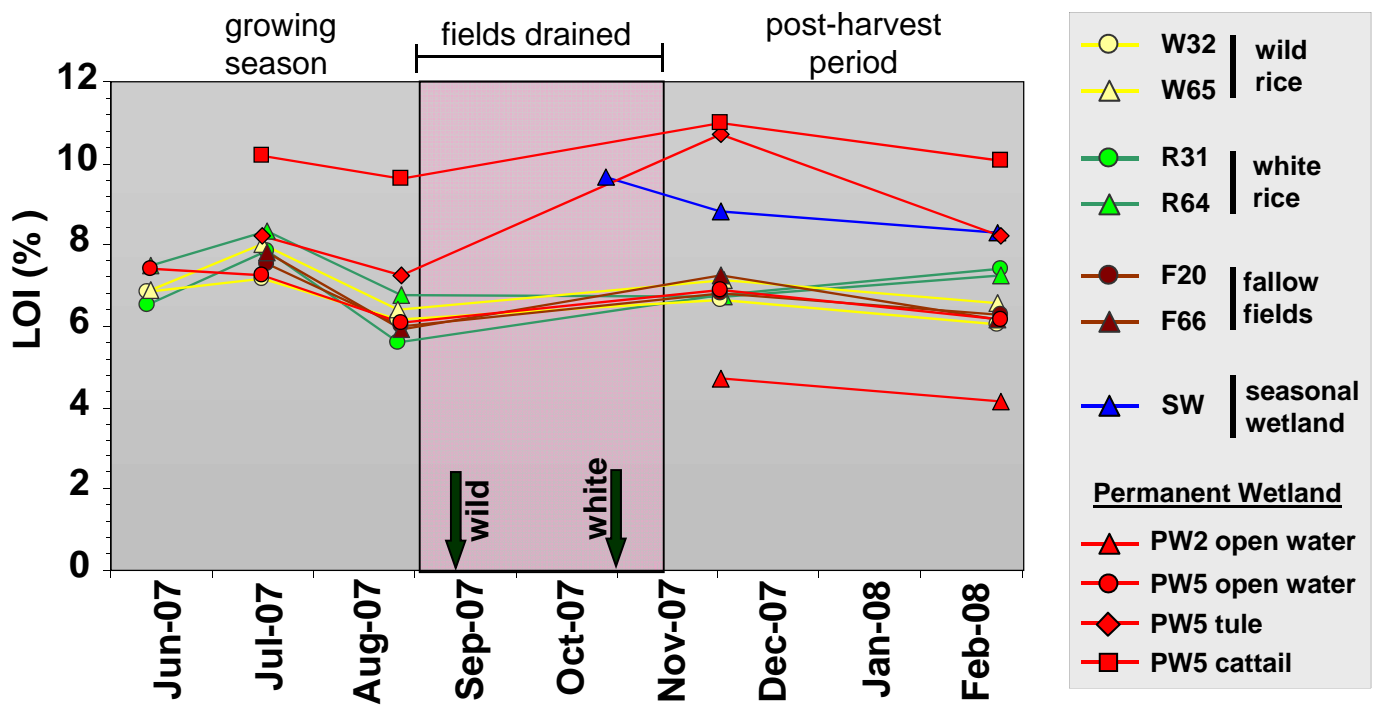


Figure 6.13. Time series plot of sediment organic content, as percent loss on ignition (%LOI), by field. Arrows and seasonal groupings are described in Figure 6.1.

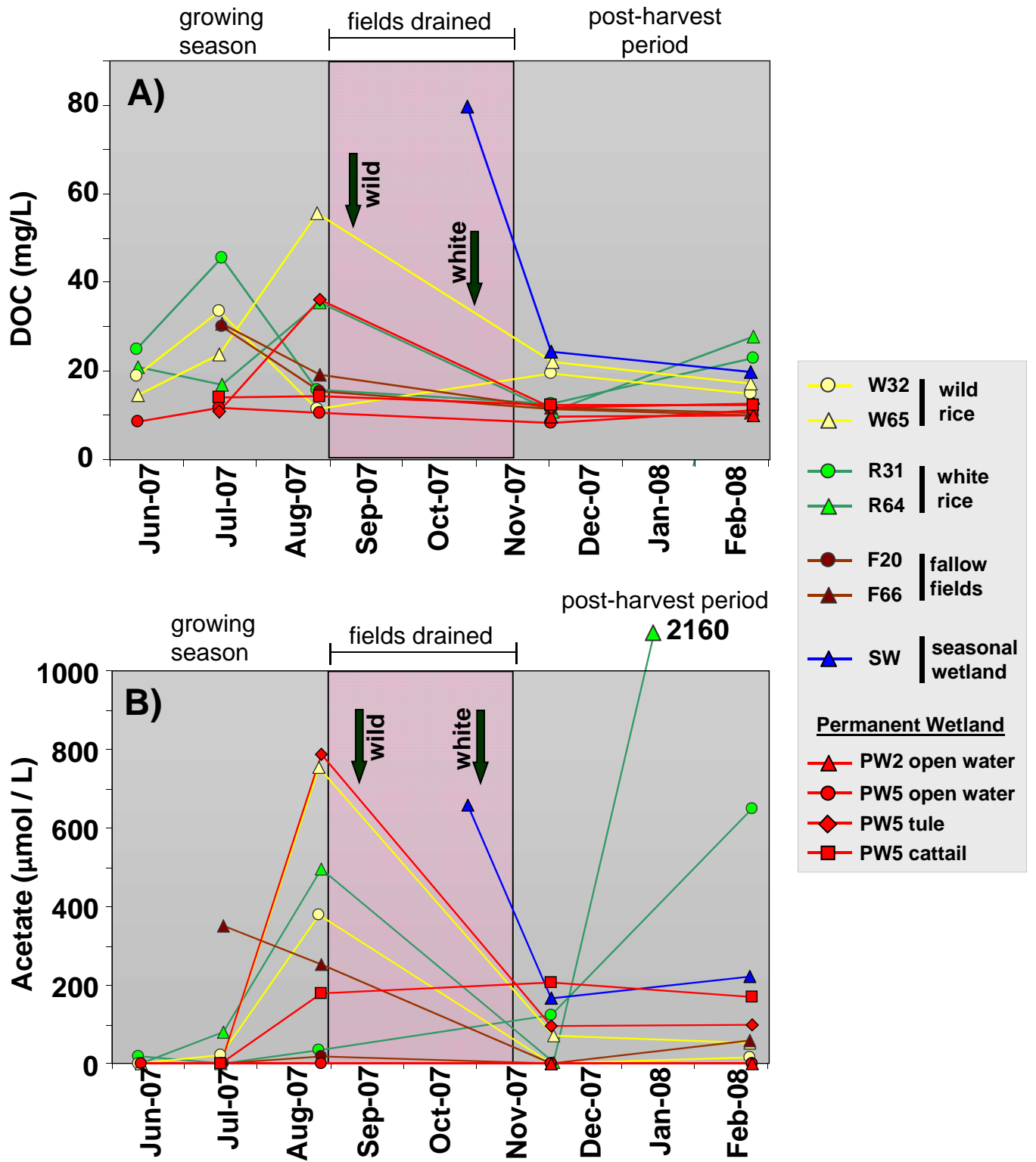


Figure 6.14. Time series plots of pore water (A) dissolved organic carbon (DOC) and (B) acetate, by field. Arrows and seasonal groupings are described in Figure 6.1.

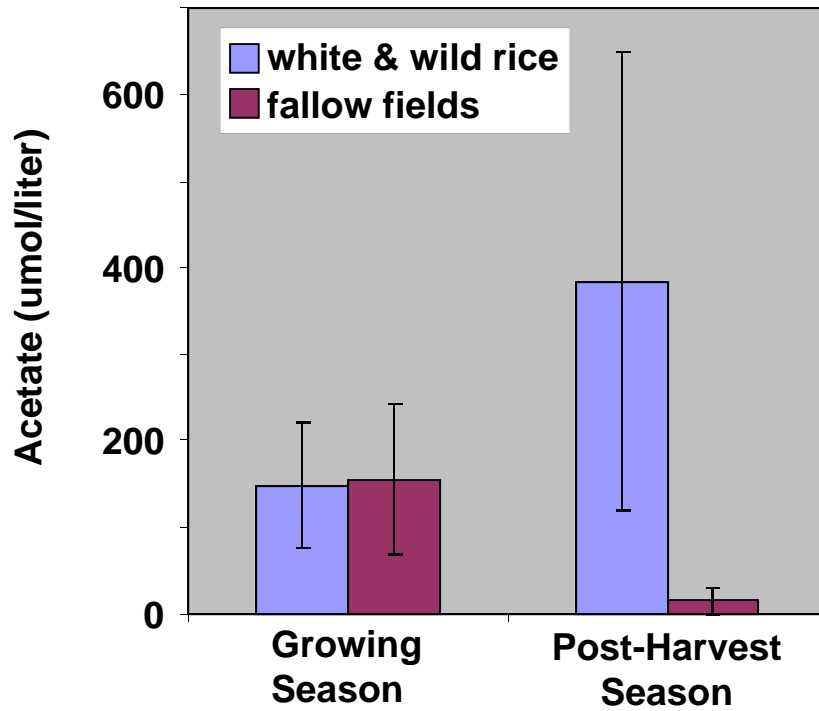


Figure 6.15. Bar graph of pore water acetate concentration by season (growing vs post-harvest) for rice (white and wild) fields and fallow fields. Error bars represent ± 1 standard error.

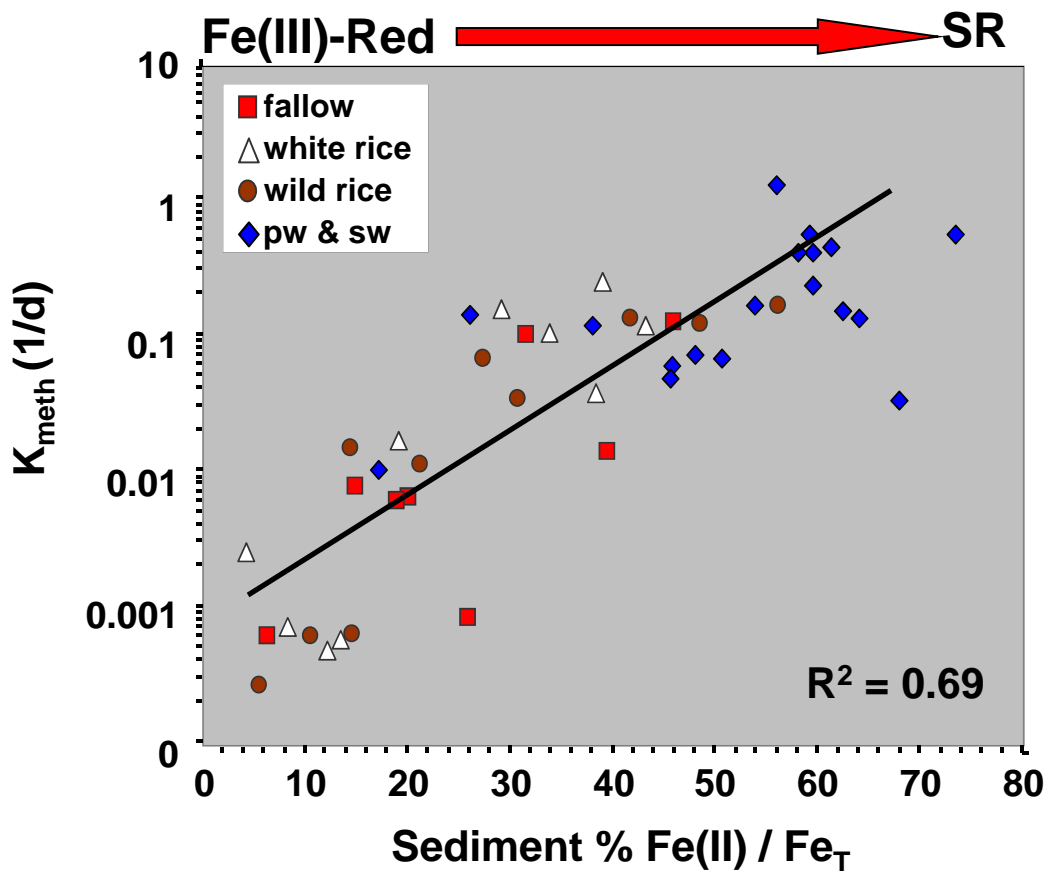


Figure 6.16. Linear-Log plot of sediment ferrous iron to total iron ratio (Fe(II)/Fe_T) versus ²⁰³Hg(II)-methylation rate constant (k_{meth}). Where: Fe_T = aFe(III) + cFe(III) + Fe(II). The solid line represents the linear least squares fit. The increase in the %Fe(II)/Fe_T metric can be thought of as a surrogate for geochemical conditions transitioning from a state poised for microbial Fe(III)-reduction, to one poised for microbial sulfate reduction (SR), as available Fe(III) becomes exhausted. This is indicated with the red arrow above the graphic.

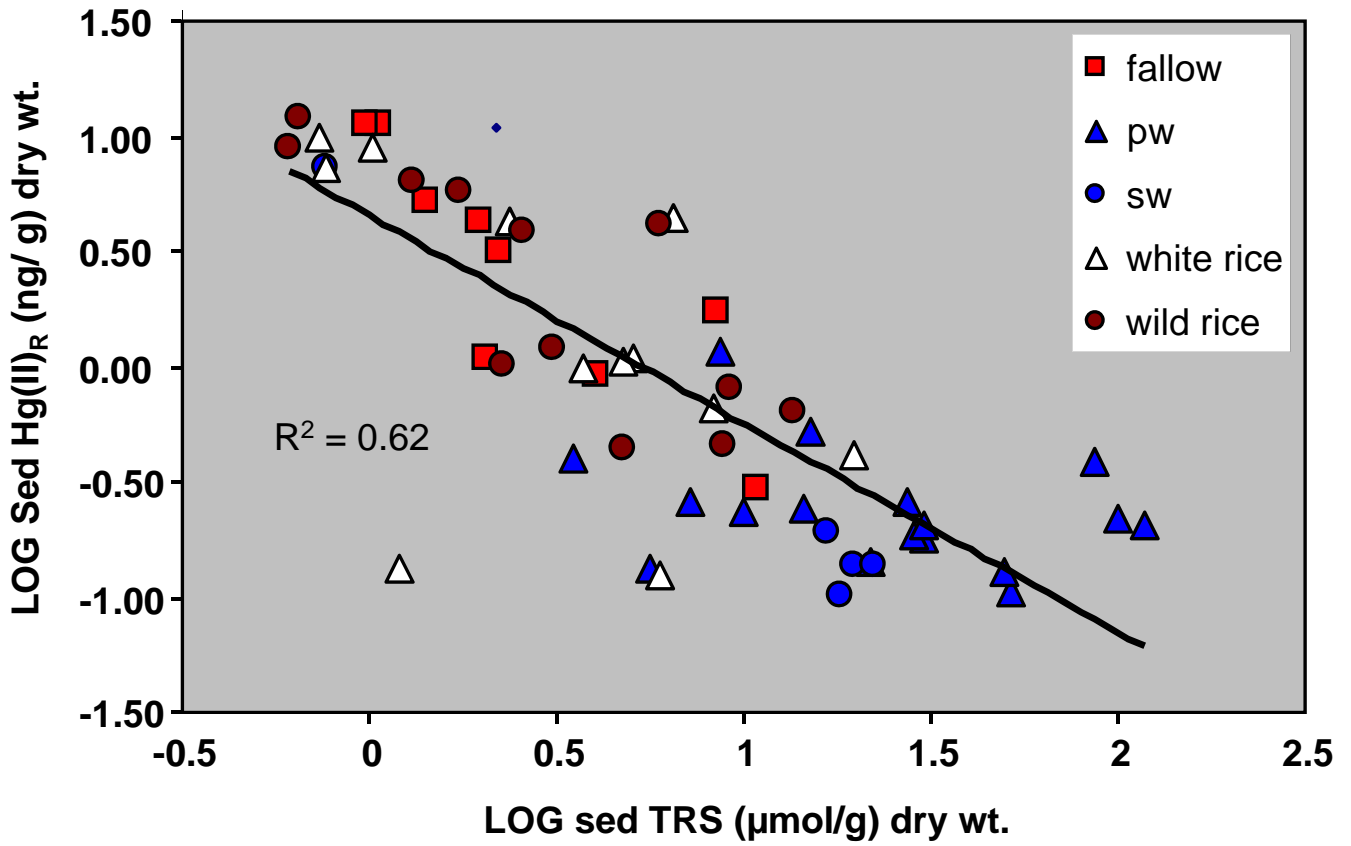


Figure 6.17. Log-Log plot of sediment total reduced sulfur (TRS) versus reactive inorganic mercury (Hg(II)_R). The solid line represents the linear least squares fit.

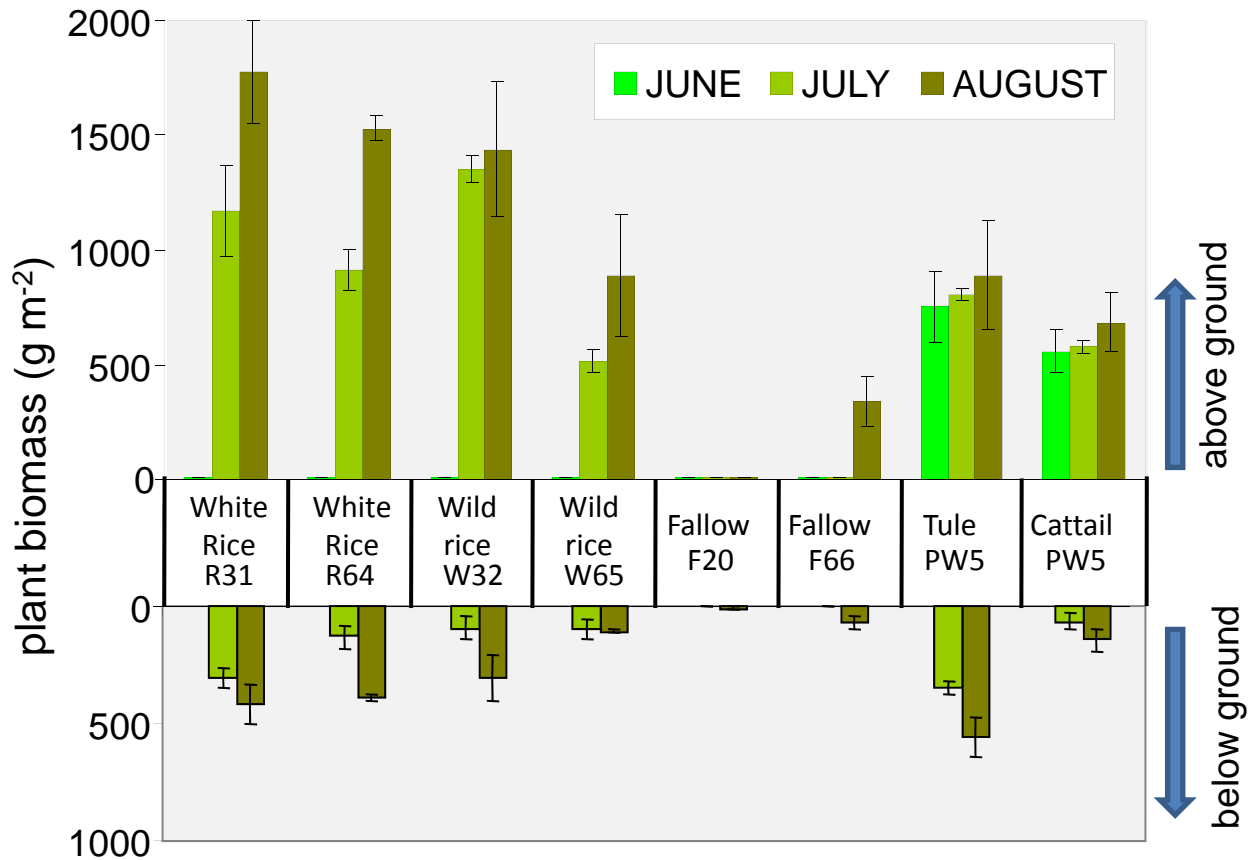


Figure 7.1 Bar graph of above and below-ground plant biomass in each field during the summer growing season, June–August 2007. Plant biomass is given on a dry weight basis. Error bars denote ± 1 standard deviation ($n=3$).

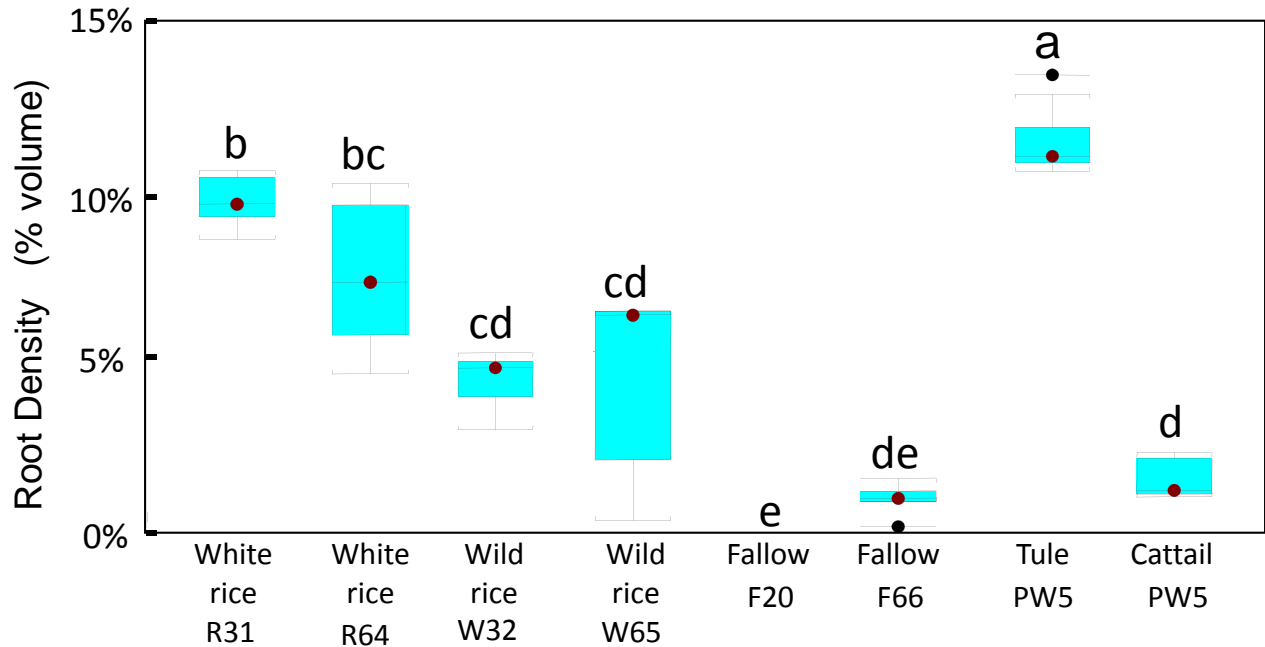


Figure 7.2. Box-and-whisker plot of live root density, expressed as the percentage of soil volume occupied by live roots in the top two centimeters of soil. Data from July (n=3) and August 2007 (n=3) are represented. Letters denote statistically significant ($p < 0.05$) differences as assessed by ANOVA with Bonferonni post-hoc test. Boxes that share a common letter are not significantly different.

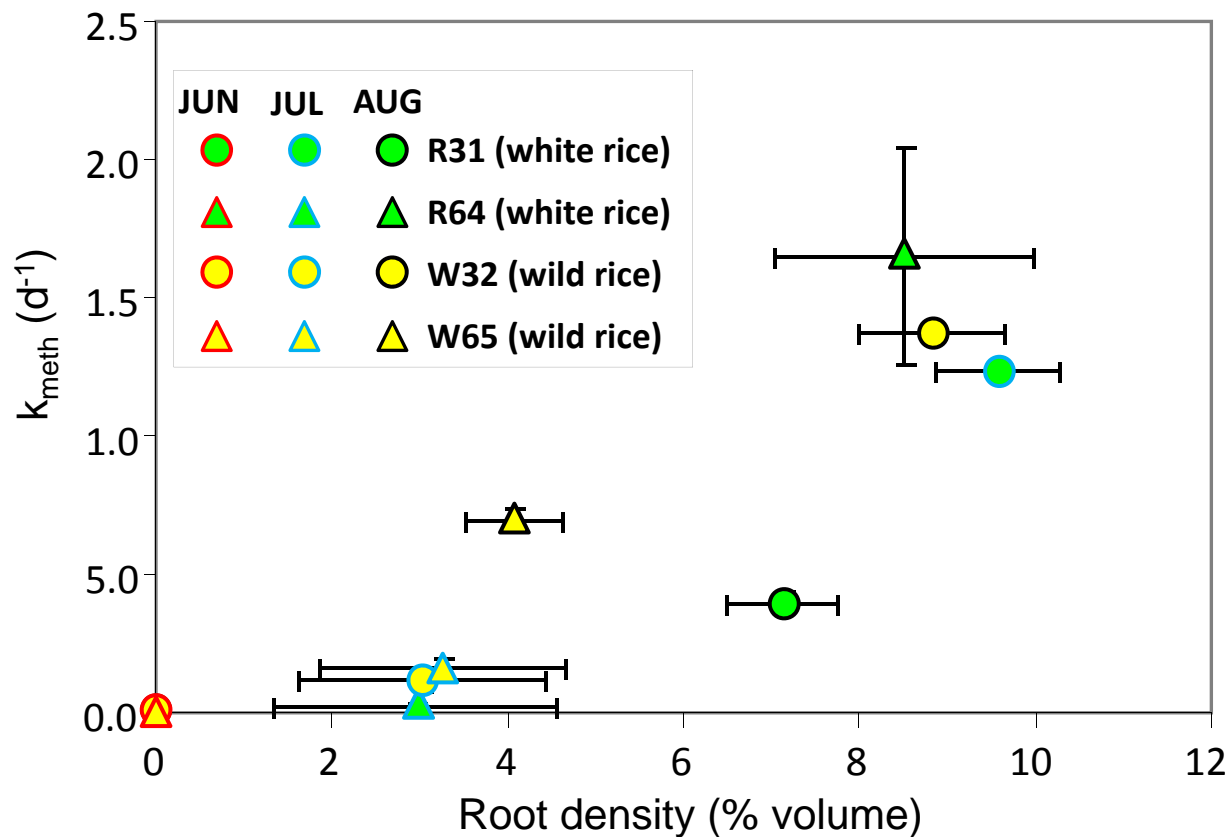


Figure 7.3. Scatterplot of live root density versus mercury methylation rate constant in actively growing rice fields during June, July and August 2007. X-axis error bars denote ± 1 standard deviation based upon $n=3$ observations. Y-axis error bars denote $\pm [\text{absolute difference}]/2$ based upon $n=2$ observations. Months coded by symbol outline: red = June, blue = July, black = August.

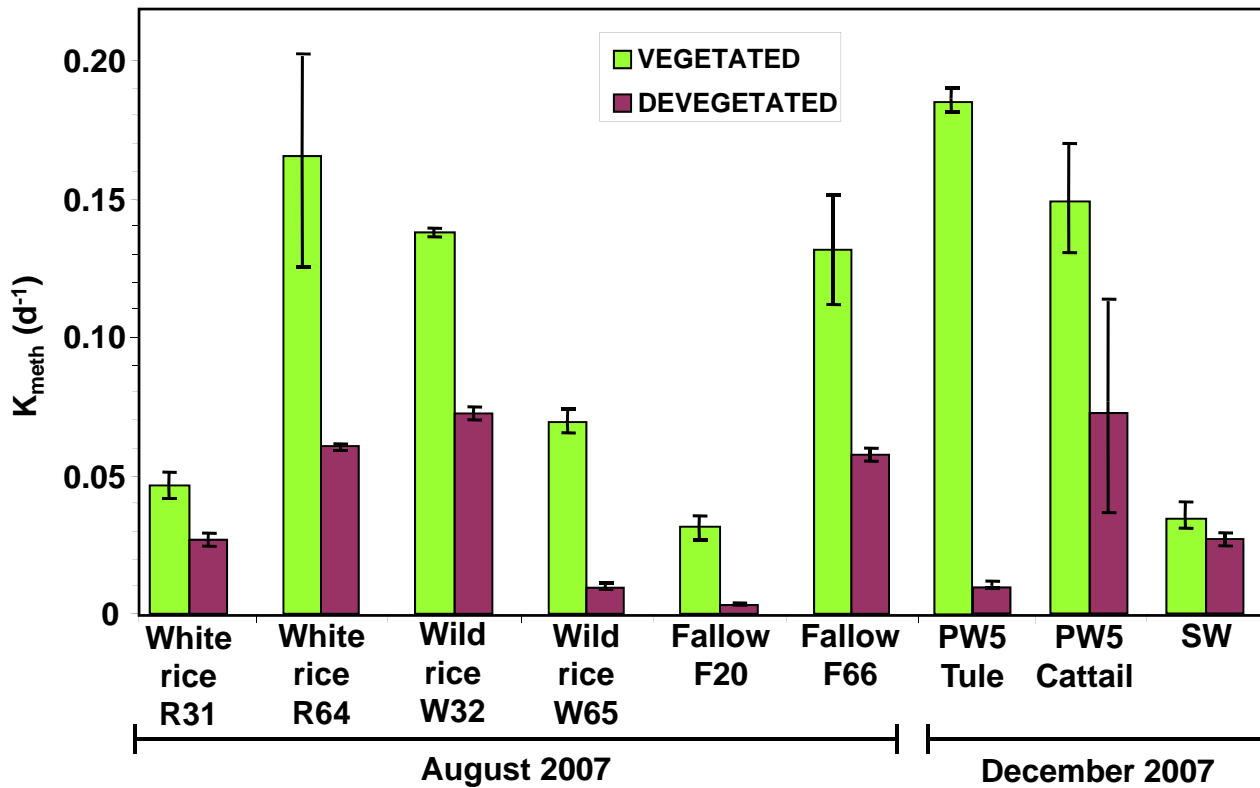


Figure 7.4. Bar graph depicting the 'devegetation effect' on the microbial mercury methylation rate constant in agricultural fields (August 2007) and non-agricultural fields (December 2007). N=2 observations for each treatment. Error bars denote \pm [absolute difference]/2.

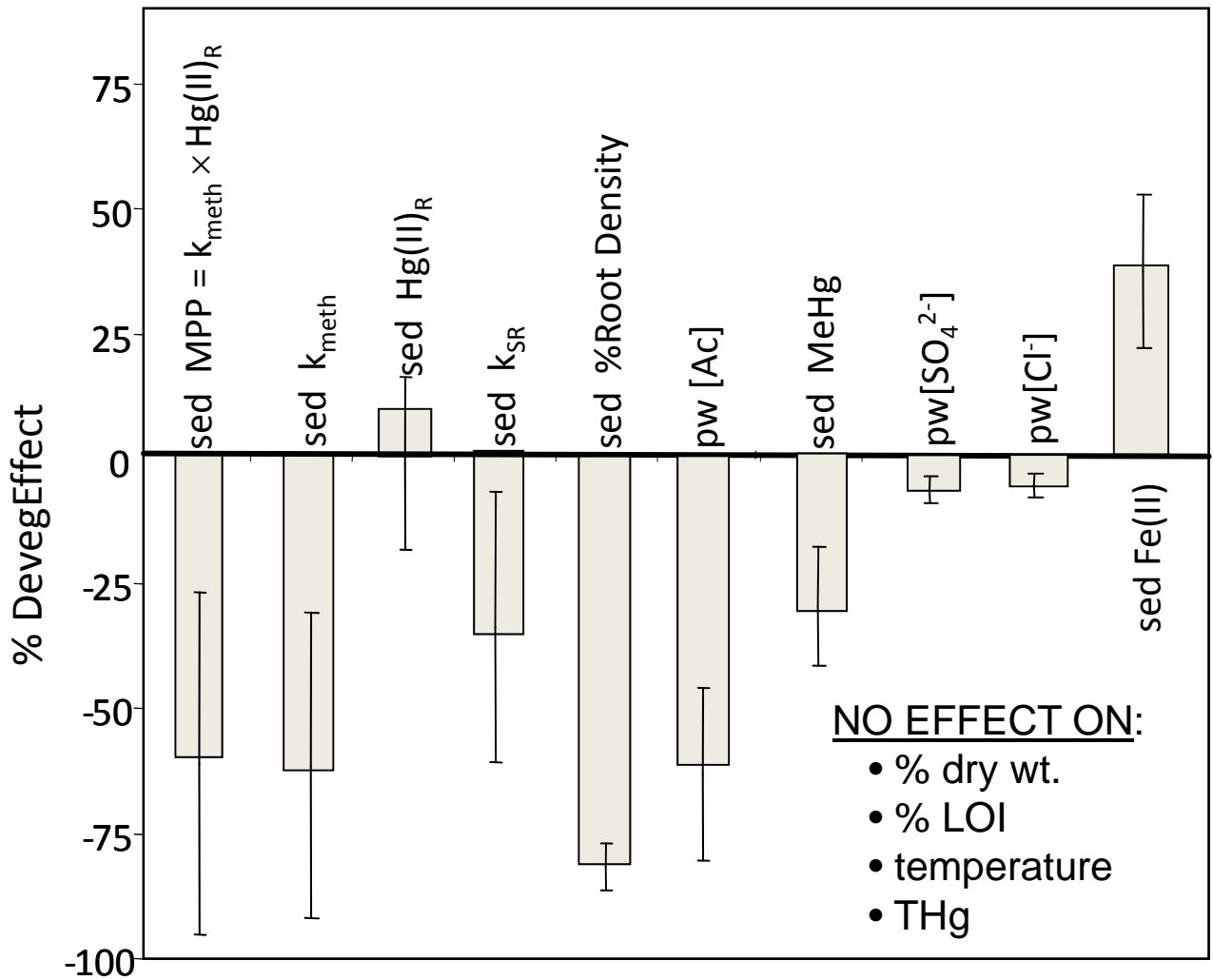


Figure 7.5. Bar graph of the percent devegetation effect on sediment and pore-water parameters in agricultural fields during the period of peak biomass (August 2007). Parameter notation as per **Table 6.1**. Percent devegetation effect (%DevegEffect) was calculated as per **Equation 7.1**. Significance assessed at $p < 0.05$ with pairwise t-tests. Error bars denote ± 1 standard deviation for $n=5$ agricultural fields. Non-significant comparisons (e.g. percent moisture, percent loss on ignition, temperature, total mercury) are not shown.

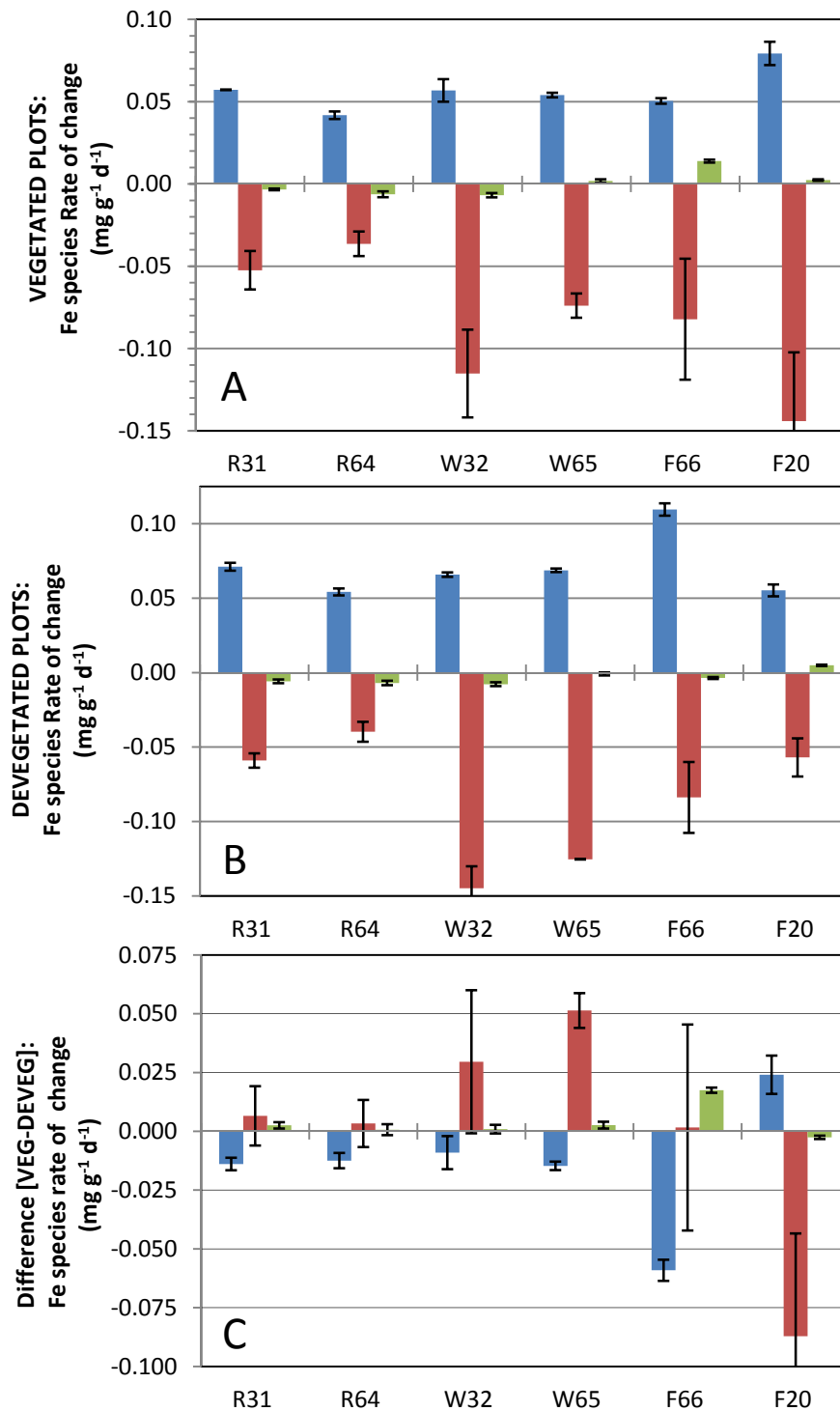


Figure 7.6. Bar graph of time-integrated daily rates of change in iron species in the surface (0-2 cm) sediment interval of individual agricultural fields for A) vegetated plots and B) devegetated plots, and C) the difference of vegetated plots minus devegetated plots. Error bars represent compounded errors. Rates were calculated based on an initial time-point of flood-up (June for white rice and wild rice, July for fallow) and a mid-season time point of peak temperatures and biomass (August for all sites). All rates are reported on a sediment dry weight basis. Iron species: Fe(II), acid-extractable ferrous iron; cFeIII, crystalline ferric iron; aFeIII, amorphous ferric iron.

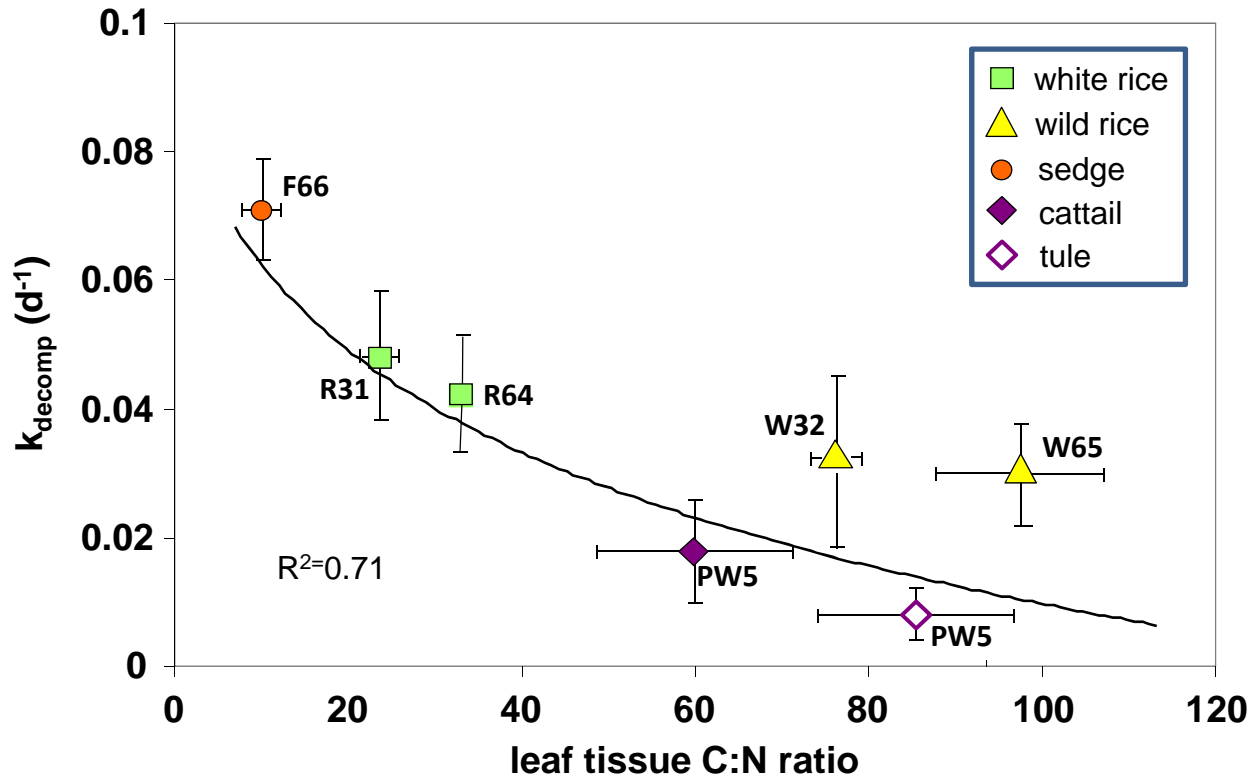


Figure 7.7. Scatterplot of leaf tissue carbon-to-nitrogen ratios versus litter decomposition rate constants for the dominant plant species in each field type. Plant tissue decomposition rate constants (k_{decomp}) were assessed experimentally in the laboratory during 28 days of incubations at 30°C. Error bars denote ± 1 standard deviation. An exponential regression was fit to the data ($y = -0.12 \ln(x)$) and was significant at $p < 0.05$.

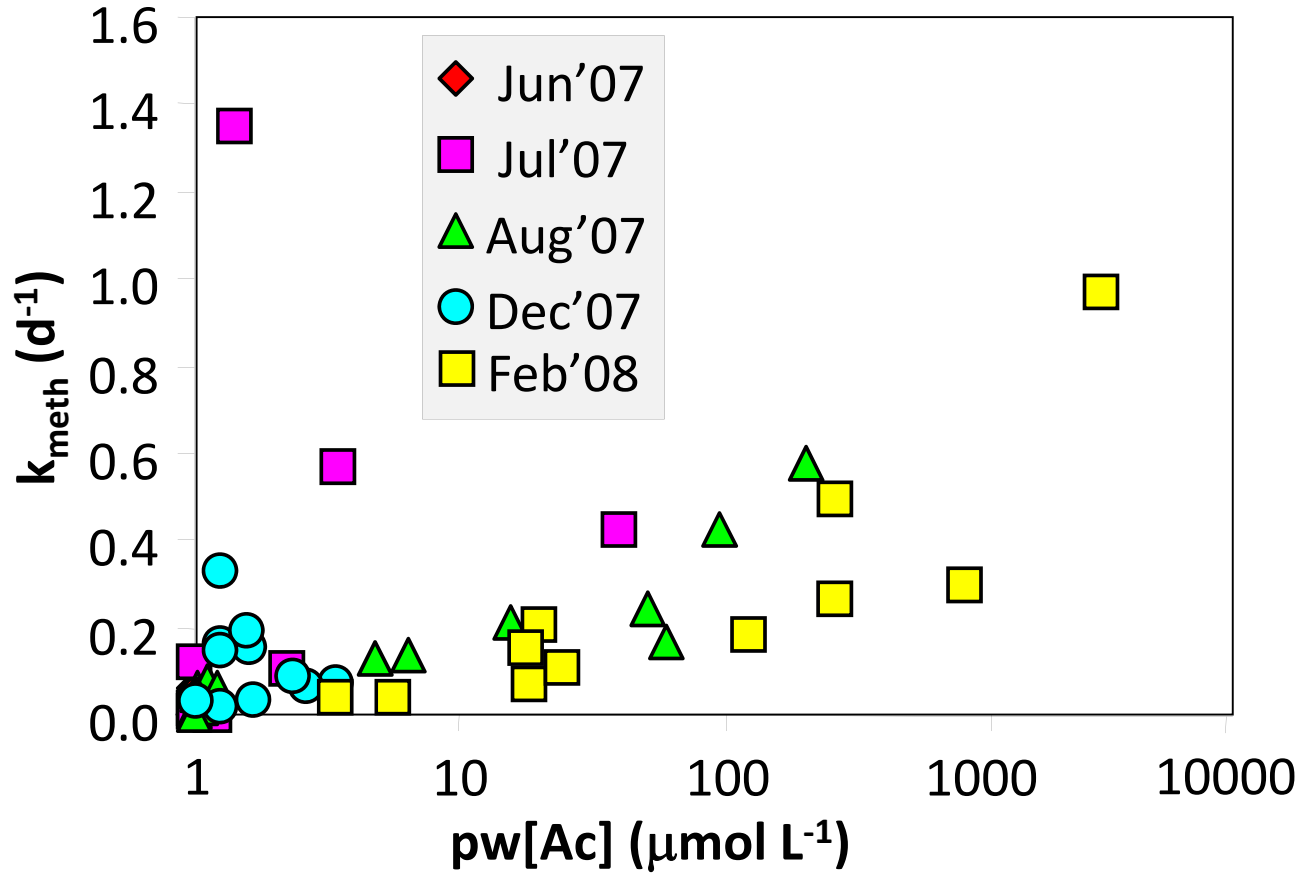


Figure 7.8. Log-linear plot of sediment pore water acetate concentration versus the mercury methylation rate constant, by sampling period. Significant ($p < 0.05$) non-linear relationships were observed for the peak of the growing season (August 2007; $y = 0.02 \ln(x)$, $r^2 = 0.42$) and for the mid-winter period during rice-straw decay (February 2008; $y = 0.02 \ln(x)$, $r^2 = 0.39$).

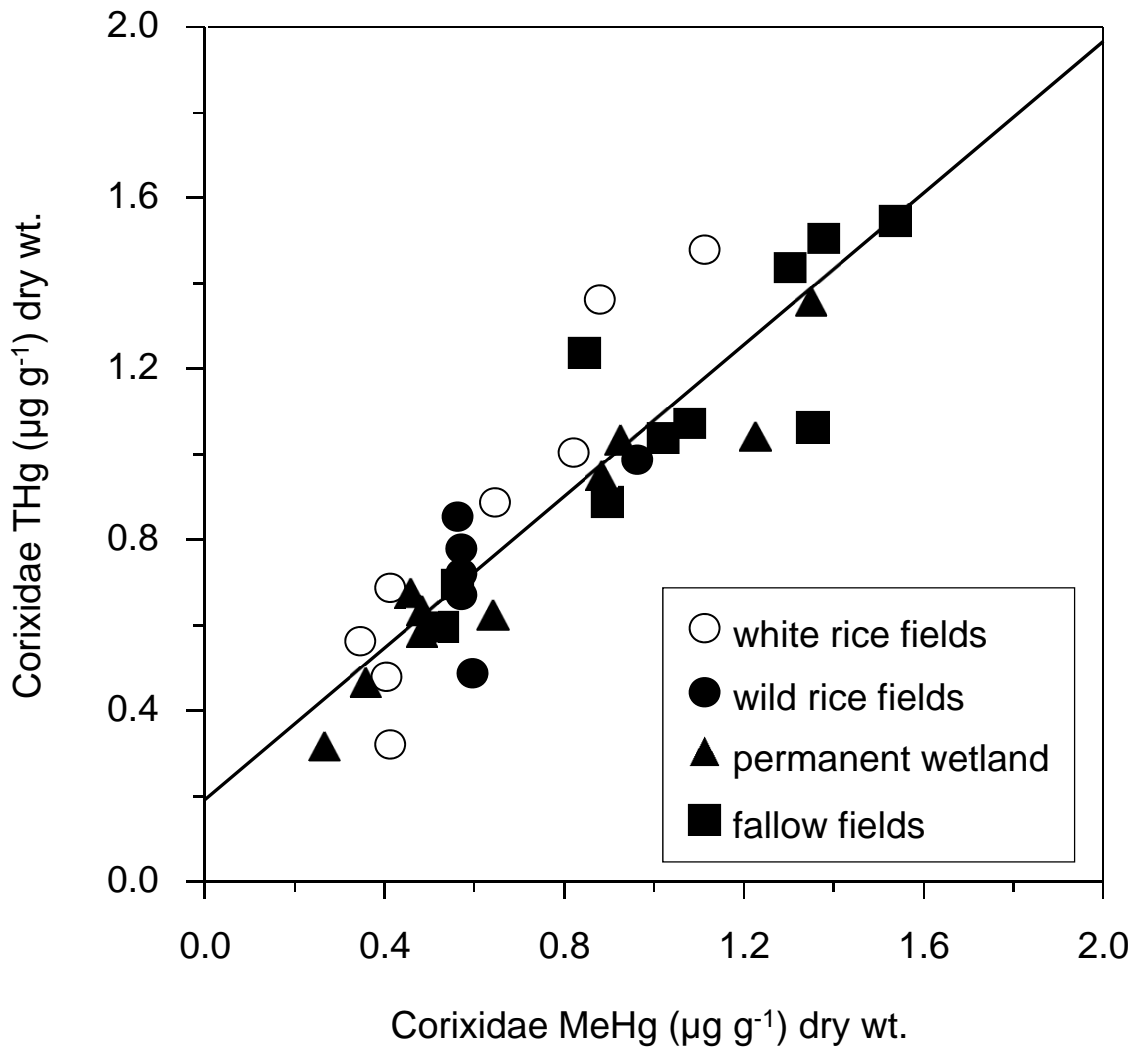


Figure 8.1. Scatter plot of Corixidae (water boatmen) methylmercury concentration versus total mercury concentration, by habitat type, in the Yolo Bypass Wildlife Area. Linear regression N=34, $R^2=0.80$, $P<0.0001$.

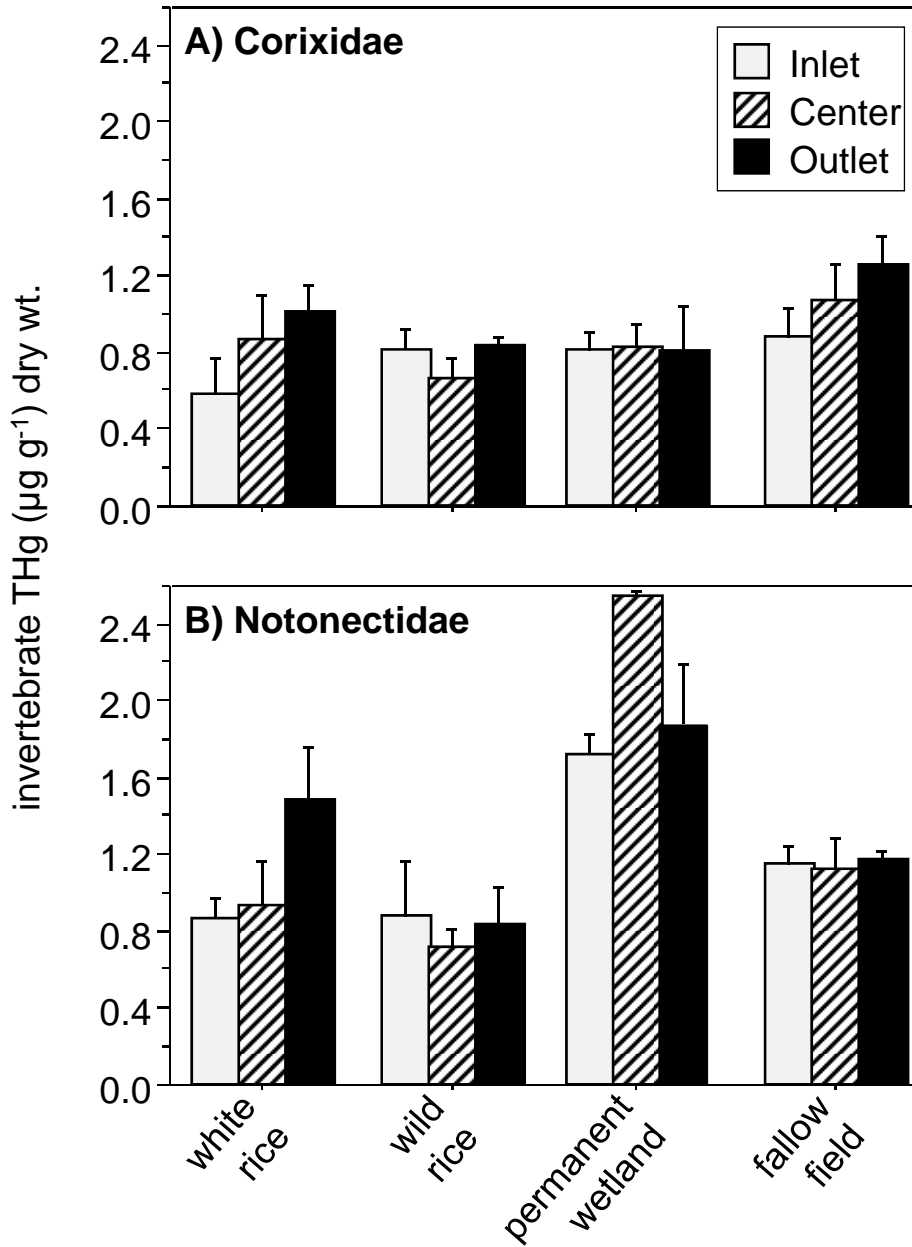


Figure 8.2. Bar graph of total mercury concentration in (A) Corixidae (water boatmen) and (B) Notonectidae (back swimmers) in agricultural fields of the Yolo Bypass Wildlife Area. Error bars reflect the standard error of the mean.

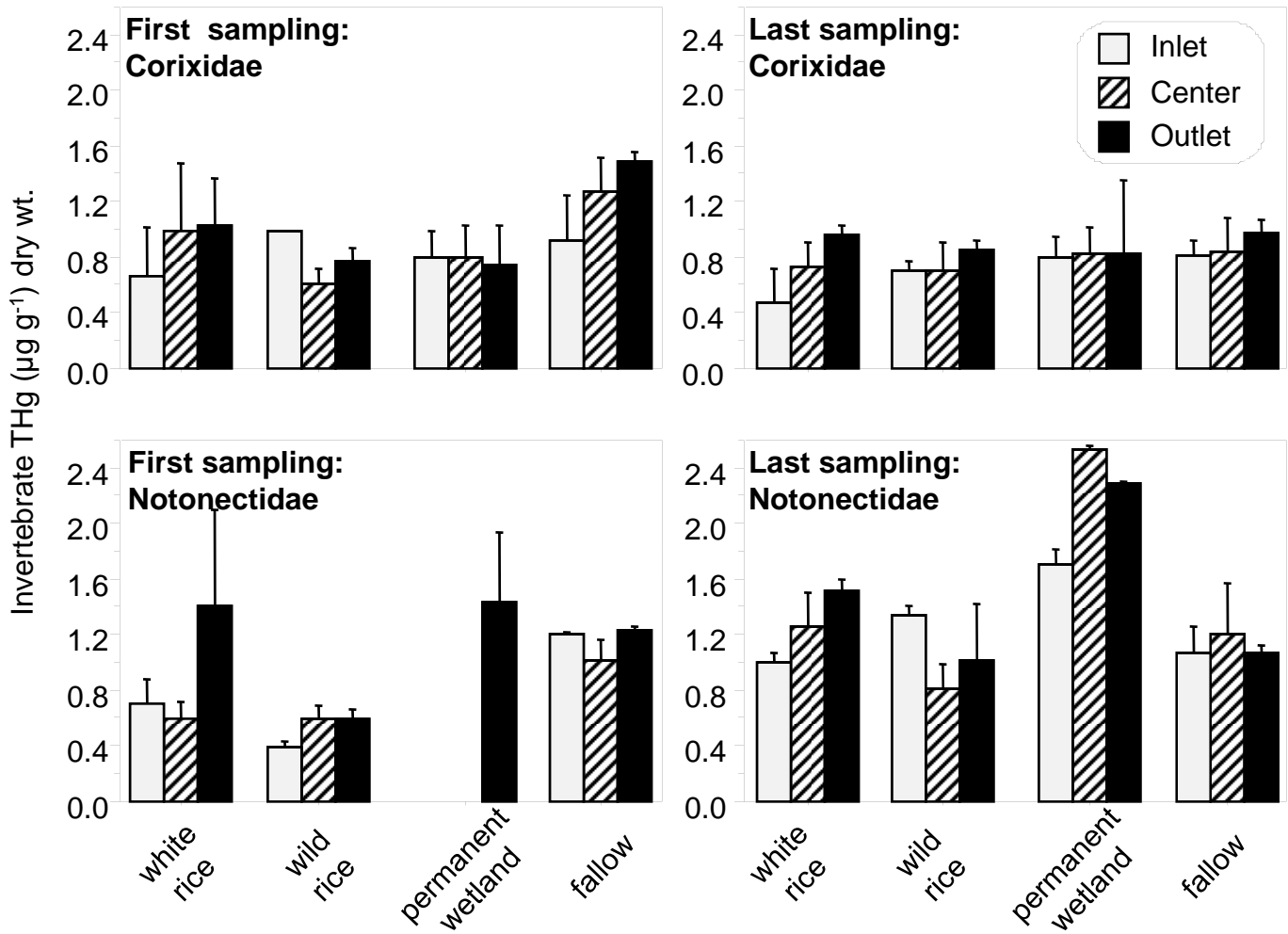


Figure 8.3. Bar graphs of total mercury concentration in Corixidae (water boatmen) and Notonectidae (back swimmers) at the inlets, centers, and outlets of shallowly-flooded fallow fields, by field type, in the Yolo Bypass Wildlife Area, during the first (25 June to 6 July 2007) and last (28 August to 19 September 2007) sampling event. Error bars reflect the standard error of the mean. The total number of observations were N=36 for Corixidae and N=45 for Notonectidae.

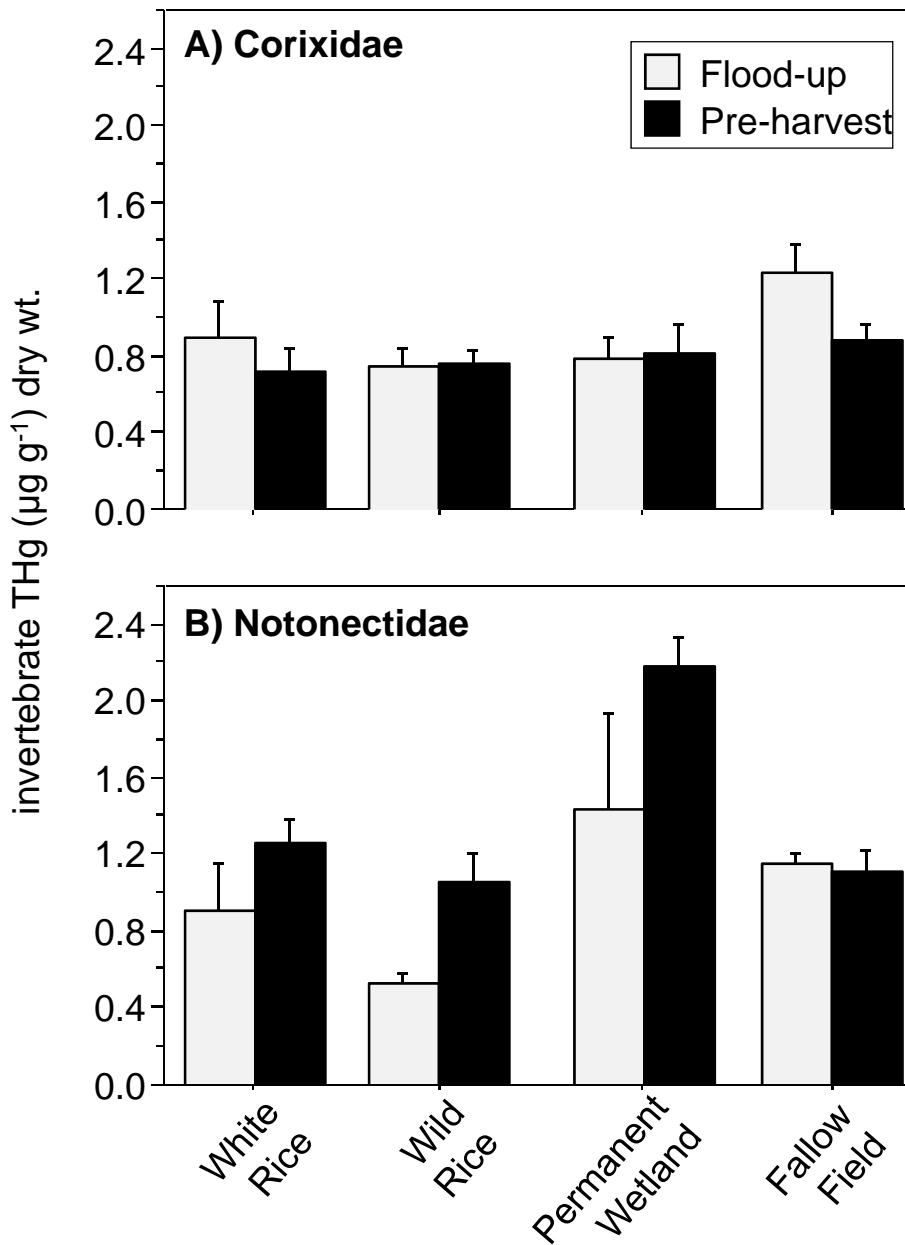


Figure 8.4. Bar graphs of total mercury concentration in (A) Corixidae (water boatmen) and (B) Notonectidae (back swimmers), by habitat type, during the field management periods of flood-up and rice pre-harvest in the Yolo Bypass Wildlife Area. Error bars reflect the standard error of the mean. The total number of observations were N=36 for Corixidae and N=45 for Notonectidae.

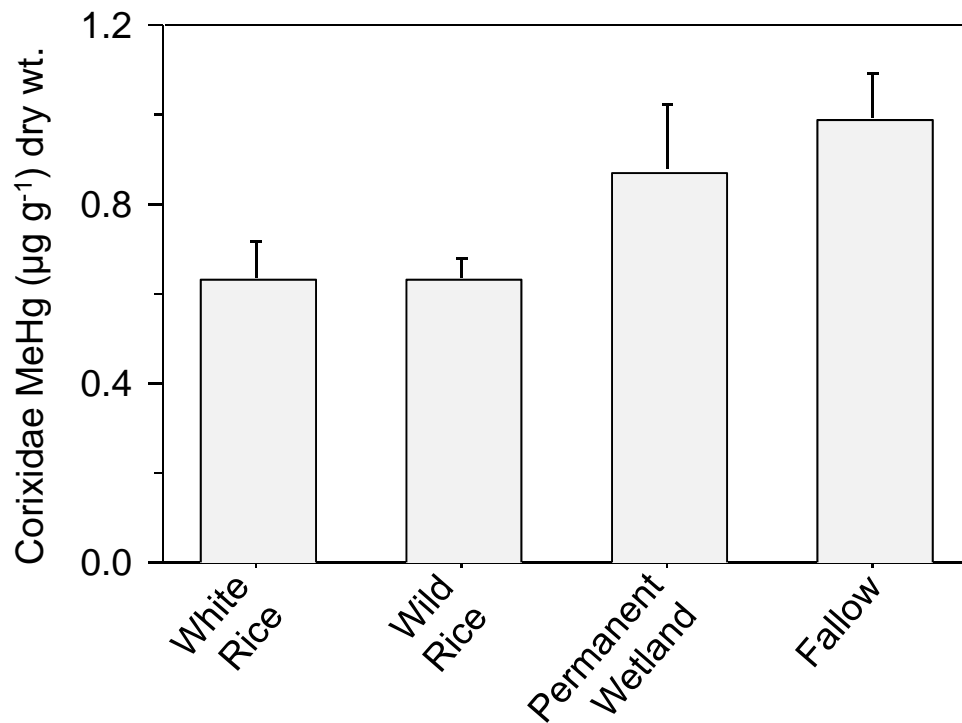


Figure 8.5. Bar graph of methylmercury concentration in Corixidae (water boatmen), by habitat type, in Yolo Bypass Wildlife Area. Error bars reflect the standard error of the mean. The total number of observations were N=36 for Corixidae and N=45 for Notonectidae.

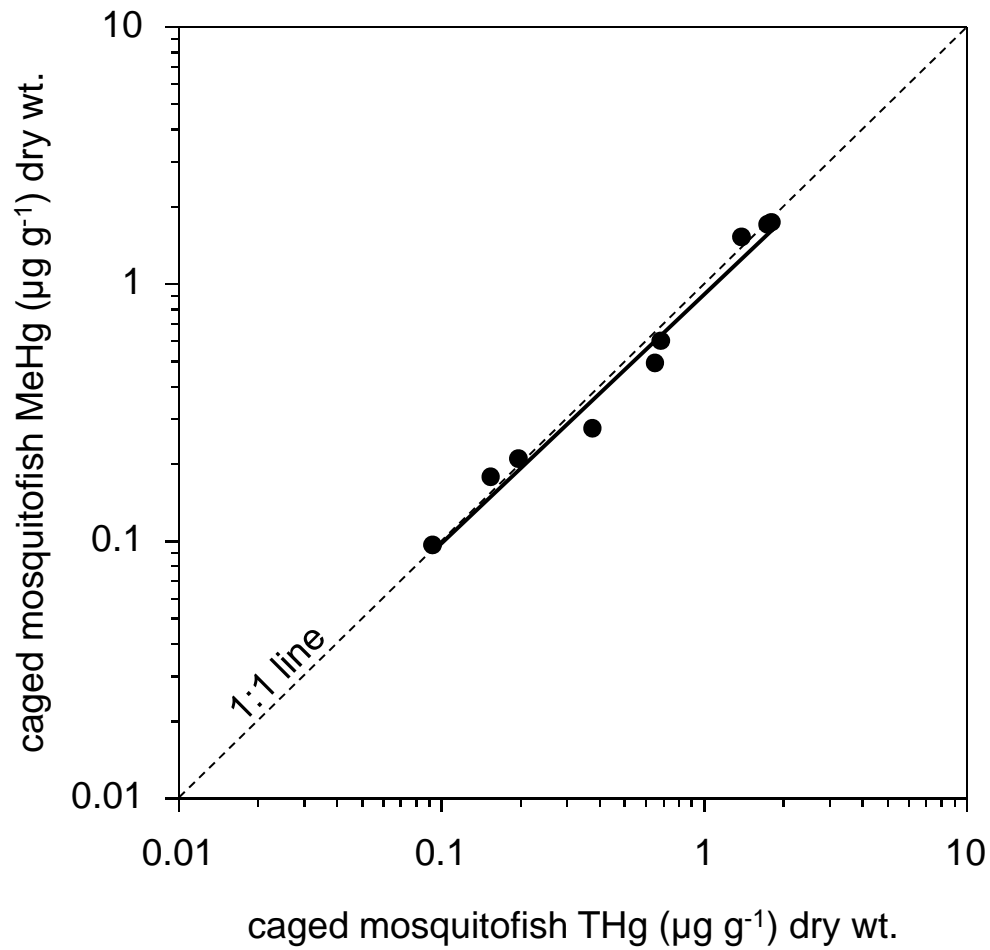


Figure 8.6. Log-Log plot of total mercury concentration versus methylmercury concentration in western mosquitofish introduced into cages within flooded agricultural fields in the Yolo Bypass Wildlife Area, California. The dashed line indicates the 1:1 relationship.

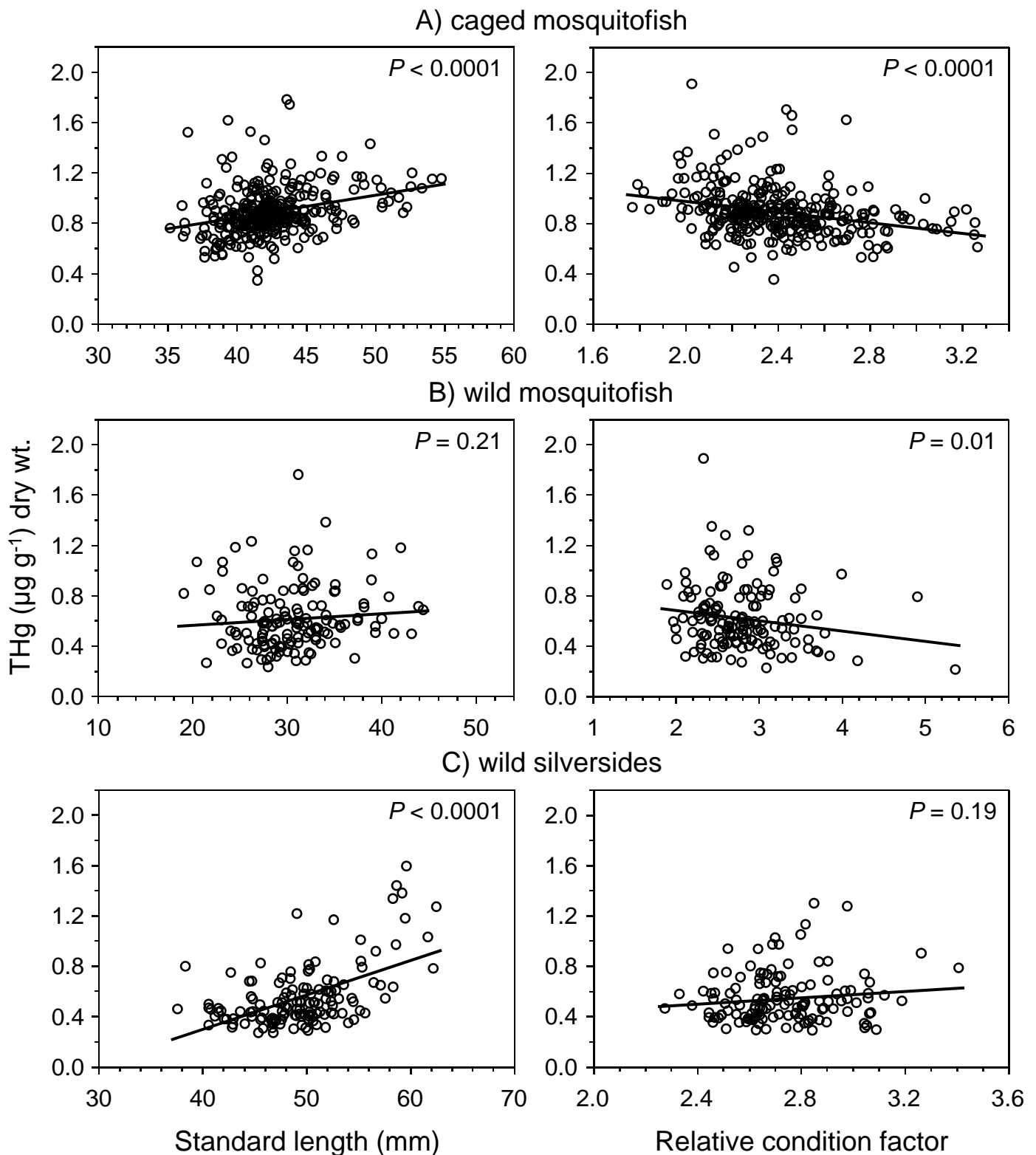


Figure 8.7. Partial leverage plots depicting the relationship between total mercury concentration and standard length or relative condition factor of (A) caged western mosquitofish, (B) wild western mosquitofish, and (C) wild Mississippi silversides in wetlands at the Yolo Bypass Wildlife Area. Partial leverage plots account for the potential effects of wetland habitat type, site within the wetland, habitat \times site interaction, standard length, and the relative condition factor as fixed effects, and wetland replicate as a random effect.

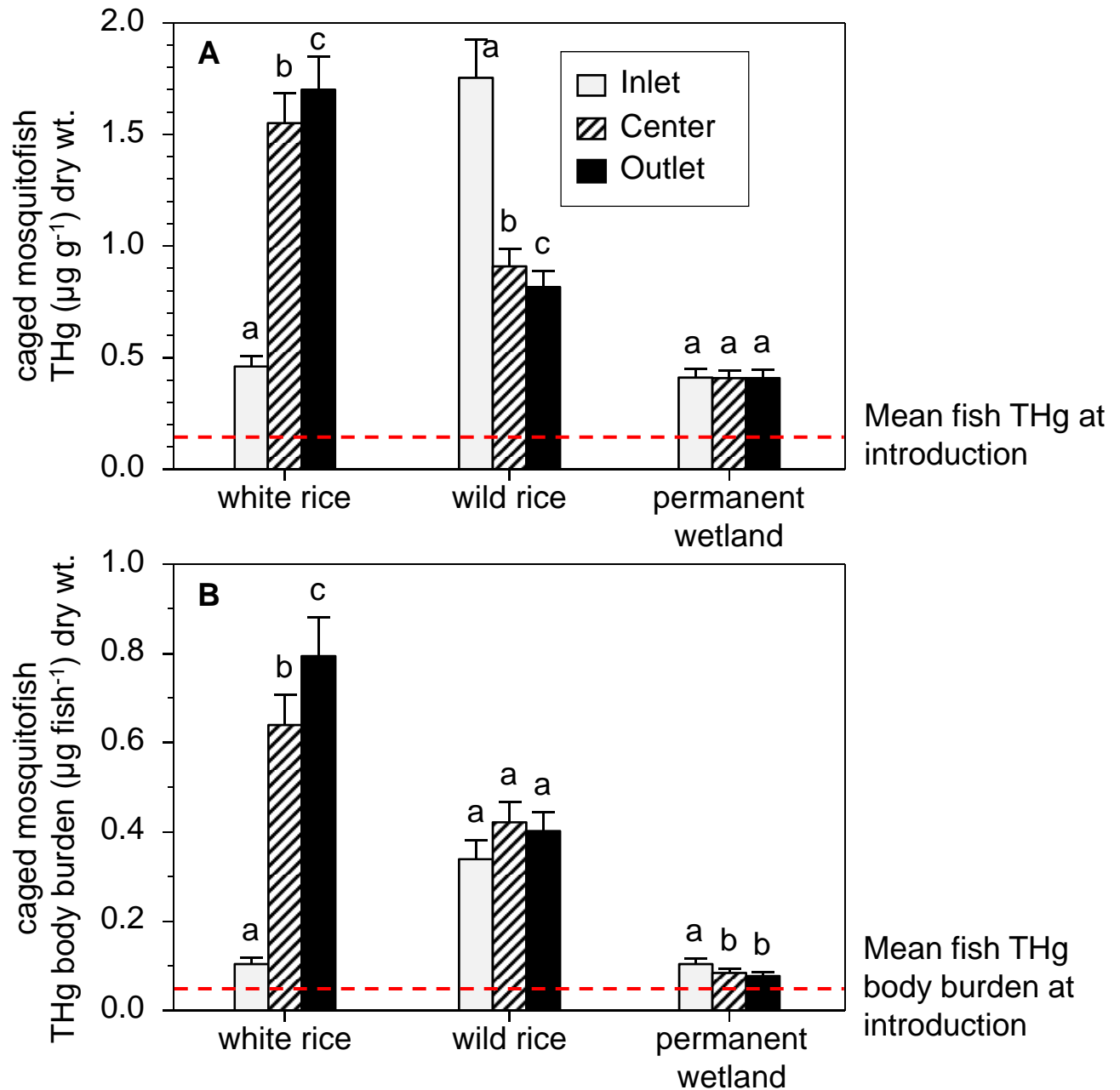


Figure 8.8. Bar graphs of (A) total mercury concentration and (B) total mercury body burden in western mosquitofish removed from cages after a 60-day of exposure period at the inlets, centers, and outlets of white rice, wild rice, and permanent wetland fields during the 2007 rice growing season at the Yolo Bypass Wildlife Area, California. The dashed lines indicate mean THg concentrations and body burdens of reference mosquitofish ($N = 37$) at the time of introduction into the cages. Different lowercase letters above bars indicate that values within a wetland habitat are statistically different ($p < 0.05$). Error bars reflect the standard error of the mean. The total number of observations was $N=304$ caged mosquitofish at removal.

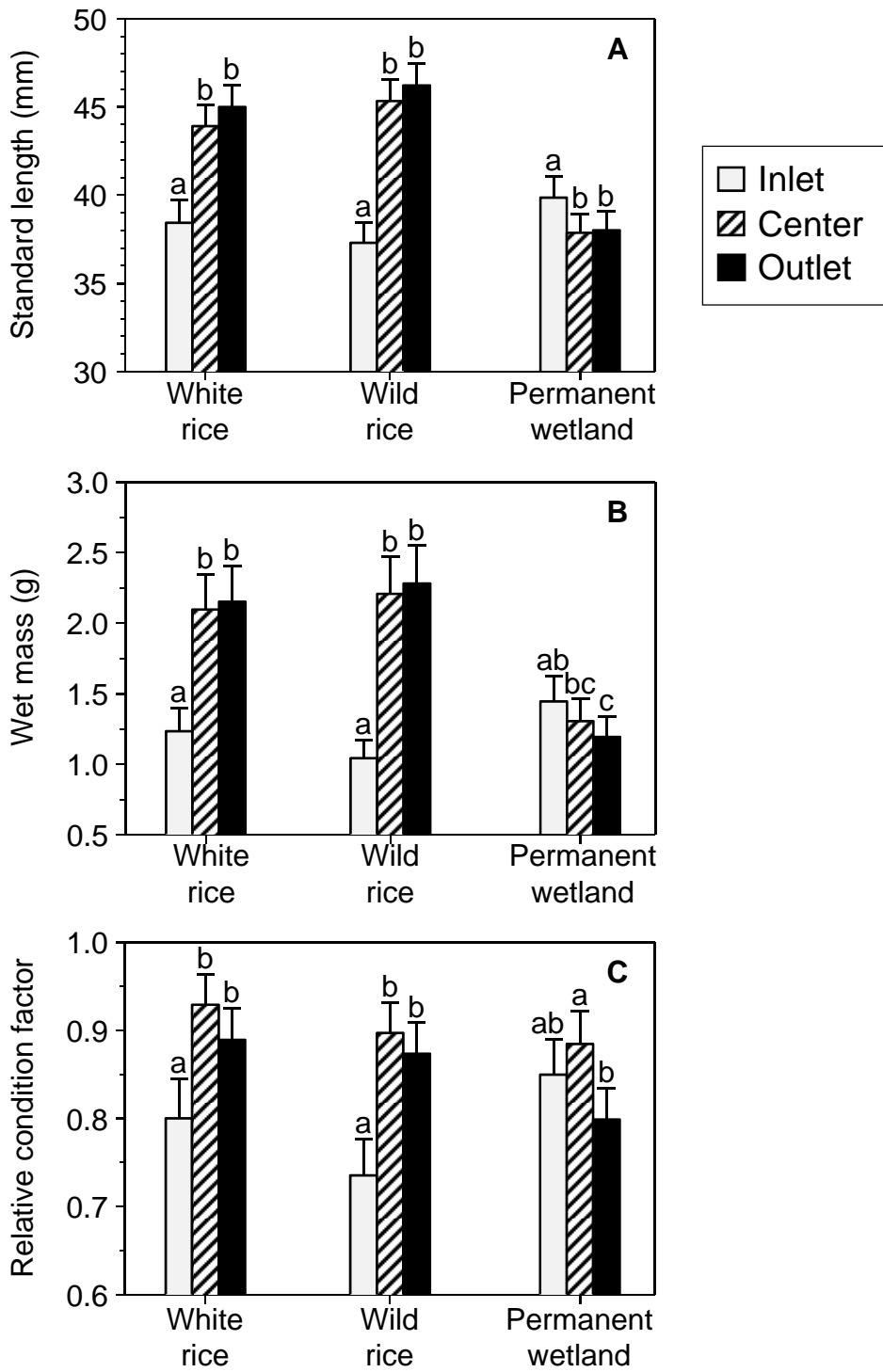


Figure 8.9. Bar graphs of (A) Standard length, (B) fresh wet mass, and (C) relative condition factor for western mosquitofish removed from cages after a 60-day exposure period at inlets, centers, and outlets of white rice fields, wild rice fields, and permanent wetlands during the 2007 rice-growing season, in the Yolo Bypass Wildlife Area, California. Different lowercase letters above bars indicate that values within a wetland habitat are statistically different ($P < 0.05$). Error bars reflect the standard error of the mean.

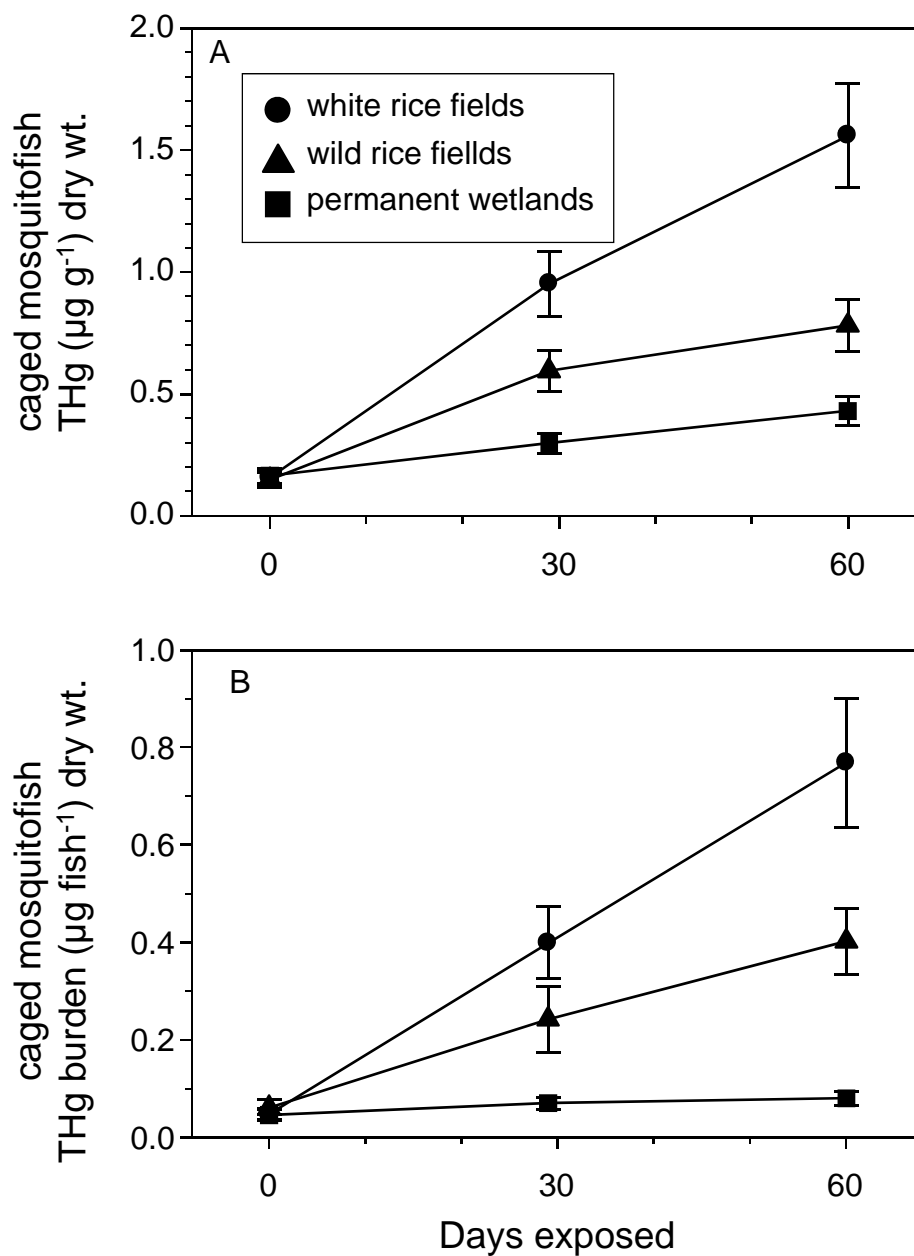


Figure 8.10. Time series plots of (A) total mercury concentration and (B) total mercury body burden of caged western mosquitofish over 60 days of exposure at the outlets of white rice, wild rice, and permanent wetland fields, during the 2007 rice growing season at the Yolo Bypass Wildlife Area, California. Error bars reflect the standard error of the mean.

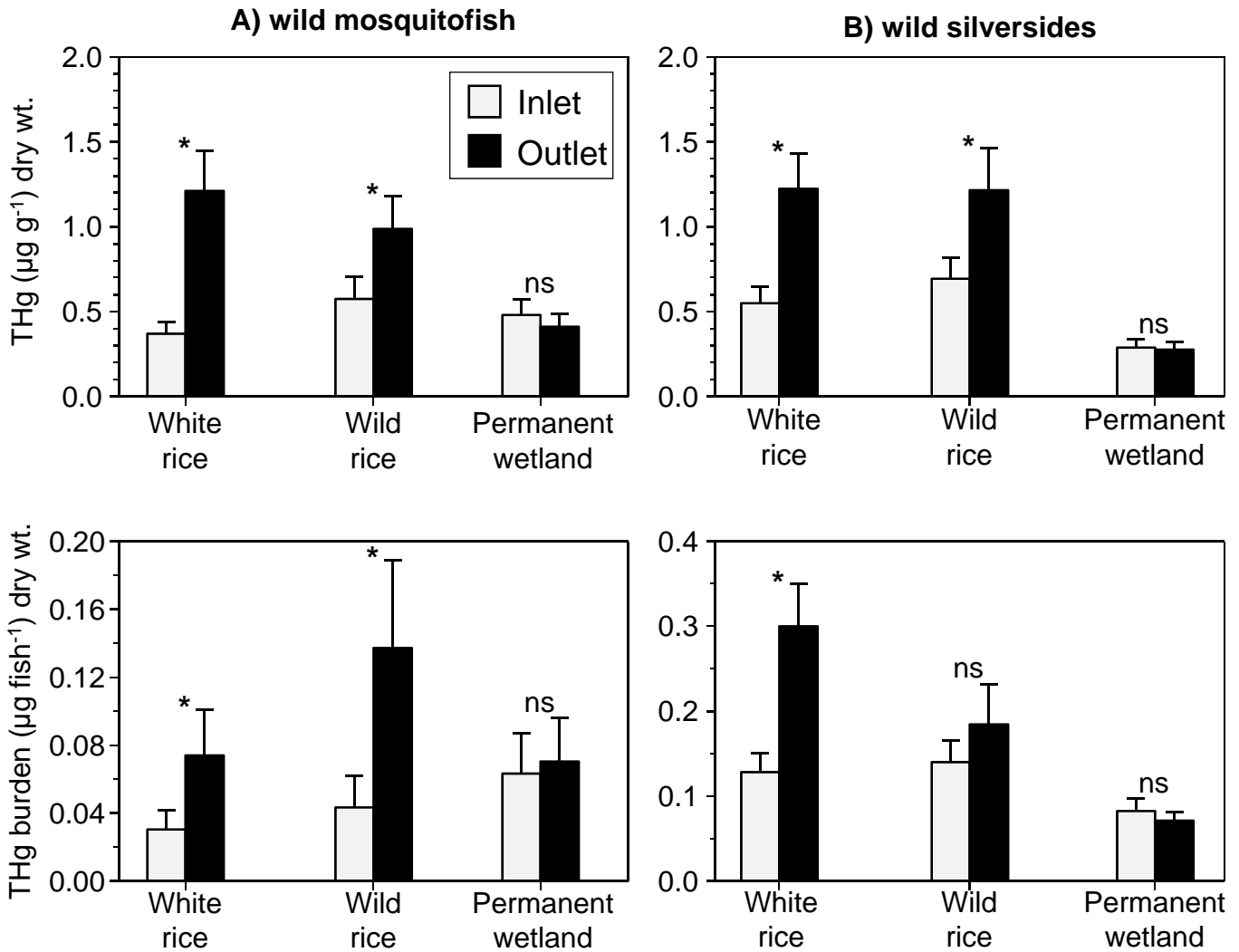


Figure 8.11. Bar graphs of total mercury concentrations and total mercury body burden in (A) wild western mosquitofish and (B) wild Mississippi silversides caught at the inlets and outlets of white rice, wild rice, and permanent wetland fields during the 2007 rice growing season at the Yolo Bypass Wildlife Area. Asterisk symbols above bars indicate that inlets and outlets within a wetland habitat are statistically different ($P < 0.05$) and “ns” indicates that values are not statistically different. Error bars reflect the standard error of the mean.

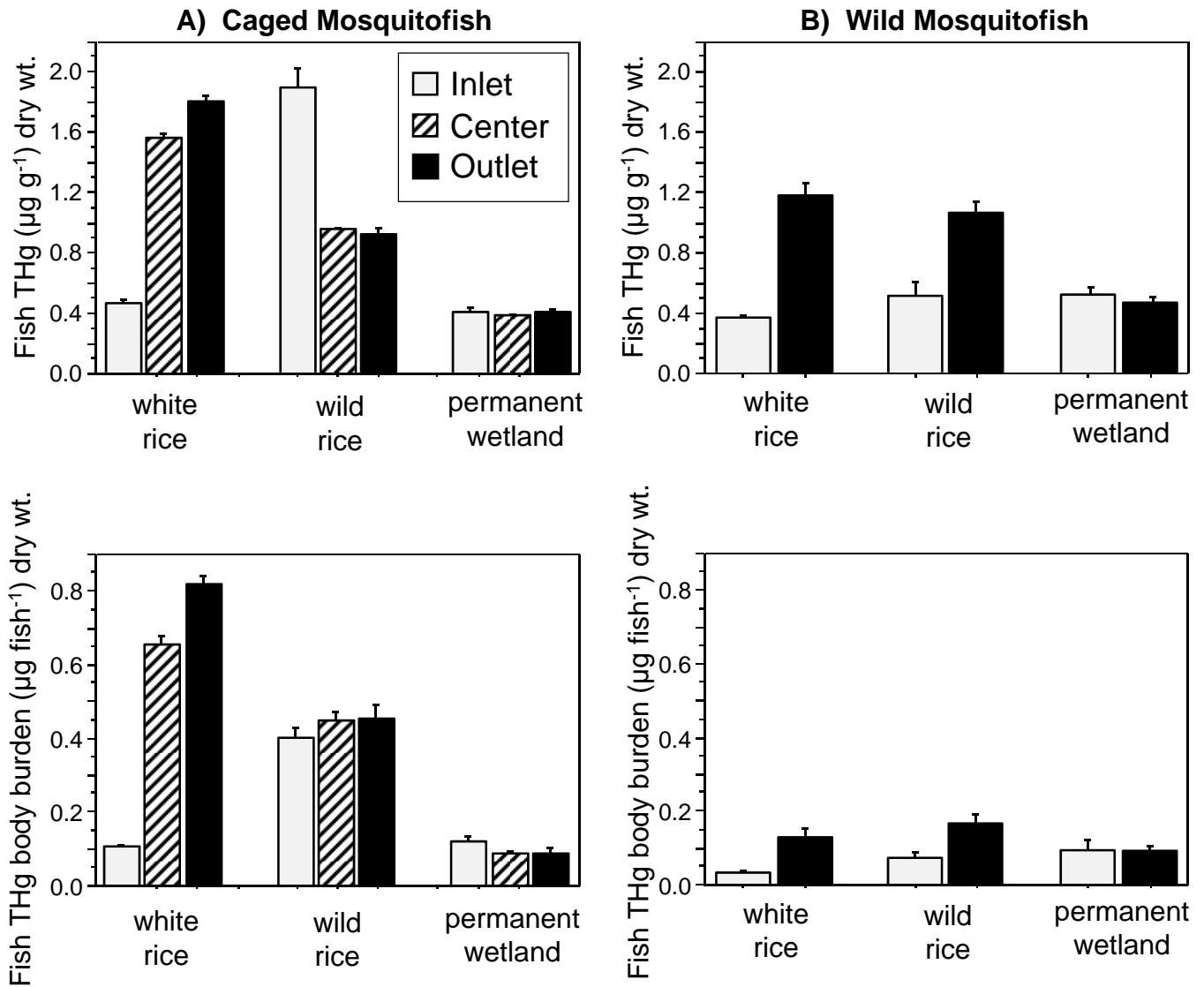


Figure 8.12. Bar graphs of (A) caged mosquitofish and (B) wild caught mosquitofish total mercury concentrations and total mercury body burden at the inlets, centers (caged only), and outlets of white rice, wild rice, and permanent wetlands during the 2007 rice growing season at the Yolo Bypass Wildlife Area. Error bars reflect the standard error of the mean.

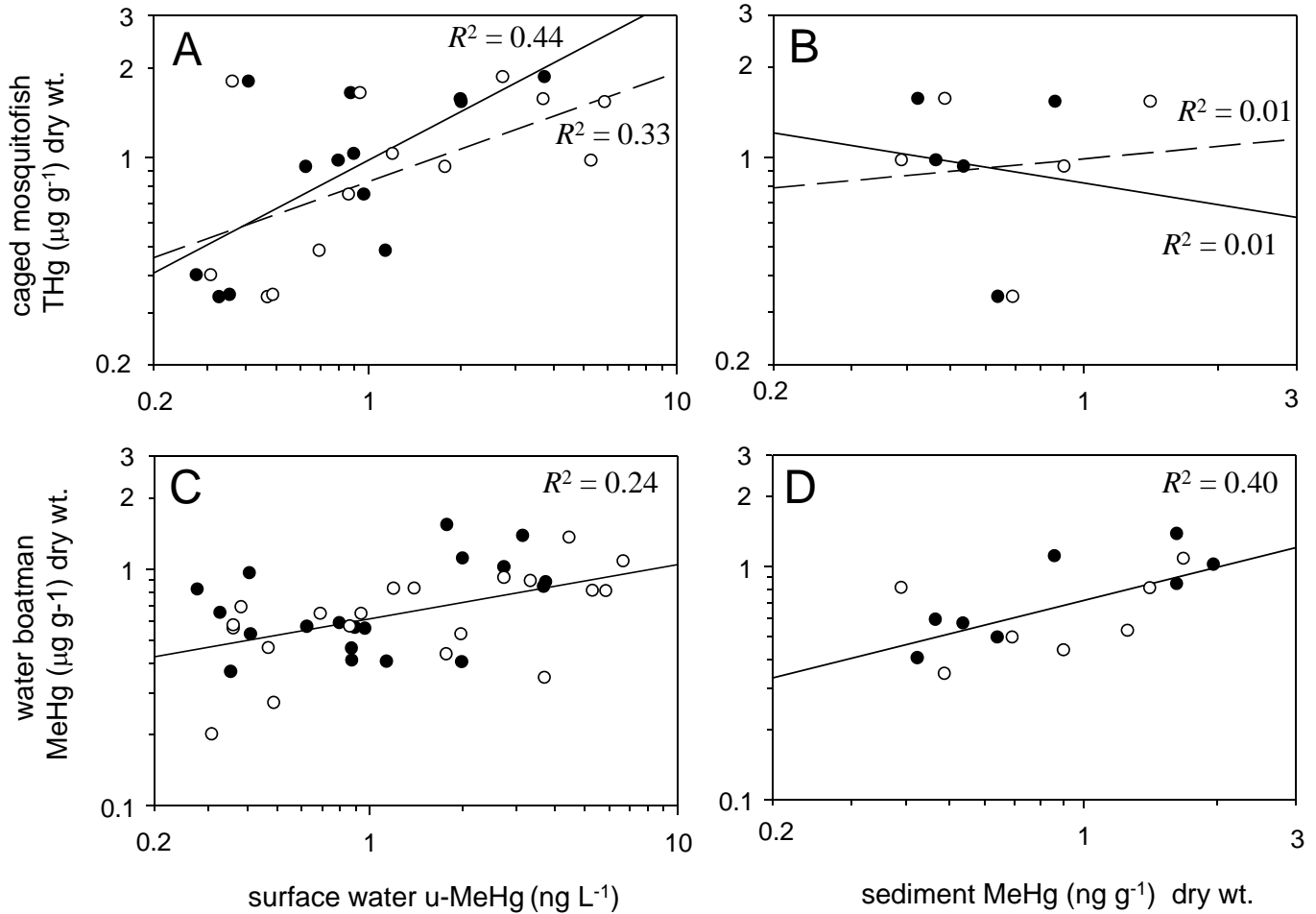


Figure 8.13. Log-Log plots of caged mosquitofish total mercury concentration versus (A) surface water unfiltered methylmercury concentration and (B) sediment methylmercury concentration, and Corixidae (water boatman) methylmercury concentration versus (C) surface water unfiltered methylmercury concentration and (D) sediment methylmercury concentration in agricultural and non-agricultural wetlands of the Yolo Bypass Wildlife Area during 2007. Closed symbols and solid lines indicate samples collected following flood-up of rice fields (early June) and open symbols and dashed lines indicate samples collected just before rice harvest (early September). Sediment only collected at centers of fields.



Figure 9.1. Photograph of photodemethylation experiment in the Yolo Bypass Wildlife Area, Calif.. Opaque Teflon® bottles were used as dark controls and clear Teflon® bottles were used for photo-sensitive treatments, reflecting conditions in surface waters.

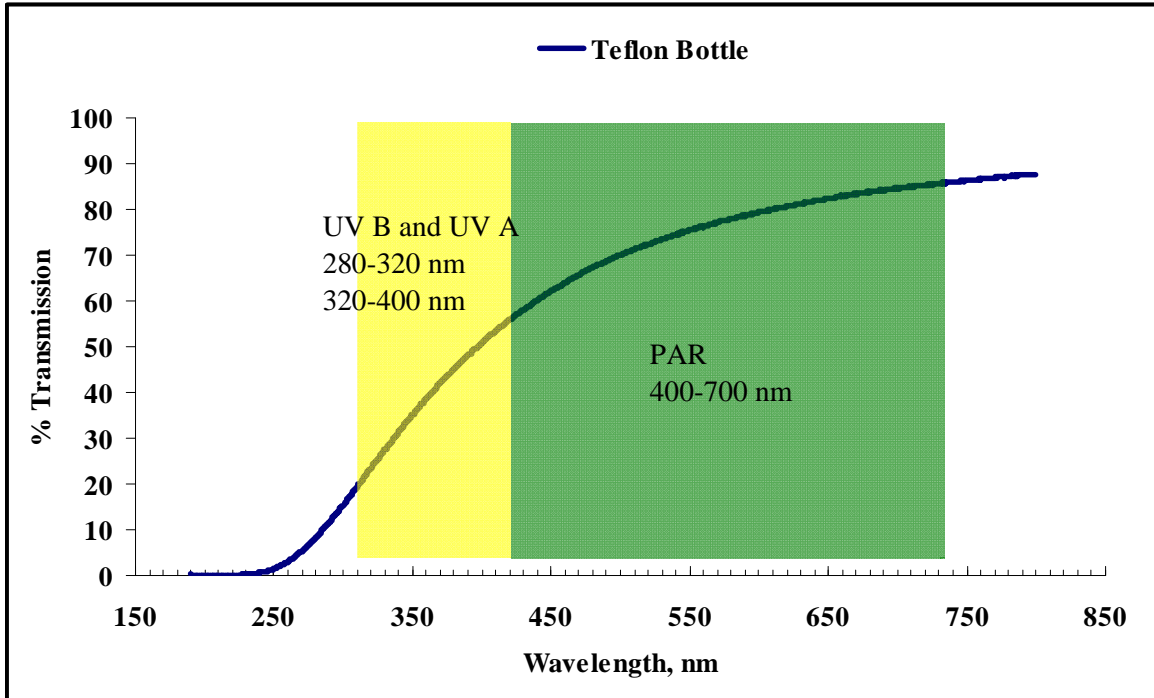


Figure 9.2. Graph showing light wavelength versus the percentage of light transmission through the incubation bottles used in the photodemethylation experiments. The percentage (%) transmission of UV-visible wavelengths through a clear FEP Teflon® bottle was determined in the laboratory with a spectrophotometer. The average light transmission in the photosynthetically available radiation (PAR) and ultra violet (UV) regions were estimated to be 69% and 35%, respectively. Figure from **Byington (2007)**.

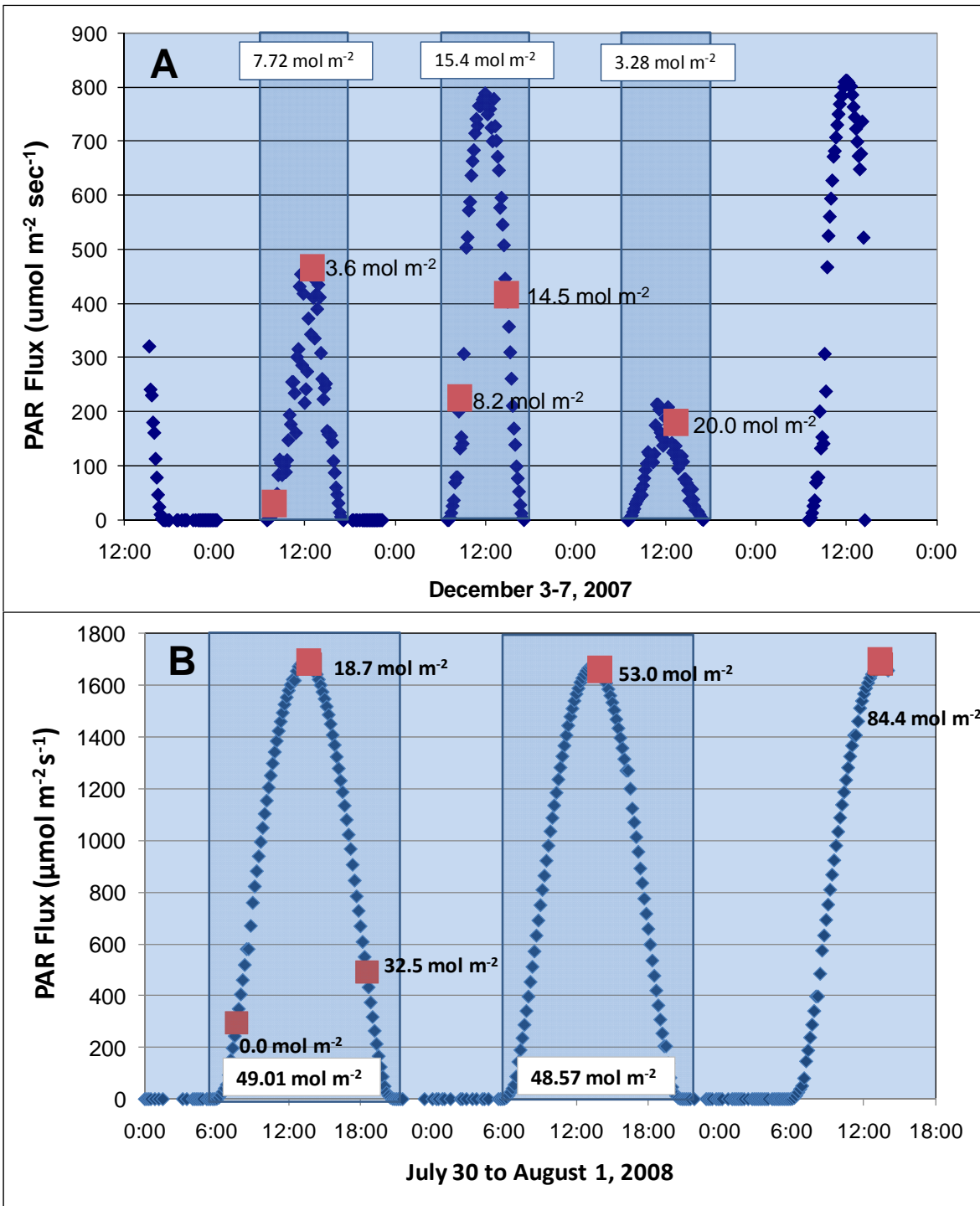


Figure 9.3. Time series plots of instantaneous flux of photosynthetically available radiation for A) December 3–7, 2007 and B) July 30 – August 1, 2008. Shaded areas for both time series are annotated with the total ultraviolet (UV, Uva + UVb) radiation flux (mol m^{-2}) for a given day, illustrating the daily variability in winter UV flux and more consistent summer UV flux. Shown in both figures are the time points (red square) and average, cumulative total in-bottle PAR flux (mol m^{-2}) at the time of sample collection.

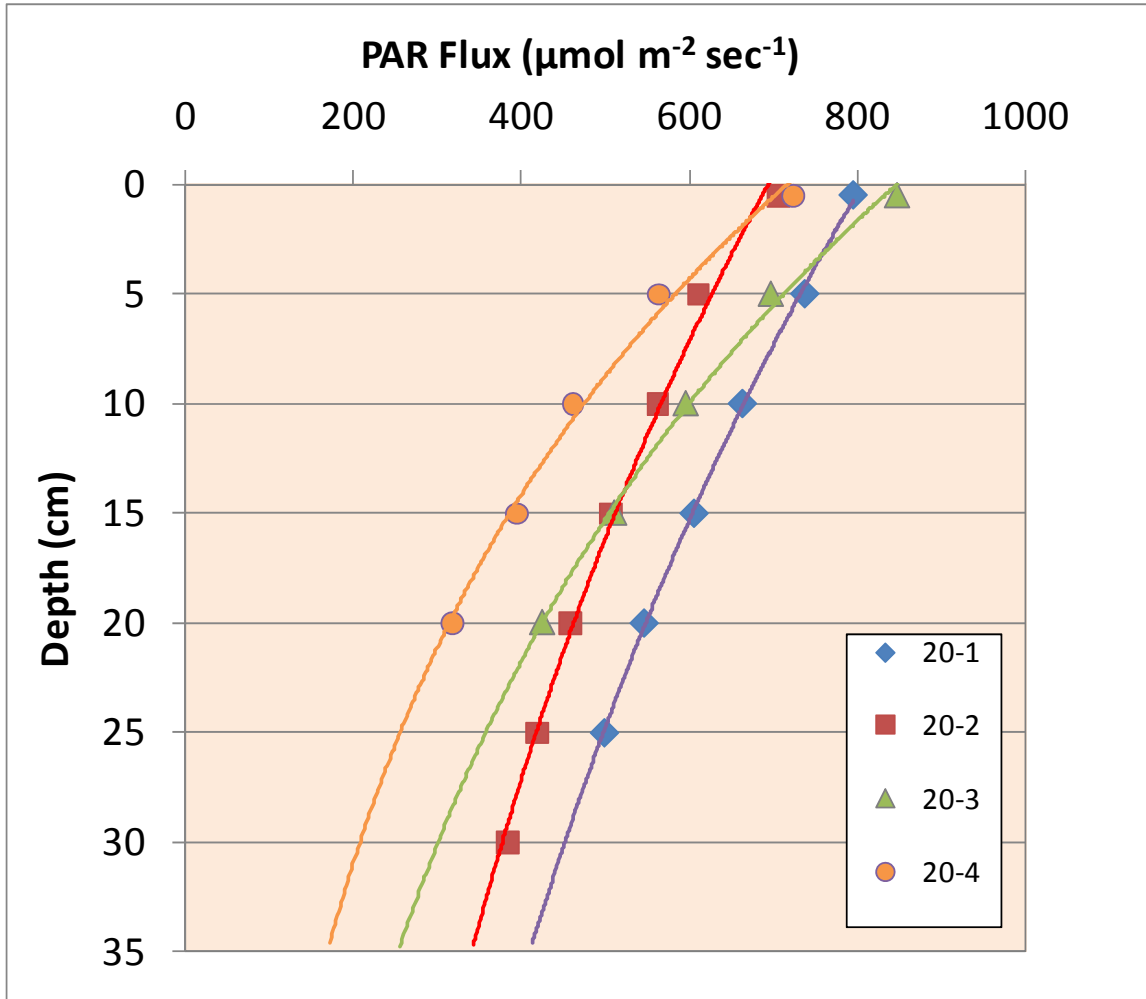


Figure 9.4 Graph showing instantaneous flux of photosynthetically available radiation versus water column depth, as a measure of light attenuation. Data collected at four replicate sites of open-water areas of field R20 on June 26, 2008. Extinction coefficients varied from 0.019 (site 20-1) to 0.041 cm^{-1} (site 20-3).

A) PAR wavelengths (400–700 nm)

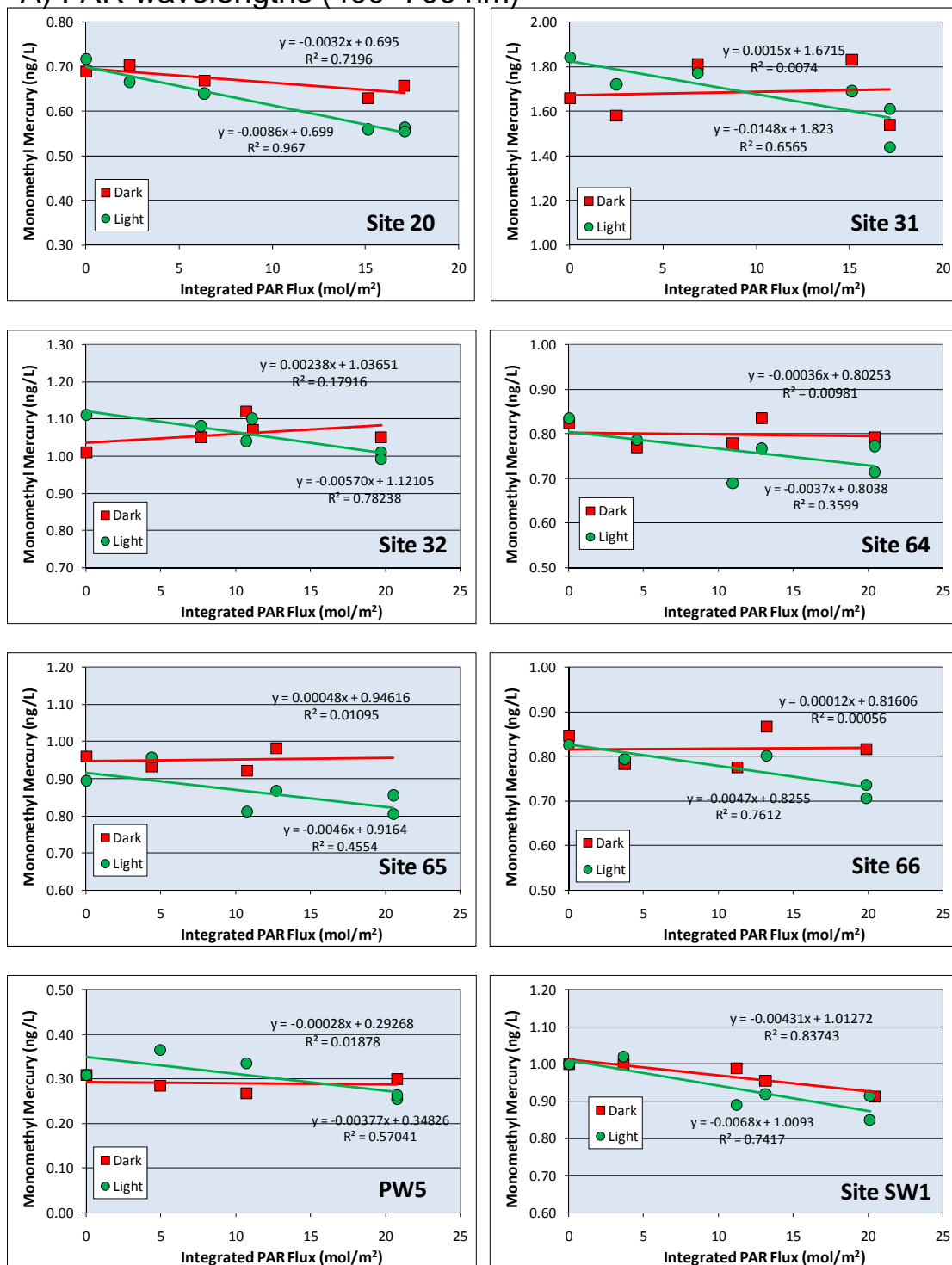
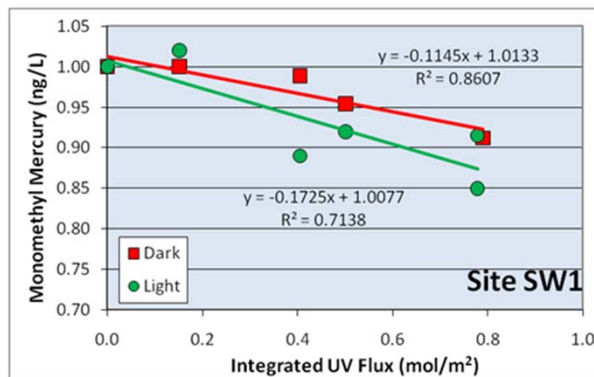
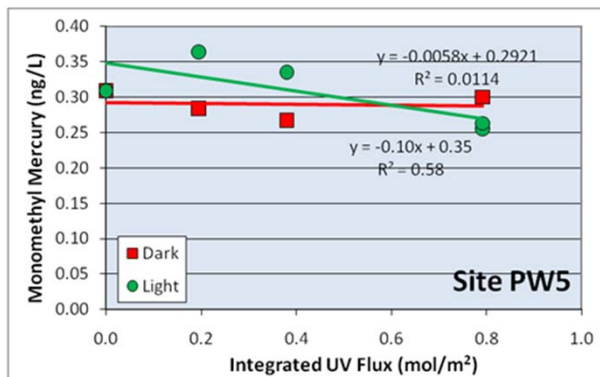
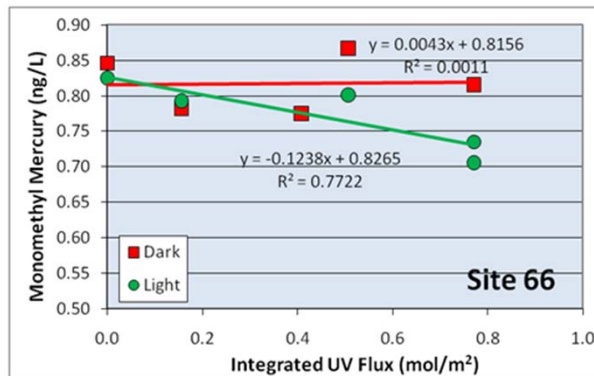
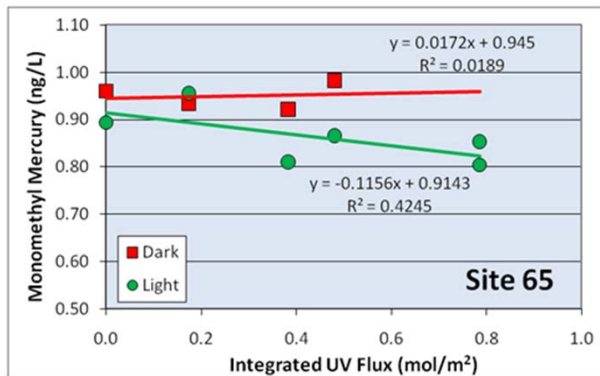
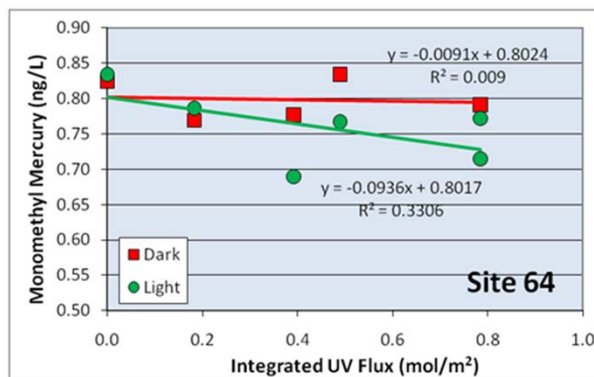
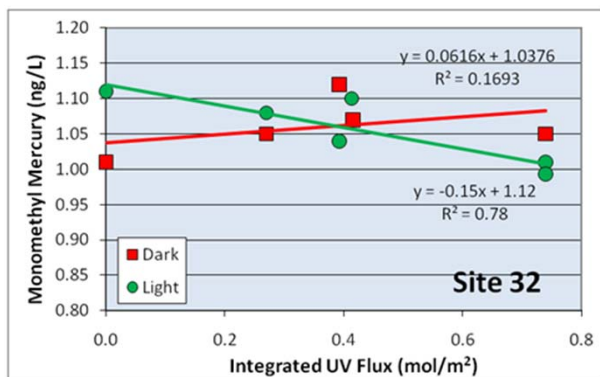
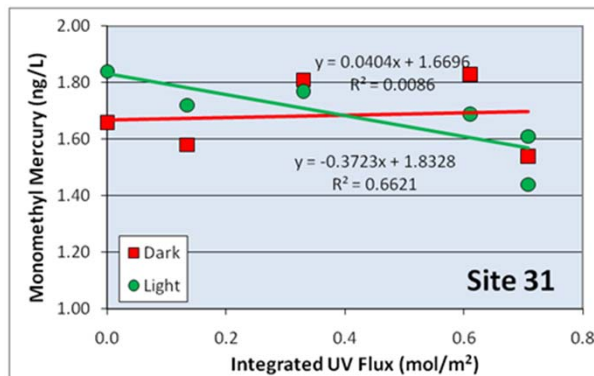
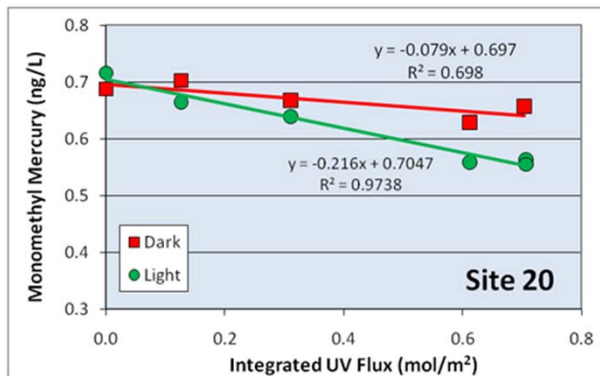


Figure 9.5. Scatter plots showing least-squares linear regressions of integrated (cumulative) solar radiation versus aqueous methylmercury concentration for December 3–7, 2007 based on A) PAR wavelengths (400–700 nm) and B) total UV wavelengths (UVA + UVB). Samples exposed to light shown in green, samples from dark control bottles shown in red.

B) UV wavelengths (UVA + UVB; 280–400 nm).



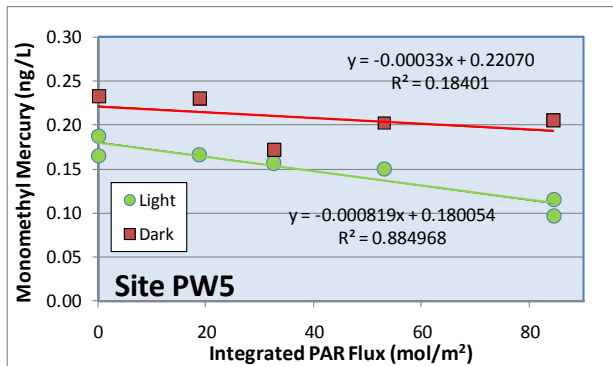
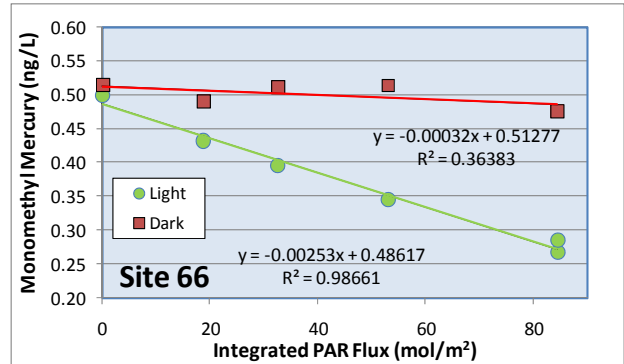
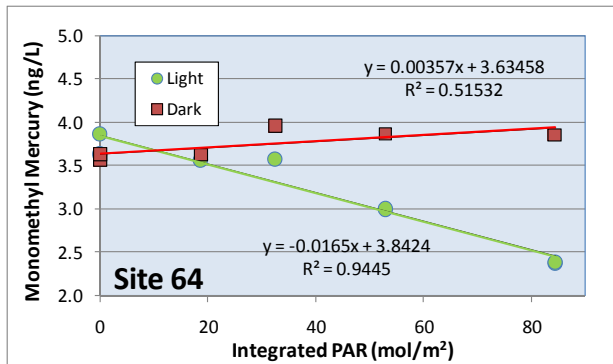
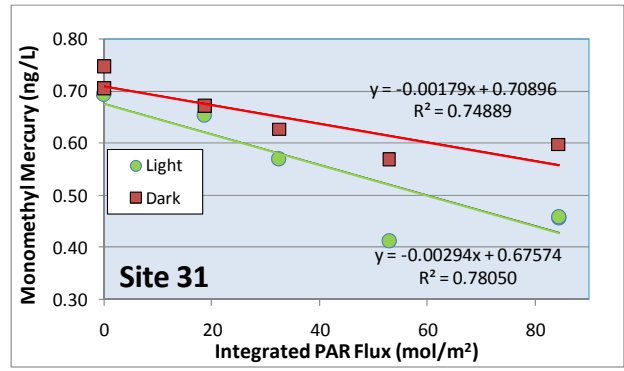
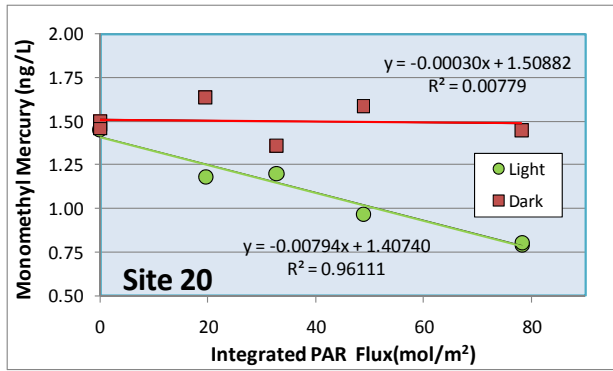


Figure 9.6. Scatter plots showing least-squares linear regressions of integrated photosynthetically available radiation versus aqueous methylmercury concentration for July–August 2008 incubations. Samples exposed to light shown in green, samples from dark control bottles shown in red.

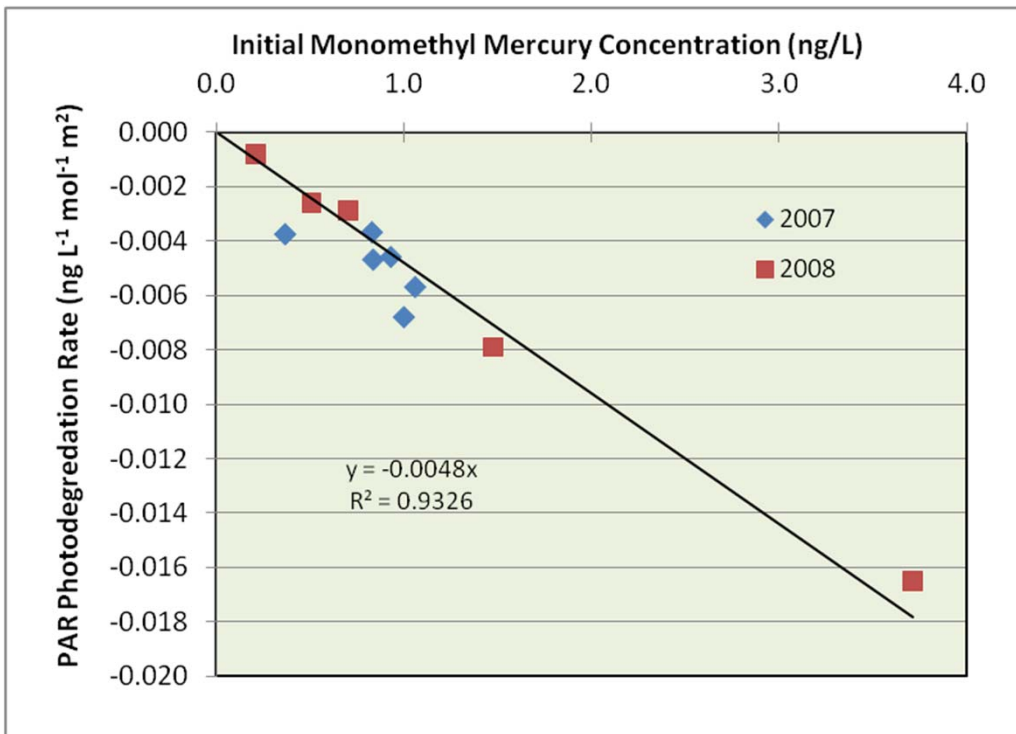
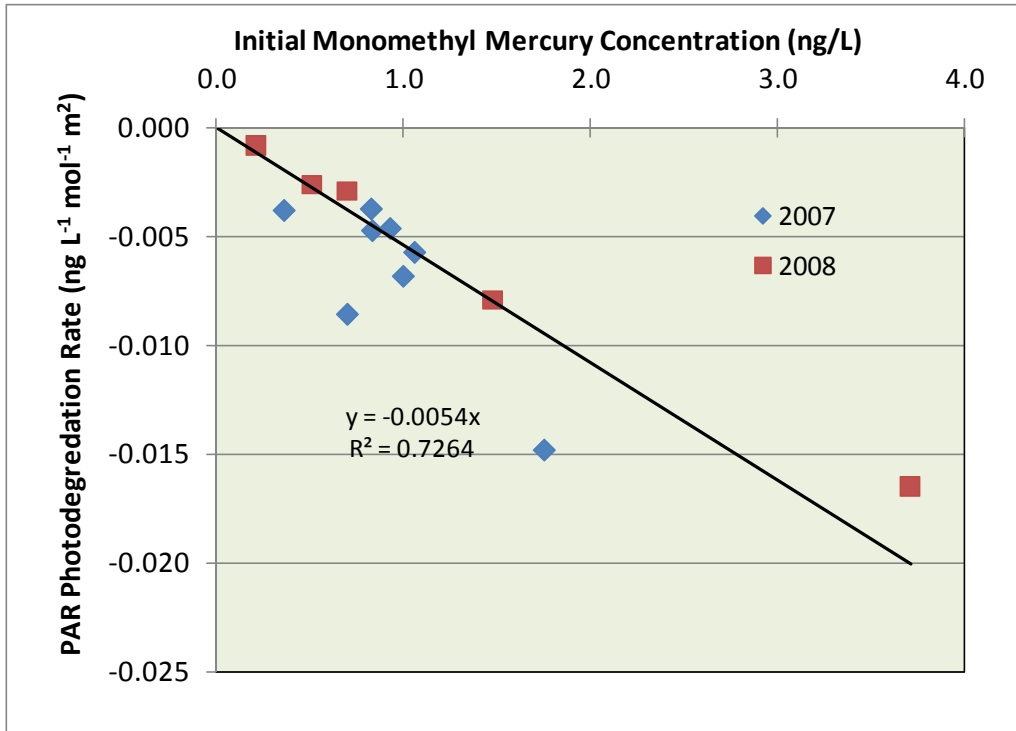


Figure 9.7. Scatter plots showing least-squares linear regressions of initial aqueous methylmercury concentration versus PAR-dependent photodecomposition rate A) data from all 13 experiments and B) data from 11 experiments (2007 data from 2 northern fields, F20 and R31, not included).

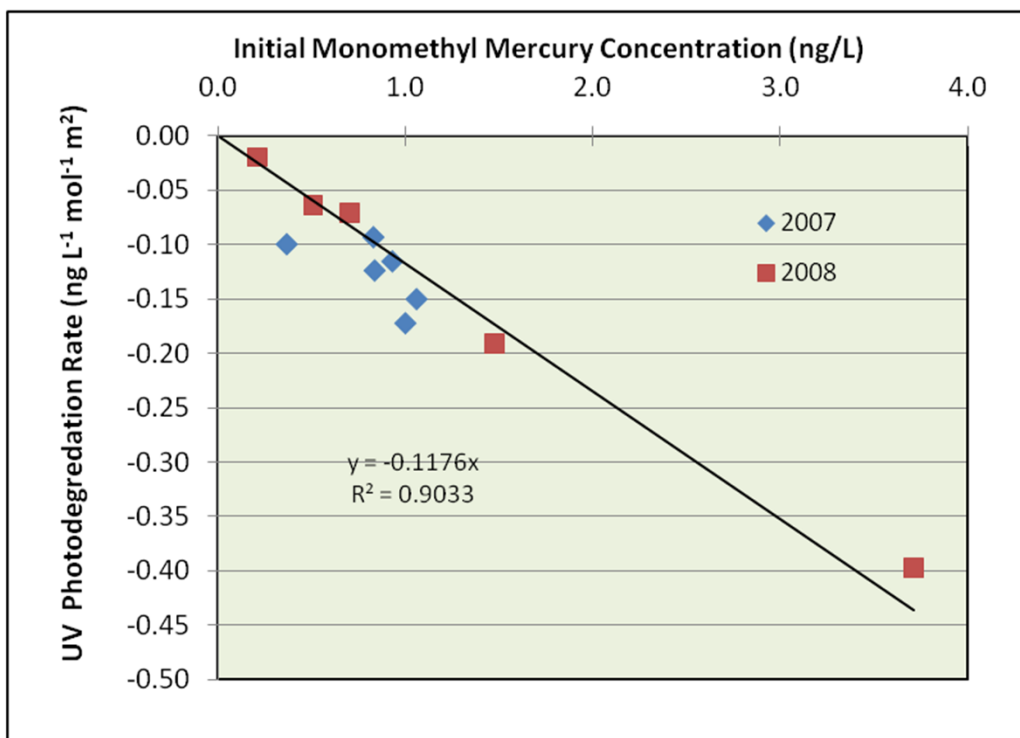
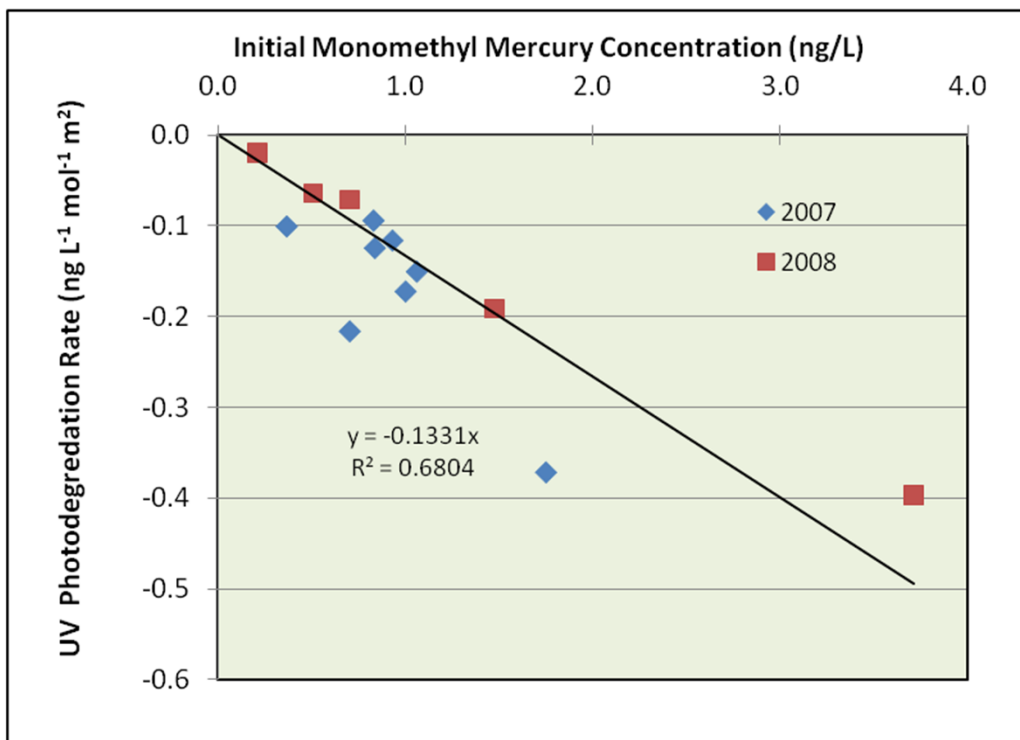


Figure 9.8. Scatter plots showing linear least-squares regressions of initial aqueous methylmercury concentration versus UV-dependent photodecomposition rate A) data from all 13 experiments and B) data from 11 experiments (2007 data from 2 northern fields, F20 and R31, not included).